Spring 5-2017

An Investigation of the Use of Cerium and Polyhedral Oligomeric Silsesquioxanes for the Protection of Polymeric Epoxy Compounds in the Low Earth Orbit Environment

Jessica Miriam Piness
University of Southern Mississippi

AN INVESTIGATION OF THE USE OF CERIUM AND POLYHEDRAL OLIGOMERIC SILSESQUIOXANES FOR THE PROTECTION OF POLYMERIC EPOXY COMPOUNDS IN THE LOW EARTH ORBIT ENVIRONMENT

by

Jessica Miriam Piness

A Dissertation
Submitted to the Graduate School
and the School of Polymers and High Performance Materials
at The University of Southern Mississippi
in Partial Fulfillment of the Requirements
for the Degree of Doctor of Philosophy

Approved:

_____
Dr. Robert Y. Lochhead, Committee Chair
Professor Emeritus, Polymers and High Performance Materials

_____
Dr. William L. Jarrett, Committee Member
Research Associate Professor, Polymers and High Performance Materials

_____
Dr. Sarah E. Morgan, Committee Member
Professor, Polymers and High Performance Materials

_____
Dr. Sergei I. Nazarenko, Committee Member
Professor, Polymers and High Performance Materials

_____
Dr. Derek L. Patton, Committee Member
Associate Professor, Polymers and High Performance Materials

_____
Dr. Karen S. Coats
Dean of the Graduate School

May 2017

Published by the Graduate School

ABSTRACT

AN INVESTIGATION OF THE USE OF CERIUM AND POLYHEDRAL OLIGOMERIC SILSESQUIOXANES FOR THE PROTECTION OF POLYMERIC EPOXY COMPOUNDS IN THE LOW EARTH ORBIT ENVIRONMENT

by Jessica Miriam Piness

May 2017

Low Earth orbit presents many hazards for composites including atomic oxygen, UV radiation, thermal cycling, micrometeoroids, and high energy protons. Atomic oxygen and vacuum ultraviolet radiation are of concern for space-bound polymeric materials as they degrade the polymers used as matrices for carbon fiber composites, which are used in satellites and space vehicles due to their high strength to weight ratios. Epoxy-amine thermosets comprise a common class of matrix due to processability and good thermal attributes. Polyhedral oligomeric silsesquioxanes (POSS) have shown the ability to reduce erosion in polyimides, polyurethanes, and other polymers when exposed to atomic oxygen. The POSS particle is composed of a $SiO_{1.5}$ cage from which up to eight organic pendant groups are attached at the silicon corners of the cage. POSS reduced atomic oxygen impact on polymers by a process known as glassification wherein the organic pendants are removed from the cage upon atomic oxygen exposure and then the cage rearranges to a passive silica network. In addition, POSS shows good UV absorbance in the UVb and UVc ranges and POSS can aid dispersion of titanium dioxide in a nanocomposite.

In this work, Chapter I focuses on hazards in low Earth orbit, strategies for protecting organic material in orbit, and the capabilities of POSS. Chapter II details the experimental practices used in this work. Chapter III focuses on work to induce POSS phase separation and layering at the surface of an epoxy-amine thermoset. Generally, POSS is dispersed throughout a nanocomposite, and in the process of erosion by atomic oxygen, some polymer mass loss is lost before enough POSS is exposed to begin glassification. Locating POSS at a surface of composite could possibly reduce this mass loss and the objective of this research was to investigate the formation of POSS-rich surfaces. Three POSS derivatives with different pendant groups were chosen. The POSS derivatives had a range of miscibilities with the epoxy-amine matrix. A sedimented layer of the most incompatible POSS moiety was observed at the bottom of bars at the highest loading level of 5 wt% POSS. It was concluded that POSS could form a sedimented layer in this epoxy during cure. Epoxy amine materials containing POSS derivatives were tested by exposure to atomic oxygen at NASA Glenn Research Center with each POSS derivative present in separate samples at 2.5 wt% loading levels. Mass loss did not decrease against an unfilled control and glassification was not observed, leading to the conclusion that POSS could not be effectively concentrated at a surface to reduce degradation given the methods used.

Taking this into account, the study transitioned into seeking ways to integrate highly UV absorbent cerium compounds with POSS. This part of the study is reported in Chapter IV. It was anticipated that POSS with a polar

pendant group would interact through intermolecular forces with cerium (IV) oxide and produce a suspension that could be cured at the surface of polymers. However, in every experiment, the cerium (IV) oxide was not dispersed. However, a homogeneous dispersion of a cerium-containing compound was achieved by combining trisilanol phenyl POSS with cerium (III) nitrate hexahydrate. NMR and mass spectrometry showed that the mixture of Cerium nitrate and trisilanol phenyl POSS did not result in the formation of a chemical compound but FTIR studies indicated the presence of hydrogen bonding between the POSS silanols and cerium-associated water. The resulting material was termed “CePOSS”. CePOSS was more UV absorbent in the UVc region than POSS or other cerium compounds as measured by solution UV-vis spectroscopy. In addition, CePOSS could be mixed into a POSS-epoxy coating, after pre-blending with poly(ethylene glycol) POSS, to produce films that were essentially opaque in the UV region below a wavelength of about 300 nm, and transparent in the visible region above 300 nm. The discovery of a ‘window of transparency’ in the visible region is significant in view of the fact that the epoxy-amine polymers, *sans* the POSS and cerium additives, were opaque across the entire UV/ visible range.

The investigation of the UV transmittance and glassification response of these CePOSS-POSS-epoxy films is described in Chapter V. UV transmittance of the POSS-epoxy coating was predicted to decrease below 275 nm with the presence of CePOSS given the solution UV-vis spectroscopy results. However, there was no difference seen in transmittance between coatings with and without

CePOSS below 275 nm. The transparent region above 300 nm was seen in all samples with any type of POSS. In addition, UV/ozone exposure was completed on epoxy, POSS-epoxy, and CePOSS-POSS-epoxy coatings to examine the effect of cerium on POSS glassification. Oxidation was achieved even in the presence of CePOSS as verified by x-ray photoelectron spectroscopy, scanning electron microscopy, and contact angle. Finally, UV transmittance was done on pre and post exposed materials.

ACKNOWLEDGMENTS

Special thanks to Dr. Robert Y Lochhead of the School of Polymers and High Performance Materials and Dr. Joe Lichtenhan at Hybrid Plastics, without whom this work would not have been completed. Thanks to my committee members, Dr. William L. Jarrett, Dr. Sarah E. Morgan, Dr. Sergei I. Nazarenko, and Dr. Derek L. Patton, and the graduate advisor, Dr. Bret Calhoun, for their assistance. I appreciate the help of various individuals and research groups at USM with experiments and instrumentation including Jessica Douglas (microscopy), Dr. Mohammad Hassan (dielectric spectroscopy), Dr. Katrina Knauer (AFM), Tina Masterson (mass spectroscopy) and the Azoulay, Morgan, Nazarenko, Patton, Rawlins, and Wiggins research groups. Funding for this work was provided by a NASA Harriet Jenkins Graduate Fellowship (NASA award: NNX13AR82H) and I appreciate the assistance of Candy Sigler and David Walker at USM and Elizabeth Cartier at NASA Ames Research Center in the administration of this grant. Dr. Tiffany Williams, Sharon Miller and Deborah Waters at NASA Glenn Research Center and Miria Finckenor at NASA Marshall Space Flight Center provided invaluable technical mentorship during the fellowship. Brian Wells at Xeel Corporation completed the UV/ozone exposures and UV transmittance measurements presented in Chapter V and was an invaluable technical consultant. Finally, I greatly appreciate lab space, supplies, and technical help offered by Hybrid Plastics, especially from Joe Lichtenhan, Mike Carr, and Greg Brust.

TABLE OF CONTENTS

LIST OF TABLES

LIST OF ILLUSTRATIONS

LIST OF SCHEMES

LIST OF ABBREVIATIONS

33DDS	3,3'-diaminodiphenyl Sulfone
44DDS	4,4'-diaminodiphenyl Sulfone
AFRL	Air Force Research Laboratory
amu	Atomic Mass Unit
ATR FT-IR	Attenuated Total Reflectance Fourier Transmission Infrared Spectroscopy
CNT	Carbon Nanotubes
CTE	Coefficient of Thermal Expansion
CVD	Chemical Vapor Deposition
DDS	Diaminodiphenyl Sulfone
DGEBA	Diglycidyl Ether of Bisphenol-A
DGEBF	Diglycidyl Ether of Bisphenol-F
DI	Deionized
DMA	Dynamic Mechanical Analysis
DMTA	Dynamic Mechanical Thermal Analysis
DSC	Differential Scanning Calorimetry
E_D	Dispersion Cohesive Energy
E_H	Electron Exchange Parameter
E_P	Polar Cohesive Energy
E_{vap}	Energy of Vaporization
f	Frequency

f_D	Fractional Dispersion Solubility Parameter
f_H	Fractional Hydrogen Bonding Solubility Parameter
f_P	Fractional Polar Solubility Parameter
FT-IR	Fourier Transmission Infrared Spectroscopy
G'	Storage Modulus
G"	Loss Modulus
IB-POSS	Isobutyl POSS
ICP-OES	Inductively Coupled Plasma Optical Emission Spectrometry
IO-POSS	Isooctyl POSS
ISS	International Space Station
IV	Ion Viscosity
LEO	Low Earth Orbit
MA	Methacrylic Acid
MALDI	Matrix-Assisted Laser Desorption/Ionization
MISSE	Materials International Space Station Experiment
NASA	National Aeronautics and Space Administration

NMR	Nuclear Magnetic Resonance
PDMS	Poly(dimethyl siloxane)
PEG	Poly(ethylene glycol)
PGMEA	Propylene Glycol Monomethyl Ether Acetate
PI	Polyimide
PISX	Poly(imide-siloxane
PMMA	Poly(methyl methacrylate)
PMSQ	Poly(dimethyl silsesquioxane)
POSS	Polyhedral Oligomeric Silsesquioxanes
PTFE	Polytetrafluoroethylene
RMS	Root Mean Square
STS	Space Transport System
T	Temperature
t-BMA	tert-Butylmethacrylate
TEM	Transmission Electron Microscopy
T_g	Glass Transition Temperature
TGA	Thermogravimetric Analysis
TGDDM	Tetraglycidyl 4,4′-diaminodiphenylmethane
THF	Tetrahydrofuran
TMA-POSS	Octa(tetraethylammonium) Polyhedral Oligomeric Silsesquioxane

TMS	Tetramethylsilane
TSIB-POSS	Trisilanol Isobutyl POSS
TSIO-POSS	Trisilanol Isooctyl POSS
TSP POSS	Trisilanol Phenyl POSS
TSPH POSS	Trisilanol Phenyl POSS
USM	The University of Southern Mississippi
UTS	Ultimate Tensile Strength
UV	Ultraviolet
UVa	UV Radiation from 400-320 nm
UVb	UV Radiation from 320-280 nm
UVc	UV Radiation from 280-100 nm
V	Volume
Vol %	Volume Percent
VUV	Vacuum Ultraviolet Radiation, UV Radiation from 200-100 nm
Wt %	Weight Percent
XPS	X-ray Photoelectron Spectroscopy
δ	Solubility Parameter
δ_D	Dispersion Solubility Parameter
δ_H	Hydrogen Bonding Solubility Parameter
δ_P	Polar Solubility Parameter
ε''	Dielectric Loss Permittivity

ε_o	Vacuum Permittivity
σ	Ionic Conductivity

CHAPTER I – INTRODUCTION

Polymeric composites have high strength to weight ratios as compared to metals, making them desirable structural materials for space applications.[1] However, low Earth orbit presents non-terrestrial environmental hazards such atomic oxygen and UV radiation can cause chain scission inorganic materials.[2] These processes lead to erosion and reduced thermal and mechanical properties.[3,4,5,6,7]

Polymers used in low Earth orbit applications include polyimides, poly(tetrafluoroethylene), epoxies, and cyanate esters. Oxides spray coated onto polymer surfaces can provide erosion protection but must be applied properly to avoid defects.[8] Nanocomposites using bulk inorganic oxides such as cerium oxide can also provide protection; however, these nanoparticles tend to aggregate.[9,10] Polyhedral oligomeric silsesquioxanes (POSS) are nanoparticles composed of an inorganic silicon-oxygen cage with organic pendant groups.[11] These pendant groups aid in dispersing or aggregating POSS particles depending on the nature of the matrix. Under exposure to atomic oxygen or oxygen plasma of sufficient energy, POSS undergoes “glassification” when pendant groups are removed by oxidization and the cage rearranges to form a passive silica layer that reduces erosion of the underlying polymer.[12, 11] In addition, POSS exhibits high UV absorbance from 200-300 nm.[13] These properties make POSS a potential candidate filler for anti-degradation nanocomposites used for low Earth orbit applications.

Low Earth Orbit Environment

Low Earth orbit (LEO) extends from 180 to 2,000 km above sea level.[14] This orbit includes the International Space Station (ISS) as well as many communications, weather, and science satellites.[14] Unfortunately, this orbit is not without hazards, including atomic oxygen, ultraviolet (UV) radiation, micrometeoroids, and thermal cycling.[2] The National Aeronautics and Space Administration (NASA) has been concerned about these hazards and their effects on materials for space structures since the early 1960s.[15,16] Initially, space structures were made of metal with polymer seals for select components.[16] Weight is of primary importance when transporting vehicles to low earth orbit.[1] Launching payloads can cost up to $4000/kg, which provides an incentive to use lightweight, high strength materials, such as polymer composites.[17,18] For example, a common aluminum alloy, 6061-T6, has a density of 2.7 g/cm3 whereas a carbon-epoxy composite has a density of 1.6 g/cm3.[1] However, organic materials in low Earth orbit are degraded by environmental factors such as UV radiation.[2]

Ultraviolet radiation is classified into three types, UVa, UVb, and UVc, dependent on wavelength (Figure 1).[19, 20]

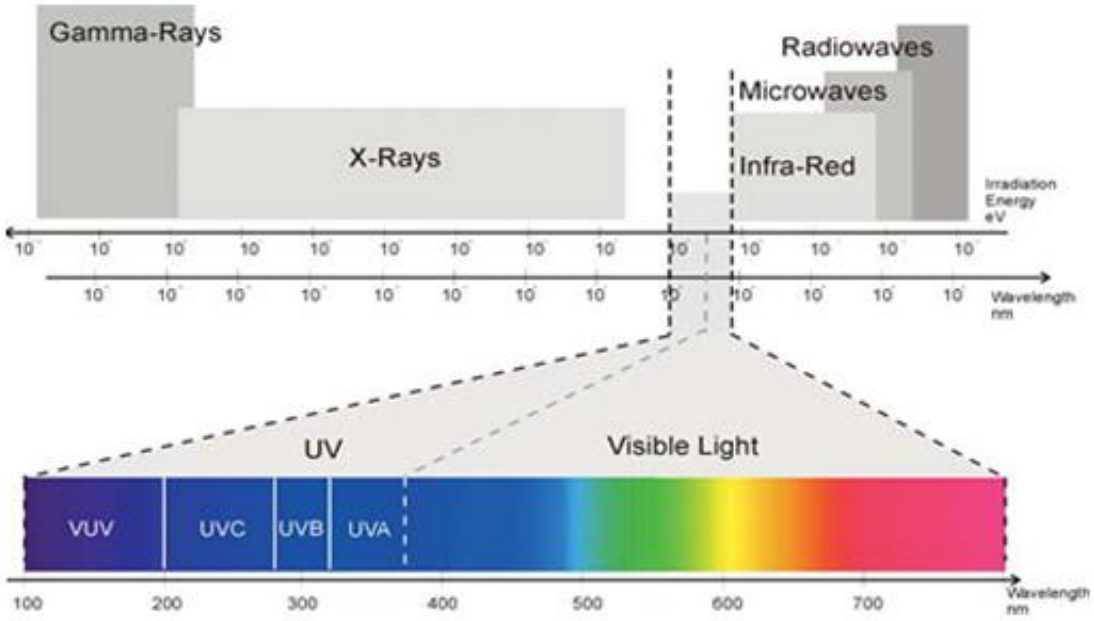

Figure 1. Electromagnetic spectrum.[21]

UVa (400-320 nm) and UVb (320-280 nm) are experienced terrestrially (Figure 1).[21, 19] The ozone layer blocks wavelengths shorter than 320 nm.[22] Photons of wavelengths less than 320 nm are classified as UVc and includes the subcategory of vacuum ultraviolet (VUV) radiation at less than 200 nm because VUV radiation can be transmitted in a vacuum.[21, 23] These higher energy UVc photons are more destructive than UVa or UVb photons.[20]

VUV radiation causes erosion and mass loss in a variety of polymers.[24,25,26] An example of VUV degradation is ground based exposure of Teflon® fluorinated ethylene propylene by Dever et al.[24] In this experiment, researchers at NASA Glenn Research Center exposed thin films to VUV radiation of wavelengths in the range 115-400 nm for a time period equivalent to 0.2 hours of sun exposure in low Earth orbit.[24] Even with this short exposure, the damaged films showed an eroded, brittle surface with a less degraded,

underlying bulk material.[24] The films also showed a statistically significant decrease in elongation at break, even when protected from radiation by a variety of inorganic solar cell glasses.[24]

There is a common misconception that the atmosphere of Earth abruptly ends and space begins. In reality, the Earth/space barrier is actually a gradient where the atmosphere is gradually decreasing in concentration.[14] As a result of this, atmospheric species such as diatomic oxygen are exposed to higher energy UV radiation that is normally blocked at lower altitudes by the ozone layer.[22] UVc radiation at less than 243 nm can cleave the 5.12 eV double bond in O_2, creating extremely reactive monoatomic oxygen radicals termed atomic oxygen, which causes additional damage on top of UV radiation.[20] Atomic oxygen is 90 % of the residual atmosphere between 300-700 km above sea level.[27] At the 400 km altitude of the International Space Station, the average flux of atomic oxygen is on the order of 10^{21} atoms atomic oxygen/cm^2 of material.[3,28]

Atomic oxygen degrades organic material either by a hydrogen abstraction mechanism or through direct scission of carbon-carbon bonds.[29] On average, the energy imparted by atomic oxygen is 4.5 eV, above the approximately 4 eV needed to break a carbon-carbon bond.[30, 31] Reaction with atomic oxygen alters the surface morphology of polymeric materials as demonstrated on the surface of Kapton H® polyimide exposed to 1.64 x 10^{20} atoms/cm^2 of atomic oxygen in a ground-based chamber (Figure 2).[31]

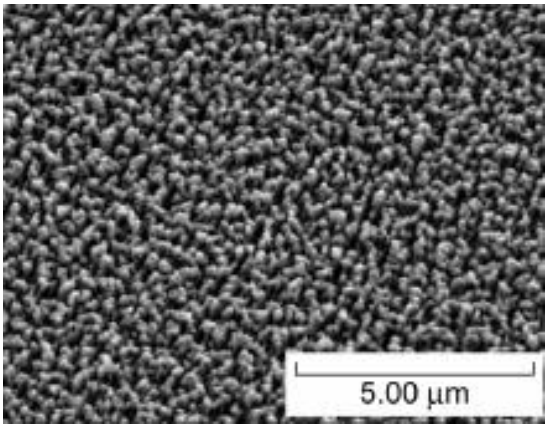

Figure 2. Kapton H® surface morphology after atomic oxygen exposure.[31] Surface etching patterns are dependent on the atomic oxygen flux and angle of exposure.[31] This erosion contributes to sample mass loss and discoloration.[32]

In addition to atomic oxygen, and UV radiation, spacecraft collide with micrometeoroids and orbital debris as well as experience thermal cycling.[33, 34] Thermal cycling in LEO can also affect materials. [35,36] Temperatures swing from -150 to +150 °C, depending on whether a satellite or spacecraft is on the sun or dark side of Earth.[35,37] This can result in fatigue cracking and issues with coefficient of thermal expansion (CTE) mismatch.[35]

In Orbit Exposure Testing of Polymers

Several exposure experiments have been conducted by NASA since the advent of the Space Shuttle program, where polymer films, coatings, and composites have been exposed to the low Earth orbit environment with mass loss and surface erosion studied before and after flight.[3,13] The first major *in orbit* experiment was the Long Duration Exposure Facility (LDEF).[13] Launched on Space Shuttle mission STS-41 in 1984, LDEF was a school bus-sized satellite

(Figure 3) with surface panels of materials that were exposed to LEO conditions for almost 6 years.[13]

Figure 3. LDEF exposure satellite.[13]

After LDEF, the International Space Station hosted a set of eight external exposure experiments known as Materials International Space Station Experiment or MISSE from 2001-2011.[3] The MISSE experiments were unprecedented in terms of data collected but were expensive and time intensive in terms of sample tray assembly, deployment, and retrieval and return to Earth.[3] Figure 4 shows an astronaut opening MISSE 2 above an ISS airlock.[3]

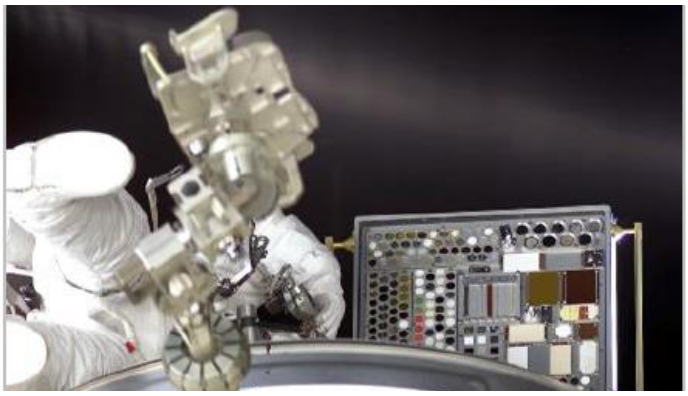

Figure 4. Astronaut placing MISSE 2 experiment on International Space Station.[3]

During the second MISSE experiment, films of various neat (unfilled) polymers were exposed primarily to atomic oxygen for four years and analyzed for erosion yield, or the mass removed per each atomic oxygen contact event.[3] The average atomic oxygen fluence was measured to be 8.43×10^{21} atoms/cm^2.[3] Fluence is defined as the amount of monoatomic oxygen atoms contacting a defined area during the duration of a test.[3] Selected results are listed in Table 1.[3]

Table 1

Polymer erosion yields from MISSE 2 experiment[3]

Polymer	Erosion Yield (cm^3/atom)
Poly(tetrafluoroethylene)	1.42×10^{-25}
Kapton H® Polyimide	3.00×10^{-24}
Epoxy (Trigycidyl-p-aminophenyl with aliphatic amine crosslinkers[38,39])	4.21×10^{-24}
Acrylonitrile butadiene styrene	1.09×10^{-24}
Cellulose acetate	5.05×10^{-24}
Poly(ethylene)*	$>3.74 \times 10^{-24}$*
Poly(acrylonitrile)	1.41×10^{-24}
Poly(styrene)	3.74×10^{-24}
Poly(methyl methacrylate)*	$>5.60 \times 10^{-24}$*
Poly(propylene)	2.68×10^{-24}
Polysulfone (Thermalux® P1700-NT11 and Udel® P-1700[s])	2.94×10^{-24}
Polyurethane (Dureflex® PS8010[s])	1.56×10^{-24}
Poly(ether ether ketone)	2.99×10^{-24}
Poly(ethylene terephthalate)	3.01×10^{-24}
Poly(amide-6)	3.51×10^{-24}
Poly(carbonate)	4.29×10^{-24}
Poly(p-phenylene terephthalamide) (Kevlar® 29 fabric[s])	6.28×10^{-25}

*Sample eroded completely before end of exposure[2]

The most commonly used neat polymers in LEO are polyimides, poly(tetrafluoroethylene), cyanate esters, epoxies, and siloxanes.[3,24,40,41,42] In general, highly aromatic polymers, such as Kapton H®, Kevlar®, poly(acrylonitrile), and the perfluorinated polymer, poly(tetrafluoroethylene), had less erosion than aliphatic hydrocarbon polymeric materials, such as poly(ethylene), poly(propylene), and poly(methyl methacrylate).[3]

Currently Used Materials in Low Earth Orbit

Given the cost of launching material to low Earth orbit, there is growing use of polymeric composites in satellites and space vehicles.[17,18] The major environmental hazards in low Earth orbits are atomic oxygen, vacuum ultraviolet radiation, micrometeoroids, and thermal cycling. [21,27,33,35] Highly aromatic or fluorinated polymers and oxides, used as spray coatings or fillers, are some of the strategies used to reduce degradation. Each of these strategies has its advantages and drawbacks. [3, 24, 40, 41, 43,44] Neat polymers can be directly used in applications such as composite structures and thermal insulation, but will eventually degrade regardless of structure.[24,40,41] In addition, different mechanical, thermal, and rheological properties govern applications for each class of polymer.[45-49] Oxide coatings applied to polymers can provide more protection, especially against atomic oxygen and UV radiation, but require complicated post-cure processing.[8,44]

Selection of Polymers for Low Earth Orbit

Polyimides. One frequently used class of thermoplastic for low Earth orbit are polyimides.[40] The basic repeat unit of a polyimide is shown in Figure 5.[50]

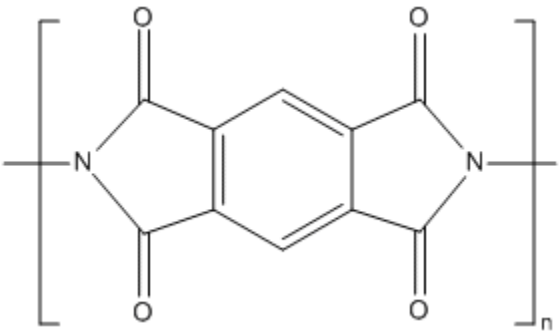

Figure 5. Basic structure of polyimide repeat unit.[50]

Polyimides are most commonly prepared from a combination of aromatic diamines and aromatic dianhydrides, resulting in a condensation reaction with the loss of water.[46] These polymers are valued for their thermal stability; the aromatic polyimide Kapton® exhibits <2 wt% loss up to 500 °C under nitrogen and only 30 wt% loss up to 1000 °C.[46] In air, degradation is more substantial but only starts above 500 °C.[46] Glass transition temperature is an important parameter for polymer chemists to understand when designing polymers.[51] The T_g of polyimides range from 50-400 °C, depending on the structure.[46] Aromaticity contributes to polymer rigidity, increasing the glass transition temperature compared to aliphatic networks. Polyimides are often used to replace metal parts, due to their high stiffness, tensile strength, flexural strength, and modulus.[46] Brittleness can be an issue that can be remedied by copolymerization at the expense of decreased mechanical properties.[46]

Because of their high thermal stability and suitable mechanical properties, polyimides are used in space as thermal blankets for solar cell arrays and as general structural components.[40] The Kapton® family of polyimides are some of the most studied polymers with regard to atomic oxygen and VUV resistance.[40] In Figure 6, electron pair resonance between the central phenyl and two heteroatom-rich rings can stabilize radicals formed after hydrogen abstraction.[18]

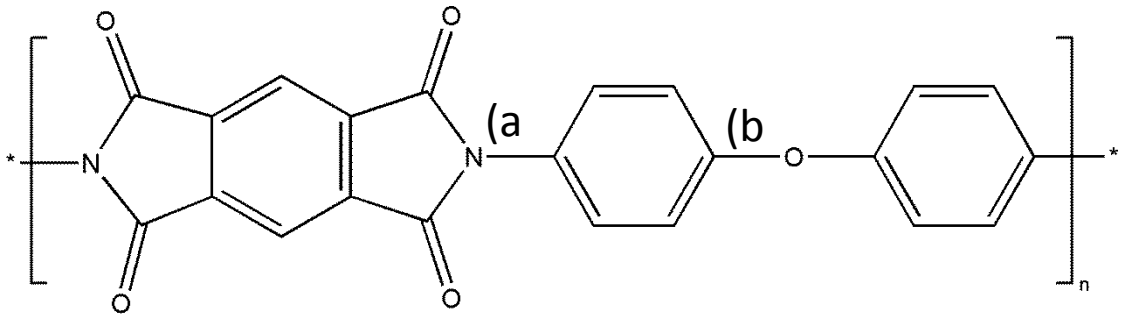

Figure 6. Structure of Kapton® repeat unit.[50]

Nevertheless, the C-N bond labeled as a) in Figure 6 has a dissociation energy of 3.2 eV, making it susceptible to UV radiation wavelengths lower than 390 nm or the approximately 5 eV energy of atomic oxygen in low Earth orbit.[43] Bond b) between oxygen and a phenyl carbon, is also vulnerable to atomic oxygen and UV radiation below 320 nm.[43]

Poly(tetrafluoroethylene). Poly(tetrafluoroethylene) (PTFE), known by the tradename Teflon®, has been used in low Earth orbit applications.[41] This polymer features a $–[–CF_2–CF2–]_n–$ repeat unit.[47] Discovered in 1938, PTFE can be manufactured from either suspension or emulsion polymerization from chloroform and hydrogen fluoride.[47] The halo of fluorine atoms around the carbon-carbon backbone prevents most attacks on the backbone and is the source of its the inert character.[47] This material is highly crystalline (92-98 %) and does not melt until approximately 300 °C.[47] It is not recommended to use PTFE above 260 °C in order to maintain optimal thermal stability.[47] However, two transitions in crystal structure and order occur at 19 and 30 °C, which substantially affect mechanical properties below the 260 °C barrier.[47] Compared to polyimides, PTFE is

extremely flexible in terms of elongation at break but has lower tensile and flexural moduli by an order of magnitude.[46,47]

Poly(tetrafluoroethylene) can be used for non-structural applications in low Earth orbit such as thermal insulation blankets.[41] This material withstands the effects of atomic oxygen and UV radiation due to the strength of the C-F bond (dissociation energy of 5.6 eV compared to 3.49 eV for C-H).[43] However, the backbone CF_2-CF_2 bond is only 4.3 eV, which can be severed by atomic oxygen and UV photons at wavelengths less than 290 nm.[43] Structural insulation on the Hubble Space Telescope consisted of PTFE blankets 127 μm thick with an 100 nm aluminum layer deposited on the coating surface to help reflect heat.[41] During spacewalks to repair the telescope in the mid-1990s, large cracks were observed in this layer and material was removed and eventually had to be replaced.[41]

Epoxies. Due to the lower viscosities of their precursors; thermosets are easier to process as composite matrices compared to thermoplastics.[52] First sold in 1946, epoxy thermosets are characterized by three-membered rings of two carbon atoms and one oxygen atom that can be easily ring opened by nucleophilic attack.[53] Epoxies are used for applications including corrosion protection coatings, electrically insulating materials, and composite matrices.[48] Monomers are generally multifunctional with aromatic species most commonly used in aerospace applications.[53] Viscosities of aromatic monomers can range from 0.55 to 20 Pa·s at 25 °C.[53] Thermal stability after cure increases with increasing aromaticity of the monomer and crosslinker.[53] Epoxy thermosets are valued for resistance to solvent ingress as well as good dimensional stability.

They become more mechanically rigid with greater aromaticity or crosslink density.[53]

Epoxy-amine systems have been used in aviation and space applications since the late 1950s.[54] Glass-epoxy composites were introduced in aircraft in 1952, with carbon fiber-epoxy composites first used in aviation in 1969.[44] The initial use of epoxies for space applications was in composite rocket nozzles studied by the National Research Council, Battelle Memorial Institute, and NASA in 1959, 1961, and 1966, respectively.[54,55] Use of epoxy composites in spacecraft and satellites began in 1971 and the number of applications continued to grow, such as satellite buses, antennas, and truss structures due to its high strength to weight ratio.[1,44]

The diglycidyl ether of bisphenol A (DGEBA) is a common epoxy monomer used for a variety of polymer and composite materials.[48] This epoxy monomer can react with various functional groups including other epoxies, esters, anhydrides, and amines.[48] The structure of the monomer is displayed in Figure 7.[56]

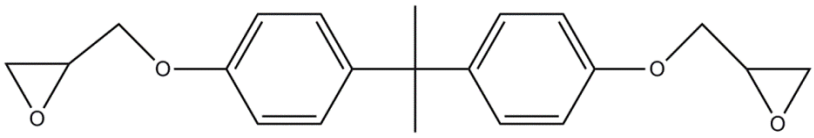

Figure 7. Structure of diglycidyl either of bisphenol A.[56]

In composite applications, DGEBA and other epoxies are generally thermally crosslinked with aromatic amines.[48] One such commericially available amine is 4,4’-diaminodiphenyl sulfone (44DDS, Figure 8), a white powder with a melting point range of 175-177 °C.[57]

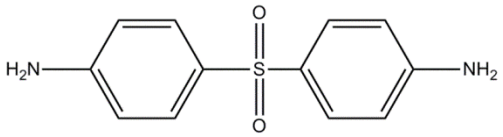

Figure 8. Structure of 4,4'-diaminodiphenyl sulfone.[58]

The glass transition temperature (T_g) of this system is approximately 204 °C as measured by dynamic mechanical analysis in tension in the current study.

Using peroxide radicals formed by UVb radiation, Musto et al. determined that hydrogen abstraction and resultant degradation for the DGEBA-4,4-DDS network were most likely to occur at the sites circled in red, shown in Figure 9.[29]

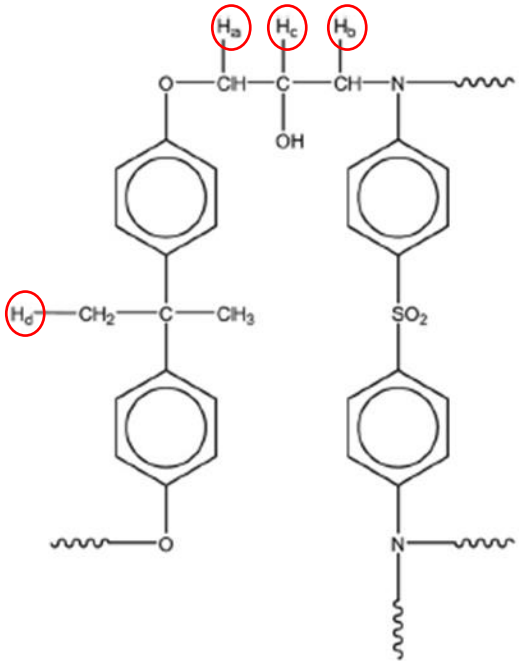

Figure 9. Hydrogen abstraction points on DGEBA-44DDS network.[29]

After the C-H bond cleavage, a radical is formed, which turns into a peroxy radical. A hydroxyl radical is then eliminated, followed by chain scission. This results in new end groups, smaller networks, and small molecule byproducts.

Any leftover radicals are stabilized by the oxygen radical and resonance from surrounding heteroatoms or phenyl groups (Scheme 1).[29]

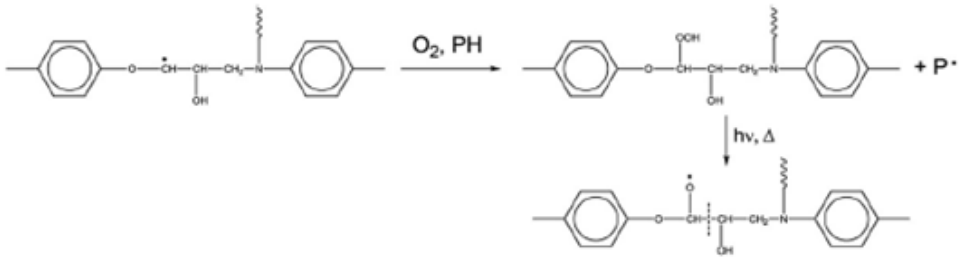

Scheme 1. Chain scission of DGEBA-44DDS network.29

Chain scission adversely affects epoxy thermal, mechanical, and optical properties due to decreases in modulus.[4,5,6,7] The glass transition temperature is also inversely related to E in epoxies.[4] Thus, network degradation impacts thermal stability.[4] In addition, epoxies yellow and become hazy after chain scission occurs, especially from UV radiation exposure.[5] Fracture toughness exhibits a maximum as a function of the molecular weight between crosslinks and then decreases at higher molecular weights.[59] Although not a direct cause of mechanical failure, this limits the use of epoxies in solar cell cover glass adhesives or as thermal radiation coatings, as these applications rely on optical and color stability.[6, 7]

Cyanate Esters. Another commonly used class of thermosets in aerospace applications are cyanate esters.[45] Cyanate esters have been used since 1983 in aerospace applications such as radomes, nose cones, and structural components for airplanes, satellites, and missiles.[44] These resins are generally aromatic and have cyanate functional groups as shown in Figure 10.[45]

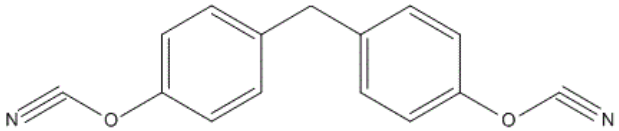

Figure 10. General structure of aromatic cyanate ester monomer.[45]

Monomers crosslink via a cyclotrimerization that transforms two cyanate groups into a triazine ring.[45] No crosslinking agent is required but carboxylate salts and transition metal chelates are needed as catalysts at parts per million levels.[45] These polymers provide high-temperature durability with glass transition temperature values generally above 250 °C, higher than most epoxies.[45,48] The degradation temperature for a variety of cyanate ester resins is over 400 °C, compared to 306-371°C for epoxy-amine and bismaleimide-amine networks.[45] However, cyanate esters have lower ductility and toughness and are more expensive than most epoxies.[45]

Inorganic Coatings

An alternative anti-degradation strategy is the use of inorganic coatings sprayed or deposited onto the surface of a polymer after cure.[8,44] As mentioned in the previous section, bond dissociation energies in Kapton® and PTFE range from 3.2-5.5 eV and are thus vulnerable to UVb photons or atomic oxygen.[43] Inorganic oxides such as silica (SiO_2) and alumina (Al_2O_3) have higher bond dissociation energies with the Si-O bond at 8.3 eV and the Al-O bond at 5.3 eV, respectively.[43] Thus, the Si-O bond can resist atomic oxygen and photons above 150 nm wavelength.[43] The Al-O bond can be broken by particularly energetic atomic oxygen species but is resistant to photons above 230 nm wavelength, a much lower limit than all organic bond energies except C-F in PTFE.[43]

Inorganic coatings on cured composites or polymer parts can provide protection again LEO hazards.[44] For example, a graphite-epoxy composite with a post-cure spray coat of SiO_2 was exposed to atomic oxygen in low Earth orbit for 42 hours during Space Shuttle mission STS-46.[44] Compared to the neat composite, no measurable mass loss was observed for the coated composite.[44]

These coatings are susceptible to a degradation mechanism known as underpinning.[8] Cracks or pinhole defects in the coating layer expose underlying organic material.[8] If a degradative agent such as a photon or monoatomic oxygen radical enters through this defect, it becomes trapped in the organic layer, causing more damage than just reflecting or absorbing into an uncoated polymer.[8] One example of underpinning is shown in Figure 11.[8]

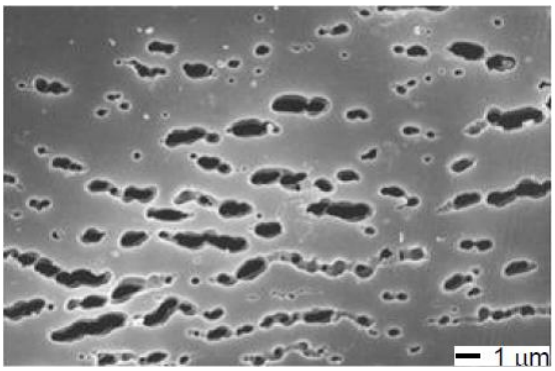

Figure 11. Underpinning erosion of Kapton®.[8]

In this study by Banks et al., Kapton® coated with aluminum was exposed for 5.7 years in low Earth orbit on the LDEF satellite.[8,13] After return to Earth and subsequent removal of the aluminum coating, severe erosion was revealed in Kapton® as darker, pitted areas approximately 1 µm deep by several microns long.[8] This was attributed to poor surface coverage of the deposited coating.[8]

Leveling coatings can reduce defects in spray coatings.[60] A leveling coating is a coating applied to an organic part after cure to create a smoother surface.[60] This coating is thick enough to obscure any surface defects or impurities stuck to the part, creating a flatter surface for adhesion of oxides.[60] This process is represented in Figure 12.[60]

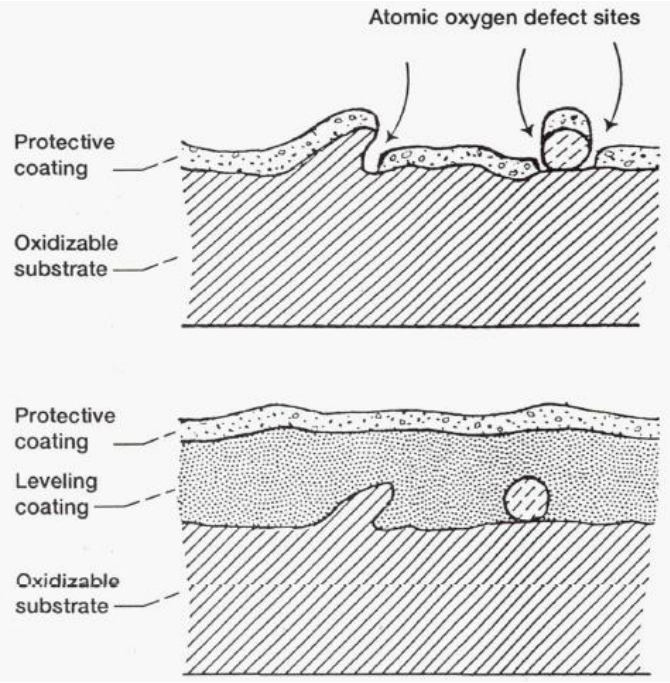

Figure 12. Surface changes from leveling coating.[60]

One example of leveling coating application is from a study by researchers at NASA Glenn Research Center and Cleveland State University.[60] Aluminum substrates were either dipped in diglycidyl ether of bisphenol-A and thermally cured or left unaltered before being coated with a layer of 1000 Å of SiO_2 by electron beam evaporation deposition.[60,61] After exposure to atomic oxygen, defects in the SiO_2 such as cracks or holes were visually identified through scanning electron microscopy (SEM).[60] The substrate with no epoxy leveling

coating had 21,000 defects per cm^2 of SiO_2.[60] This was reduced to 5,700 defects per cm^2 with one leveling coating but increased to 7,600 defects per cm^2 with two leveling coatings.[60] The authors concluded that the leveling coatings obscured any roughness or dirt on the surface of a substrate.[60] This smoothing process allowed for a more uniform surface for the silica coating, reducing coating defects.[60] However, leveling coatings and spray coatings both require additional post-processing of composite parts.

Cerium Oxide Filler

Oxide additives such as titanium dioxide, silicon dioxide, and cesium dioxide are common anti-UV additives.[62] Cerium (IV) oxide, CeO_2, is the most widely applicable of these three based on its low band gap of 3.1 eV.[62] Bonds can only absorb photons at or above a certain energy level, therefore, the cerium (IV) oxide band gap allows it to absorb relatively lower energy photons in the UVa and UVb range.[63] Cerium (IV) oxide has been used terrestrially to improve UV resistance of polymers such as poly(methyl methacrylate) and polyurethane, and in low Earth orbit as a UV absorber to prevent darkening in silica glass.[9,10,64,65] Nonetheless, dispersion and darkening are issues when using this oxide.[9,10,64,65]

Carbon Nanotubes

Carbon nanotubes (CNT) are cylindrical structures made exclusively of carbon atoms.[66] Well dispersed CNTs add electrically conductive pathways to a polymer allowing for additional functionalization of a nanocomposite.[66] In 2015, Atar, Minton, Grossman, Gouzman, and other collaborators published a study in

Applied Materials and Interfaces on a POSS-polyimide (PI) blend infused in carbon nanotube sheets.[67] Polyhedral oligomeric silsesquioxanes (POSS) are fillers with a $SiO_{1.5}$ cage that can have up to eight organic pendant groups.[11] POSS copolymers are electrical insulators and cannot dissipate charging that occurs when exposed to plasmas present in space.[67] This phenomenon can cause solar array and electronics failures in satellites and spacecraft when POSS coatings are used for antidegradation protection.[67] Atar et al. sought to remedy this issue by combining anti-atomic oxygen POSS-polyimides with conductive CNT sheets.[67] The CNT sheets were grown as a 9 μm thick, tangled layer using chemical vapor deposition (CVD) on silica substrates.[67] Solutions of polyamic acid and trisilanol phenyl POSS (Figure 13) at 5 and 15 wt% were mixed and infused into the CNT sheets.[67]

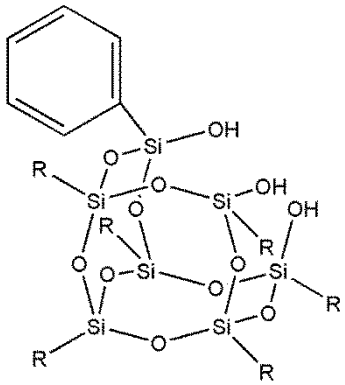

Figure 13. Structure of trisilanol phenyl POSS where R = phenyl.[68]

The POSS-polyimide matrix was cured thermally under nitrogen as temperature increased to 350 °C.[67] The resultant POSS-polyimide/CNT sheets were peeled from the silica substrate to create flexible films.[67]

Examination by SEM revealed a homogenous, tangled morphology of CNTs after polyimide infusion with no CNT aggregation.[67] The authors measured the resistivity of manufactured films and sheets as a function of increasing length (l) in rectangles at constant width (w). As shown in Figure 14, resistivity per increasing rectangular area was always higher with CNT-POSS-polyimide films compared to CNT sheets.[67] However, the inclusion of POSS did not substantially increase resistivity compared to the CNT-polyimide film.[67]

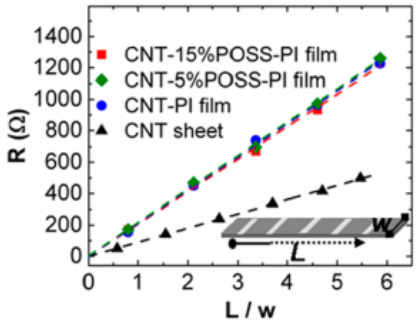

Figure 14. Resistivity of various films and sheets measured as a function of increasing rectangular area.[67]

Atar et al. also conducted tensile testing on the CNT-polyimide and CNT-POSS-polyimide films.[67] The CNT only sheet was not tested because it was too brittle.[67] Young's modulus was 2.3 GPA for the CNT-polyimide film and both CNT-POSS-polyimide films.[67] This compares to the 2.5 GPa value for commercially available Kapton HN®. Ultimate tensile strength decreased from 231 MPa for Kapton HN® to 78 MPa for the CNT-polyimide film.[67] A decrease is also observed for CNT-5 wt% POSS-polyimide and CNT-15 wt% POSS-polyimide, each having values of 61 to 77 MPa, respectively.[67] In addition, elongation of the films at break decreased from 72 % with Kapton HN® to 4.9 % for CNT-polyimide.[67] The CNT-5 wt% POSS-polyimide film had a elongation at

break of 6.1 %, but CNT-15 wt% POSS-polyimide was similar to that of CNT-polyimide.[67] The ultimate tensile strength and elongation at break results emphasize the strong decrease in ductility using fillers such as CNT or POSS.[67] The CNT-polyimide and CNT-POSS-polyimide films were rolled and unrolled 300 times per sheet, with resistivity measured ten times on each film after every 50 rolls.[67] There was no resistivity change greater than -3 % after the 300 total rolls for any of the materials.[67] The authors stated this was a significant result, because most conductive materials, such as neat CNT sheets, are too brittle to withstand constant bending.[67] However, no further mechanical testing was performed to determine properties such as flexural modulus. In addition, there were no comparisons with other flexible electronics.

Both the CNT-5 wt% POSS-polyimide and CNT-15 wt% POSS-polyimide films were cycled between -100 and +140 °C for 29 cycles under nitrogen.[67] Sheet resistance was measured every two cycles at the maximum and minimum temperatures.[67] Figure 15 summarizes the resistance changes, which never exceeded +/- 0.4 %.[67] The authors believed this demonstrated the ability of the CNT-POSS-polyimide films to retain electrical properties during temperature swings.[67] The Kapton HN® CNT sheet and CNT-polyimide film materials were not evaluated.

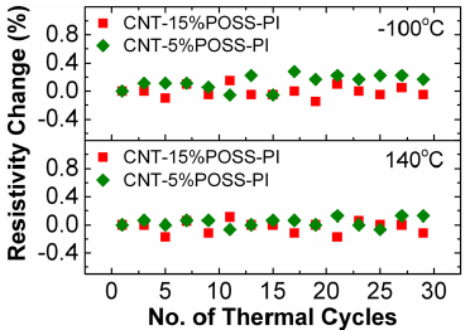

Figure 15. Resistivity change versus thermal cycling of CNT-POSS-polyimide films.[67]

The final experiment was with atomic oxygen.[67] Films of CNT-polyimide, CNT-5 wt% POSS-polyimide, and CNT-15 wt% POSS-polyimide were exposed to fluences of 6.0×10^{19} and 2.3×10^{20} atoms/cm^2 using a previously described hyperthermal oxygen beam.[67,69] Samples were examined by SEM and erosion yields and resistivity change were measured.[67] Micrographs of each of the three materials unexposed (top row), at 6.0×10^{19} atoms/cm^2 (middle), and 2.3×10^{20} atoms/cm^2 are displayed in Figure 16.

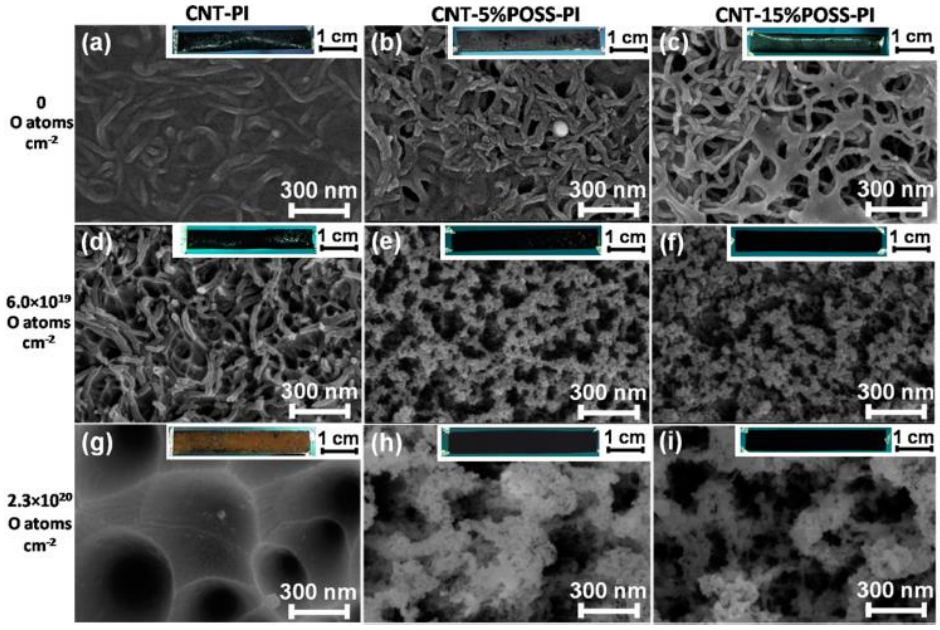

Figure 16. SEM micrographs of films after atomic oxygen exposure.[67]

Atar et al. stated that CNTs and matrix eroded from the CNT-polyimide film at 6.0×10^{19} atoms/cm^2 (d), leaving only polyimide to erode at 2.3×10^{20} atoms/cm^2 (g).[67] Films with POSS showed aggregate formations of CNT-SiO_2 after POSS glassification due to atomic oxygen (e, f).[67] Erosion did occur with increasing fluence (h, i) even with POSS.[67] At all fluences, the CNT-15 wt% POSS-polyimide film had the least erosion yield, followed by CNT-5 wt% POSS-polyimide, and Kapton HN® with CNT-polyimide film as the worst performer.[67] According to Atar et al., the erosion yields of the POSS materials could be fit to the following equation:

$$E = Ae^{-F/\tau} + y_o$$

where E is the erosion yield (cm^3/O atom), F was the fluence (atoms/cm^2), y_o was the erosion rate (cm^3/O atom) and A and τ were empirical constants.[67] The fluence can be related to the time of exposure. This equation indicates after the initial erosion loss there is a leveling off and eventual plateau of erosion. Following this relationship, erosion yield for the CNT-POSS-polyimide films began to level off at approximately 1.5×10^{20} atoms/cm^s.[67] The authors attributed this to POSS being converted to SiO_2 at the surface of the films by the atomic oxygen, creating an inert surface and thus slowing further erosion even with increasing fluence.[67]

Six films of each material, CNT-polyimide, CNT-5 wt% POSS-polyimide, and CNT-15 wt% POSS-polyimide, were measured for resistivity change according to fluence.[67] Figure 17 highlights the ability of films with POSS to retain resistivity against atomic oxygen fluence greater than 1×10^{20} atoms/cm^2.[67]

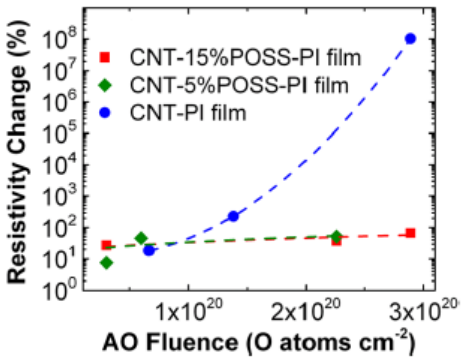

Figure 17. Resistivity change versus atomic oxygen fluence for CNT-polyimide and CNT-POSS-polyimide films.[67]

The CNT-15 wt% POSS-polyimide had an etch depth of 1.45 μm after 2.3×10^{20} atoms/cm^s.[67] Given the erosion rate of this material at 3.0×10^{-25} cm^3/O atom, Atar et al. calculated that 2.4×10^{20} atoms/cm^2 would be needed to erode the remaining 7.55 μm of film.[67] Therefore, a fluence of 4.7×10^{20} atoms/cm^s or approximately 4 years in low Earth orbit would be needed to erode the full 9 μm CNT-15 wt% POSS-polyimide and the film would be conductive for much of that time.[67] Thicker films would be able to last longer before destruction.[67] Overall, the resistivity change and erosion rate studies indicated that POSS was the filler that prevented atomic oxygen degradation and CNTs had little effect.

Transformation of Silica Species in Low Earth Orbit

In the previously discussed paper, Atar et al. referenced a phenomenon in which POSS became SiO_2 under exposure to atomic oxygen, creating an inert, protective surface layer.[67] This process also occurs in siloxane polymers but POSS provides advantages in that it can be integrated in a variety of polymers allowing for a wider range of applications.[12, 57]

Siloxane Polymers

Silicon-oxygen bonds are utilized in polymers to prevent degradation.[43] As previously mentioned, the bond dissociation energy of Si-O is 8.3 eV.[43] This is higher than low Earth orbit atomic oxygen at approximately 5 eV, and can only be cleaved by UV photons at wavelengths lower than 150 nm.[43] Polydimethylsiloxanes used to exploit this, with an Si-O backbone and organic pendant groups, are shown in Figure 18.[70]

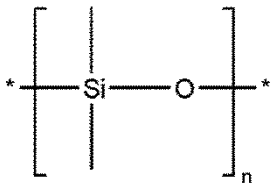

Figure 18. Siloxane repeat unit.[70]

Crosslinked polysiloxanes are commonly referred to as silicone rubbers, silicone resins, or elastomers.[70] These materials are much weaker and softer than epoxies or cyanate esters, with tensile strengths ranging from 2.4-5.1 MPa depending on the loading of fillers such as silica or metal oxides.[49] Silicone elastomers are recommended for use between -60 to +200 °C, and that can increase with thermal stabilizers to -110 to +250 °C.[49] These materials do have an advantage over epoxies and cyanate esters since silicone rubbers can remain flexible from -93 to +125°C, depending on the size of the pendant groups incorporated into the silicone structure.[70,42]

Silicone rubber is currently used for adhesives and seals on areas of the International Space Station that experience cold temperatures.[42] Even with the Si-O backbone, silicone rubber does darken under exposure to VUV radiation

and will react with atomic oxygen to form an SiO_x-rich, organic-poor surface.[42] This surface transformation causes cracking and releases an excessive amount of organic contaminants, compared to other polymers that have been exposed to atomic oxygen.[42] This loss of organic components during conversion to silica also occurs with uncrosslinked siloxanes, such as poly(dimethyl siloxane).[71] As the methyl groups are burned off by atomic oxygen or UVc photons, a SiO_x glass layer forms at the surface.[71] However, this causes the polymer to shrink and introduces stresses that crack the silica, exposing the underlying poly(dimethyl siloxane) and allowing degradation similar to the underpinning seen with defective inorganic coatings.[8,71]

Polyhedral Oligomeric Silsesquioxane Filler

Polyhedral oligomeric silsesquioxanes also lose organic material when converted from $RSiO_{1.5}$ to SiO_2 glass under exposure to atomic oxygen.[12] This phenomenon was first reported in 1996 by Gilman et al., at the Air Force Research Laboratory (AFRL).[12] This study compared poly(imide-siloxane) (PISX) and POSS-siloxane copolymers (Figure 19 and 20) to a simulated LEO environment.[12]

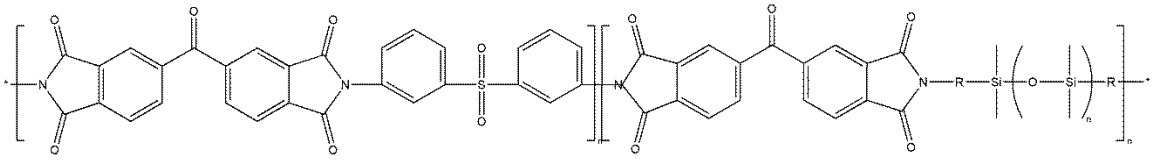

Figure 19. Poly(imide-siloxane) copolymer structure used by Gilman et al.[12]

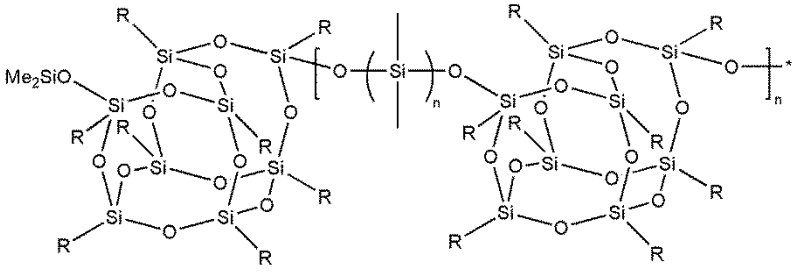

Figure 20. POSS-siloxane copolymer structure used in Gilman et al.[12]

Both copolymers were exposed to 4.3x10^{21} atoms/cm^2 atomic oxygen or atomic oxygen and far-UV radiation.[12] The PISX copolymer lost up to 0.15 mg/cm^2 after exposure whereas the POSS-siloxane copolymer gained up to 0.02 mg/cm^2.[12] Gilman et al. proposed that this result was due to altered copolymer chemistry. X-ray photoelectron spectroscopy (XPS) was used to detect the types of covalent bonds at the surface.[72] In this study, XPS showed increased silicon and oxygen content at the surface regardless of treatment with atomic oxygen or atomic oxygen and far UV.[12] The authors also noted that surface cracking was healed after exposure as seen left to right in Figure 21 where a cracked film converts to a smooth, rippled morphology.[12]

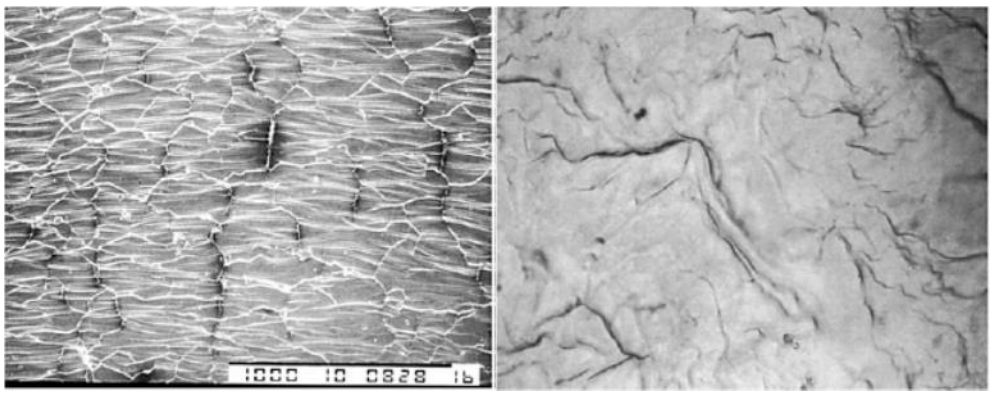

Figure 21. Pre-exposure cracked (left) and post-exposure healed POSS-polysiloxane (right).[12]

Gilman et al. attributed the morphological transformation to enthalpic heat of reactions between the POSS-siloxane and atomic oxygen as well as the absorption of energy after atomic oxygen collisions at the copolymer surface.[12]

During the early 2000s, the study of POSS exposure to atomic oxygen was continued by Rene Gonzales, an AFRL researcher also completing his Ph.D. under the supervision of Dr. Gar Hoflund at the University of Florida.[73] In a 2000 AFRL report, Gonzales and co-authors studied the atomic oxygen resistance of a POSS-poly(dimethyl siloxane) (PDMS) copolymer (Scheme 2) and a polyurethane polymer with POSS as a pendant group (Scheme 3).[74] Portions of this report were also published the same year in the *Journal of Spacecraft and Rockets*.[73,74]

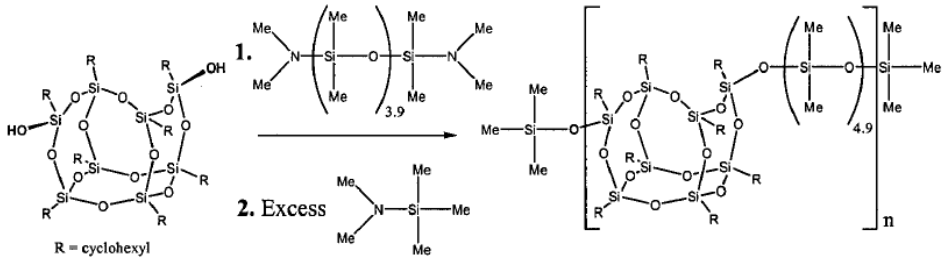

Scheme 2. Synthesis by Gonzales et al. of POSS-PDMS copolymer.[73,74]

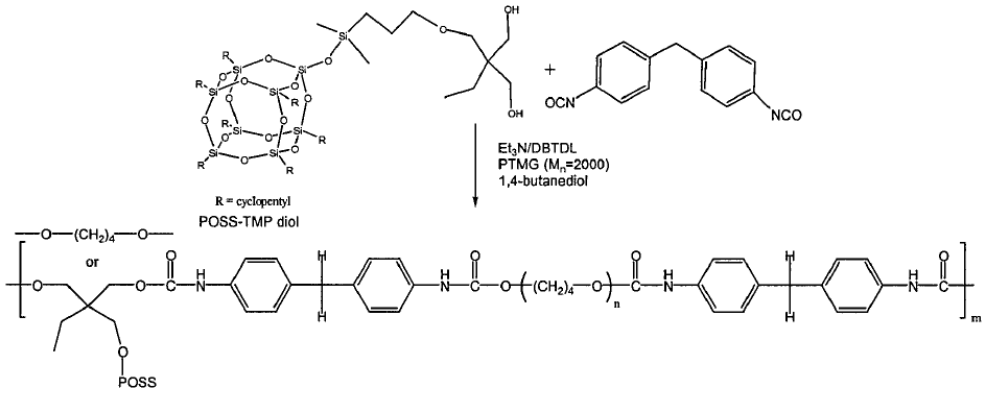

Scheme 3. Synthesis by Gonzales et al. of polyurethane with POSS pendant.[73,74]

Films of POSS-polymer were exposed on average 3.6 eV atomic oxygen that was generated by electrically stimulated desorption of O_2 while under vacuum.[73,74] Testing occurred at different atomic oxygen fluences.[73,74] Surface composition, determined by XPS on both copolymers, showed a similar increase in percent oxygen atom after atomic oxygen treatment as detailed in the previously discussed Gilman et al. paper.[12,73,74] The silicon atom percent also increased as a proportion of the total composition.[73,74] However, the O/Si atom percent ratio increased from 1.11 to 1.91 in POSS-PDMS and from 1.61 to 2.16 in POSS-polyurethane with increasing exposure to atomic oxygen.[73,74] In both samples, XPS showed a shift of the Si *2p* peak originally 102.7 eV, typical of $RSiO_{1.5}$, to approximately 103.5 eV, showing SiO_2 bond formation.[73,74] This shift was approximately equal regardless of type of copolymer or atomic oxygen fluence, indicating a self-extinguishing reaction that relied on the presence of atomic oxygen, not the amount.[73,74] The Gilman et al. paper did not remark on the carbon surface content but Gonzales and collaborators also noted that the percent carbon decreased 45.5 % at the surface of the POSS-PDMS film and 21.6 % in the POSS-polyurethane sample after the highest fluence test.[73,74] Considering both the decrease in carbon and silicon bonding shift to SiO_2, Gonzales et al. concluded that the atomic oxygen separated the organic pendant groups from the POSS cages at the copolymer surfaces and transformed those cages into layers of SiO_2 as depicted in Scheme 4.[73,74]

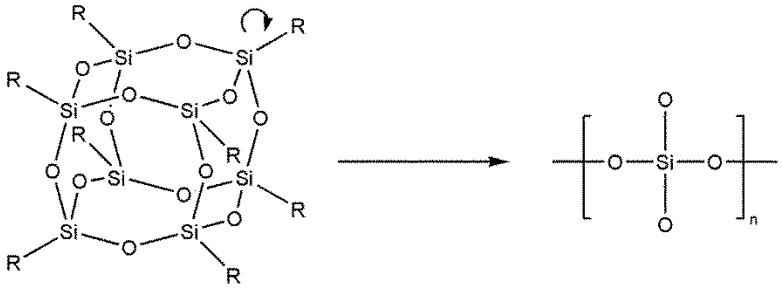

Scheme 4. Conversion of POSS to SiO_2 glass.

These layers were inert and prevented further surface alteration.[73] The authors provided no information on the possible depth of the SiO_2 layers or surface morphology.

Gonzales and other AFRL researchers continued to collaborate with Hoflund at University of Florida and reported a POSS-polyurethane study in the Journal of Adhesion Science and Technology in 2001.[75] POSS with six cyclopentyl and two reactive diols pendants was combined at a loading level of 20 % with 4,4-methylenebis(phenyl isocyanate) monomer to form the polymer structure shown in Figure 22.[75] The authors did not specify whether the loading level of POSS was in weight percent, volume percent, or another unit of measurement.

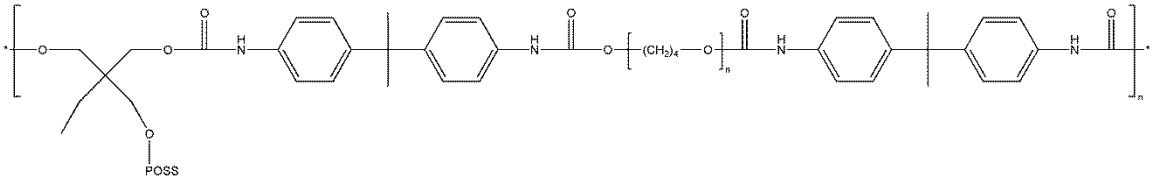

Figure 22. POSS-polyurethane copolymer synthesized by Hoflund, et al.[75]

Solvent cast films of unspecified thickness were exposed for 2, 24, and 63 hours to $2x10^{13}$ atoms/cm^2 atomic oxygen estimated at approximately 2.0 eV from electrically stimulated desorption of O_2.[75] The same film specimens were

characterized by XPS before and after exposure.[75] The XPS peak of the Si *2p* binding energy shows silicon in unexposed films, (spectrum (a) in Figure 23) primarily in the $RSiO_{1.5}$ bonding state at a binding energy of 102.7 eV.[75]

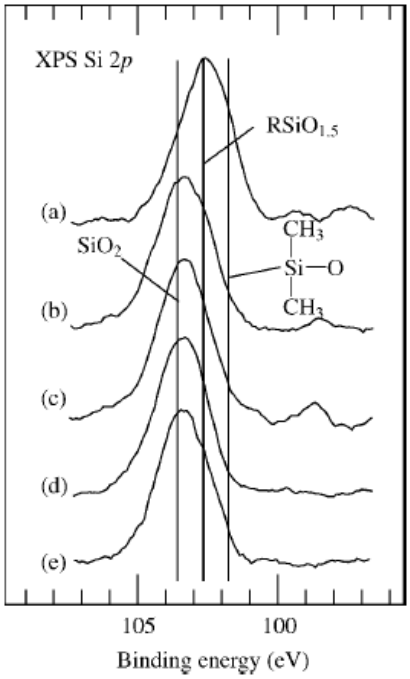

Figure 23. Si *2p* peak from XPS of (a) unexposed POSS-polyurethane and atomic oxygen exposed films after (b) 2 h, (c) 24 h, (d) 63 h, and (e) 63 h with a 4 h delay in air atmosphere before XPS analysis.[75]

This $RSiO_{1.5}$ structure corresponds to the POSS cage.[75] Beginning with 2 h of atomic oxygen exposure (spectrum (b)), the Si *2p* peak shifted towards the binding energy of SiO_2 at approximately 103.7 eV.[75] Visually, there did not appear to be further shifting of the Si *2p* peak with further exposure, although the authors stated that there was continued change up to 24 h of exposure (spectrum (c)).[75] The minor shift or lack thereof after 2 h of exposure was attributed to a passivating SiO_2 surface layer.[75] The XPS was assumed to

penetrate 4-6 nm into the material but no further investigation was completed into the depth of the SiO_2.[75]

Hoflund, et al. also analyzed the XPS binding energy of the carbon *1s* orbital.[75] The authors noted that the pre-exposed peak was centered at 285 eV, indicative of aliphatic groups, with a shoulder at 284.7 eV for aromatics.[75] With atomic oxygen testing, the C *1s* peak broadened to include other, higher binding energy species such as alcohols and acids.[75] Hoflund et al. explained this trend as selective attack at the aliphatic POSS pendant groups by atomic oxygen.[75]

Also of note in the 2001 study, select samples were exposed to atomic oxygen for 63 h and then left exposed to air for an additional 4 h before XPS analysis.[75] Compared to XPS of samples immediately examined after 63 h of exposure, the additional 4 h of air exposure increased surface carbon content by 5.6 atom%.[75] Hoflund et al. attributed this to atomic oxygen generating a reactive surface on the POSS-polyurethane that then reacted with organic species after removal from the vacuum test chamber.[75] Although this is a plausible explanation, due to the radicals that can be formed from oxygen radical attack, it does negate the conclusion that after formation the SiO_2 layer is a completely passive, unreactive material.

Polyhedral Oligomeric Silsesquioxanes

As filler, polyhedral oligomeric silsesquioxane is generally a closed Si-O cage with eight organic pendant groups of formula $RSiO_{1.5}$.[11] A variant known as open cage POSS also exists where one corner of the cage is replaced by three

silanols.[11] Both structures are shown in Figure 24.[68] Individual particles are 1-3 nm in size.[76]

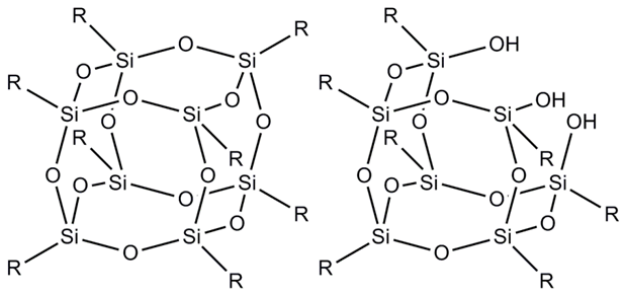

Figure 24. Structures of L) closed cage and R) open cage POSS.[68]

POSS is synthesized by two main methods, hydrolysis and condensation of eight $RSiCl_3$ molecules or the addition of one $RSiCl_3$ molecule to a partially completed silsesquioxane under basic conditions.[11] Depending on the functionality of the pendant group, POSS can be dispersed to a targeted degree when mixed into a polymer, or it can be attached to both thermosets or thermoplastics directly via a pendant group or through a crosslinking agent.[43,75,77,78] POSS nanocomposites have been created through copolymerization reactions using POSS as a monomer, POSS/polymer solution casting, and physical methods such as melt extrusion or mechanical blending of POSS in thermoplastics.[67,74,79,80]

POSS can aggregate when blended into nanocomposites if the selected functional groups are not compatible with the polymer matrix.[76] For example, Morgan et al. demonstrated that a POSS cage having attached phenyl groups has greater miscibility and dispersion in polystyrene as compared to POSS having an isobutyl pendant.[80] Surface energy measurements in this system concluded that only 15 percent of the surface area was covered with the phenyl

inclusive POSS compared to 78 percent of the area by the isobutyl POSS.[80] Surface aggregation of POSS can be beneficial; in Nylon-6 systems this phenomenon increased surface hardness, scratch resistance, and hydrophobicity, and resulted in decreased surface friction.[79] Understanding interactions between POSS and polymers is important since POSS fillers provide several functions, such as viscosity reduction, thermal stabilization, and degradation resistance.[76,80]

Polyhedral Oligomeric Silsesquioxanes and UV Radiation

Italian and American researchers examined the effects of UV radiation on POSS-polystyrene blends and reported the results in a 2012 *Polymer Degradation and Stability* paper.[81] Dintcheva, et al. disclosed commercially available, neat polystyrene blended with 5 wt% of five types of POSS: closed cage octafunctional iso-butyl (IB-POSS), octafunctional iso-octyl (IO-POSS), trisilanol iso-butyl (TSIB-POSS), trisilanol iso-octyl (TSIO-POSS), and trisilanol phenyl (TSPH-POSS) POSS.[81] Each type of POSS along with neat polystyrene was mixed in ratios of 1 mg/10 mL tetrahydrofuran (THF) and the resulting mixture was measured by UV-vis spectroscopy.[81] Figure 25 shows the absorbance per wavelength from 200-800 nm for polystyrene and each of the five POSS additives.[81]

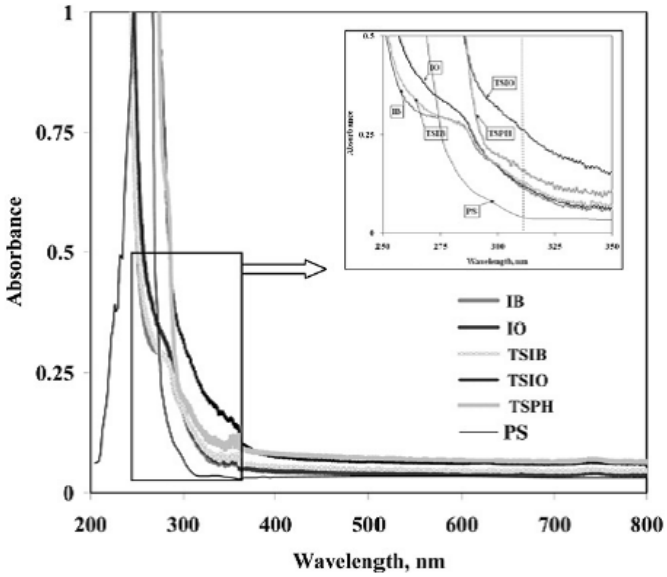

Figure 25. Absorbance versus wavelength for polystyrene and five types of POSS in THF (1 mg/10 mL).[81]

These spectra show the high absorbance of POSS in the 200-350 wavelength range, corresponding to all UVb radiation (280-320 nm) and a portion of the UVc range (100-280 nm).[81] This was a broader absorbance band than neat polystyrene, from approximately 210-280 nm.[81]

Films approximately 70 μm thick of each of the six materials were exposed simultaneously to eight UVb lamps of wavelength 313 nm.[81] Fourier transmission infrared (FT-IR) spectroscopy monitored the generation of carbonyl and hydroxyl group byproducts through chain scission.[81] No changes were observed until 24 hours of exposure for the closed cage POSS-polystyrene films and there was a delay of 48 hours for degradation to occur in open cage POSS-polystyrene.[81] The inclusion of POSS did suppress degradation with trisilanol phenyl POSS being the most effective filler.[81] Dintcheva et al. proposed that open cage POSS provides greater UV protection due to a possible mechanism where the silanols

can donate hydrogen to radicals along the polystyrene chain, while they are converted to a silanone.[81] Although this particular mechanism has not been definitively established, the UV-vis data supports the ability of POSS to perform as an anti-UV filler for polystyrene and potentially other, unexamined polymers such as epoxies.[81]

Ultraviolet radiation has also been used to glassify POSS.[82] A 2010 patent describes exposing a coating with up to 100 % POSS to UV light of wavelength less than 300 nm. Lamps producing primarily 185 or 172 nm light were preferred and exposure times ranging from 1-8 min for a 25-100 wt% POSS-polymer was suggested.[82] Such exposure caused oxidation of the POSS surface, leading to scratch-resistant coatings.[82] Although glassification is not specifically mentioned, the patent authors do state that the UV radiation breaks bonds in the POSS molecules and that the surface treatment is irreversible.[82]

Polyhedral Oligomeric Silsesquioxanes and Atomic Oxygen

As mentioned previously, polyimides are commonly polymer used for thermal blankets and other components but it does degrade over time in low Earth orbit.[3,40] Gonzales and Hoflund explored the use of POSS to protect polyimide against atomic oxygen with Sandra Tomczak, also of AFRL, and Timothy Minton and Amy Brunsvold of Montana State University. The results were presented at the 9th International Conference on Materials in a Space Environment in 2003.[69] Using condensation polymerization, a diamine POSS was reacted with aromatic diamine and dianhydride monomers to form a POSS-

polyimide copolymer with POSS at 5, 10, and 20 wt% loadings (Figure 26).[69] The non-reactive POSS pendant groups were cyclopentyl rings.[69]

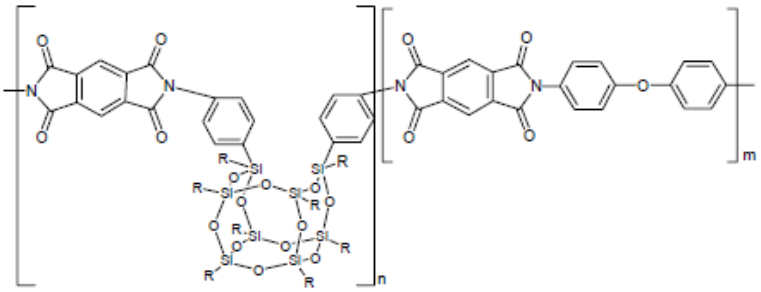

Figure 26. POSS-polyimide copolymer synthesized by Gonzales, et al.[69]

Terrestrial pre-exposure characterization of the copolymer focused on modulus and thermal degradation.[46-49,69] Measurements of storage modulus as a function of temperature for the neat polyimide and POSS-polyimide copolymers showed a sharp decrease in modulus at approximately 400 °C.[69] The decrease in modulus above 400 °C was not as pronounced with the POSS copolymers.[69] Gonzales, et al. attributed this finding to POSS-POSS interactions limiting chain motion.[69] However, the specific interaction was not disclosed. Degradation of the neat polyimide and the POSS-polyimides was measured by loss of weight percent with increase of temperature by thermogravimetric analysis (TGA) both under nitrogen and air.[69] The addition of up to 20 wt% POSS decreased the onset of degradation under nitrogen by up to 100 °C.[69] This phenomenon was not observed under air and neither result was explained in detail by the authors.[69]

The POSS-polyimide was exposed to a hyperthermal atomic oxygen beam under a stainless steel mesh.[69] Surface profilometry was used to detect etching between sample areas covered by the mesh and areas exposed to the beam.[69,83] The atomic oxygen exposure fluence was 8.47 x 10^{20} atomic oxygen

atoms/cm^2 and was meant to approximate 10 days in low Earth orbit.[69] During this test, the neat Kapton® was etched 25.4 μm between areas covered by mesh.[69] In contrast, with 10 wt% POSS copolymerized with the Kapton®, the average etch depth was 2.2 μm.[69] A second exposure added an additional loading level of POSS in the polyimide.[69] After an exposure of 2.62 x 10^{20} atoms/cm^2 of atomic oxygen for approximately 3 days of LEO, neat Kapton®, 10 wt% POSS-polyimide, and 20 wt% POSS-polyimide had average etch depths of 7.85, 1.17, and 0.41 μm, respectively.[69] This trend was confirmed by root mean square (RMS) roughness measurements with atomic force microscopy (AFM).[69,83,84] After being exposed to a fluence of 8.47 x 10^{20} atoms/cm^2 of atomic oxygen, the RMS roughness was 102 nm in neat Kapton®, 17.7 nm in 10 wt% POSS-polyimide, and 6.75 nm in 20 wt% POSS-polyimide.[69] Both the AFM and earlier etch depth results indicated the ability of POSS to reduce atomic oxygen related erosion in polyimides.

Surface analysis with XPS of the Si *2p* spectrum showed a definite shift in bonding from $RSiO_{1.5}$ to SiO_2 resulting from exposure to atomic oxygen.[69] This confirmed that the POSS glassification phenomenon, described by Gilman and Gonzales in POSS-PISX, PDMS, and polyurethane copolymers, also occurred in POSS-polyimides.[12, 69, 73, 74, 75] Exposure to air after testing pushed the Si *2p* peak towards a peak that was characteristic of $RSiO_{1.5}$. This is an indication of a more reactive surface after exposure.[69] Unlike the POSS-polyurethane study by Gonzales et al., carbon composition at the surface of the POSS-polyimide

increased while silicon and oxygen decreased with increasing atomic oxygen fluence (Table 2).[69, 75]

Table 2

Atomic composition through XPS of POSS-Polyimide copolymer[69]

Sample Treatment	**Atomic Oxygen Fluence (atoms/cm^2)**	**O (atom %)**	**Si (atom %)**	**C (atom %)**	**N (atom %)**	**O:Si ratio**
Untreated	n/a	15.9	4.6	74.5	4.9	3.4
2 h Atomic Oxygen	1.44 x 10^{17}	14.3	4.9	72.6	8.2	2.9
24 h Atomic Oxygen	1.77 x 10^{18}	11.1	4.4	79.6	4.9	2.5
40 h Atomic Oxygen	4.53 x 10^{18}	9.1	3.7	81.5	5.6	2.4
40 h Atomic Oxygen + Air exposure	4.53 x 10^{18}	13.9	3.5	76.8	5.8	3.9

The authors attributed the reduction in oxygen to destruction of carbonyl groups at the copolymer surface.[69] Since the atomic compositions must sum to 100 %, it was then stated that increases in C and Si were expected with the loss of oxygen.[69] However, only the carbon composition increased.[69] The XPS spectra of C *1s* and N *1s* confirm the loss of carbonyl species but the decrease in silicon atom content was not further explained.[69] Still, this study that oxidation occurred at the surface and that POSS could protect polyimides against atomic oxygen.

Minton, Brunsvold, and Gonzales continued their work on POSS-polyimides with Israeli collaborators Gouzman and Grossman.[85] The same POSS-polyimide copolymer used in the previous study (Figure 26) was synthesized with 10 or 20 wt% POSS.[85] These three materials along with a Kapton H® standard were exposed to a hyperthermal oxygen beam of 70 % atomic oxygen at an average of 5 eV for fluences up to 8.47x10^{20} atoms/cm^2.[85] Selected samples were exposed under a steel mesh with open areas 500 μm wide between 100 μm wires.[85]

The etch depth of the 0, 10, and 20 wt% POSS-polyimide copolymers was plotted against the etch depth of the Kapton H® standard, which also correlated to specific atomic oxygen fluences.[85] As shown in Figure 27, the 0 wt% POSS-polyimide copolymer etched linearly compared to the fluence, indicating its similarity to the commercial polyimide, Kapton H®.[85]

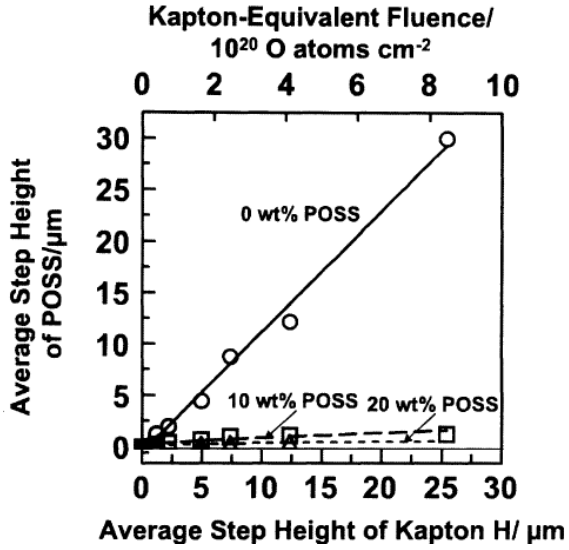

Figure 27. Etching of POSS-polyimide copolymers compared to Kapton H®.[85]

The 10 and 20 wt% POSS-polyimide copolymers had significantly smaller step heights compared to Kapton H® at equivalent fluences.[85] This reiterated the ability of POSS to prevent atomic oxygen-based erosion in polyimides as detailed in the previous study by Gonzales and Minton.[69, 85]

This phenomenon was confirmed by changes in RMS roughness as measured by atomic force microscopy on 500x500 nm modulus maps of the three copolymers (Table 3).[85]

Table 3

RMS roughness per sample and atomic oxygen fluence[85]

Atomic Oxygen Fluence	**0.0 atoms/cm^2**	**3.8x10^{19} atoms/cm^2**	**1.6x10^{20} atoms/cm^2**	**4.1x10^{20} atoms/cm^2**
0 wt% POSS-Polyimide RMS	2.48 nm	70 nm	120 nm	126 nm
10 wt% POSS-Polyimide RMS	2.47 nm	22.4 nm	34.3 nm	78.9 nm
20 wt% POSS-Polyimide RMS	2.86 nm	17.2 nm	23.7 nm	39.1 nm

Unexposed material had approximately equal roughness values, except for a small increase for the 20 wt% POSS copolymer.[85] The modulus map for that sample showed some phase separation of POSS, indicated by regions of significantly different moduli.[85] For the 0 wt% POSS-polyimide, the increase in roughness began to level off at 1.6x10^{20} atoms/cm^2.[85] In comparison, the 10 and 20 wt% POSS-polyimides had significant increases even from 1.6x10^{20} atoms/cm^2 to the highest fluence of 4.1x10^{20} atoms/cm^2.[85] Still, all of the POSS-inclusive samples never approached the roughness at each fluence of the 0 wt% POSS materials.[85] This indicates the neat polymer degraded rapidly and significantly in contrast to the POSS-polyimide films that degraded slowly and not to the same extent with added atomic oxygen. In addition, the 0 wt% POSS-polyimide copolymer showed a very jagged morphology compared to a smoother, rippled, morphology of polyimide with POSS, after each exposure.[85]

As with many other studies, XPS was used to examine compositional changes at the surface of exposed samples.[85] With the 0 wt% POSS-polyimide copolymer, carbon atom percent decreased with fluence while oxygen atom percent increased.[85] The spectra of the carbon C *1s* orbital displayed a peak attributed to C-C/C-H bonding and added a C=O peak that grew with fluence,

indicating oxidation of the surface with increased atomic oxygen exposure.[85] Carbon atom percent also decreased at the surfaces of the 10 and 20 wt% POSS-polyimide copolymers with corresponding increases in oxygen and silicon.[85] The spectra of Si *2p* bonding for the 20 wt% POSS-polyimide copolymers shifted almost exclusively from $RSiO_{1.5}$ to SiO_2 only at the highest fluence of $4.1x10^{20}$ atoms/cm^2.[85] This is attributed to the transformation of POSS to silica seen at the surface, similar to other POSS copolymers under exposure to atomic oxygen.[69,74,75] However, this work does establish that there is a minimum fluence necessary for full conversion to silica to occur in POSS-polyimide systems, although degradation is still reduced compared to neat polymer under this fluence.

Minton, Gonzales, Gouzman, and other collaborators including Sandra Tomczak at AFRL, continued this study and presented their results in a paper given at a Materials Research Society symposium in 2004.[86] Molecular dynamics simulated reactions between POSS cages with –H pendants and 5 eV atomic oxygen atoms.[86] A reaction between the POSS cage and the oxygen radical occurred in 39 % of collisions.[86] Three specific reactions dominated:

1. Abstraction of H from the cage, resulting in OH and a POSS cage with radical Si· in one corner.[86]
2. O· addition to a corner of the POSS cage, resulting in the ejection of H to form H· and an oxidized cage.[86]
3. Addition of O· to an Si-O bond in the POSS cage, resulting in bond scission and eventual destruction of the cage.[86]

Reactions 2 and 3 were the dominant reactions.[86] Similar modeling was completed with 5 eV atomic oxygen atoms and a polyimide monomer.[86] The most prevalent reaction was O· addition to the monomer, which could result in scission of C-C, C-H, or C-N bonds.[86] The monomer was more reactive than the POSS cage with 67 % of collisions resulting in a reaction.[86] These simulations offered a possible explanation of the ability of POSS-polyimide copolymers to mitigate etching and morphology changes after atomic oxygen exposure compared to neat polyimide.[86]

Tomczak et al. also analyzed 0, 10, 20, and 25 wt% POSS-polyimide copolymers using dynamic mechanical thermal analysis (DMTA).[86] The glass transition temperature as measured from the tan δ curve was approximately 410 °C for the 0 wt% POSS-polyimide and decreased to under 400 °C for the POSS-containing copolymers.[86] The largest decreases were with the 20 and 25 wt% POSS-polyimide copolymer, which had approximately equal glass transition temperatures near 380 °C.[86] The authors attributed this decrease to the POSS cages disrupting packing and intermolecular interactions between polyimide chains.[86] This effect is magnified with increasing amounts of POSS.[86] Storage modulus was also measured for each of the 4 polymers.[86] Below T_g, the neat polyimide had a higher modulus but the POSS-polyimide copolymers had larger values above the glass transition.[86] Tomczak et al. proposed that crosslinking was occurring between chains due to heating and that this reaction was slowed by the presence of POSS.[86] However, no spectroscopy was provided to substantiate this hypothesis.[86]

In a 2005 presentation at Pacifichem and a 2006 *Macromolecules* paper, Tomczak, Minton, and collaborators compared POSS-polyimide main chain copolymers with POSS side chain polyimide copolymers in terms of resistance to atomic oxygen and the low Earth orbit environment.[87,88] The *Macromolecules* paper by Wright et al. detailed the how 3-aminopropylisobutyl POSS was used as a side chain pendant to the selected polyimide.[87] Figure 28 shows the POSS moiety pendant to a phenyl ring on the polymer backbone.[88]

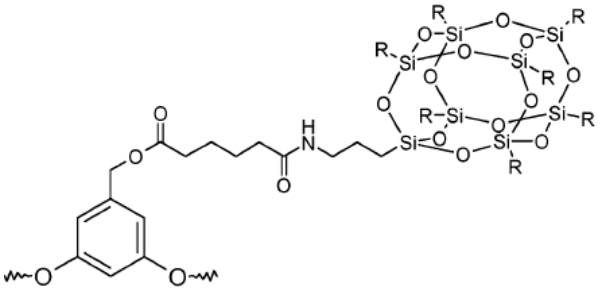

Figure 28. POSS pendant from polyimide backbone.[88]

Other phenyl rings in the polyimide backbone were modified with isocyanate or acrylate pendants to enable crosslinking of the polyimide chains.[88] In the *Macromolecules* paper, Wright et al. exposed commercially available Kapton H® and an uncrosslinked polyimide with 15 wt% POSS to atomic oxygen under a steel mesh (Figure 29), as was done in previous studies.[27,69,87,88]

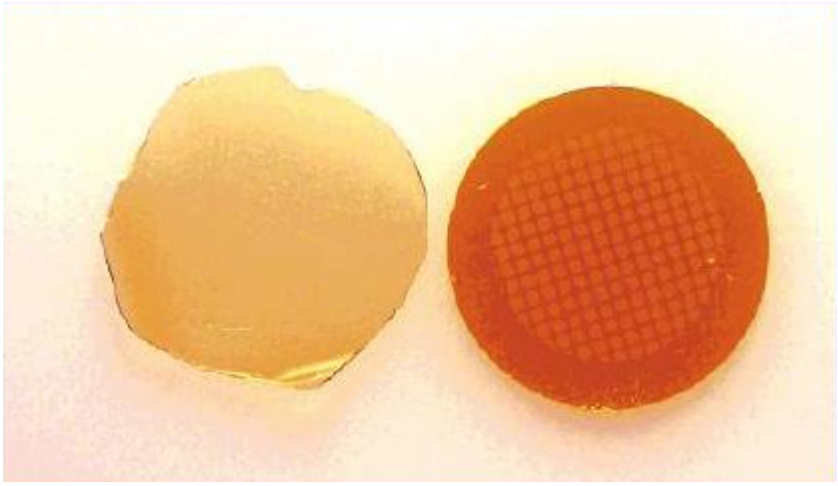

Figure 29. 15 wt% side chain POSS-polyimide (L) and Kapton H® (R) films exposed to atomic oxygen.[88]

The atomic oxygen fluence was not specified in their publication. The authors stated that there was no detectable erosion or discoloration in the side chain POSS-polyimide compared to the darkened Kapton H®, which eroded approximately 11-12 μm.[88] This adds more data to support the ability of POSS to protect organic material against atomic oxygen.

In a more detailed study, Tomczak et al. compared the exposure response of the main chain POSS-polyimide shown in Figure 26 to the side chain POSS-polyimide synthesized by Wright et al.[27,87,88] Weight percent of the POSS was measured based on the weight percent of the POSS cage in the copolymer.[27,87] As in other studies, films were covered by a steel mesh and exposed to a hyperthermal oxygen beam with atomic oxygen having an average kinetic energy of 5.2 eV.[27,85,87] After exposure to an atomic oxygen fluence of 8.47×10^{20} atoms/cm^2, the worst performing main chain copolymer, at 3.5 wt% Si_8O_{11}-polyimide, had an erosion rate of only 3.7 % of the erosion of Kapton H® at the

same fluence.[27,87] Main chain copolymers with higher POSS content had less erosion. [27,87]

To better understand the passivation protection afforded by POSS, the authors exposed films of Kapton H®, Kapton HN® coated with SiO_2, and 8.75 wt% main chain Si_8O_{11}-polyimide to $2.3x10^{20}$ atoms/cm^2. [27,87] Tabulation of etch depth measurements was somewhat inconsistent. [27,87] After the first exposure, Kapton H® eroded 5.5 μm according to a table of erosion values, but the authors stated the etch depth was 7.0 +/- 0.2 μm in the text of the paper. [27,87] No erosion could be detected on the Kapton HN® coated with SiO_2 and only 0.2 μm was measured for the 8.75 wt% main chain Si_8O_{11}-polyimide. [27,87] Then, each of the three materials was intentionally scratched to make marks approximately 20 μm wide and 1 μm deep. [27,87] A portion of the scratch and surrounding material was covered with a mask and the entire sample and mask exposed again to $2.3x10^{20}$ atoms/cm^2 fluence of atomic oxygen.[87] Thus, the samples received a total atomic oxygen fluence of $4.6x10^{20}$ atoms/cm^2 but the material exposed after scratching was only in contact with atomic oxygen for the second exposure of $2.3x10^{20}$ atoms/cm^2.[87]

The Kapton H® sample scratch was 1.0 μm deep before exposure and 1.4 μm after exposure, although the surrounding material was also eroded 5.5 μm. [27,87] The Kapton HN® coated with SiO_2 only etched where the coating was removed, with the atomic oxygen removing 7 μm of exposed Kapton HN®.[27,87] Tomczak et al. emphasized this result as proof that damage to SiO_2 coatings can result in a loss of protective capability. [27,87] The 8.75 wt% main chain Si_8O_{11}-

polyimide eroded only 400 nm in the scratch and less than 200 nm between the unscratched exposed and covered areas. [27,87] Again, this result indicates the advantage of having the anti-degradation particle integrated into the film during processing, rather than applied afterward in the manner of spray or vapor deposited coatings.

In an additional study, 0, 3.5 and 7.0 wt% main chain Si_8O_{11}-polyimide samples were exposed to atomic oxygen at different temperatures. [27,87] The neat polyimide with no POSS showed increasing erosion as the temperature increased from 25 to 300 °C, but the POSS-inclusive polymers had a slight increase from 250 to 300 °C with 3.5 wt% Si_8O_{11} and no statistically significant change across the entire temperature range with 7.0 wt% Si_8O_{11}.[87] In previous studies, POSS has been used to increase thermal stability of polymers.[80]

Glass transition temperatures were determined from tan δ as measured by DTMA. [27,87] The glass transition decreased with increasing POSS content in the main chain. [27,87] The inclusion of POSS generally increases the T_g but there are examples of the POSS cage disrupting chain packing or crosslinking to decrease T_g.[89,90] A polyimide with 7.0 wt% Si_8O_{12} as a side chain pendant was exposed to atomic oxygen to $2.3x10^{20}$ atoms/cm^2. [27,87] After this test, the T_g of the Si_8O_{11}-polyimide dropped 22 °C, likely due to chain scission.[87] In this study, no measurements were made on neat Kapton H®.[27,87] In previous testing with $3.53x10^{20}$ atoms/cm^2 of atomic oxygen, the main chain 7.0 wt% Si_8O_{11}-polyimide eroded 3.8 % of the erosion depth of Kapton H® at that fluence, whereas the side chain 7.0 wt% Si_8O_{12}-polyimide eroded 3.3 %.[27,87] The authors used this data to

state that the resistance to atomic oxygen of main chain and side chain 7.0 wt% POSS cage-polyimide was equivalent. [27,87] However, the change in T_g was not measured for the main chain copolymer and it is doubtful that it would be equivalent given the different packing of POSS in the main versus side chain of a polymer and the resultant effects on free volume.

As previously discussed, the coefficient of thermal expansion (CTE) of protective films is important due to thermal cycling experienced in low Earth orbit.[35,37] Mismatches in layer coefficients can result in cracking and delamination of the protective coating.[35,37] The CTE of Kapton H® was 30.25 μm/(m*°C).[27,87] This increased to 33.5 μm/(m*°C) with main chain 7.0 wt% Si_8O_{11}-polyimide and 35.86 μm/(m*°C) for side chain 7.0 wt% Si_8O_{12}-polyimide.[27,87] The highest loading level of POSS measured, main chain 8.75 wt% Si_8O_{11}-polyimide, resulted in a CTE of 35.00 μm/(m*°C).[27,87] After exposure to $2.3x10^{20}$ atoms/cm^2 of atomic oxygen, the CTE of side chain 7.0 wt% Si_8O_{12}-polyimide decreased to 33.64 μm/(m*°C).[27,87] The authors estimated that the glassified POSS at the surface had a CTE equivalent to fused silica at 0.55 μm/(m*°C).[27,87] This mismatch between the underlying copolymer with a greater CTE was predicted to cause cracking in the glassified surface.[27,87]

Tomczak et al. also had 0, 1.75, and 3.5 wt% main chain Si_8O_{11}-polyimide films exposed to low Earth orbit on the ISS for 3.9 years as part the MISSE-1 experiment. [27,87] This was a unique testing opportunity due to aforementioned issues with the expense and effort needed for *in orbit* exposures.[3] Samples were fixed to aluminum and obscured at the edges by an aluminum mask so erosion

depth between exposed and unexposed areas could be quantified. [27,87] The control polyimide at 32.55 +/- 0.87 μm thick eroded completely. [27,87] The 1.75 and 3.5 wt% main Si_8O_{11}-polyimide eroded 5.79 +/- 1.31 μm and 2.12 +/- 0.34 μm, respectively. [27,87] Analysis by XPS showed exposed copolymer surfaces that were mainly silicon and oxygen but no pre-exposure measurements were provided for comparison. [27,87]

Minton, Tomczak, Brunsvold, and other collaborators continued studying POSS-polyimides and their interaction with atomic oxygen and reported their results in a 2012 paper in *Applied Materials and Interfaces*.[27] Side chain Si_8O_{12}-polyimides were exposed to atomic oxygen at $2.7x10^{20}$ atoms/cm^s.[27] Erosion of the 1.75 wt% side chain Si_8O_{11}-polyimide was 24.5 % of Kapton H® at equivalent fluence.[27] This decreased to 4.9% with 7.0 wt% side chain Si_8O_{11}-polyimide and erosion was undetectable at 14 wt% side chain Si_8O_{11}-polyimide.[27] Main and side chain 7.0 wt% Si_8O_{11}-polyimides were exposed to an atomic oxygen fluence of $2.68x10^{20}$ atoms/cm$^{2.}$[27] The main chain copolymer eroded 4.25 +/- 0.48 % of Kapton H® at that fluence whereas the side chain copolymer eroded slightly more at 4.86 +/- 0.47 % of Kapton H®.[27]

The authors also stated that these side chain Si_8O_{11}-polyimide exposure results could be compared to their previous 2004 study of main chain Si_8O_{11}-polyimides. [27,87] Although the same exact fluences were not used in both papers, it did seem that the main chain Si_8O_{11}-polyimide provided more erosion resistance when results were extrapolated between fluences.[27,87] Minton, et al. did note that the side chain POSS cage was Si_8O_{12} compared to Si_8O_{11} for the

main chain POSS and that the effects of this molecular difference were not studied.[27] However, they concluded that their erosion results, from this and previous studies, indicated that loading level of POSS was more important than its structural incorporation into the polymer.[27] Based on this, it would be interesting to see if POSS continues to protect against atomic oxygen when reacted into a network versus simply mixed in as a filler.

The rest of the paper focused on previously reported studies involving scratched films and temperature dependent erosion. [27,87] More details were provided on the films flown on the MISSE-1 experiment that were exposed to approximately $8x10^{21}$ atoms/cm^2.[27] As previously stated, the control 0 wt% Si_8O_{11}-polyimide eroded completely, as can be shown in Figure 30.

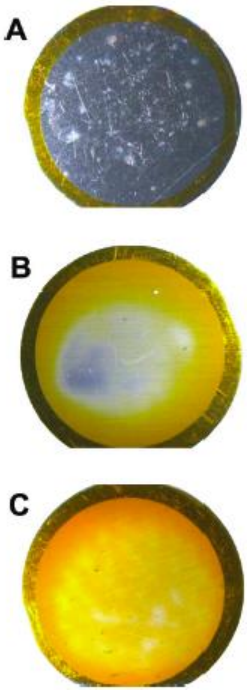

Figure 30. A) 0 wt%, B) 1.75 wt%, and C) 3.5 wt% Si_8O_{11}-polyimide fixed to aluminum and exposed to LEO for 3.9 years.[27]

The surface of the 1.75 and 3.5 wt% Si_8O_{11}-polyimide films appeared textured and possibly brittle in SEM micrographs taken at 1370X (Figure 31).[27]

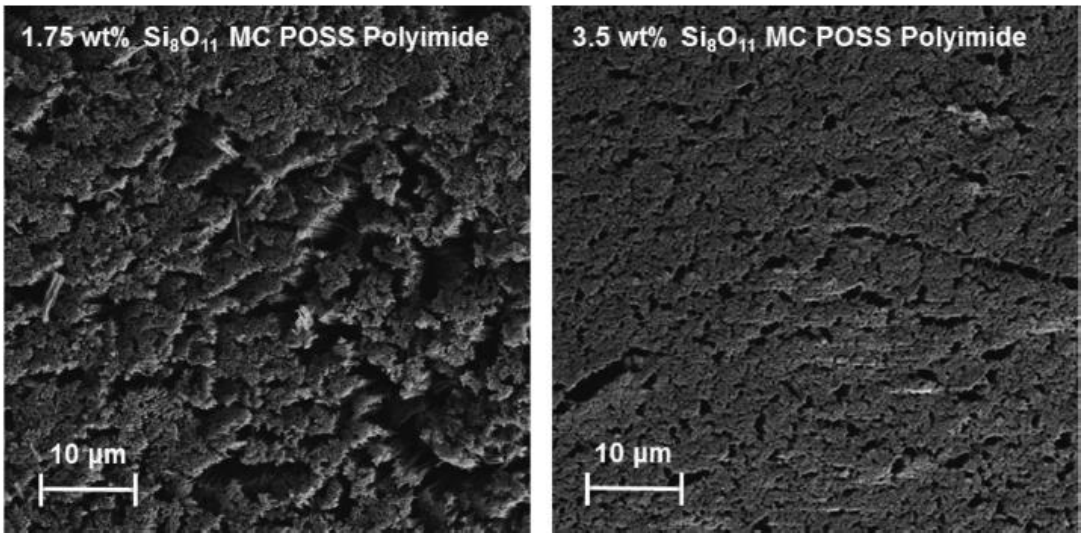

Figure 31. L) 1.75 wt% and R) 3.5 wt% Si_8O_{11}-polyimide surfaces after LEO exposure.[27]

Minton and collaborators attribute the decrease in roughness on the 3.5 wt% Si_8O_{11}-polyimide surfaces to a more interconnected silica layer due to the higher loading level of POSS.[27]

More main and side chain POSS-polyimides were flown on MISSE 5 and 6 experiments.[27] Conclusions from MISSE-5 data showed yet again that erosion depth decreased with increasing weight percent of main chain POSS and was always less than the erosion depth of Kapton H®.[27] Both 7 and 8.8 wt% main and side chain POSS-polyimides were flown on MISSE-6 along with a 0 wt% POSS-polyimide and commercially available Kapton H®.[27] Minton et al. estimated that the samples experienced an atomic oxygen fluence of 1.97×10^{21} atoms/cm^2.[27] Erosion depth of the films was measured using the contrast between exposed areas and the film edges covered by the aluminum sample fixture (Table 4).[27]

Table 4

Erosion of POSS-polyimide copolymers flown by Minton et al. on MISSE-6[27]

Polymer	Erosion Depth (μm)
Kapton H®	59.1 +/- 1.5
0 wt% POSS-polyimide	75.9 +/- 4.2
7 wt% main chain Si_8O_{11}-polyimide	1.37 +/- 0.22
7 wt% side chain Si_8O_{12}-polyimide	1.02 +/- 0.30
8.8 wt% main chain Si_8O_{11}-polyimide	0.44 +/- 0.16
8.8 wt% side chain Si_8O_{12}-polyimide	0.74 +/-0.22

All copolymers with POSS had less erosion than the neat 0 wt% POSS-polyimide or the commercially available Kapton H® polyimide.[27] At 7 wt%, there was no statistically significant different in erosion depth between the main and side chain copolymers.[27] With an increase to 8.8 wt% POSS cage, the main chain Si_8O_{11}-polyimide provided slightly more erosion resistance.[27] This does match up with earlier data that main chain POSS provides slightly more anti-atomic oxygen benefit compared to side chain POSS pendants.[27]

During MISSE-6, some side chain Si_8O_{12}-polyimide films were flown on quartz crystal microbalances for measurement of mass loss during exposure.[27] Although the microbalances failed during flight, mass loss decreased with increasing amounts of POSS.[27] Mass loss between 7.0 wt% main chain Si_8O_{11}-polyimide and 7.0 wt% side chain Si_8O_{12}-polyimide was also compared.[27] Over the 8 hours, the microbalances functioned in LEO, the side chain polymer had more mass loss at a faster rate than the equivalent 7.0 wt% main chain copolymer.[27] However, the authors did not state whether the difference of approximately 5 mg was within the error margin of the quartz crystal microbalances nor did they state the initial masses of any of the samples.[27] In all experiments, the mass loss rate never plateaued.[27] Minton et al. suggested that

this indicated the lack of complete surface passivation or that there is always some finite mass loss during LEO exposure.[27] More in-depth analysis of exposed, POSS-rich surfaces to determine the homogeneity of glassification would help to close a gap in the literature on POSS and atomic oxygen.

Branching out from the effects of atomic oxygen on electrical properties, Israeli researchers Grossman, Gouzman (from previously discussed papers) and Dr. Ronen Verker published a study in 2008 on atomic oxygen exposure and hypervelocity impacts on POSS-polyimides.[86,91] Debris in low Earth orbit travels on average at 10 km/s, meaning even millimeter-sized objects can cause major damage in the event of a collision.[2] In a 2008 publication in the journal '*High Performance Polymers',* Verker et al., reported blending trisilanol phenyl POSS with polyamic acid, to produce films of 0, 5, 10, and 15 wt% POSS.[91]

These POSS-polyimide films along with 25 μm thick samples of Kapton® HN were exposed to various fluences of atomic oxygen produced by a 15 W RF O_2 plasma system.[91] The Kapton HN® was used to calculate fluence based on the known erosion rate of the material.[91] Figure 32 contains a plot of fluence versus mass loss for the five exposed materials.[91]

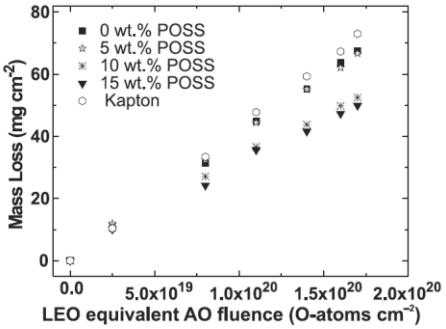

Figure 32. Mass loss versus fluence for Kapton HN® and POSS-polyimide blends.[91]

Above a fluence of $2.5x10^{19}$ atoms/cm^2, mass loss results began to show differences.[91] The most affected material was Kapton HN® (empty hexagon).[91] The lab made polyimide with 0 wt% POSS had the second largest mass loss (black square).[91] The mass loss discrepancy between the commercially available Kapton HN® and the 0 wt% POSS-polyimide has been attributed in previous papers to the narrower molecular weight distribution in lab-produced materials.[27] Molecular weight distribution can affect properties from intensity of intermolecular forces to viscosity and mechanical properties.[72] Chains with a variety of weights do not stack as well, decreasing intermolecular binding forces and possibly accounting for the change in mass loss between the Kapton HN® and the 0 wt% POSS-polyimide.[72] The 5 wt% POSS-polyimide blend (gray star) did not perform much differently than the neat polyimide.[91] However, a definite decrease in mass loss was seen starting with 10 wt% POSS (asterisk), and 15 wt% POSS (black triangle) provided incrementally more protection.[91] Verker et al. noted that 5 wt% POSS did not provide adequate atomic oxygen resistance while the decrease in mass loss from 10 to 15 wt% POSS was minimal.[91]

Films of 0, 5, 10 and 15 wt% POSS-polyimide were subjected to impacts at 1.8-2.8 km/s from 30-50 μm aluminum particles.[91] The film thickness ranged from 16-30 μm.[91] According to the authors, thicker films have more capacity to reduce impact damage due to increased stiffness, and any failures tend to be ductile rather than brittle.[91] In addition, Kapton® films experience temperatures greater than T_g at the impact area.[91] Using SEM, impact regions were reduced

67 % on average, with 10 or 15 wt% POSS compared to the 0 wt% POSS-polyimide.[91]

To examine synergistic effects, 0 and 15 wt% POSS-polyimides were subjected to aluminum particle impacts and then exposed to an atomic oxygen fluence of $2.6x10^{20}$ atoms/cm^2.[91] Initial impacts had average perforated areas of 0.47 and 0.09 mm^2 for the 0 wt% and 15 wt% POSS-polyimide, respectively.[91] After atomic oxygen, the area increased to 0.70 mm^2 for the neat polyimide but was only 0.11 mm^2 for the 15 wt% POSS-polyimide impacts.[91] Standard deviations were not provided for the area measurements, so it could not be decided whether the 0.02 mm^2 increase in area for the 15 wt% POSS-polyimide impacts was statistically significant or repeatable. Surface analysis with XPS was performed on the 15 wt% POSS-polyimide blend before and after $2.6x10^{20}$ atoms/cm^2 of atomic oxygen.[91] As in other studies, carbon atom percent decreased as silicon and oxygen content increased.[69, 74, 75, 91] In addition, the primary silicon species was SiO_2.[91] This data is consistent with glassification of the POSS film.[91]

In another experiment, neat polyimide was impacted at 2.4 km/s, exposed to $1.1x10^{20}$ atoms/cm^2 and then to an additional amount of $2.6x10^{20}$ atoms/cm^2 of atomic oxygen.[91] After the first exposure, impact holes were surrounded by smaller, newly formed holes.[91] After the second exposure, the initial hole often grew and merged with the newer holes.[91] Verker et al. attributed impact area growth in the neat polyimide to a combination of residual stresses after impact, temperature increases at the impact site, and atomic oxygen diffusion through

the already damaged film.[91] This phenomenon of impact hole expansion was not seen the 15 wt% POSS-polyimide.[91] Surfaces did appear rougher with POSS and long cracks extended from hole edges.[91] The authors concluded that the POSS filler reduced the residual stresses that persisted after impact, and was able to prevent further atomic oxygen damage through conversion to passivating silica.[91] Although POSS was previously primarily used for atomic oxygen protection, this study demonstrates another advantage of using this filler.

Building on previous work by Minton, Gonzales, Tomczak, Lei et al. noted that POSS-polyimide synthesis was not particularly effective with octafunctional amine POSS as a monomer due to the difficulty of reacting all functional groups.[92] However, methods used in previous studies to generate diamine POSS were expensive and used unstable reagents.[92] In an attempt to mitigate these issues, Lei et al. conducted silane condensation reactions with a 3:1 mixture of phenyltriethoxysilane to γ-aminopropyltriethoxysilane according to the reaction shown in Scheme 5.[92]

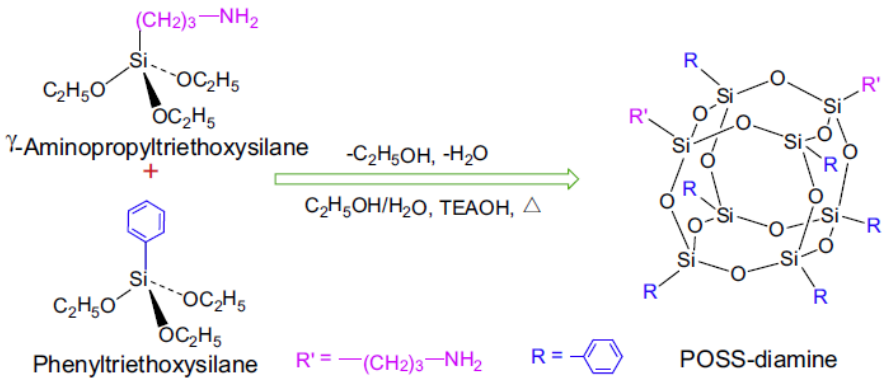

Scheme 5. Reaction of functionalized silanes to form diamine POSS.[92]

The reaction yield was 37% and the product structure was verified by Fourier transmission infrared (FT-IR) and nuclear magnetic resonance (NMR) spectroscopy.[92] The authors did not provide a yield comparison with other synthesis methods. The POSS diamines were reacted with pyromellitic dianhydride and 4,4'-diaminodiphenyl ether to create 4.1, 8.8, 14.4, 21.9, and 29.7 wt% POSS-polyimide membranes.[92]

The neat polyimide and the four copolymers were characterized for optical and thermal properties.[92] Increasing POSS decreased transmittance of visible light, and also decreased the temperature at which 5 % mass was lost during thermal decomposition (T_d).[92] Glass transition temperature did increase with POSS loading level, as is the case with many POSS-polymer combinations, whereas the coefficient of thermal expansion initially dropped and then increased.[92] After these characterizations were completed, the five materials were exposed to an atomic oxygen beam at four fluences, $0.88x10^{20}$, $1.76x10^{20}$, $2.64x10^{20}$, and $3.87x10^{20}$ atoms/cm^2.[92] As expected, the neat polyimide (PI-0) statistically had more mass loss at every fluence (Figure 33) when normalized to the mass loss of 29.7 wt% POSS-polyimide (PI-29.7).[92]

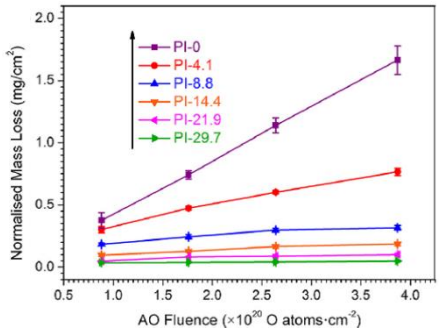

Figure 33. Mass loss of POSS-polyimide copolymers versus atomic oxygen fluence.[92]

Also as expected, POSS decreased mass loss starting with the 4.1 wt% POSS-polyimide (PI-4.1).[92] The erosion rate appeared to slow with the 8.8 wt% POSS-polyimide (PI-8.8) although, at loadings higher than 14.4 wt% POSS-polyimide, there was little statistical benefit realized by continuing to add POSS to the copolymer.[92] Similar trends were seen in erosion yield data.[92] Such plateaus for POSS-polyimide systems and any similar data for other POSS-polymer systems are useful in terms of preventing overspending and any property loss from overutilization of POSS. From the mass loss data, the curve for the 29.7 wt% POSS-polyimide (PI-29.7) was plotted to the equation:

$$y = 0.0072x^{1.9123} + 0.2500$$

where x was atomic oxygen fluence (atoms/cm^2) and y was mass loss (mg/cm^2).[92] Using this relationship and assuming a film 40 μm thick, it would take a fluence of 61.84×10^{20} atoms/cm^2 to erode half of the 29.7 wt% POSS-polyimide material.[92] The authors estimate that this fluence corresponds to approximately 15 years in low Earth orbit but do mention that other degradants could speed up erosion.[92] Currently, satellite lifetime in LEO is estimated to be up to 15 years.[93]

Surface analysis by XPS on the POSS-polyimides showed a surface of primarily SiO_2 after exposure, as seen in other studies. [69,74,75,91,92] Lei et al. examined Si *2p* bonding in the 8.8 and 21.9 wt% POSS-polyimides according to fluence.[92] As displayed in Figure 34, the Si *2p* peak in the 8.8 wt% POSS-polyimide membrane shifted from $RSiO_{1.5}$ at 102.8 eV to SiO_2 at 103.7 eV with a fluence as low as 0.88×10^{20} atoms/cm^2.[92]

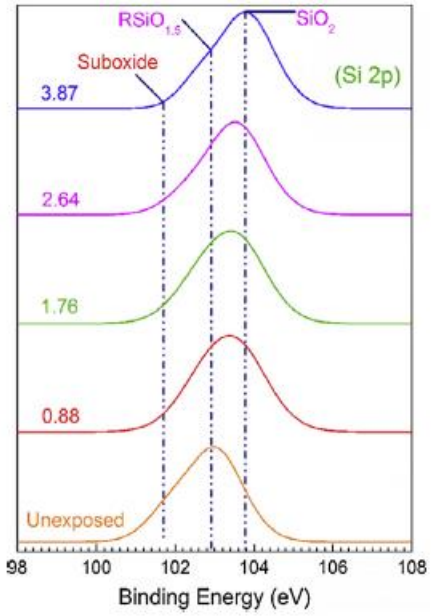

Figure 34. XPS Si *2p* bonding in 8.8 wt% POSS-polyimide by atomic oxygen fluence.[92]

The authors explained left-sided broadening in the Si *2p* peaks to a "suboxide" species that disappeared as the POSS was glassified.[92] Lei et al. used that species to support the earlier work of Tomczak et al. that monoatomic oxygen added to Si-O bonds, causing scission of Si-O and Si-C bonds.[86,92] However, the composition or exact role of this "suboxide" species was never clarified.

Oxygen plasma can also glassify POSS given adequate energy.[94] French and Greek researchers published a study in 2006 on POSS-methacrylate copolymers used for photolithography.[94] Si-O bonds have good resistance to etching plasma used in electronics processing, making POSS a good option to integrate into masking polymers.[94] Although this was not an aerospace related application, the paper focused on the results of oxygen plasma treatment on POSS.[94] Eon et al. reacted monofunctional methacrylate-POSS with tert-butylmethacrylate (*t*-BMA) to synthesize copolymers at POSS/*t*-BMA ratios of

100/0, 60/40, 40/60, and 20/80 wt%.[94] An additional monomer, methacrylic acid (MA), was used in other copolymers at POSS/*t*-BMA/MA ratios of 30/50/20 and 40/40/20 wt%.[94] Poly(dimethyl siloxane) (PDMS) and poly(dimethyl silsesquioxane) (PMSQ) polymers were also synthesized as comparison materials to the POSS-acrylate copolymers.[94] Materials were treated with oxygen plasma using a source power of 800 W under a pressure of 10 mTorr.[94] Samples were cooled to avoid maintain temperatures below 30 °C during exposure.[94] The thickness of approximately 210-200 nm films was measured by ellipsometry for up to 20 minutes of exposure.[94] Ellipsometry measures thickness changes by analyzing changes in polarized light before and after reflecting from a surface.[95]

The inclusion of POSS reduced the amount and rate of etching.[94] The POSS/*t*-BMA/MA copolymer did have approximately 10 % less thickness loss than POSS/*t*-BMA.[94] Surface analysis by XPS showed a minimum of 30 atom percent decrease in carbon content after 10 s of plasma etching in the 100/0, 60/40, 40/60, and 20/80 POSS/*t*-BMA/MA copolymers and the 30/50/20 POSS/*t*-BMA/MA copolymer.[94] The top layer of SiO_2 oxide ranged from 1.4 to 3.2 nm.[94] This data indicates that glassification from oxygen plasma happens near the beginning of a test and that the layer formed is not particularly thick but significantly changes surface composition.[94] FT-IR spectroscopy also showed a shift from the Si-O-Si from the POSS cage at 1105 cm^{-1} to SiO_2 at 1050 cm^{-1}. Although FT-IR penetrates much deeper (1-2 μm depending on the instrumentation and method) there was still enough alteration due to the glassification for the peak shift to begin after 1 min of etching.[94,96]

A similar study was conducted by Augustine, et al. in 2007 on propylmethacrylate heptaisobutyl POSS polymerized with methyl methacrylate monomer.[97] The copolymers were 10, 20, and 45 wt% POSS and were spun onto silicon substrates at thicknesses ranging from 140 to 220 Å.[97] Neat poly(methyl methacrylate) (PMMA) films were also produced as a control.[97] The plasma used consisted of various ratios of O_2/N_2 gasses at a power level of 25 W and a pressure of 350 mTorr.[97] Ellipsometry, XPS, and contact angle characterized surface changes.[97,98] The contact angle of a 45 wt% POSS-PMMA film dropped from approximately 90° to approximately 57° under 100s of 100 % N_2 gas plasma and to approximately 41° under 100s of 100 % O_2 gas.[97] The authors considered these changes to be evidence of a more hydrophilic surface after exposure, albeit with the more reactive O_2 species being capable of effecting a more significant change.[97] Under 95 % N_2/5 % O_2 plasma, thickness loss in all samples increased with time during the 2000 s total of exposure.[69] Increasing POSS content did decrease thickness loss with 45 wt% POSS-PMMA losing approximately 30 Å thickness of material at 2000 s compared to 160 Å for neat PMMA.[98] However, under 100 % N_2, all materials with or without POSS did not erode more than 10Å reinforcing conclusions on plasma gas makeup from the contact angle results.[98] In addition, data from XPS indicated no detectable SiO_2 in a 45 wt% POSS-PMMA sample, which shifted to an area containing18.8 % SiO_2 after 100s in N_2 gas, and 25.8 % after 100s in O_2 gas.[98] However, this did confirm that plasma treatment can also produce POSS glassification.[98] This

could provide a route for glassification of POSS-rich surfaces before flight, decreasing mass loss in orbit.

Reaction of POSS with Oxides

As discussed earlier, oxides such as SiO_2, TiO_2, and CeO_2 have been used in polymers as an 'anti-UV additive'.[63] However, dispersion was an issue.[9,10] Open cage POSS can complex with metal oxides through its three silanol groups (Figure 35).

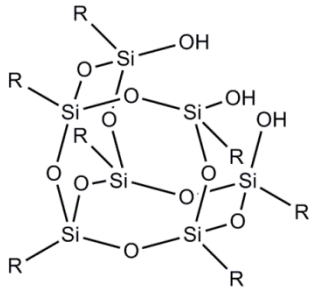

Figure 35. Structure of open cage POSS.[68]

This reaction was used by Morgan et al. to increase dispersion of TiO_2 in polypropylene.[99] These authors estimated that 5 wt% POSS would be needed to cover the TiO_2 particles (nominal particle size 21 nm) so a 10:1 ratio of TiO_2 to trisilanol isobutyl POSS was chosen to ensure adequate POSS coverage.[99] Reagents were mixed for an hour in an excess of hexanes and then placed on a rotary evaporator to remove solvent, resulting in a white powder.[99] The reaction yield by weight was 61.6 %.[99] Morgan et al. described the reaction process as hydrogen bonding between silanols, residual water, and the oxide that leads to a condensation reaction (Scheme 6).[72,99]

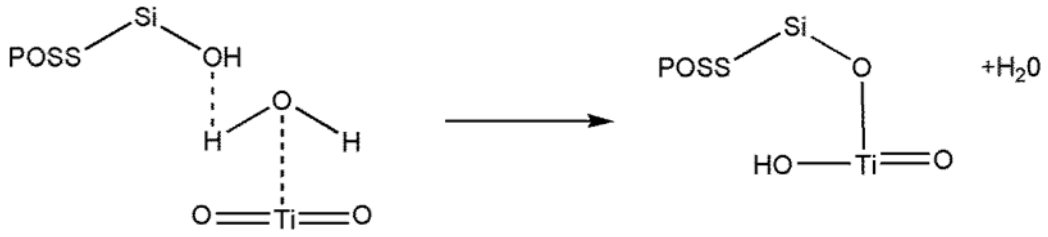

Scheme 6. Proposed reaction of TiO_2 with a trisilanol POSS.[72,99]

Thermogravimetric analysis (TGA) was used to investigate the thermal degradation behavior of neat TiO_2 (Figure 36, curve a), unwashed POSS-TiO_2 product (Figure 36, curve c), and POSS-TiO_2 washed multiple times with hexanes and tetrahydrofuran (Figure 36, curve b).[99]

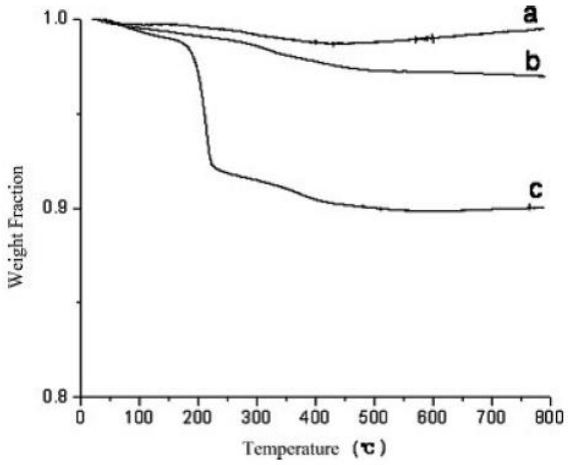

Figure 36. TGA data for (a) neat TiO2, (b) washed POSS-TiO_2, and (c) unwashed POSS-TiO_2.[99]

The unwashed POSS-TiO_2 sample lost approximately 10 % of its weight below 200 °C.[99] This decrease was attributed to the 10 wt% of trisilanol isobutyl POSS used to thoroughly cover the TiO_2 particles.[99] However, after washing the product powder to remove unreacted reagents, weight loss before 200 °C was only 3 %.[99] This indicated a reaction conversion below the 5 wt% POSS estimated to give total surface coverage of the TiO_2.[99]

Polypropylene was then melt-blended with 1 wt% neat TiO_2, a mixture of 1 wt% TiO_2 and 5 wt% trisilanol isobutyl POSS, and 1 wt% of the TiO_2-trisilanol POSS reaction product.[99] The average diameter of TiO_2 particulates was measured by transmission electron microscopy (TEM), a microscopy method that generates micrographs by transmitting electrons through <100 nm sections of materials.[72,99] The polypropylene with 1 wt% of neat TiO_2 had an average particle diameter of 70.4 +/- 31.9 nm.[99] With the unreacted 1 wt% TiO_2/5 wt% POSS blend, average size decreased to 50.1 +/- 21.4 nm but was still within the standard deviation of the neat TiO_2.[99] The 1 wt% reacted POSS-TiO_2 had an average diameter of 33.2 +/- 11.6 nm.[99] Wheeler et al. attributed the decrease in average particle diameter when TiO_2 is reacted with POSS to the miscibility of the isobutyl POSS pendants in polypropylene.[99] Reacting trisilanol isobutyl POSS and TiO_2 also improved optical properties including yellowness, haze, and gloss compared to the other two fillers.[99] Since the authors were unsure if the TiO_2 particles were fully covered by POSS, it would be interesting to see if properties continue to improve with greater POSS coverage, perhaps by examining particles with a spectroscopic technique to determine elemental composition.

This POSS-oxide condensation reaction has not been widely explored in the literature. One paper by Gomathi et al. in 2010 explored combining POSS with TiO_2, and Fe_2O_3 particles as well as ZnO nanowires.[100] The authors synthesized octa(tetraethylammonium) polyhedral oligomeric silsesquioxane (TMA-POSS) from tetraethoxysilane and tetramethylammonium hydroxide.[100] The TMA-POSS was then reacted at a 5:1 ratio with the oxides by mixing the

reagents in anhydrous ethanol for 12 h at 60 °C.[100] This process was confirmed by using FT-IR to check for both the Si-O peak from POSS and appropriate oxide functional bands in the spectra of the products.[100] Gomathi et al. stated that a surface layer of POSS on the oxides was confirmed by TEM and SEM/energy dispersive x-ray spectroscopy (EDS).[100] The latter technique determines the elemental composition of the first 0.3-3 μm below the surface of a sample.[100,101] Specific micrographs or results from EDS were not provided nor did the authors provide a specific mechanism for a reaction given that the POSS used was closed cage POSS.[100]

The TMA-POSS colloidally dispersed oxides more effectively in polar solvents such as water.[100] This is demonstrated in Figure 37 where untreated ZnO (left) has precipitated at the bottom of a vial of water compared to most of TMA-POSS-ZnO (right) seen suspended in water.[100]

Figure 37. Neat ZnO particles (L) and POSS-ZnO particles (R) in water.[100] Although this suspension has not achieved solubility, it was progress versus the original precipitation.[100] The oxides and POSS-oxides were also mixed at various loading levels in nanocomposites of poly(vinyl alcohol) and nylon-6,6.[100] Particles

treated with POSS gave more transparent and uniform samples than the neat oxide fillers.[100] Again, the authors did not propose a mechanism but both polymers have polar functional groups that might be compatible with the charged tetraethylammonium pendants groups.[100]

Hansen-Hoy Theory

As seen in previous examples, miscibility of POSS can have a strong effect on nanocomposite properties.[102] Different intermolecular forces govern compatibility between compounds, including non-polar dispersion forces, dipole-dipole interaction forces, and hydrogen bonding.[103] Hildebrand defined the solubility parameter of a solvent as:

$$\delta = (\frac{E_{vap}}{V})^{1/2}$$

where δ is the solubility parameter, E_{vap} is the energy of vaporization, and V is the molar volume of the solvent.[104] The treatment Hildebrand developed is accurate only for systems in which the intermolecular forces are entirely London dispersion forces.[104] Hildebrand theory is not accurate nor predictive for systems with polar or hydrogen bonding interactions.[104]

Dr. Charles Hansen expanded the concept of the solubility parameter to include dispersion, dipole-dipole, and hydrogen bonding forces.[104] Dispersion forces consist of attractive forces between atoms, meaning that all molecules exert these forces on their surroundings.[104] These forces can be summed as E_D, or dispersion cohesive energy.[104] Dipole-dipole forces are polar interactions between permanent dipoles in molecules and are termed polar cohesive energy,

or E_P.[104] Finally, hydrogen bonding is the interaction between a hydrogen atom and an electron-rich atom such as oxygen or nitrogen.[104] Hansen described this as the electron exchange parameter, E_H.[104] The total cohesion energy is the sum of these three energies and represents a simplified view of the energy of interactions between two equivalent molecules.[104] The Hansen Solubility Parameter can be calculated from:

$$\delta^2 = \left(\frac{E_D}{V}\right)^2 + \left(\frac{E_P}{V}\right)^2 + \left(\frac{E_H}{V}\right)^2$$

where δ is the solubility parameter, E_D is the dispersion cohesive energy, E_P is the polar cohesive energy, E_H is the electron exchange parameter, and V is the molar volume of the solvent.[104] This is more commonly expressed as:

$$\delta^2 = {\delta_D}^2 + {\delta_P}^2 + {\delta_H}^2$$

where δ is the Hansen Solubility Parameter, δ_D is the dispersion solubility parameter, δ_P is the polar solubility parameter, and δ_H is the hydrogen bonding solubility parameter.[104]

Teas diagrams arrange different solvents according to proportional contributions to their cohesive energy through three equations for each type of interaction:

$$f_D = 100\delta_D/(\delta_D + \delta_P + \delta_H)$$

$$f_P = 100\delta_P/(\delta_D + \delta_P + \delta_H)$$

$$f_H = 100\delta_P/(\delta_D + \delta_P + \delta_H)$$

where f_D is the fractional dispersion parameter, f_P is the fractional polar parameter, and f_H is the fractional hydrogen bonding parameter.[104] Each

parameter is given its own axis.[104] Figure 38 shows a Teas diagram with various common solvents.[104,105]

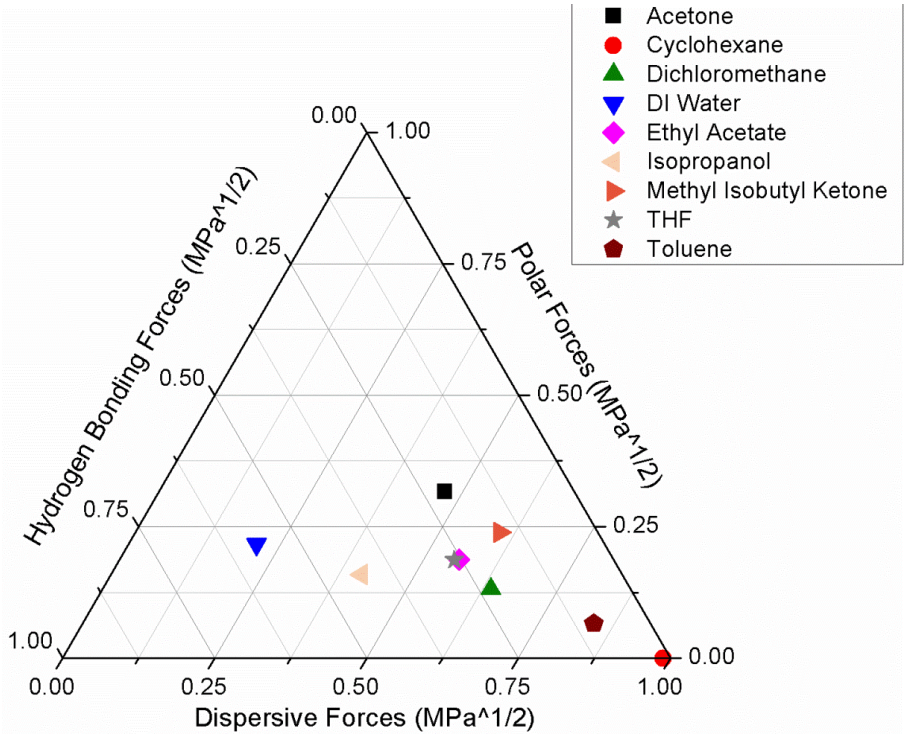

Figure 38. Teas diagram of common solvents.[105]

The Teas diagram provides a visual representation of the interaction forces in solvents.[104,105] For example, only dispersive forces are present in the non-polar, non-hydrogen bonding cyclohexane.[105] In contrast, water is characterized by strong hydrogen bonding forces and lesser polar forces, with the smallest contribution from dispersive forces.[105] Based on solubility of a solute in a solvent, Teas diagrams can be used to determine a region of solubility for the solute, which can be compared to other materials or used to find compatible solvents.[105] More specifically, this can be used to determine the compatibilities of

different POSS moieties with a selected matrix and thus, their tendencies to aggregate or disperse.

Summary

Epoxies are commonly used as matrices for carbon-fiber composites due to low viscosity, acceptable thermal stability, and good fluid resistance.[106] However, these polymers are susceptible to hydrogen abstraction leading to chain scission when attacked by oxygen radicals or high enough energy UV radiation.[29] Atomic oxygen, UV radiation, and other hazards are present in low Earth orbit.[2] Atomic oxygen is the primary hazard and has caused significant damage to polyimides and epoxies in orbit.[3] Inorganic spray coatings of oxides such as SiO_2 and Al_2O_3 have provided some protection but are difficult to apply correctly.[8,44] Cerium oxide has also been used for UV protection but often forms problematic aggregates.[9,10] Polyhedral oligomeric silsesquioxanes have shown ability to protect polymers against low Earth orbit hazards by converting from $RSiO_{1.5}$ to an SiO_2 surface layer under exposure to atomic oxygen or high energy O_2 plasma.[12,94] The POSS nanoparticle comprises a silicon-oxygen cage with pendant groups that govern POSS solubility within a polymer.[102] While POSS-polyimide blends and copolymers and POSS-polyurethane copolymers have been studied extensively for low Earth orbit hazards, the effect of atomic oxygen and UV resistance is comparatively unexplored on POSS-epoxy composites.[67,69,74] In addition, all studies on POSS for atomic oxygen resistance deal with POSS in the bulk of a matrix.[12,27,86,87] Formation of a glassified POSS layer requires erosion of the polymer for exposure of the POSS. However, oxide

spray coating is also not without drawbacks, namely underpinning of degradants due to poor surface coverage.[60] It is unknown whether the creation of a POSS-rich layer in a nanocomposite would decrease the mass loss of the organic material below.

Therefore, the initial objectives of this work were directed to answering the questions:

1. How does the type of functional group attached to the POSS moiety change phase separation and promote POSS layering?
2. Can the amount of POSS phase separation be controlled by loading level and cure protocol?

However, after experiments, it did not prove possible to form a layer of POSS at the surface of a POSS-epoxy-amine nanocomposite. Therefore, focus shifted to combining POSS and cerium for enhanced UV protection, and the questions asked were:

3. Can POSS-CeO_2 compounds be created by intermolecular complexation and/or covalent bonding?
4. Can cerium and POSS be combined to provide protection against erosion in low Earth orbit?
5. Does the addition of cerium to POSS affect POSS glassification?
6. Are there other benefits to be realized by combining cerium and POSS in epoxy-amine polymers?

CHAPTER II - EXPERIMENTAL

Introduction

Hazards in low Earth orbit such as atomic oxygen, and vacuum ultraviolet radiation damage organic material through bond scission and oxidation. Initially, the main objective of this project was to layer POSS in epoxy to provide protection against atomic oxygen. However, as the project advanced, the objectives were modified to improving the UV absorbance of POSS by including cerium and understanding how this affected glassification of POSS. A relatively broad range of experimental procedures and techniques were used to prepare samples, characterize materials, perform testing, and measure effects of Cerium/POSS inclusion as protective layers.

Initially, samples were made by mixing epoxies, amines, and POSS in various proportions and eventually this proceeded to layering of POSS/cerium-rich layers. Focus shifted to commercially available POSS-rich films for final glassification. All samples were characterized with respect to a variety of thermal and mechanical properties in order to examine how the addition of POSS affected these properties compared to the neat matrices that did not contain either POSS or cerium. The development of combinations of Cerium/POSS was also characterized for composition and miscibility. Characterization methods included a variety of spectroscopic techniques and solubility assessments including Teas Diagrams. Additionally, the Cerium/POSS (hereafter abbreviated to CePOSS) moieties were mixed with other POSS products to achieve better dispersion in the selected coatings.

Exposure testing to induce glassification was conducted at NASA Glenn Research Center, Hybrid Plastics, and Xeel Corporation. Additional properties were measured including mass loss, glass transition temperature, and contact angle before and after exposure to simulated degradation protocols. Overall, formulation and testing was directed to gaining understanding the dispersion of POSS and the effects of CePOSS on UV protection and POSS glassification under a range of exposure conditions.

Experimental

Evaluation of Mixtures

Construction of Teas Diagrams. Various compounds were examined for their interactions with a range of solvents to facilitate the construction of Teas diagrams. Solutions of octamethyl POSS, octaphenyl POSS, glycidyl POSS, diglycidyl ether of bisphenol-A, cerium (IV) oxide, $Ce(NO_3)_3 \cdot 6H_2O$, trisilanol phenyl POSS, and CePOSS (combination of $Ce(NO_3)_3 \cdot 6H_2O$ and trisilanol phenyl POSS) were mixed in solvents at 10 mg solute per 1000 mg of solvent at ambient temperature and pressure. The structures of some of these compounds are shown in Figures 39-44.

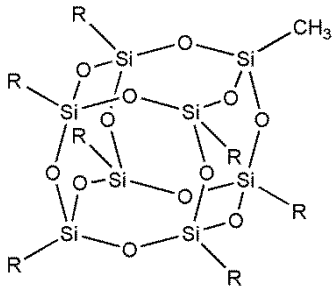

Figure 39. Structure of octamethyl POSS, where R = methyl.[107]

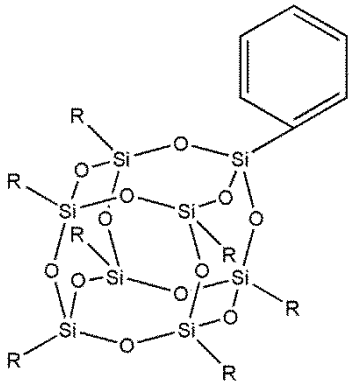

Figure 40. Structure of octaphenyl POSS, where R = phenyl.[107]

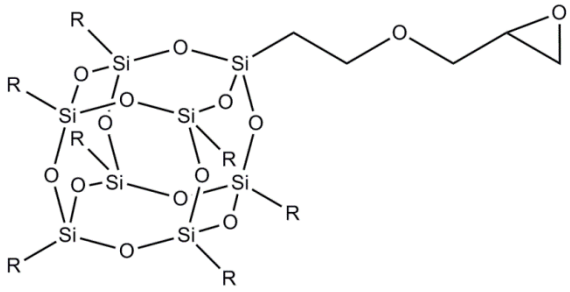

Figure 41. Structure of glycidyl POSS, where R = glycidyl.[107]

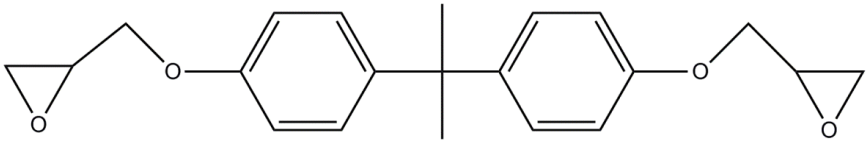

Figure 42. Structure of diglycidyl ether of bisphenol-A.[56]

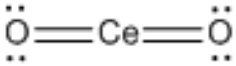

Figure 43. Structure of cerium (IV) oxide.[108]

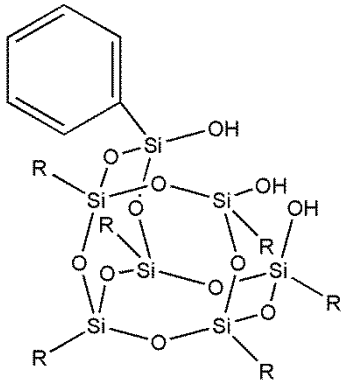

Figure 44. Structure where trisilanol phenyl POSS, where R = phenyl.[56]

The nine solvents chosen were: acetone, cyclohexane, dichloromethane, deionized water, ethyl acetate, isopropanol, methyl isobutyl ketone, tetrahydrofuran (THF), and toluene. These solvents represented common solvents that spanned the range of interest for the inclusion of POSS and Cerium entities into epoxy matrices that are already used in aerospace applications and are appropriate candidate construction materials for low Earth orbit applications. Solvent fractional solubility parameters were found in the *CRC Handbook of Solubility Parameters and Other Cohesion Parameters*.[105] Solutes considered to be miscible in a given solvent produced clear mixtures after addition to the solvent. Solutes considered partially miscible in a given solvent produced a mixture with some haze or light precipitation that appeared to be less than the 10 mg of solute added initially. Solutes considered immiscible in a given solvent produced a suspension or sediments of particulates in a solvent or complete precipitation from the solvent.

Compatibility Studies of Cerium Compounds. Various cerium containing compounds were mixed with different liquid POSS moieties and POSS-rich

coatings at room temperature. Transparency was the primary factor in evaluating the compatibility of the fillers with other POSS materials or in coatings. Cerium (IV) oxide often causes darkening and loss of optical quality in polymers.[9,10] A transparent coating with a cerium-containing compound could be useful for aerospace or space applications.

Sample Preparation

Synthesis of Epoxy-Amine-POSS Nanocomposites. Nanocomposites were synthesized from diglycidyl ether of bisphenol-A (DGEBA, EEW = 177.5, supplied by Hexion, Figure 42) and 4,4'-diaminodiphenylsulfone (44DDS, supplied by Royce Chemical Corp., >99% purity, micronized, Figure 45) at a 1:1 functional group ratio.

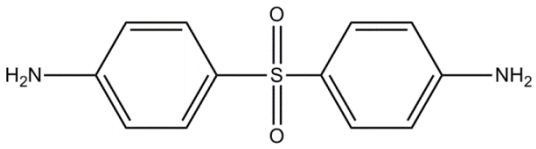

Figure 45. Structure of 4,4'-diaminodiphenylsulfone.[58]

Octamethyl (Figure 39), octaphenyl (Figure 40), and glycidyl POSS (Figure 41) moieties were selected to give a range of interactions with the epoxy. The octamethyl POSS should be the least miscible with epoxy-amine matrices due to its short, aliphatic pendant groups. The octaphenyl POSS would be more miscible with an aromatic epoxy-amine matrix due to this POSS moiety's phenyl ring pendant groups. The glycidyl POSS was contemplated to be the most miscible POSS moiety because it could react into the epoxy-amine matrix during cure. If glycidyl-POSS is miscible in the epoxy-amine matrix, it would be expected to homogeneously distribute within the epoxy-amine matrix of the cured

resin. On the other hand, incompatible particulate POSS materials would be expected to sediment under the influence of gravity in an uncured matrix.

Initially, DGEBA was degassed under vacuum, at 75 ºC with stirring, for at least 30 minutes or until major bubbling ceased. Octamethyl or octaphenyl POSS was directly added to the DGEBA at 1, 2.5 or 5 wt%. The POSS/DGEBA mixtures were stirred using a magnetic stir bar at 75 °C, 300 rpm for at least 30 minutes and then the 4,4DDS amine crosslinker was added and stirred again for at least 30 minutes at 75 ºC under vacuum. Samples were then cured in silicone rubber molds for 3 hours at 180 °C. The curing protocol was provided by collaborators in Boeing Research and Technology.

After reevaluation of the cure protocol, the solid octamethyl and octaphenyl POSS were ultrasonicated in acetone first and then added to DGEBA with thorough degassing of the DGEBA/POSS/solvent mixture until solvent and gasses were eliminated from the material. Ultrasonication broke up aggregates.[109] Glycidyl POSS (Figure 41) was a liquid phase material under ambient Earth conditions at room temperature, and so it did not require ultrasonication but was still degassed while mixing with DGEBA. After degassing, the 44DDS amine crosslinker was added and stirred for at least 30 minutes at 75 ºC under vacuum. Samples were then cured in silicone rubber molds with an alternative cure protocol of 1 hour at 110 °C and 3 hours at 180 °C, with a ramp rate of 1 °C/min. Small quantities of material were set aside before cure and frozen for differential scanning calorimetry.

Surface Coated Disk Preparation. Previous synthesis produced POSS sedimentation in DGEBA-44DDS. In an effort to create POSS-rich layers at the surface of a sample, a layer of atomic oxygen and UV protective particles were cast under a matrix and then inverted after cure, or was cast over partially cured matrix and cured. The matrix was a 1.08:1:0.067 ratio of glycidyl POSS, tetraglycidyl 4,4′-diaminodiphenylmethane (TGDDM) epoxy (Figure 46), and Lindax 1®, an imidazole curative (Figure 47). Lindax 1® is the imidazole catalyst, 1-(2-Hydroxypropyl) imidazole, supplied by Lindau Chemical Company®.

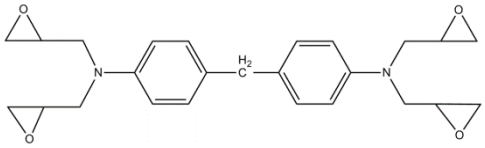

Figure 46. Structure of tetraglycidyl 4,4′-diaminodiphenylmethane (TGDDM).[110]

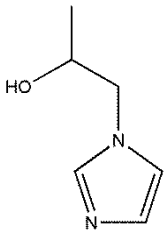

Figure 47. Structure of Lindax 1® (1-(2-Hydroxypropyl) imidazole).[111]

This composition was developed in conjunction with collaborators at Hybrid Plastics The coating layer consisted of 75-90 wt% glycidyl POSS, 0-5 wt% CeO_2, and 10-20 wt% of 3,3'-diaminodiphenyl sulfone (33DDS, Figure 48).

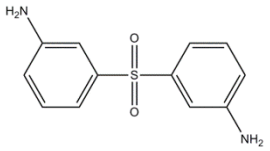

Figure 48. Structure of 33DDS.[58]

The CeO_2 used was commercially available <25 nm diameter particulates.[108] However, flocculation, agglomeration and/or aggregation of such particulates is common and the effective diameter of the dispersed particulate clusters was probably larger than the diameter of the fundamental particles.

Initially, the POSS/CeO_2/33DDS coating layer was mixed with a specialized dremel attachment termed a “tissue tearor” at ambient temperature.[112] If this was not available, the layer was mixed by hand after heating the glycidyl POSS at 70 °C for 30-60 minutes to decrease the POSS viscosity. The cure protocol was 80 °C for 1 h, 120 °C for 2 h, and 150 °C for 2 h with ramp rates of 5 °C/min when coating was placed into the mold and then the matrix cast over top of the coating If the matrix was cast first, the cure protocol was 80 °C for 1 h and 120 °C for 0.5 h with ramp rates of 5 °C/min. The coating was then cast on top of the matrix and the cure continued at 120 °C for 1.5 h, and 150 °C for 2 h with ramp rates of 5 °C/min The steel mold used had four wells each 1 in diameter and 0.2 in deep. Non-stick films were placed at the bottom of each well for sample removal. A drawing of the mold is in Figure 49.

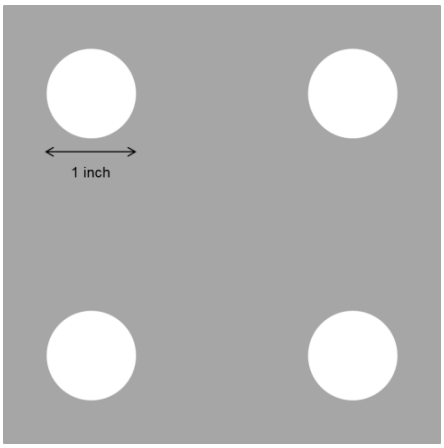

Figure 49. Drawing of mold face.

Samples were made by two methods, which were distinguished by the placement of the coating. For method 1, the POSS/CeO_2/33DDS coating was poured into the preheated mold and then the matrix was poured on top, filling up the wells. In Method 2, the matrix was poured into the mold first, leaving a gap of approximately 0.05 in at the top of the 0.2 in thick wells. Cure commenced for 80 °C for 1 h, ramped up to 120 °C at 5 °C/min, and then after 30 min at 120 °C, the coating was cast on top of the matrix. Then cure was completed at 120 °C for 1.5 h and 150 °C for 2 h with a ramp rate of 5 °C/min

Seven types of composite disks were made for full characterization:

1. Neat matrix without coating (1.08:1:0.067 ratio of glycidyl POSS, TGDDM epoxy, and Lindax 1®)
2. 5 wt% CeO_2/20 wt% 33DDS/75 wt% glycidyl POSS cured under matrix (Method 1)
3. 5 wt% CeO_2/20 wt% 33DDS/75 wt% glycidyl POSS cured over matrix (Method 2)
4. 33 wt% CeO_2/17 wt% 33DDS/50 wt% glycidyl POSS cured under matrix (Method 1)
5. 33 wt% CeO_2/17 wt% 33DDS/50 wt% glycidyl POSS cured over matrix (Method 2)
6. 10 wt% 33DDS/90 wt% glycidyl POSS cured under matrix (Method 1)
7. 10 wt% 33DDS/90 wt% glycidyl POSS cured over matrix (Method 2)

Layer thicknesses were measured with calipers.

CePOSS Formulation. Trisilanol isobutyl POSS (Figure 50) and titanium dioxide can form a compound through a condensation reaction between the silanol groups of the POSS and the titanium-oxide bonds of the TiO_2.[99] The resulting compound improved dispersion of the titanium dioxide in polypropylene.[99] Therefore, it was of interest to investigate if this method would improve dispersion of CeO_2 in an epoxy-amine matrix.

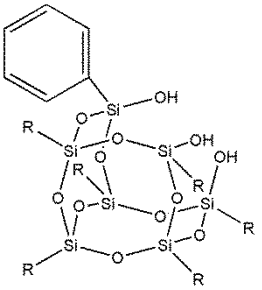

Figure 50. Structure of trisilanol phenyl POSS where R = phenyl.[107]

Trisilanol phenyl POSS was chosen for this experiment because of concerns that trisilanol isobutyl POSS with its aliphatic pendant would be less miscible in the aromatic epoxy matrix. Several methods of combining CeO2 and trisilanol phenyl POSS did not produce a mixture of the materials. A mixture of the two substances was formed by combining equal masses of $Ce(NO_3)_3 \cdot 6H_2O$ and trisilanol phenyl POSS in an excess of acetone and stirring for 30 minutes at room temperature. The mixture was then poured into metal dishes to let the acetone evaporate overnight. The resultant powder was scraped off the dishes and dried at 75 °C for at least 12 hours. The powder was a white solid and was termed “CePOSS”.

POSS Coatings with CePOSS. The CePOSS material was found to produce a transparent mixture with octapoly(ethylene glycol) POSS, or “PEG POSS” (Figure 51).

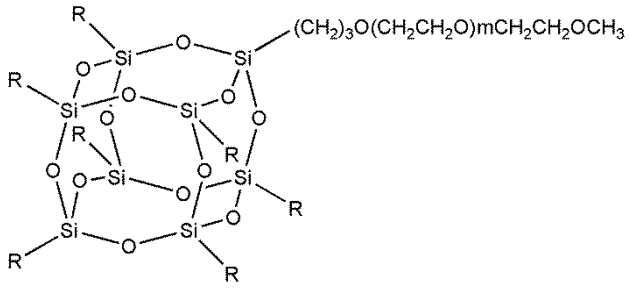

Figure 51. Structure of PEG POSS, where R = $CH_2)_3O(CH_2CH_2O)_mCH_2CH_2OCH_3$, m ~ 10.[107]

Mixtures of CePOSS and PEG POSS at ratios of 1:1 and 2:1 were mixed with two POSS-rich coatings, IM9330 and EP3510. This was done to determine if a transparent, cerium-containing coating could be produced and if cerium would interfere with POSS glassification.

The specific coatings were selected due to their bonding ability with TGDDM-glycidyl POSS-Lindax 1® disks for possible continuing development of the dual layer composite concept. The first coating selected was IM9330, a proprietary POSS-polyimide that was solvent cast in propylene glycol methyl ether acetate. However, the combination of CePOSS-PEG POSS-IM9330 produced opaque and cloudy coatings. The other selected coating was EP3510, which was 68.9 wt% glycidyl POSS, 29.4 wt% EPON 862 (diglycidyl ether of bisphenol-F), and 2 wt% of Lindax 1® and was cured for 1 hour at 80 °C and 1 hour at 100 °C.[113,114] The inclusion of CePOSS-PEG POSS did not alter the

transparency or optical quality of the sample, but the proportion of Lindax 1® was increased to 5 wt% to boost cure due to tackiness of initial samples.

Cure Analysis

Dielectric Spectroscopy. Dielectric spectroscopy can probe polymer relaxations from 10-5 to 1011 Hz through the application of an oscillating electric field, and this technique is used to track cure in thermosets.[115] The electric field polarizes and orients ions or dipoles, in the thermosets, depending on frequency, and the time to relaxation of these ions or dipoles is directly affected by the rheology of the system and the change in rheological characteristics can be used to follow the cure process .[115,116] Thus, dielectric spectroscopy can indicate and follow cure conversion and rate and the dependence of cure characteristics on factors such as temperature or filler.[115]

The Netzsch DEA 230/1 Epsilon dielectric spectroscopy system was used at frequencies from 0.1 Hz - 90 kHz to measure the shift in dielectric properties, specifically ion viscosity, during the cure of DGEBA-44DDS with and without POSS.[117] All sensors were calibrated in air for specific values of gain and phase provided by Netzsch before use. Uncured material was smeared at a thickness of 500 nm-1 μm over flat sensors of 7x9 mm integrated into polyimide strips. Cure was performed under ambient atmosphere starting at 100 ºC with temperature increasing at 1 ºC/min until 180 ºC, and then held there for 3 hours according the cure protocol recommended by collaborators at Boeing Research and Technology.[117] Changes in ion viscosity versus temperature and time were used

to indicate milestones in the cure cycle such as the onset of network formation or vitrification.

Differential Scanning Calorimetry (DSC). Uncured samples were made for DGEBA-44DDS cure conversion studies using differential scanning calorimetry (DSC). This study was completed using aluminum pans on a TA DSC Q800 at NASA Glenn Research Center. For each material, one sample was heated from room temperature to 300 °C at 5 °C/min. An additional two samples of the sample material were cured in the DSC for 1 hour at 110 °C, ramped 1 °C/min to a 3-hour hold at 180 °C, then cooled to 40 °C and immediately ramped at 5°C/min to 300 °C. A small exothermic peak was measured from the second ramp after cure and compared to the larger exotherm from the single 300 °C ramp sample to determine cure conversion. All sample masses were weighed within +/- 0.1 mg for accurate comparisons of the exothermic peaks.

In addition, the thermal transitions of the fillers $Ce(NO_3)_3 \cdot 6H_2O$, trisilanol phenyl POSS, and CePOSS were measured on a different TA DSC Q800 at Hybrid Plastics. These samples were tested in powder form and were not mixed with any matrix or coating. This was done as part of an effort to characterize CePOSS in comparison with $Ce(NO_3)_3 \cdot 6H_2O$ and trisilanol phenyl POSS. Samples were heated to 250 °C at 10 °C/min to eliminate any unreacted moieties and anneal thermal stresses, then cooled to -250 °C at 10 °C/min and heated again to 250 °C at 10 °C/min. The second heat was used to determine thermodynamic transitions such as crystallization or melting of the powders by examining the heat flow data for large endothermic or exothermic peaks.

Rheology of Disk Matrix. Rheological measurements on the TGDDM-glycidyl POSS-Lindax™ 1 matrix were conducted on a TA Aries L2 rheometer with 10 mm parallel plates to measure storage (G') and loss (G") moduli.[118,119] The test was run at a constant frequency of 1 Hz and constant strain of 0.1 % (both instrument default settings) at 80 °C for 1 h and then the temperature was immediately raised to 120 °C for an isothermal hold until gelation occurred as defined by the crossover of G' over G".[119] The frequency was fixed because the test was focused on the effects of temperature on G' and G" and no frequency sweeps were conducted.

Spectroscopy and Chemical Composition

Attenuated Total Reflectance Fourier Transmission Infrared (ATR FT-IR) Spectroscopy. A Nicolet 6700 FT-IR with a Smart Orbit diamond crystal ATR accessory was used for ATR FT-IR on a variety of powders and liquids.[120] For each sample, 32 scans were taken at a resolution of 2 cm^{-1} to assemble each spectrum. Omnic software was used for spectral analysis such as detection of peak shifts after exposure testing or reaction of reagents.

Nuclear Magnetic Resonance Spectroscopy (NMR) Nuclear magnetic resonance spectroscopy was conducted with the assistance of Dr. William L. Jarrett on trisilanol phenyl POSS and CePOSS in deuterated acetone as solvent. Trisilanol phenyl POSS was mixed with deuterated acetone at a concentration of 40 mg/1 mL. CePOSS was theorized to be a 1:1 mixture of trisilanol phenyl POSS and cerium (III) nitrate hexahydrate, so the CePOSS was mixed with deuterated acetone at a concentration of 80 mg/1 mL. Therefore, theoretically,

there would be an equal amount of trisilanol phenyl POSS in each solution, eliminating peak shifts due to concentration differences. Samples were run on a Bruker Avance III 600 MHz NMR spectrometer. For each sample, ^{1}H, ^{13}C, and ^{29}Si were acquired with a 90° pulse. Proton decoupling was used for the ^{13}C and ^{29}Si acquisitions to avoid decreases in peak intensity due to a negative nuclear Overhauser effect.[121] In addition, longer recycling delays were used for ^{29}Si acquisition to allow for complete dipole relaxation. The spectra of trisilanol phenyl POSS and CePOSS were then compared for differences between peak shifts and splitting that could indicate covalent bonding of the trisilanol phenyl POSS to cerium (III) nitrate hexahydrate.

Mass Spectroscopy. The fragmentation patterns of trisilanol phenyl POSS, cerium (III) nitrate hexahydrate, and CePOSS were determined using a Microflex LT Bruker Matrix-Assisted Laser Desorption/Ionization (MALDI) mass spectrometer by Ms. Tina Masterson. Samples were prepared based on the method proposed by Wallace et al. for POSS-rich materials.[122] Analytes were mixed with acetone to create a saturated solution.[122] The matrix was a 45 mg/mL solution of sinapinic acid in acetone.[122] To create samples for ionization, 0.5 µm of the analyte solution and 0.5 µm of the matrix were either layered or mixed on a target, dried, and then analyzed.[122] Spectra of the two reagents, trisilanol phenyl POSS and cerium (III) nitrate hexahydrate, were compared to the spectrum of CePOSS to determine molecular weight of CePOSS.

Elemental Analysis. Elemental analysis was completed on CePOSS at in the Microanalysis Laboratory of the School of Chemical Sciences at the

University of Illinois at Urbana-Champaign.[123] The atom percentages of carbon, hydrogen, and nitrogen in the compounds were determined with a CHN analyzer, an Exeter Analytical CE 440.[123] This instrument heats samples in oxygen until combustion and detects elemental composition via thermal conductivity.[123] For silicon and cerium, the CePOSS were digested in a solution of 70 vol% HNO_3, 20 vol% HCl, and 10 vol% HF and then analyzed with a Perkin Elmer Optima 2000DV inductively coupled plasma optical emission spectrometry (ICP-OES).[123] Inductively coupled plasma optical emission spectrometry converted samples to plasma and used optical emission spectroscopy to detect metallic elements in the plasma.[123]

Thermomechanical Properties

Dynamic Mechanical Analysis (DMA). For characterization of the DGEBA-44DDS-POSS samples, storage modulus, and tan delta were measured in tensile mode at constant strain of 0.005 % and frequency of 1 Hz during temperature sweeps from -125 to +250 °C at a rate of 5 ºC/min as recommended by TA Instruments.[117] All samples were run on a TA Instruments Q800 DMA.[117]

For the atomic oxygen study, the mode was switched to single cantilever to avoid noise from edge defects in samples.[124] Storage modulus and tan delta were measured from three unexposed samples and two exposed samples per material due to limitations on the amount of material that could be exposed.[124] Glass transition temperature was measured as the peak of the tan delta curve. All tests were run on a TA Instruments Q800 DMA either at the University of Southern Mississippi or at NASA Glenn Research Center.[124]

Thermogravimetric Analysis (TGA). Thermal degradation by weight percent was measured under nitrogen in a platinum pan with a TA Q500 TGA at NASA Glenn Research Center or a TA Instruments TGA500 at the University of Southern Mississippi from room temperature to 800 °C at 10 °C/min as recommended by TA Instruments.

Microscopy

Optical Microscopy. Given the relative transparency of the DGEBA-44DDS matrix, micron scale and above POSS aggregates could be seen with optical microscopy. Optical microscopy at the University of the Southern Mississippi was conducted with a Zeiss Discovery. V8 stereomicroscope with AxioVision 4.8 software and Image Pro Plus 7.0 was used to measure sample features. Optical microscopy at NASA Glenn Research Center was conducted with a Olympus Infinity SZH with LAS v4.0 software.

Scanning Electron Microscopy (SEM). In this work, SEM was used to examine surface morphology and composition to assess the impact of processing changes on aggregate locations or the impact of exposure testing on samples. For the DGEBA-44DDS-POSS atomic oxygen study, squares were cut of unexposed and exposed material and mounted with carbon tape on 15 mm diameter SEM posts with the POSS-rich faces pointing up. For the dual layer composite samples, disks were submerged in liquid nitrogen for approximately 5 minutes, removed, wrapped in a soft material, and then broken with a hammer to crack disks to produce internal cross sections. Any smooth fracture surfaces produced were mounted on posts. Other disks were cut to an area approximately

15x15 mm and mounted top up on posts for surface analysis. Powders were aspirated onto carbon film on SEM posts. Films with CePOSS were directly cured onto posts. All samples were sputter coated with platinum or silver.

Scanning electron microscopy was conducted on an FEI Quanta 200 Environmental SEM or Zeiss Sigma VP FEG-SEM. Most work was completed on the FEI SEM, with higher resolution (>6000X) microscopy done on the Zeiss SEM due to the capabilities of each SEM. Energy dispersive x-ray spectroscopy (EDS) for dual layer disks and CePOSS powder was conducted on the Thermo System 7 EDS X-ray detector attached to each microscope at a beam voltage of 10-20 kV. This range of accelerating voltage was chosen to avoid substantial damage to samples while providing enough secondary electrons for EDS.

Atomic Force Microscopy (AFM). AFM work was conducted by Dr. Katrina Knauer according to standard AFM parameters. Quantitative nano-mechanical mapping (QNM) studies were conducted on a Bruker Dimension Icon 3000 scanning probe microscope in tapping mode in a temperature (23 C) and humidity (50 %) controlled room with a standard Veeco RTESP silicon probe (cantilever length, 125 mm; nominal force constant, 40 N/m; and resonance frequency, 350 kHz).[124] Height, phase, DMT modulus, and adhesion images were collected simultaneously. The DMT modulus and adhesive forces measured in QNM are not absolute measurements but are based on calibration of the instrument and are therefore used as a means of comparison between the different samples. The image size ranged from 500 x 500 nm to 5 x 5 µm, while the resolution was held constant at 512 x 512 data points. At least three

macroscopically separated samples of the film were selected randomly for analysis. All standard image processing techniques were performed using Nanoscope version 5.30 r2 image analysis software.[124]

Mechanical Testing

Tensile and Flexural Testing. Tensile and three-point bend flexural testing was done according to ASTM standards D638 and D790.[125,126] Flexural bars were 127x12.7x3.175 mm, meeting the 16:1 length to thickness requirement.[126] Testing was conducted on an MTS Insight frame with a 1 kN load cell using Test Works 4.0 software.

Contact Angle and Surface Energy Measurements

Water contact angle was measured 3 times on dual layer disk surfaces before and after exposure to plasma by collaborators at Surfx Plasma in an attempt to quantify oxidation or glassification of the POSS-rich surface.[127] Contact angles of EPON 862, EP3510, and CePOSS and EP3510 were measured at the University of Southern Mississippi on a Ramé Hart Model 200 goniometer for 2 films each before and 1 film each after UV/ozone exposure. The solvents used were water and diiodomethane, a common solvent used for contact angle of silica-rich material.[128] Due to the use of two solvents, the surface energy of each sample could be calculated using a geometric method that takes into account dispersion, polar, and hydrogen bonding forces between the surface and solvent.[129]

UV-vis Spectroscopy

UV-vis Spectroscopy of Fillers. Measurements of ultraviolet and visible light absorbance for powders were conducted on a Cary 5000 UV-vis-near Infrared spectrophotometer. Cerium (IV) oxide, cerium (III) nitrate hexahydrate, trisilanol phenyl POSS, and CePOSS were mixed with chloroform at 0.25 mg of solute per 1 mL of solvent. Absorption data was collected from 175-500 nm but displayed from 200-350 nm to avoid noise due to solvent absorption below 200 nm. This range covers part of the UVa radiation range (400-320 nm), all of the UVb radiation range (320-280 nm), and part of the UVc radiation range (280-100 nm).[19] Spectra were compared to determine whether incorporating cerium-containing compounds with POSS increases UV absorbance compared to reagents.

UV-vis Spectroscopy of Films. UV-vis transmission measurements for epoxy films either unexposed or exposed to UV/ozone were collected on a bench top custom fixture.[130] Visible spectrum illumination was provided via fiber optic cable to the sample using the SpectraNet SL1 light source.[130] Ultraviolet spectrum illumination was provided concurrently with the L7293 lamp mounted in the exposure fixture port.[130] The spectrometer was a SpectraNet Black Comet Spectrometer running SpectraWiz spectrometer software V5.3.[130]

Exposure Testing

Atomic Oxygen Exposure Testing. Specimens were exposed to atomic oxygen in an SPI Plasma Prep II asher for 68 h at NASA Glenn Research Center.[124] This time was selected to ensure a minimum fluence of $1x10^{21}$

atoms/cm^2 as verified by Kapton H witnesses. Samples were dehydrated under vacuum for 48 h before exposure, weighed, and wrapped on all sides except the exposed face by aluminum foil that had been previously atomic oxygen exposed to remove coatings. After exposure, samples were dehydrated again for 48 h, unwrapped, and reweighed.[124]

Plasma Treatment of Surface Coated Disks. Dual layer composite disks were provided for plasma treatments at Surfx Plasma using an Atomflo 500 plasma system. For this experiment, the plasma used was a 100:1 ratio of argon to oxygen gas at a power level of 120 W. One pass at 1 mm/s was made over each disk at the coating surface at a 4 mm distance. The effects of plasma treatment were assessed through water contact angle and SEM/EDS.

Films of neat EP3510 were treated by oxygen plasma at Hybrid Plastics using a Harrick Plasma Basic Plasma Cleaner.[131] This instrument applies up to 18W of power to coils that produce plasma.[131] Three samples each were exposed for 1, 2.5, 5, 10, 15, 30, or 45 min and were analyzed before and after for carbon content through SEM/EDS. In addition, water contact angle was measured on unexposed and the 45 min exposed films. The overall objective of this experiment was to determine if the Harrick Plasma cleaner had enough power to glassify a POSS-rich surface. Oxygen plasma has been used for glassification by other researchers and could prove a simple method to alter POSS surfaces without cost and time-intensive atomic oxygen testing.[31,91]

Xeel UV/Ozone Treatment of EP3510 Films. Atomic oxygen testing requires specialized and expensive testing equipment but is a proven method to

glassify POSS.[12,31,73,74] However, Özçam, et al. glassified poly(dimethyl siloxane) with a combination of UV radiation and ozone.[132] This procedure inspired efforts to glassify POSS-rich materials with UV radiation and ozone with collaborators at Xeel Corporation.[133]

Coatings of EPON 862, neat EP3510, and EP3510 with 1 wt% CePOSS-0.5 wt% PEG POSS, 2.5 wt% CePOSS-1.25 wt% PEG POSS, or 5 wt% CePOSS-2.5 wt% PEG POSS were prepared and exposed to UV/ozone environment to evaluate whether or not the Ce in the Ce-POSS cage structure adversely inhibited the formation of a glassified layer. The sample disks of 2 mm thickness were subjected to high-intensity UV in an ozone rich environment at standard temperature and pressure.[134]

For the testing, ozone was generated using a commercial ozone unit (Ozone Solutions VMUS-2) supplied with ultra-high purity oxygen (Grade 5.9).[134] The generated ozone was supplied to a sealed enclosure with the outlet port leading to an ozone destructor unit. Using a commercial ozone analyzer unit (EcoSensors UV-100), the enclosure concentration exceeded the instrument measurement range of 1000 ppm. UV illumination is provided by a Hamamatsu L7293 Deuterium lamp. This model lamp produced a broad emission spectrum ranging between 116 to 650 nm with a total intensity of 11.7 mW/cm^2. The lamp's long nose form factor allowed it to pass through an ozone enclosure compression port to direct a narrow beam onto the sample stage positioned ~5 mm from the end of the lamp. Since ozone is a strong UV absorber, a small sample set back from the lamp was utilized to maximize the incident spectrum reaching the

sample surface.[134] Exposure effects were quantified by SEM/EDS, contact angle, and x-ray photoelectron spectroscopy (XPS).

X-ray Photo Electron Spectroscopy (XPS). X-ray photoelectron spectroscopy was conducted at Auburn University with a Kratos XSAM 800 unit. X-ray photoelectron spectroscopy can detect the type of molecules present at a surface by bombarding the surface with x-rays and the measuring the binding energies of the ejected electrons.[72] Shifting of the Si 2p bond from Si_3N_4, Si_2O_3, or SiC to SiO_2 or SiO_2nH_2O indicates glassification.[73,74]

Summary

Epoxy-amine nanocomposites were cured as DMA bars, tensile bars, coated disks or coatings. The miscibilities of various fillers in DGEBA were evaluated by using Teas Diagrams. Samples and fillers were evaluated for chemical composition, morphology, rheological, thermal, and mechanical properties. UV-vis spectroscopy was used to evaluate the UV absorbance or transmittance of fillers such as CePOSS and cerium (IV) oxide and the EP3510 coating with CePOSS. Selected POSS nanocomposites and films were exposed to atomic oxygen or a combination of UV radiation and ozone and examined for POSS glassification after exposure

CHAPTER III – POSS SEDIMENTATION IN DGEBA-44DDS

Introduction

Atomic oxygen and other hazards degrade organic material in low Earth orbit.[2] Polyhedral oligomeric silsesquioxanes (POSS) have shown promise in reducing mass loss and other impacts of atomic oxygen and UV radiation.[12,81] POSS converts to a glassy layer of SiO_2 under exposure to atomic oxygen and high energy plasma.[74] This creates a passive surface layer that blocks further degradation.[74] The materials that have been used to establish this glassification phenomenon have been primarily POSS-polysiloxane, POSS-polyurethane, and POSS-polyimide copolymers.[12,69,73,74] However, copolymerization with POSS as a monomer requires synthesis of specialized POSS moieties. [12,69,73,74] Atar et al. and Verker et al. have shown that POSS glassification can also be achieved with blending of POSS and other polymers.[67,91] However, as other studies have shown, dispersion of POSS can be dependent on the nature of its pendant groups.[102]

Epoxies are a common system for carbon fiber composites and have been used in a variety of aerospace applications since the 1960s.[44, 54] For this work, the monomer chosen was diglycidyl ether of bisphenol-A (DGEBA). This is a commonly used epoxy monomer as reviewed in the introduction.[48] The symmetrical 4,4'-diaminodiphenyl sulfone (44DDS) was chosen as the amine crosslinker. This material is a white solid that can be mixed into DGBEA as a suspension. The structures of DGEBA and 44DDS are shown in Figures 52 and 53.[56,82]

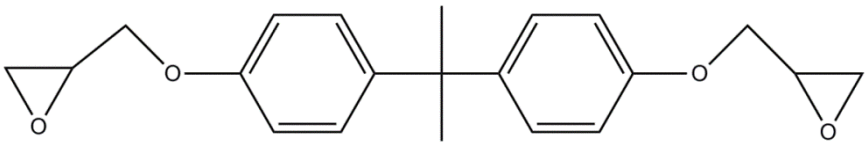

Figure 52. Structure of diglycidyl ether of bisphenol-A.[56]

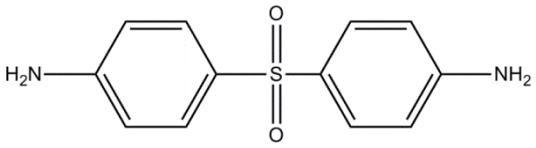

Figure 53. Structure of 4,4'-diaminodiphenylsulfone.[58]

As previously discussed in the introduction, the compatibility of POSS with a matrix is mainly governed by the POSS pendant groups used.[76] For this project, initially two closed cage POSS moieties were used: octamethyl POSS and octaphenyl POSS (Figures 54 and 55). Both of these POSS moieties are solid and cannot react with the epoxy matrix.[68] Octafunctional glycidyl POSS (Figure 56), which can react into the epoxy matrix, was used later to give a broader range of pendant diversity among the three types of POSS.[68]

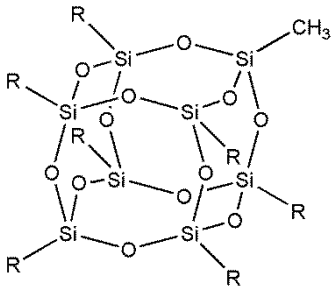

Figure 54. Structure of octamethyl POSS, where R = methyl.[107]

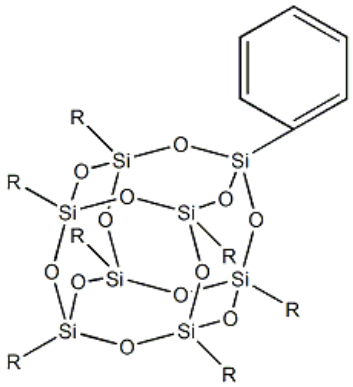

Figure 55. Structure of octaphenyl POSS, where R = phenyl.[107]

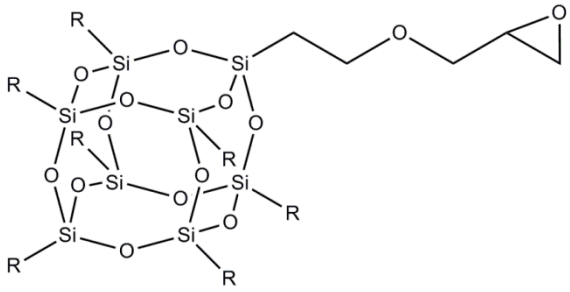

Figure 56. Structure of glycidyl POSS, where R = glycidyl.[107]

In this project, these three types of POSS with varying solubility were mixed with DGEBA-44DDS and characterized based on POSS dispersion and their effects on thermal and mechanical properties.

Results and Discussion

Initial Efforts

Initially, octamethyl and octaphenyl POSS were mixed with DGEBA-44DDS at 1, 2.5, or 5 wt%. Higher loading levels produced materials that were too brittle. To manufacture samples, POSS was placed in DGEBA at approximately 75 °C and stirred while being degassed to remove impurities. The 44DDS crosslinker was added at stoichiometric 1:1 ratio of functional groups to the DGEBA monomer. Both the POSS and the 44DDS were suspended in the

epoxy by stirring. This caused the initially clear DGEBA to become opaque. The mixture of DGEBA, 44DDS, and POSS was degassed and stirred while heated until the mix became transparent, indicating that cure was beginning. The mixture was then transferred to silicone rubber molds to produce DMA bars 60 mm long, 5 mm wide, and 1.5 mm thick and cured at 180 °C for 3 hours as recommended by collaborators at Boeing Research and Technology.

Neat DGEBA-44DDS produced transparent but yellow tinted bars for dynamic mechanical analysis (DMA) as seen from the top down in Figure 57.

Figure 57. Top view of neat DGEBA-44DDS DMA bar at 6X.

The bars did occasionally display bubbling and were also sometimes susceptible to scratching. Addition of octamethyl POSS caused POSS sedimentation both at the top and bottom surface of bars, as shown in Figure 58 which shows an example of a DGEBA-44DDS sample containing1 wt% octamethyl POSS. Although both POSS moieties were denser than the DGEBA-44DDS matrix, it is possible that POSS was well dispersed in the epoxy-amine during mixing and then was frozen into place by network formation during the cure cycle.[135] The

size of many of these POSS particles was greater than the shortest wavelength of visible light, 400 nm, and the samples appeared opaque.[136]

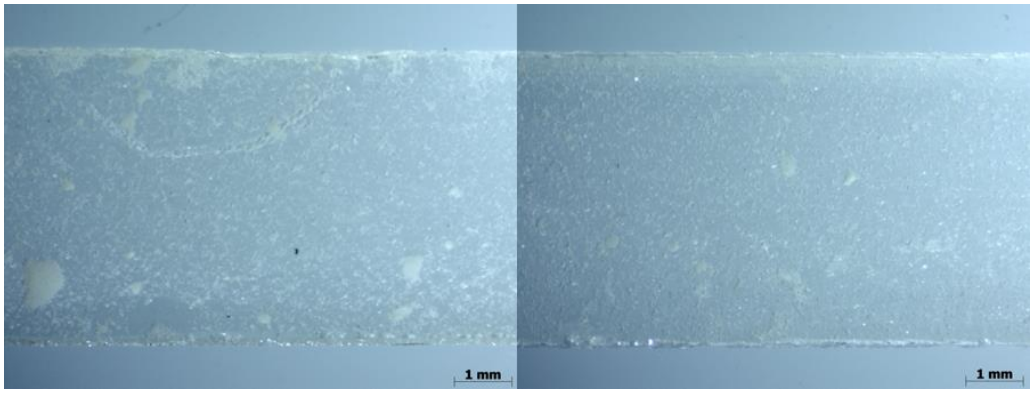

Figure 58. Bottom (l) and top (r) of 1 wt% octamethyl POSS in DGEBA-44DDS DMA bar at 6X.

Octamethyl POSS particles could be as large as 1 mm in diameter. The variation in sizes increased with increasing loading levels. Octaphenyl POSS also had aggregation issues on both top and bottom bar surfaces as shown in the 2.5 wt% octaphenyl POSS in DGEBA-44DDS sample shown in Figure 59.

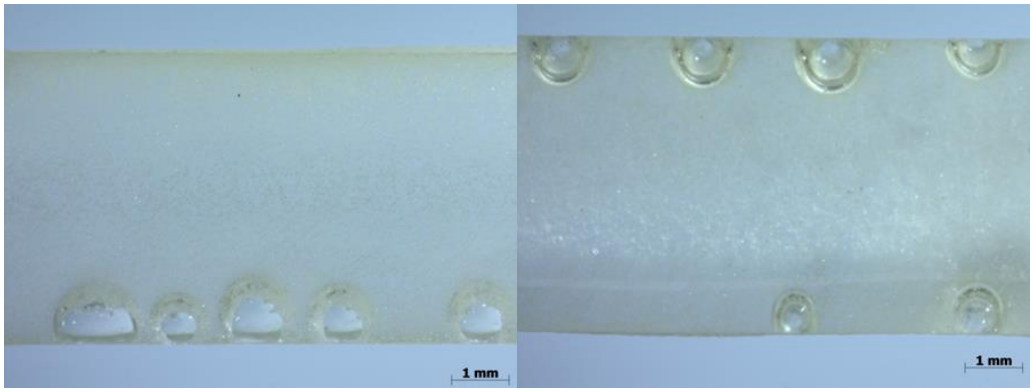

Figure 59. Bottom (l) and top (r) of 1 wt% octaphenyl POSS in DGEBA-44DDS DMA bar at 6X.

Initially, the octaphenyl POSS particles were not as large as those seen with octamethyl POSS, although octaphenyl POSS-DGEBA-44DDS samples were at least semi-opaque at the lowest loading level of 1 wt% octaphenyl

POSS. Particulates began to approach 1 mm in diameter or greater at 5 wt% octaphenyl POSS. In addition, a white region of sedimented POSS was observed at the bottom of the bar as shown in Figure 60. This region was 0.39 mm thick on average in a bar of 1.21 mm average thickness.

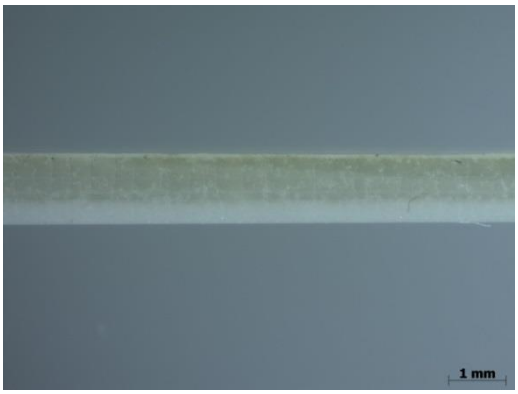

Figure 60. Side view of sedimented octaphenyl POSS in a 5 wt% octaphenyl POSS in DGEBA-44DDS DMA bar at 6X.

Dynamic mechanical analysis (DMA) was conducted in tensile mode on three bars of each material from -125 to +250 °C. The peak of the tan delta curve was used to determine glass transition temperature (T_g). Results are in Table 5.

Table 5

Glass transition temperatures for DGEBA-POSS materials cured at 180°C for 3 hours

Neat DGEBA-44DDS	**T_g (°C)**
0 wt%	193.7 +/- 2.9
Octamethyl POSS	**T_g (°C)**
1 wt%	195.9 +/- 4.4
2.5 wt%	206.5 +/- 3.8
5 wt%	205.9 +/- 3.6
Octaphenyl POSS	**T_g (°C)**
1 wt%	208.2 +/- 2.2
2.5 wt%	216.4 +/- 1.7
5 wt%	201.0 +/- 4.2

Octamethyl POSS did not increase the T_g above that of neat DGEBA-44DDS until a loading level of 2.5 wt%. The octaphenyl POSS increased T_g compared to the neat matrix regardless of loading level. The standard deviations for each measurement were worth noting. The standard deviation for the neat DGEBA-44DDS T_g measurement was +/- 2.9 °C, whereas all samples with octamethyl POSS had larger deviations. This was attributed to the large variability in POSS particle size as observed by optical microscopy (Figure 58).

Teas Diagrams

Initial efforts to make POSS nanocomposites with a DGEBA-44DDS matrix resulted in samples with POSS aggregations dispersed throughout with particle sizes ranging from millimeter to micron-sized. The octamethyl and octaphenyl POSS were originally chosen because they were assumed to be immiscible in DGEBA-44DDS, and therefore, might sediment and form a protective layer. This assumption was based on their unreactive pendant groups and their existence as solids at room temperature as opposed to the liquid DGEBA. However, these POSS moieties produced large, heterogeneous aggregates that were distributed throughout the DGEBA-44DDS. It is possible that these two POSS moieties aggregated due to their incompatibility with DGEBA-4DDS and lack of any colloid-stabilizing entities on their surfaces. Teas diagrams were employed to better understand the miscibility of POSS moieties in DGEBA-4DDS. If a solute is miscible in a set of solvents, then a region of miscibility can be marked on the Teas diagram of the solute (Figure 61).[104]

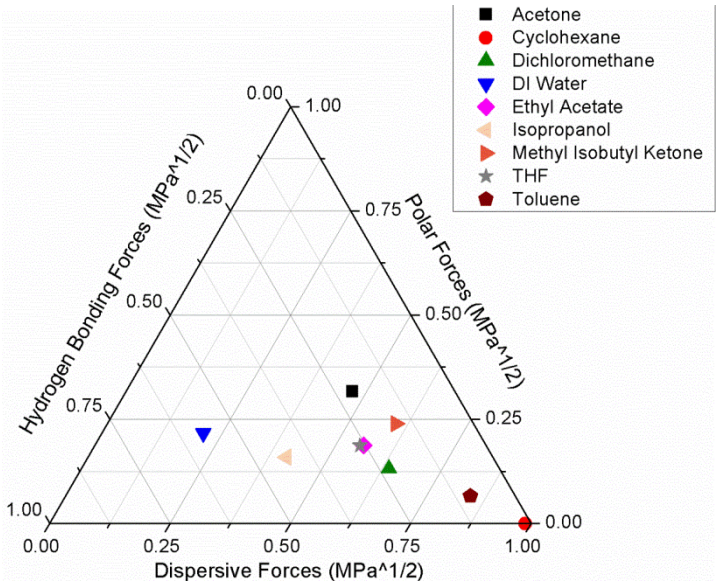

Figure 61. Teas diagram of selected solvents.

This information can help predict miscibility or immiscibility in other solvents as well as allowing for comparisons with other solutes.[104] All three POSS moieties were mixed at a concentration of 10 mg POSS/1000 mg solvent in acetone, cyclohexane, dichloromethane, deionized water, ethyl acetate, isopropanol, methyl isobutyl ketone, tetrahydrofuran (THF), and toluene. In the following Teas diagrams, the miscible solvents for each type of POSS are labeled in green. Partial miscibility is labeled in yellow. Immiscibility is labeled in red.

Miscibility of octamethyl POSS is governed mostly by dispersion forces due to the non-polar, non-hydrogen bonding methyl pendants. There is also a small contribution from dipole-induced dipole interaction. This can be observed in the octamethyl POSS Teas diagram (Figure 62) where the only solvent with even partial miscibility was toluene.

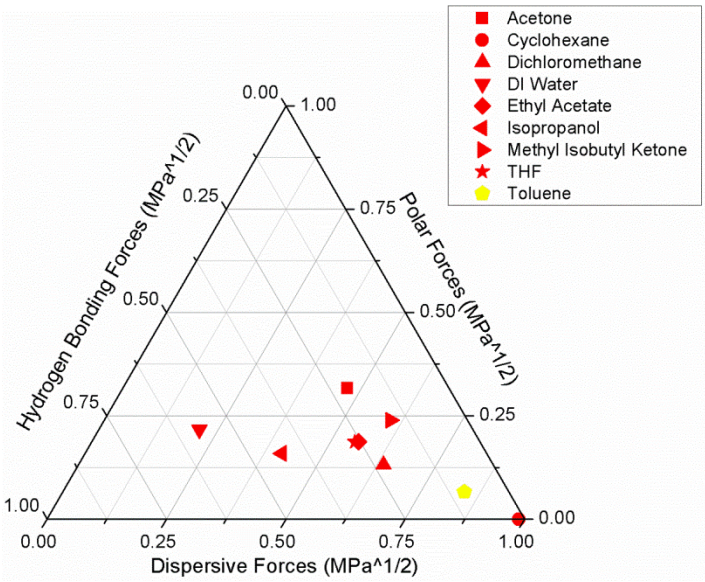

Figure 62. Teas diagram of octamethyl POSS.

The phenyl pedants on octaphenyl POSS are more polar than methyl groups but cannot hydrogen bond. Therefore, a larger contribution from dipole-induced dipole interaction would be expected. The only compatible solvent in the octaphenyl POSS Teas diagram (Figure 63) was dichloromethane.

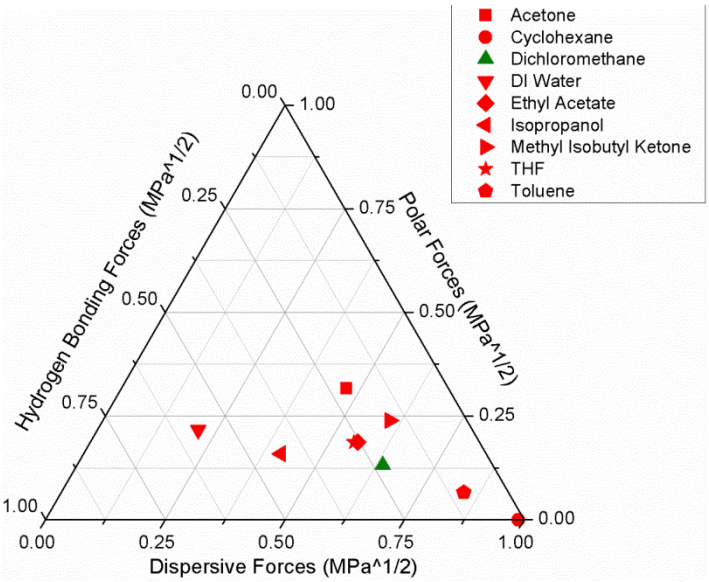

Figure 63. Teas diagram of octaphenyl POSS.

The glycidyl POSS pendant groups contain relatively polar bonds and the epoxy group can also act as a hydrogen bond acceptor. As a consequence, glycidyl POSS had the widest range of compatible solvents (Figure 64).

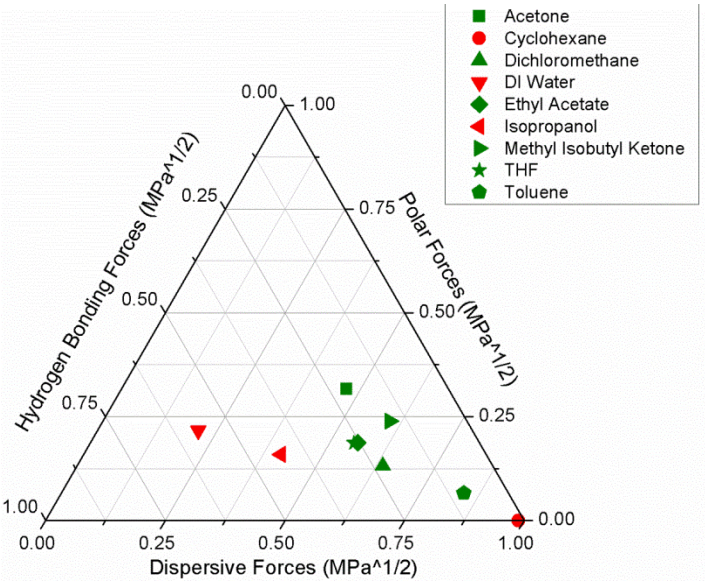

Figure 64. Teas diagram of glycidyl POSS.

Glycidyl POSS was immiscible with deionized water, cyclohexane, and isopropanol. Deionized water and isopropanol required more hydrogen bonding and dipole-dipole interactions whereas cyclohexane was probably not sufficiently polar to confer miscibility on POSS with glycidyl pendant groups.

The epoxy monomer, DGEBA, had similar solubility characteristics to glycidyl POSS (Figure 65).

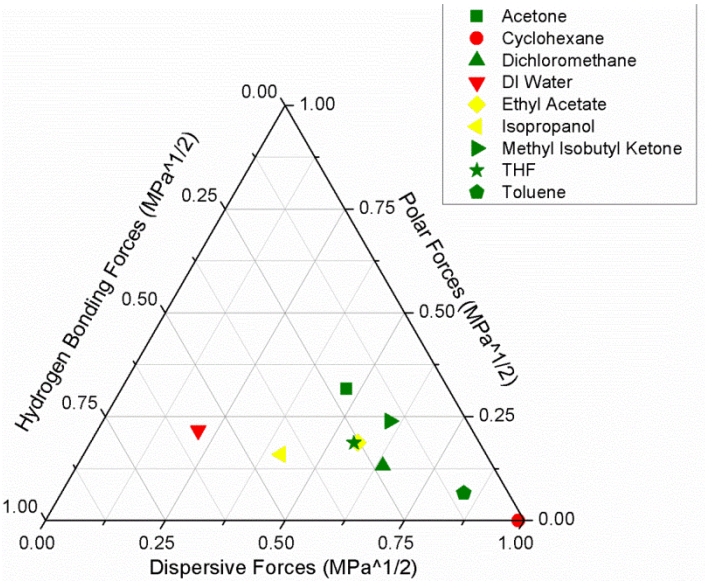

Figure 65. Teas diagram of DGEBA.

The DGEBA was miscible in the same solvents as glycidyl POSS except for ethyl acetate and isopropanol. Therefore, the glycidyl POSS would be expected to be more miscible in the epoxy than the octamethyl and octaphenyl POSS. As for the octamethyl and octaphenyl POSS, these do share miscible solvents with DGEBA, but the overall miscibility regions are much smaller for these two POSS moieties compared to glycidyl POSS. This may explain why the octamethyl and octaphenyl POSS sedimented in DGEBA-44DDS.

In-situ Dielectric Spectroscopy

Dielectric spectroscopy (DS) contributes nuance to DMA results with the ability of the method to record dynamic response during cure. It requires specialized electrodes capable of withstanding the cure environment as well as producing and measuring an electric field. As shown in Figure 66, the sensors are two interdigitated comb electrodes on an inert substrate.

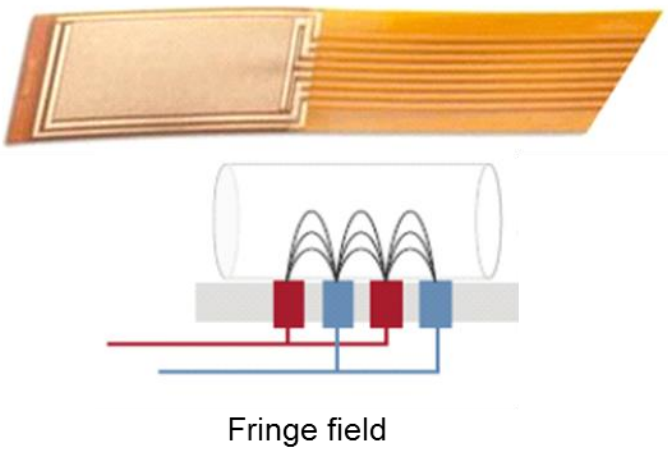

Figure 66. In-situ dielectric sensor and fringe field diagram.[117]

The electric field applied during measurement is a fringe pattern; a localized measurement of the dielectric properties is performed near the sensor/sample interface. A fixed sample thickness is not necessary as long as the active sensor area is well covered and the penetration depth of the electric field lines into the sample is approximately the same magnitude as the electrode spacing. For the interdigitated electrode sensors used in this study, electrode spacing was 115 μm and sample thickness was at least 300 μm (based on the fully cured sample).[117]

Ion viscosity versus time plots are commonly used to identify resin gel points and to analyze kinetics.[137-139] Dielectric spectroscopy can monitor resin cure by measuring electrical properties which are closely tied to viscoelastic properties. One relation is between viscosity and the ion viscosity (IV), resulting from the dielectric loss permittivity, ε”. Ion viscosity is a measure of ion mobility, which is a function of polymer chain mobility. This is related to ε” through:

$$\text{Ion viscosity} = \text{IV} = 1/\sigma; \qquad \sigma = 2\pi f \varepsilon'' \varepsilon_o$$

σ is electrical conductivity reflective of long range charge migration and ε_o is the vacuum permittivity. Sodium hydroxide is the literature standard catalyst during DGEBA synthesis; small quantities of Na^+ and Cl^- (less than 50 ppm) are usually present in DGEBA resins. [140,141] The mobility of these ionic impurities in the presence of an applied electric field causes changes in the ionic conductivity, which is tracked during dielectric experiments.[142] As the fluid system of monomers becomes increasingly polymerized and cross-linked, there is an increase in viscosity, with gel point is defined as the point at which the curve reaches a plateau after the rapid increase.[117]

Figure 67 shows change in IV vs. time at 900 Hz for the curing of DGEBA monomer using 44DDS crosslinker with 1-10 wt% of octamethyl POSS.[117] Curing was achieved in one step by coating the dielectric sensor with reaction mixture in an oven which was preheated to 100 ºC, then oven temperature was raised to 180 ºC at a ramp rate of 1 ºC/min and kept there for 3 hours.[117]

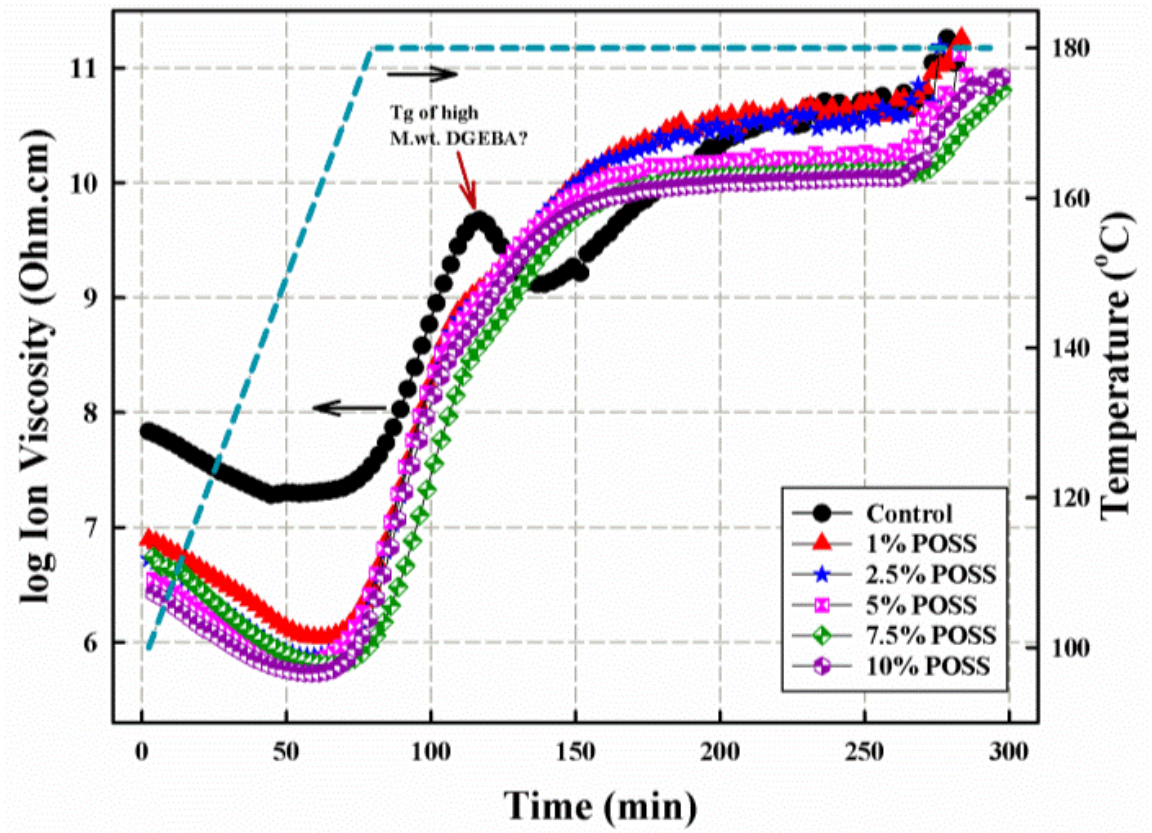

Figure 67. Log IV vs. time at 900 Hz for the curing of DGEBA-44DDS with 1 to 10 wt% octamethyl POSS.[117]

As the oven temperature rose from 100 ºC, IV for all samples dropped by almost equivalent amounts due to decreasing viscosity as temperature approaches 180 ºC.[117] At this point, there were two competing processes, namely increased ion mobility as a result of thermal activation, and crosslinking. With increasing time, the crosslinking process overwhelmed the effect of thermally-increased ion mobility and IV started to rise again for all samples after approximately 60 min.[117]

The gel point for resin curing is defined to be the cure time at which IV reaches an asymptote, which occurs beyond approximately 236 min. for the control sample. The gel point shifted earlier with increasing POSS weight percent

as indicated by the dashed lines. An expanded view of Figure 67 is shown in Figure 68.[117]

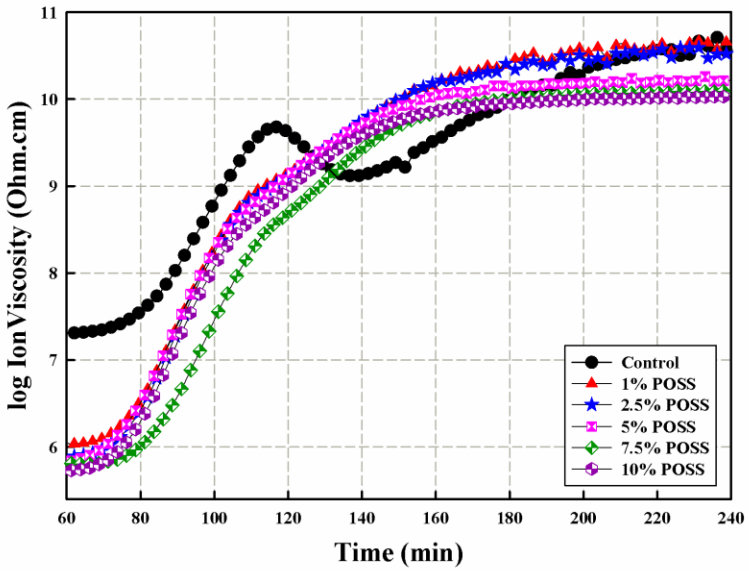

Figure 68. Expanded view of Figure 67 to show shift in IV curves for 1 to 10 wt% octamethyl POSS.[117]

The rise in IV reflects the progress of crosslinking, with the rate of this process seeming to increase with additional POSS as evidenced by the time after which IV reaches an asymptote value. Finally, the rise in IV shown in Figure 68 after 260 min. is due to the drop of oven temperature at the completion of the curing cycle. The behavior of the IV throughout the entire cure cycle is very descriptive of changes in thermal steps during curing. As a reflection of the changing ionic mobility during epoxy-amine curing, IV thus represents a very sensitive tool for examining the physical and chemical alterations happening during the cure process.[117,130]

Cure Protocol Modification

As mentioned previously, initial DGEBA-44DDS-POSS samples had a range of POSS aggregation sizes and no consistent sedimented bottom layer of POSS. Two strategies were employed to address these issues. Octamethyl and octaphenyl POSS were ultrasonicated for 15 min in acetone before addition to DGEBA.[143] This extra step required thorough degassing of the DGEBA before addition of 44DDS for up to 2-3 hours. In addition, once the 44DDS was mixed in and degassed for another 30 min, the mixture was immediately transferred to molds instead of waiting for cure to begin in the flask to avoid reaggregation of POSS. A dwell was also added in the cure protocol. Instead of a single isothermal hold at 180 °C, samples were placed in an oven at 100 °C, ramped 1°C/min to 110 °C, held for 1 h, and then ramped 1°C/min to the 180 °C, 3-hour isothermal hold. This was done to take advantage of some of the drop in ion viscosity with heating seen through in-situ dielectric spectroscopy and allow the POSS particles time to sediment.

The more soluble glycidyl POSS was also used as an additive (Figure 56). This POSS moiety was liquid at room temperature and could react with the epoxy. Neat DGEBA-44DDS and DGEBA-44DDS with octamethyl, octaphenyl, or glycidyl POSS at 1, 2.5, and 5 wt% were cured as DMA bars and small quantities of uncured material was reserved for differential scanning calorimetry (DSC).

Effects of Cure Protocol Modification. The purpose of adding the hold at 110 °C in the cure cycle was to allow POSS particles time to sediment into a region at the bottom of sample bars. Overall, POSS aggregates present were

smaller on average and appeared more evenly distributed throughout samples. Figure 69 displays DMA bars of 1, 2.5 or 5 wt% octamethyl or octaphenyl DMA bars. The bars are oriented as removed from the mold with the bottom surface originally flush with the bottom of the DMA mold.

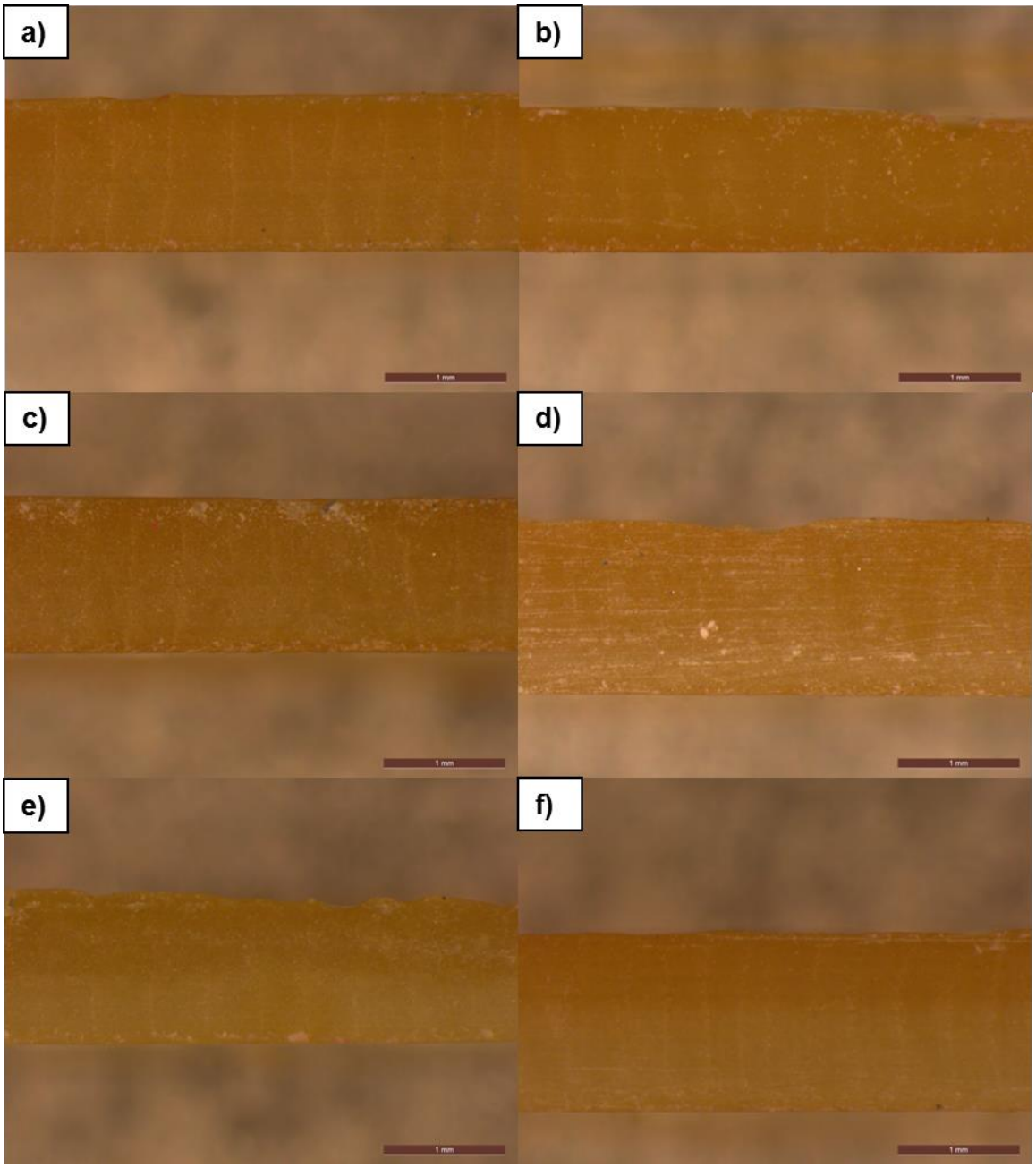

Figure 69. Side views of 1 wt% a), 2.5 wt% c), and 5 wt% e) octamethyl POSS and 1 wt% b), 2.5 wt% d), and 5 wt% f) octaphenyl POSS DMA bars at 24X.

POSS particles were seen depth wise throughout every sample but appeared as a gradient with a higher concentration of particles at the bottom of each bar, as opposed to the scattered dispersion of aggregates with the original cure cycle in Figures 58 and 59. Loading level seemed to influence the thickness of the POSS sediment at the bottom of the bars. The 2.5 wt% octaphenyl sample had a layer of sedimented POSS of thickness 0.353 +/- 0.009 mm in a bar of 1.44 mm whereas the 5 wt% octaphenyl POSS bar had a layer 0.825 +/- 0.002 mm thick in a bar 1.47 mm thick. The 5 wt% octamethyl POSS bar had a POSS sediment layer of 0.534 +/- 0.033 mm in a bar 1.214 mm thick. Variation in bar thicknesses was due to using an open top mold that does not prevent under or over filling before cure. The reasons for different thicknesses of the 5 wt% octaphenyl and octamethyl POSS sediment regions are likely related to the miscibility of the moieties in the DGEBA-44DDS and any variations in particle size. It can be interfered from these results that with a longer cure cycle, POSS has more time to sediment at the bottom of samples.

Glycidyl POSS did not show any such sedimentation (Figure 70). This was expected as glycidyl POSS can react into the epoxy-amine matrix and had the most similar region of miscibility to DGEBA as charted in Teas Diagrams. If any aggregates were present their size would be less than 400 nm. The white flecks were contamination from the silicone mold.

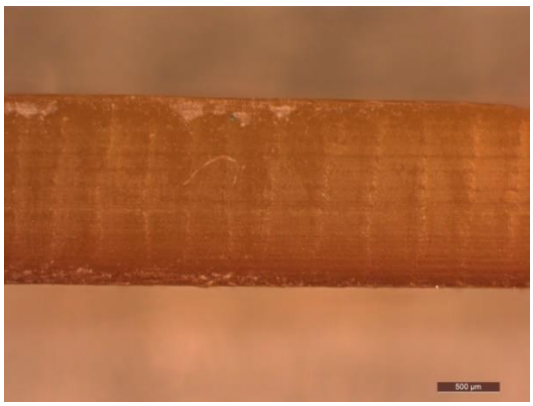

Figure 70. Side view of 5 wt% glycidyl POSS DMA bar at a magnification of 24X.

Cure Conversion

One major concern with modifying cure cycles is the possible change of network conversion. Samples of equal weight (+/- 0.1 mg) were placed in DSC pans and heated through the updated cure cycle with the 110 °C dwell time. Samples were then cooled to 40 °C and heated to 300 °C at 5 °C/min. Any remaining exotherm was compared to the exotherm during cure, with percent change in exotherms corresponding to the network conversion. Because this process was very time consuming (one test could be 8+ hours), cure conversion was measured twice for only neat DGEBA-44DDS, and samples with 1 or 5 wt% octamethyl, octaphenyl, or glycidyl POSS (Table 6).

Table 6

Network conversion with modified cure cycle

Material	Conversion (%)
Neat DGEBA-44DDS	94.1 +/- 6.9
1 wt% octamethyl POSS-DGEBA-44DDS	89.6 +/- 2.4
5 wt% octamethyl POSS-DGEBA-44DDS	94.7 +/- 3.9
1 wt% octaphenyl POSS-DGEBA-44DDS	95.9 +/- 4.4
5 wt% octaphenyl POSS-DGEBA-44DDS	97.9 +/- 2.9
1 wt% glycidyl POSS-DGEBA-44DDS	93.0 +/- 1.2
5 wt% glycidyl POSS-DGEBA-44DDS	89.2 +/- 1.0

The conversion data for the neat DGEBA-44DDS did have a relatively large standard deviation. Therefore, it was statistically uncertain whether POSS positively or negatively affected conversion compared to the neat matrix. However, none of the DGEBA-44DDS-POSS samples had an average conversion lower than 89.2 %, which was considered acceptable

The effect of cure prescription alteration on glass transition temperature (T_g) was measured using dynamic mechanical analysis. As with previous experiments, cured samples were placed in tension from -125 to +250 °C and the peak of the tan delta curve was used to determine T_g. Table 7 displays a comparison of average T_g values between the original, 180 °C for 3 h, cure and the modified cure of 110 °C for 1 h and then 180 °C for 3 h.

Table 7

Glass transition temperatures for DGEBA-POSS materials cured with original or modified cure prescriptions

Neat DGEBA-44DDS	**Tg Original Cure (°C)**	**Tg Modified Cure (°C)**
0 wt%	193.7 +/- 2.9	203.5 +/- 2.3
Octamethyl POSS	**Tg Original Cure (°C)**	**Tg Modified Cure (°C)**
1 wt%	195.9 +/- 4.4	209.5 +/- 3.0
2.5 wt%	206.5 +/- 3.8	200.1 +/- 0.8
5 wt%	205.9 +/- 3.6	196.8 +/- 2.3
Octaphenyl POSS	**Tg Original Cure (°C)**	**Tg Modified Cure (°C)**
1 wt%	208.2 +/- 2.2	204.8 +/- 1.7
2.5 wt%	216.4 +/- 1.7	200.2 +/- 1.0
5 wt%	201.0 +/- 4.2	201.1 +/- 3.2
Glycidyl POSS	**Tg Original Cure (°C)**	**Tg Modified Cure (°C)**
1 wt%	Not Measured	210.0 +/- 0.8
2.5 wt%	Not Measured	197.9 +/- 1.9
5 wt%	Not Measured	195.5 +/- 2.2

The modified cure increased the glass transition temperature of neat DGEBA-44DDS. This was probably due to the longer cure cycle time (approximately 5.5 h

compared to 3 h) allowing the system to achieve a higher degree of cure, thus improving conversion.

The glass transition temperatures of octamethyl and octaphenyl POSS samples could be compared between the original and modified cure. In every case, the T_g standard deviation decreased with the modified cure cycle, indicating more uniform samples. This is consistent with the optical microscopy images that showed a more uniform size of sedimented particles compared to the original cure. Unlike the neat DGEBA-44DDS, the modified cure produced POSS materials having T_g data lower than that from the original cure except for two cases, the 1 wt% octamethyl POSS-DGEBA-44DDS (higher T_g) and the 5 wt% octaphenyl POSS-DGEBA-44DDS (equal T_g). Factors affecting glass transition temperature include intermolecular forces between chains.[144] POSS aggregates became evenly dispersed throughout a network, and the surface of these aggregates interacted with the chains and increased excluded volume, causing a decrease in T_g.

Being the least soluble additive, octamethyl POSS aggregates will more easily form, creating provide minimal interfacial area for polymer adsorption. This could explain the 12.7 °C decrease in T_g from 1 to 5 wt% loadings. The aggregates could be reducing chain end mobility, and therefore, decreasing conversion. This is consistent with decreased T_g, however, further study using a technique such as dynamic scanning calorimetry or Fourier infrared transmission spectroscopy is needed to quantify this effect. Glycidyl POSS was the only one of the three moieties that could react into the epoxy matrix. The 14.5 °C drop in T_g

with increasing glycidyl POSS content might be explained by an increase in excluded volume by the bulky glycidyl POSS reacting into the network. Octaphenyl POSS exhibited the lowest decrease in T_g (3.7 °C) from 1 to 5 wt% loading level.

Mechanical Properties of Modified Cure Materials

Mechanical properties such as strength and flexibility are of interest in the design of structural materials for use in low-Earth orbit. Therefore ultimate tensile strength (UTS), Young's modulus, and flexural modulus of the previously produced POSS nanocomposites were measured. Measurement of the Young's modulus provided insight concerning the ductility of a material.[145]

As shown in Figure 71, ultimate tensile strength clearly increased with increasing loading levels of octaphenyl POSS (black). In contrast, the octamethyl samples did not have statistically significant changes in UTS compared to DGEBA-44DDS.[146]

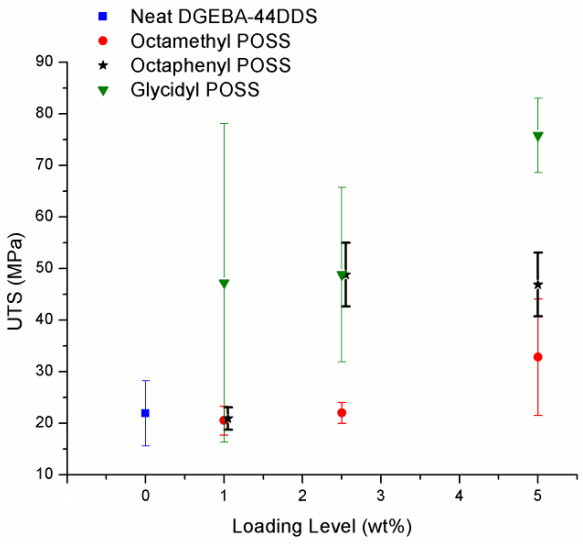

Figure 71. Ultimate tensile strength versus loading level of POSS moieties in DGEBA-44DDS.[146]

The UTS only increased in octaphenyl and glycidyl POSS samples above 2.5 wt%.[146] The lack of improvement in the UTS data with octamethyl POSS inclusion could indicate that this additive promotes crack growth. POSS decreased Young's modulus (Figure 72).[146]

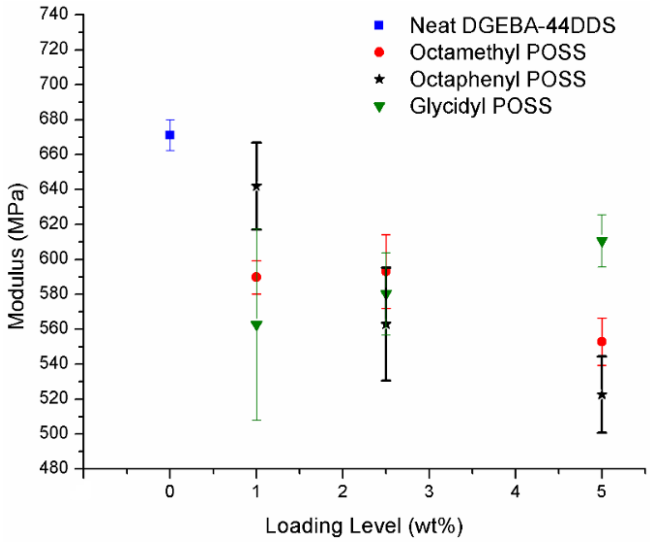

Figure 72. Young's modulus versus loading level of POSS moieties in DGEBA-44DDS.[146]

The decreases indicate that the addition of POSS has shifted the failure mechanism from ductile to brittle.[146]

Another property potentially affected by a layer of POSS sediment was flexural modulus.[146] Three-point bend testing was conducted for each nanocomposite type; here testing was done with five samples having the POSS sediment layer facing down in the fixture (Figure 73, Orientation A) and five samples having the POSS sediment layer facing up in the fixture (Figure 73, Orientation B). The POSS sediment is represented in Figure 73 as the dark orange line on the yellow sample bar. During flexural testing, the top of a sample experiences compressive forces at the top of the sample and tensile forces at the

bottom of the sample.[145] Therefore, in Orientation A, any region of POSS sediment would experience extension versus experiencing compression forces in Orientation B.[146]

Figure 73. Sample orientations for flexural testing. POSS sediment represented by orange line at bottom of base.[146]

Figure 74 demonstrates the effect of POSS sediment layer orientation on flexural modulus.[146] As was expected, test orientation had a distinct effect on the modulus of almost all nanocomposites.

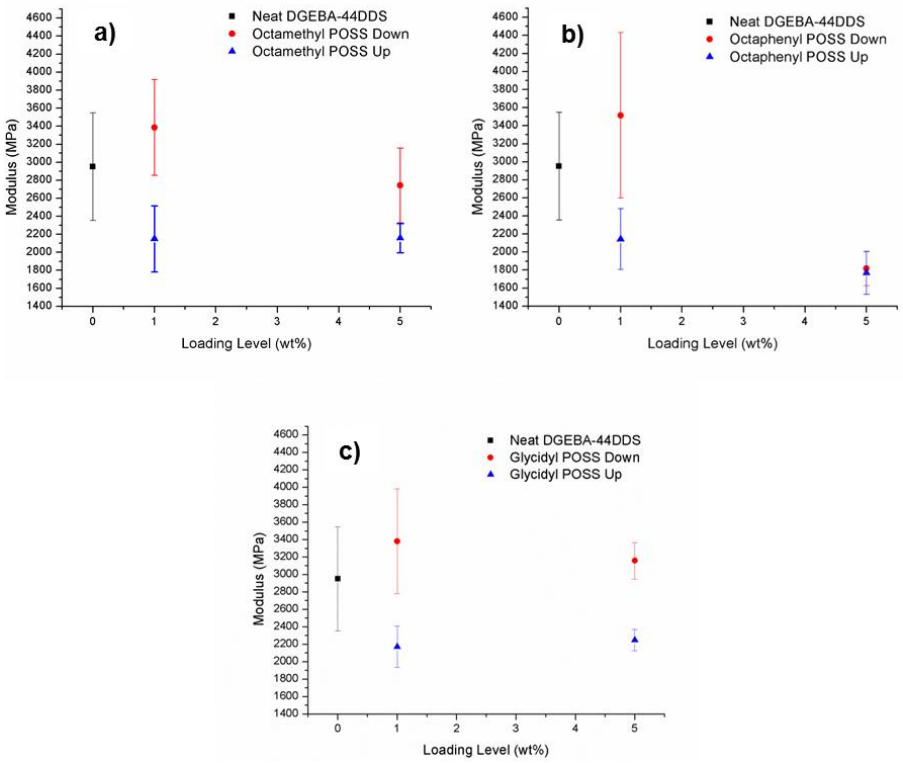

Figure 74. Flexural modulus of a) octamethyl, b) octaphenyl, and c) glycidyl POSS in DGEBA-44DDS where down is Orientation A and up is Orientation B.[146]

Having the POSS sediment experience maximum compression at the top of the bar (Orientation B) clearly decreases the modulus with increasing loading levels, regardless of pendant group. In contrast, POSS nanocomposites had higher moduli when the sediment experienced extension forces, meaning that POSS is stronger in tension. The orientation of POSS sediment does substantially affect flexural modulus but a definitive comparison between the neat DGEBA-44DDS samples and POSS nanocomposites was not possible again due to large standard deviations. This is another example of issues with sample consistency within each type of material.[146]

Atomic Oxygen Exposure Testing

Sample Preparation. Atomic oxygen testing was used to evaluate the DGEBA-44DDS-POSS nanocomposites.[124] Given that the POSS pendant group choice could affect properties such as aggregation and mechanical properties, 2.5 wt% octamethyl, octaphenyl, and glycidyl POSS samples were exposed to better understand the effects of pendant group selection on atomic oxygen resistance. Each sample was flipped upside down after removal from the mold, thereby exposing the POSS-rich regions. Any additional surfaces were wrapped in aluminum foil that was pre-treated to remove industrial coatings.[124] For each material, three 50x5x1.5 mm bars were exposed to atomic oxygen for 68 h in a plasma asher, resulting in an exposure fluence of $1x10^{21}$ atoms/cm^2.[124]

Mass Loss. Mass loss was calculated based on the area of the exposed surface. Samples were dehydrated before and after exposure for 48 hrs. The average mass loss per area for each material is shown in Table 8.

Table 8

Mass loss per area from atomic oxygen exposure.[124]

Sample	Average Mass Loss per Area (g/cm^2)
Neat DGEBA-44DDS	$6.57e^{-3}$ +/- $5.99e^{-4}$
2.5 wt% Octamethyl	$7.43\ e^{-3}$ +/- $1.58e^{-4}$
2.5 wt% Octaphenyl	$9.02e^{-3}$ +/-$2.58e^{-4}$
2.5 wt% Glycidyl	$8.07e^{-3}$ +/- $3.98e^{-4}$

The neat DGEBA-44DDS material had the least average mass loss per area. None of the POSS-filled samples showed a statistically significant decrease in mass loss per area compared to the neat epoxy. The octaphenyl specimens had the worst average performance compared to the octamethyl and glycidyl groups. The octamethyl and glycidyl POSS materials had similar results and were within a positive standard deviation of the average mass loss per area for the neat DGEBA-44DDS. These results were unexpected based on the previously referenced literature describing the mitigation of atomic oxygen effects on thermoplastics by POSS additives.[86,87,91] It was concluded that the POSS loading level was not sufficient to form a protective surface layer of silica glass. Thus additional property and morphology testing was implemented to investigate the impact of atomic oxygen on the exposed specimens in order to determine an appropriate POSS loading level.[124]

Dynamic Mechanical Analysis of Atomic Oxygen. Exposed Samples

Dynamic mechanical analysis was used to measure the glass transition temperature (T_g) of samples and storage moduli before and after exposure.[124] Figure 75 displays the storage moduli and tan delta curves for neat (black), 2.5 wt% octamethyl (red), 2.5 wt% octaphenyl (green), and 2.5 wt% glycidyl (blue)

before and after exposure. The glass transition temperature decreased with exposure for each material except the 2.5 wt% octaphenyl composite (Figure 75).

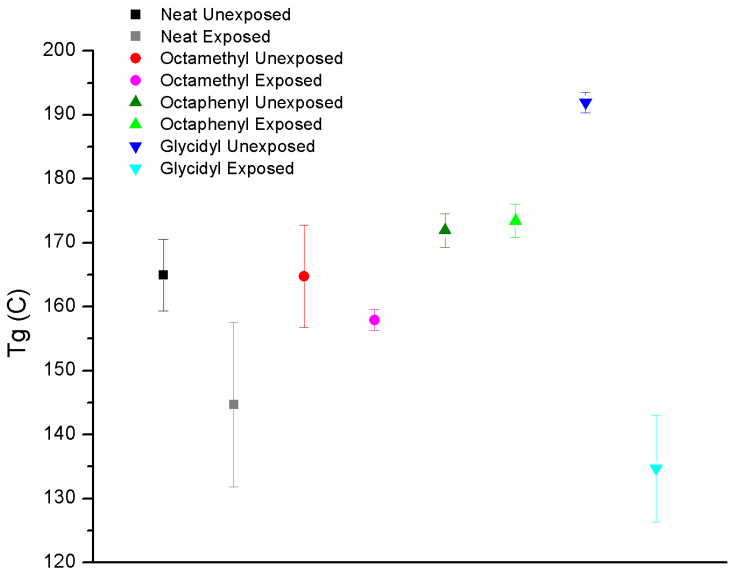

Figure 75. Change in T_g per sample after atomic oxygen exposure.[124]

The glycidyl specimens exhibited the largest decrease. Again, because this is the only moiety that can react into the epoxy thermoset, it may have been more adversely degraded by chain scission.[86,124]

The storage modulus and tan delta curves for the neat DGEBA-44DDS, 2.5 wt% octamethyl POSS, 2.5 wt% octaphenyl POSS, or 2.5 wt% glycidyl POSS in DGEBA-44DDS for exposed and unexposed samples are presented in Figures 76-79.[124]

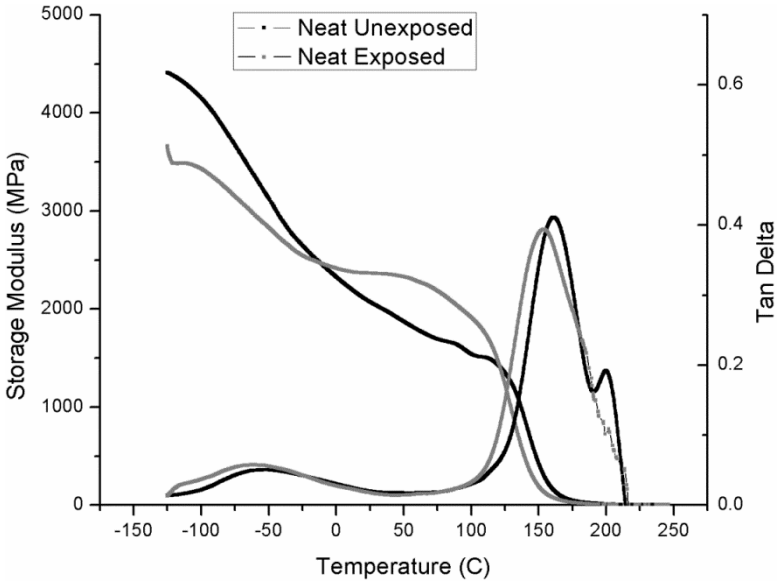

Figure 76. Neat DGEBA-44DDS DMA before and after atomic oxygen exposure.

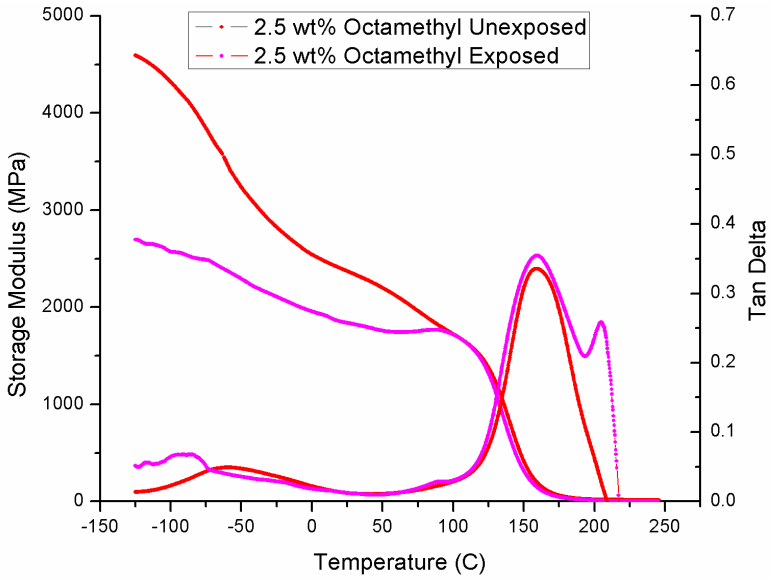

Figure 77. 2.5 wt% octamethyl POSS DMA before and after atomic oxygen exposure.[124]

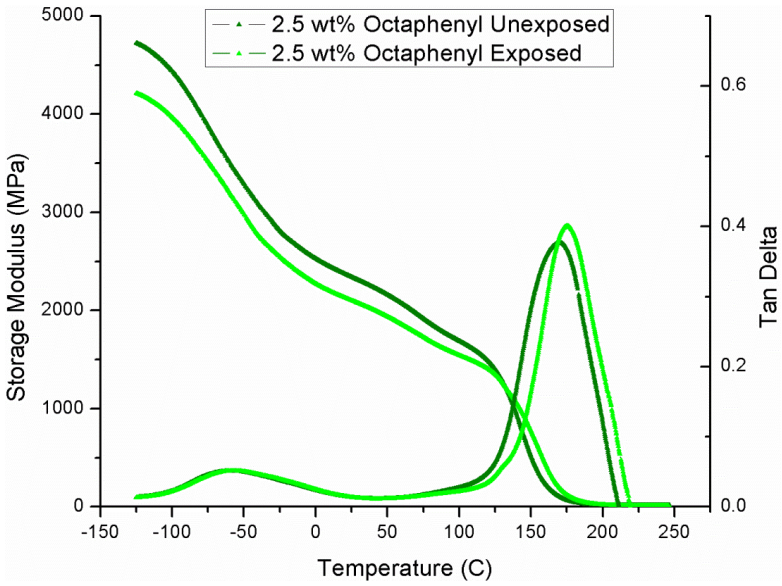

Figure 78. 2.5 wt% octaphenyl POSS DMA before and after atomic oxygen exposure.

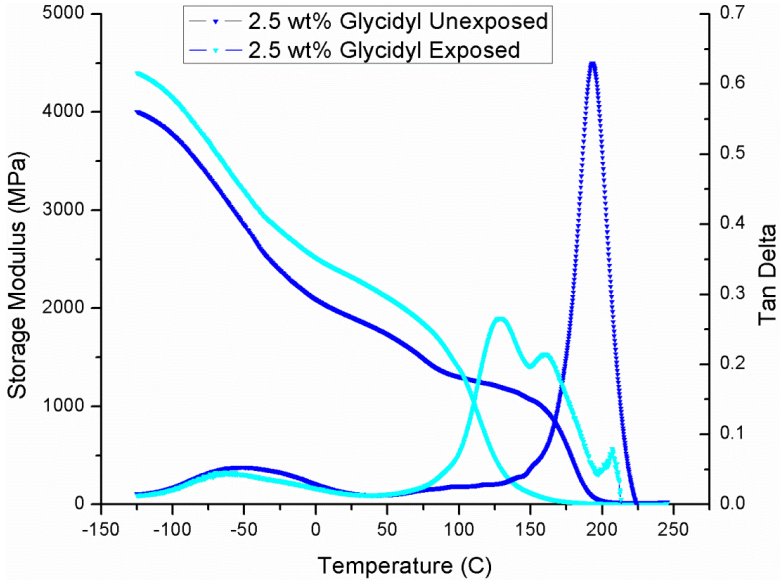

Figure 79. 2.5 wt% glycidyl POSS DMA before and after atomic oxygen exposure.

The storage modulus decreases and the tan delta curve reflected an additional peak for all sample types except octaphenyl POSS. Oxygen radical attack leading to chain scission is one of the main mechanisms of degradation, reducing

the integrity of the thermoset resin and leading to a decrease in modulus. Additionally, as the network fragments, areas of varied molecular weight are formed, leading to multiple glass transitions. A homogenous distribution of lower molecular weight areas would widen the tan delta curve, whereas a bimodal tan delta curve results from two differently eroded regions, indicating that degradation is heterogeneous.

Thermogravimetric Analysis of Atomic Oxygen Exposed Samples. Thermogravimetric analysis (TGA) was used to determine the thermal stability of unexposed and exposed specimens.[124] All three POSS materials (octamethyl in red, octaphenyl in green, glycidyl in blue) had similar mass losses to the neat DGEBA-44DDS (black) up to approximately 475 °C (Figure 80).

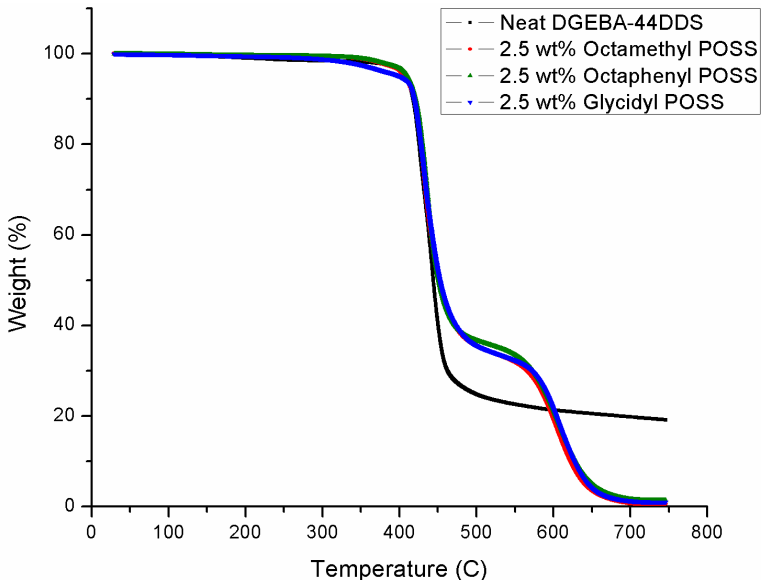

Figure 80. Thermal degradation of unexposed specimens.[124]

The second transition observed for the nanocomposite specimens only 575-625 °C was attributed to the inorganic content of the POSS cage. This is reasonable as POSS is often used as an additive for thermal stability.[11,124]

Exposed specimens showed the same initial transition, with a broader second transition extending past 750 °C (Figure 81 Top).[124]

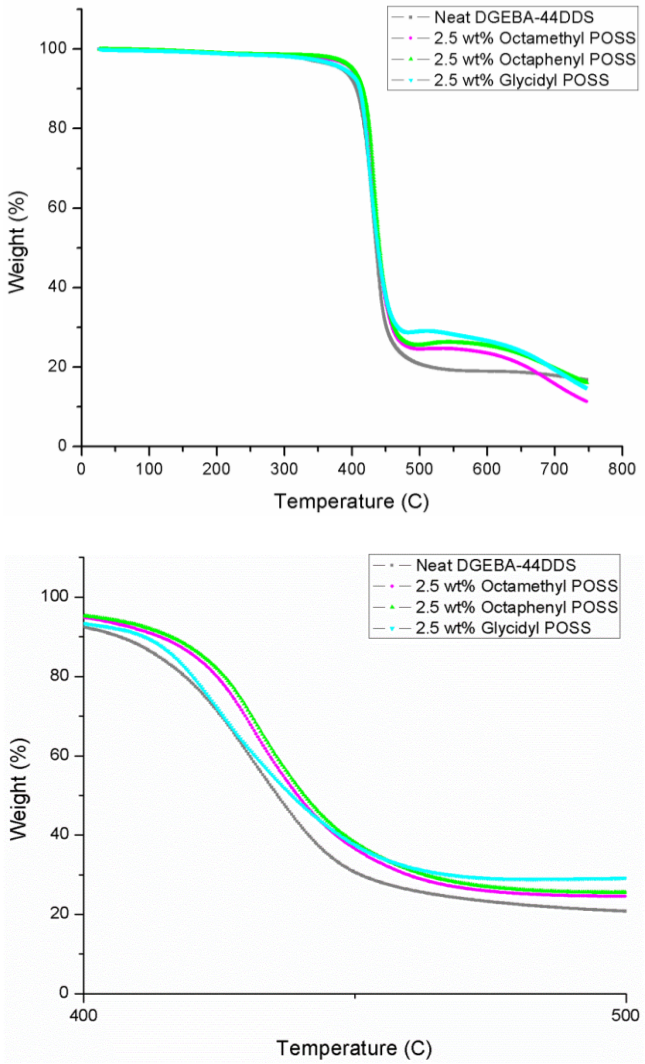

Figure 81. Top: thermal degradation of exposed specimens from 0 to 800 °C, and bottom: from 400 to 500 °C.[124]

The octamethyl and octaphenyl POSS additives did delay the onset of significant mass loss by approximately 5 °C (see the bottom plot of Figure 81). Thus, the POSS moieties did provide some protection against atomic oxygen degradation albeit not to the degree theoretically predicted with glassification of the POSS cage. Again, glycidyl POSS behaved differently in that it did not provide as

significant enhancement of protection against degradation by exposure to atomic oxygen[124]

Scanning Electron Microscopy. Scanning electron microscopy (SEM) was used to focus on the effects of atomic oxygen exposure on the surface morphology of the exposed specimens.[124] Micrographs were taken off the bottom sample-mold surface for both unexposed and exposed specimens. The unexposed neat thermoset surface displayed in Figure 82 did not exhibit any distinguishing features.

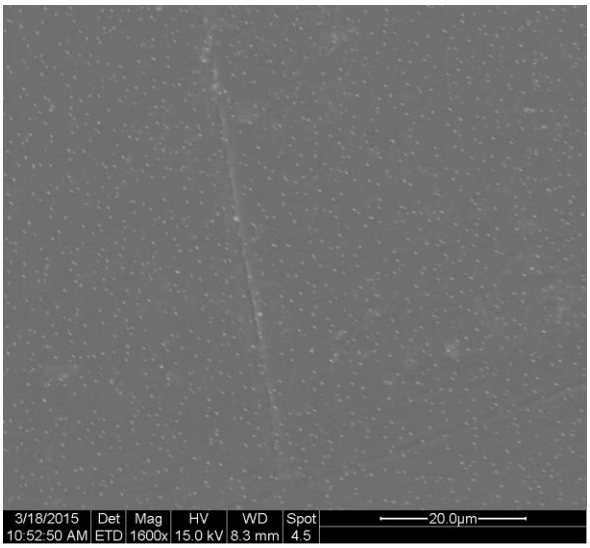

Figure 82. Unexposed surface of neat DGEBA-44DDS at 1600X.[124]

Energy dispersive (x-ray) spectroscopy (EDS) confirmed that the white speckles shown in Figure 82 were due to surface contamination or unreacted amine crosslinker.[124]

The unexposed surface of the 2.5 wt% octamethyl nanocomposite was covered with small holes (Figure 83).[124] This could be from off-gassing due to residual acetone.

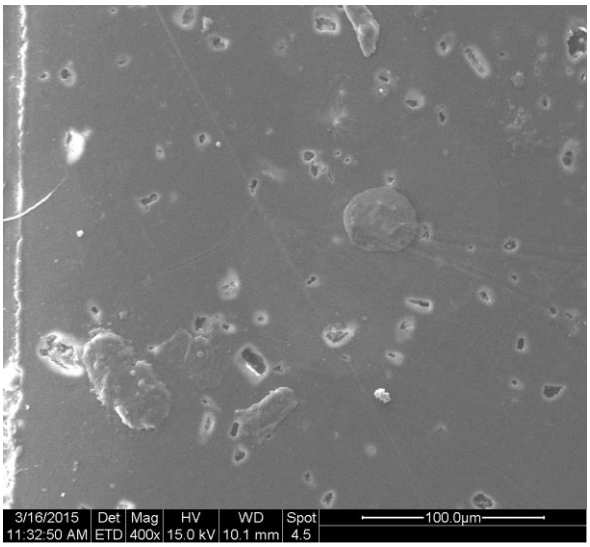

Figure 83. Unexposed surface of 2.5 wt% octamethyl specimen at a magnification of 400X.[124]

However, pores were not seen on the opposite surface, suggesting the source is related to the mold surface. The larger, unordered shapes were POSS-rich. The octaphenyl and glycidyl surfaces did not have pores but did have a variety of round aggregates in various sizes as shown in a representative view of a glycidyl POSS surface in Figure 84. At high magnification, these structures appear to consist of much smaller particles. The distribution and size of these circular features was random across the surfaces.[124]

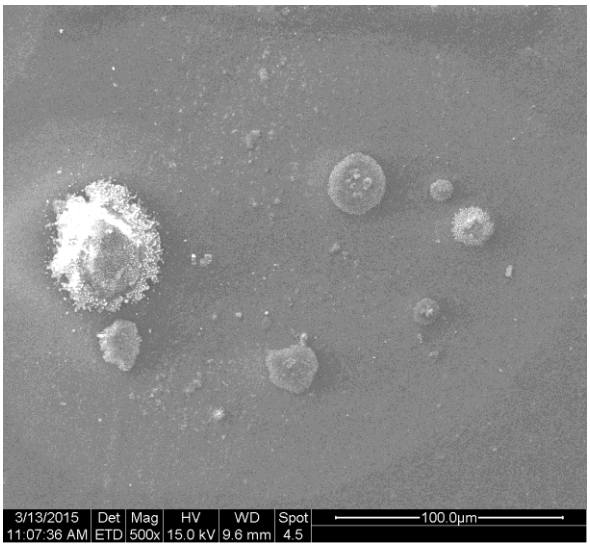

Figure 84. Unexposed surface of 2.5 wt% glycidyl specimen at a magnification of 500X.[124]

All four exposed sample types showed evidence of erosion after exposure. Neat DGEBA-44DDS (Figure 85) was covered with 2-5 µm diameter nodules.[124]

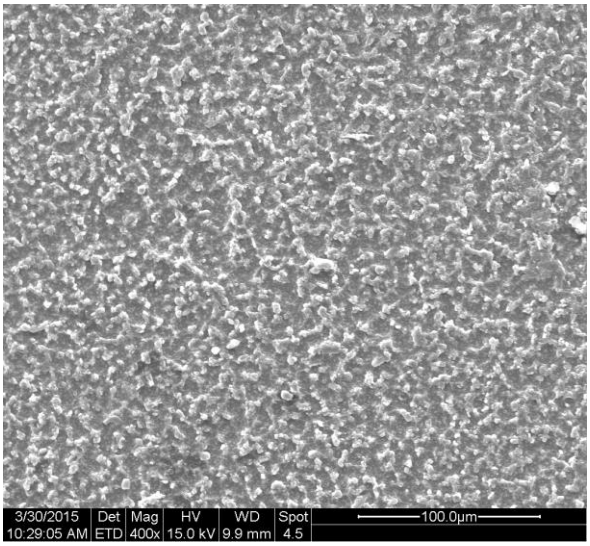

Figure 85. Exposed surface of neat DGEBA-44DDS at a magnification of 400X.[124]

The 2.5 wt% octamethyl surface featured occasional square POSS crystallites (Figure 86). The short octamethyl pendant allows the POSS cage to pack well, leading to the square shape.

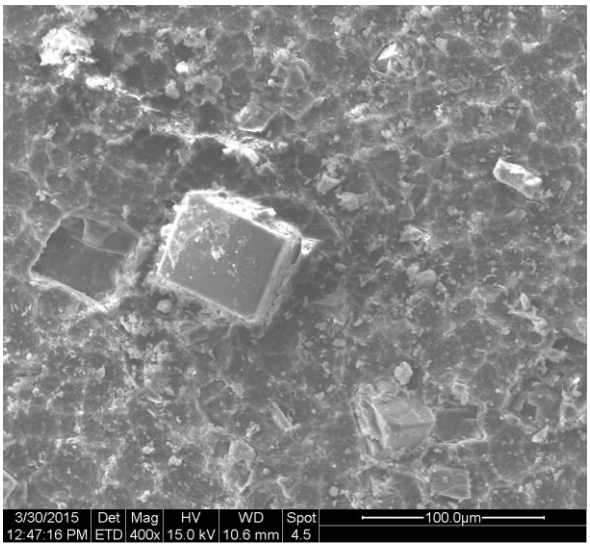

Figure 86. Exposed surface of 2.5 wt% octamethyl specimen at 400X.[124]

Although crystallites are present in the octaphenyl and glycidyl samples (Figure 87, 88), their shapes are not as uniform because the larger pendant groups prevent more efficient packing.

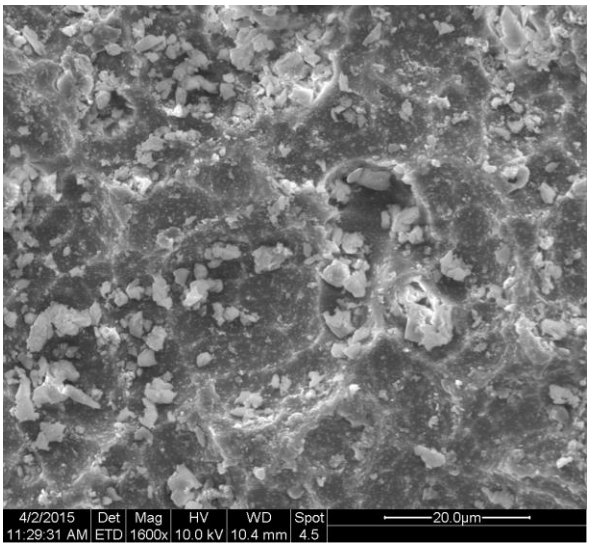

Figure 87. Exposed surface of 2.5 wt% octaphenyl specimen at a magnification of 400X.[124]

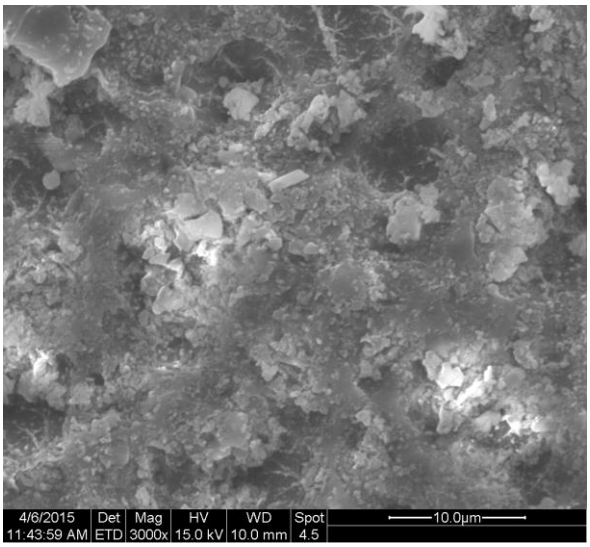

Figure 88. Exposed surface of 2.5 wt% glycidyl specimen at a magnification of 400X.[124]

No continuous film glassification of the POSS was observed for POSS-modified DGEBA-44DDS. A resultant –$[SiO_2]_x$– network generally displays a smooth morphology with limited cracking.[12] The lack of such morphology supports the idea that the concentration of POSS at the surface, and therefore the overall loading level, was insufficient for glassification and the resultant atomic oxygen protective layer.[124]

Atomic Force Microscopy. Atomic force microscopy (AFM) was performed on exposed surfaces. The neat DGEBA-44DDS exposed sample (Figure 89) was uniform and did not reflect the nodules shown in Figure 85. This can be explained by the ~100 µm scale of SEM compared to the AFM modulus map size of 1.5x1.5 µm.

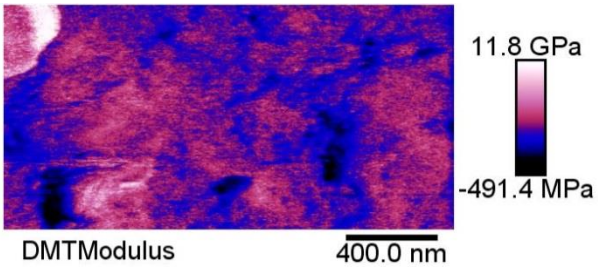

Figure 89. Exposed surface of neat DGEBA-44DDS.[124]

However, some octamethyl crystallites are small enough to be visible in a larger, 5x5 µm map of exposed 2.5 wt% octamethyl-DGEBA-44DDS. These show up as the white, high modulus, regions of Figure 90. The rest of the map is primarily lower modulus matrix.

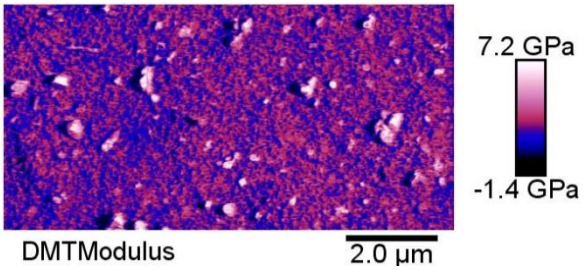

Figure 90. Exposed surface of 2.5 wt% octamethyl specimen.[124]

More POSS-rich regions were shown in the octaphenyl map as higher modulus, pink areas (Figure 91). No white, POSS crystallites were seen.

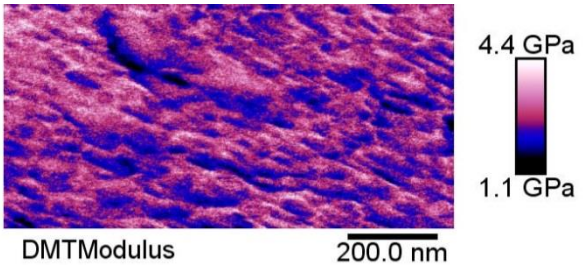

Figure 91. Exposed surface of 2.5 wt% octaphenyl specimen.[124]

Fairly homogeneous glycidyl-rich regions are circled in green on the 2.5 wt% glycidyl surface (Figure 92). The overall map was the most homogenous of all

exposed samples and may predict cohesive protection from glycidyl POSS at a higher loading level.

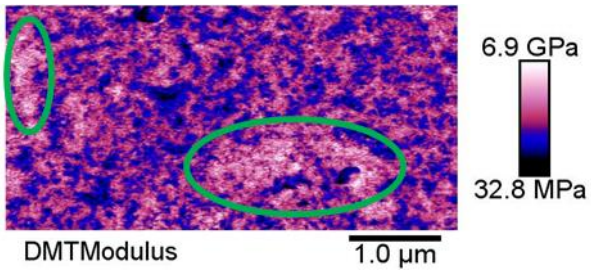

Figure 92. Exposed surface of 2.5 wt% glycidyl specimen.[124]

The 2.5 wt% glycidyl POSS in DGEBA-44DDS surface exhibited no morphological evidence of POSS glassification in any of the samples investigated.[124]

Conclusions

Atomic oxygen is a harsh oxidizing agent that can cause chain scission and network degradation in polymers, limiting the use of organic materials in low Earth orbit.[2,29] Thermoplastic coatings with polyhedral oligomeric silsesquioxanes have shown reduced mass loss and other property benefits when exposed to atomic oxygen and UV radiation.[12,81] The main protective mechanism is the transformation of POSS to a surface layer of passivating silica glass.[74] However, there is a gap in the understanding of POSS protection of thermosets against such hazards. In addition, it is not known if creating POSS-rich surfaces would result in less mass loss before glassification rather than dispersing POSS throughout the bulk of a matrix.

Octamethyl, octaphenyl, and glycidyl POSS were mixed in DGEBA-44DDS. Initially, only octamethyl and octaphenyl were cured in the epoxy-amine

matrix, which resulted in aggregations with a wide range of particle sizes and locations. Only 5 wt% octaphenyl POSS produced a POSS-rich surface at the bottom of bars due to POSS sedimentation. After this initial result, the miscibility of the three POSS moieties was evaluated with Teas diagrams. The glycidyl POSS had a similar miscibility region to the DGEBA monomer. However, the octamethyl and octaphenyl POSS moieties had significantly smaller miscibility regions, possibly explaining their aggregation in DGEBA-44DDS.

Modifying the cure protocol to allow POSS more time to sediment at the interface resulted in more pronounced regions of octamethyl and octaphenyl at the bottom of 2.5 and 5 wt% octaphenyl POSS-DGEBA-44DDS and 5 wt% octamethyl-DGEBA-44DDS bars. The thickness of the sediment layer was dependent on loading level and POSS type. Standard deviations in glass transition temperature decreased, indicating more uniform samples with the modified cure prescription. However, high standard deviations were observed in the tensile and flexural test results, preventing definite conclusions to be reached on the relationships between the composite attributes and mechanical properties of the materials.

In an atomic oxygen exposure study, neat DGEBA-44DDS and 2.5 wt% octamethyl, octaphenyl, and glycidyl POSS in DGEBA-44DDS were examined for mass loss, and changes in glass transition temperature, thermal degradation, and morphology.[124] Unexpectedly, POSS-inclusive samples did not decrease mass loss per area compared to the neat DGEBA-44DDS. This was attributed to insufficient loading level of POSS. After exposure, glass transition temperatures

dropped significantly for the neat and glycidyl samples. Thermal stability after exposure differed from control specimens in that the neat DGBEA-44DDS specimen began to show mass loss at a slightly lower temperature than the POSS-filled specimens and the secondary transition of the composites broadens. Scanning electron microscopy showed that neat DGEBA-44DDS was eroded by the atomic oxygen, leading to a pattern of micron-scale nodules. Erosion was also seen in the 2.5 wt% POSS-DGEBA-44DDS surfaces but as a less homogeneous pitted motif. Atomic force microscopy established that the glycidyl POSS nanocomposite had the most homogeneous surface in terms of POSS coverage. Neither SEM nor AFM studies found evidence of POSS glassification during exposure, indicating the need for a higher concentration of the additive.[124]

The homogenous surfaces of the 2.5 wt% glycidyl POSS-DGEBA-44DDS focused attention on this specific POSS moiety. In addition, this may disprove the hypothesis that POSS layered at a surface would provide enhanced protection against atomic oxygen compared to well dispersed POSS in the bulk of a material. Therefore, focus shifted to making POSS-rich coatings to be placed over polymers. Additional work was then done to add cerium oxide for UV radiation protection.

CHAPTER IV – POSS AND CERIUM COMPOUNDS

Introduction

Previous experiments that mixed POSS moieties in an epoxy-amine matrix resulted in sedimentation of POSS particulates unless the POSS could react into the matrix. This sedimentation did not glassify under exposure to atomic oxygen and did not reduce mass loss compared to neat epoxy-amine. This was thought to be due to the lack of nanoscale dispersion of the additives, leaving large gaps of exposed matrix between micron-sized aggregates as detected by atomic force microscopy of the exposed surfaces. A different approach was needed to use POSS to protect epoxies against atomic oxygen.

Spray coating of oxides with an epoxy binder is a common method of protecting composites in orbit. These coatings are difficult to apply consistently and suffer from defects that lead to underpinning damage.[60] Pinhole defects in coatings allow for the infiltration of degradants such as photons or atomic oxygen atoms into the matrix that are then trapped underneath. These degradants then spend more time in the matrix, causing a greater degree of damage. Thus, the overall goal of this entire study is to construct a dense layer of POSS over the surface of an epoxy matrix composite in order to provide better protection to composite materials in low Earth orbit. The initial approach, inducing POSS transport to the surface of the matrix during cure, was not effective. A matrix with a surface coating of POSS may provide an alternative route to protection against atomic oxygen and other hazards. In addition, open cage trisilanol POSS could

be used to act as a dispersant for CeO_2 in a matrix, creating a particle with both atomic oxygen and UV radiation resistance.

Results and Discussion

The objectives of this project were to combine POSS and CeO_2 for enhanced protection of an epoxy matrix in low Earth orbit. This was attempted by casting a coating of POSS, CeO_2 and crosslinker over an epoxy-POSS-imidazole matrix. Additionally, trisilanol POSS and CeO_2 were reacted to synthesize a particle with UV radiation and atomic oxygen durability. Trisilanol phenyl POSS and cerium (III) nitrate hexahydrate created a mixture termed CePOSS that was more UV absorbent than either precursor.

X-37 Project

In March 2014, Boeing Defense, Space, and Security Division offered Polymer researchers at USM the opportunity to fly samples on the X-37b Air Force experimental test vehicle (Figure 93).[147] The experiment proposed would be a “suitcase” exposure similar to the Materials International Space Station Experiments (MISSE).[3] Samples of 1 in diameter would be placed in slots, such as the ones shown in Figure 94, in a closed case and then opened while the payload bay doors of the X37b were open in low Earth orbit (LEO).

Figure 93. X37b experimental test vehicle.[147]

Figure 94. MISSE samples deployed on the International Space Station.[3]

Due to aforementioned issues with POSS phase segregation and a 6-week timeline for sample production, the decision was made to cure a POSS-rich coating over an epoxy matrix. Cerium (IV) oxide would be added to this coating to enhance UV protection and a relatively small amount of an amine crosslinker, 3,3'-diaminodiphenyl sulfone (33DDS) was added to bond the layers together.[63] After dynamic mechanical analysis (DMA) testing to ensure ductility based on storage modulus, the matrix chosen was a combination of glycidyl POSS, tetraglycidyl 4,4′-diaminodiphenylmethane (TGDDM) epoxy, and Lindax 1, an imidazole curative. Four samples were produced for flight:

1. Matrix without coating (exposed control)

2. 5 wt% CeO_2/20 wt% 33DDS/75 wt% Glycidyl POSS coating over matrix
3. 5 wt% CeO_2/20 wt% 33DDS/75 wt% Glycidyl POSS coating over matrix

*Sample treated for 15 min in 10 W plasma oven before shipment to MSFC to attempt to form passivating layer before flight.

4. 15 wt% CeO_2/20 wt% 33DDS/65 wt% Glycidyl POSS coating over matrix

The coating layer was prepared first by mixing with a specialized rotor attached to a dremel known as a “tissue tearor” (Figure 95).

Figure 95. Tissue tearor mixing rotor.

Once mixed, the mixture was cast into a steel mold of 1 in diameter and 0.2 in thickness preheated to 80 °C. The coating was measured volumetrically to attempt to create a layer 0.05 in thick. After letting the coating adjust to temperature and mold, the matrix was poured over to finish filling the mold slots. Cure commenced immediately. After completion, samples were gently removed from the mold to produce the disk shown in Figure 96.

Figure 96. Surface coated composite disk.

The white coating layer was distinct from the darker, maroon matrix and there were no issues with cohesion when handled manually. This is due to the 33DDS crosslinker acting as a bridge between epoxy functionalities in both layers.

The X37b vehicle launched in May 2015 and is thought to currently be in a polar LEO orbit.[147] Due to mission security, no other information is available on the status of the samples. Hopefully, upon return, samples will be evaluated for mass loss, surface morphology, and other properties. Although flight samples are unavailable for analysis as of Fall 2016, these surface coated disks were thought to be still worth investigating further given the issues with sedimentation of POSS in DGEBA-44DDS as detailed in the previous chapter.

Processing of Surface Coated Epoxy Disks

At the time of production, no timeline was given by collaborators as to when the X-37b samples would fly and then be returned for analysis. Therefore, additional surface coated disks were made to better understand the system before the flight samples returned. Samples were made by two methods, which were different in the placement of the coating. Method 1 was described above wherein the coating is placed into the heated mold, allowed to settle, and then the matrix is cast on top. Cure starts immediately after addition of the matrix.

During the casting process, the matrix displaced the coating, pushing it out to the sides of the mold well. However, because the coating is denser than the matrix, it settled to the bottom of the well during cure, producing the separation shown in Figure 97. This was the method used for the X-37b samples.

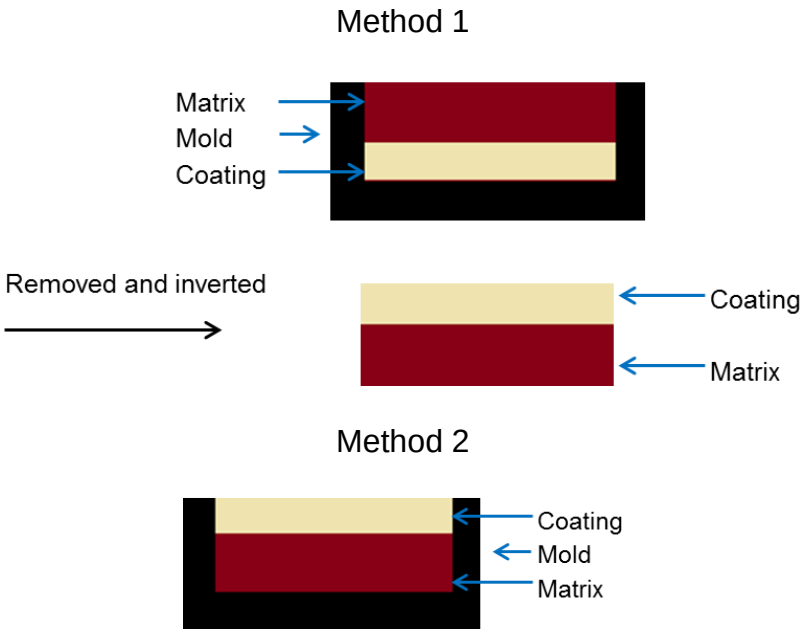

Figure 97. Method 1 (top) and Method 2 (bottom) of disk preparation (layer size not to scale).

Method 2 consists of the matrix being poured into the mold, leaving a gap at the top of the wells. To avoid mixing, rheological measurements were conducted on the TGDDM-glycidyl POSS-Lindax 1® matrix (Figure 98) during cure using parallel plate rheology at constant strain of 0.1% and constant frequency of 1 Hz. The cure conditions were as follows: each sample was held for 2 h at 80 °C and then was immediately heated to 120 °C until gelation. Gelation was defined as the point at which the storage modulus, G', becomes greater than G", the loss modulus.[118] This indicated when the polymer

transitioned from “liquid-like” to “solid-like” and marked the onset of significant crosslinking in the thermoset network.[118]

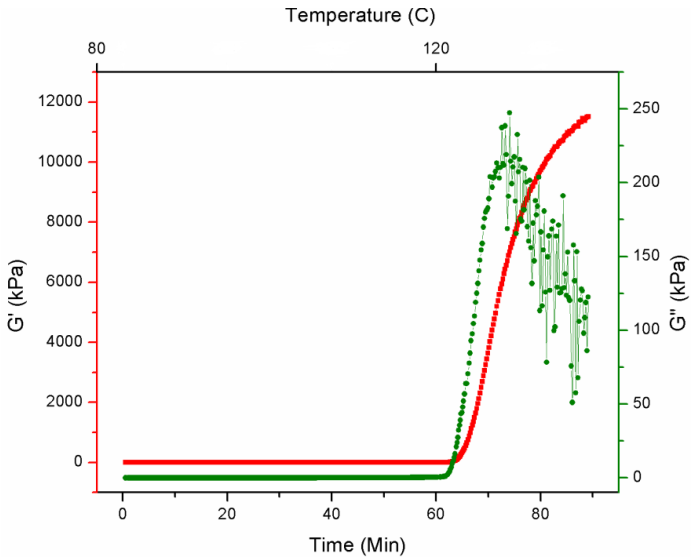

Figure 98. G’ (red) and G” (green) versus temperature and time for TGDDM-glycidyl POSS-Lindax 1 matrix.

From the rheological data, gelation occurred at approximately 15 minutes into the 120 °C isothermal hold time. This experiment did not correspond exactly to Boeing’s cure prescription due to the lack of ramp between the 80 °C and the 120 °C isothermal hold-time. However, this ramp is conducted at 5 °C/min and only lasts for 4 minutes. Therefore, for method 2, the matrix is added to the mold with some space left at the top of the mold wells for the coatings. Cure commenced as usual, and then after 30 min at 120 °C, the coating was cast on top of the matrix. At this point, gelation had almost certainly begun, and therefore, matrix viscosity should have been high enough to prevent the coating from substantially diffusing into the matrix. However, vitrification of the matrix had not occurred at that point in the process, so there was still the opportunity for the coating to bond to the matrix through the 33DDS amine crosslinker.

Seven types of composites were made:

1. Neat matrix without coating
2. 5 wt% CeO_2/20 wt% 33DDS/75 wt% glycidyl POSS cured under matrix (Method 1)
3. 5 wt% CeO_2/20 wt% 33DDS/75 wt% glycidyl POSS cured over matrix (Method 2)
4. 33 wt% CeO_2/17 wt% 33DDS/50 wt% glycidyl POSS cured under matrix (Method 1)
5. 33 wt% CeO_2/17 wt% 33DDS/50 wt% glycidyl POSS cured over matrix (Method 2)
6. 10 wt% 33DDS/90 wt% glycidyl POSS cured under matrix (Method 1)
7. 10 wt% 33DDS/90 wt% glycidyl POSS cured over matrix (Method 2)

Both methods produced a distinct coating over the matrix after cure. Each specimen was cast to a total thickness of 0.2 in. However, the thickness of the individual layers did vary depending on the processing method and chemical composition. The specific thickness of the coating layers for 3-4 specimens for each sample type were measured with calipers and recorded in Table 9.

Table 9

Thickness of Coating Layers

Sample	Coating Thickness (in)
5 wt% CeO_2/20 wt% 33DDS/75 wt% Glycidyl POSS Method 1	0.064 +/- 0.015
5 wt% CeO_2/20 wt% 33DDS/75 wt% Glycidyl POSS Method 2	0.088 +/- 0.017
33 wt% CeO_2/17 wt% 33DDS/50 wt% Glycidyl POSS Method 1	0.109 +/- 0.032
33 wt% CeO_2/17 wt% 33DDS/50 wt% Glycidyl POSS Method 2	0.084 +/- 0.011
10 wt% 33DDS/90 wt% Glycidyl POSS Method 1	0.083 +/- 0.011
10 wt% 33DDS/90 wt% Glycidyl POSS Method 2	0.057 +/- 0.08

As can be seen above, coating thickness did vary by approximately 25 % of the total sample thickness. This variation arose from the difficulty of measuring out the viscous coating and matrix by hand into the mold. In addition, the coatings that included CeO_2 were thicker than the POSS/33DDS combinations.

Neat DGEBA-44DDS. Specimens of neat matrix had an opaque, maroon appearance (Figure 99).

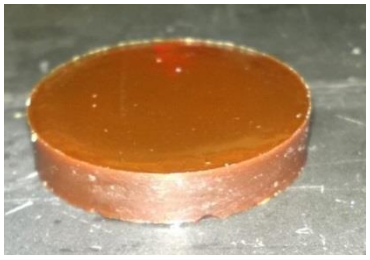

Figure 99. Neat DGEBA-44DDS disk.

The top of the sample was slightly concave, due to cure shrinkage. Disks did not exhibit cracking or chipping around the edge unless removed from the mold before completely cooling.

5 wt% CeO_2/20 wt% 33DDS/75 wt% glycidyl POSS – Method 1. The first trials with the 5 wt% CeO_2 coating were cast with the coating at the bottom of the mold and were then flipped over when removed, termed Method 1 (Figure 100).

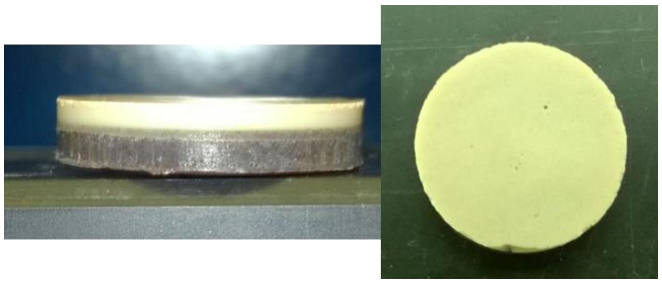

Figure 100. (L) Side and (R) top of 5 wt% CeO_2/20 wt% 33DDS/75 wt% glycidyl POSS Method 1 specimen.

The CeO_2 coating produced an opaque, cream-colored layer. This is the same color as the CeO_2 additive. The matrix looked duller compared to the neat specimen in Figure 99. During Method 1, the coating mixes with the matrix pushing the coating out to the sides of the well before the denser coating settles back to the bottom. Therefore, there may be some CeO_2-rich residue at the sides of the sample. Some porosity was also seen on top of the coating layer. This was attributed to off-gassing that was trapped by the bottom of the mold to create these defects.

One disk was cryo-fractured for scanning electron microscopy/energy dispersive x-ray spectroscopy (SEM/EDS) analysis. Figure 101 presents a broad view of the coating layer at 40X.

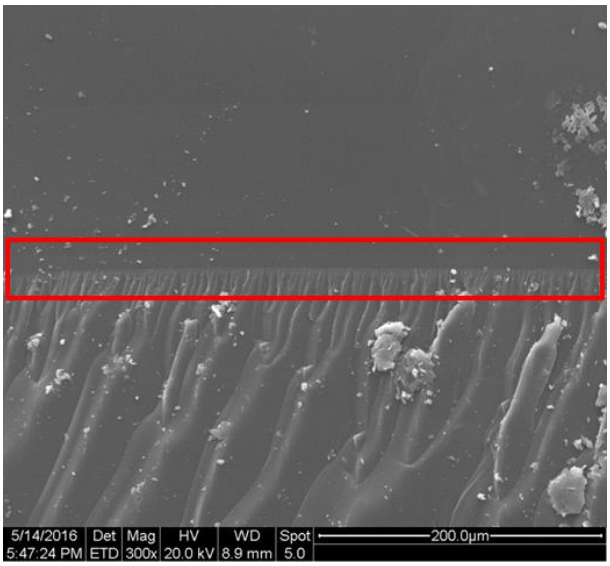

Figure 101. Coating over matrix in 5 wt% CeO_2/20 wt% 33DDS/75 wt% glycidyl POSS Method 1 disk at 300X.

The red box in Figure 101 indicates the division between coating (above) and matrix (below). Elemental analysis with EDS at 3000X was done for the

presence of Ce depthwise through the disk at four spots: middle of matrix, interface between matrix and coating, middle of coating, and the top of the coating. Results in Table 10 indicate the highest concentration of Ce resided at the top of the coating layer. EDS revealed that the larger white flecks in Figure 101 did not contain Ce, but are probably artifacts of the fracture surface or post-fracture contaminants.

Table 10

Ce wt% by depth via EDS in 5 wt% CeO_2/20 wt% 33DDS/75 wt% glycidyl POSS specimen Method 1

Position	Ce Weight Percent (wt%)
Coating Top	5.55 +/- 0.04
Coating Middle	2.84 +/- 0.05
Interface Coating/Matrix	0.00 +/- 0.00
Matrix	0.00 +/- 0.00

Figure 102 demonstrates the higher density of Ce at the coating surface. The lighter, gray areas were found to be indicative of CeO_2-rich spots and showed up as higher intensity green in EDS mapping.

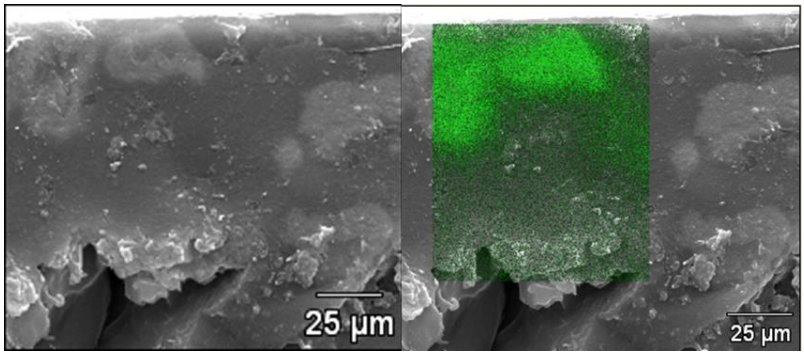

Figure 102. (L) Top of coating and (R) Ce overlay (green) at 3000X.

The density of CeO_2 is 7.13 g/mL at 25 °C, much higher than the density of glycidyl POSS (1.25 g/mL at 25 °C).[108,135] Therefore, as the coating mixture fell to

the bottom of the mold because of density differences with the matrix, within the coating the CeO_2 also settled at the bottom mold surface through a gravity driven sedimentation. After removal from the mold, this bottom surface became the top of the disk as part of the disk inversion characteristic of Method 1. This sedimentation of CeO_2 was verified from observing the coating surface in Figure 103 at 1000X.

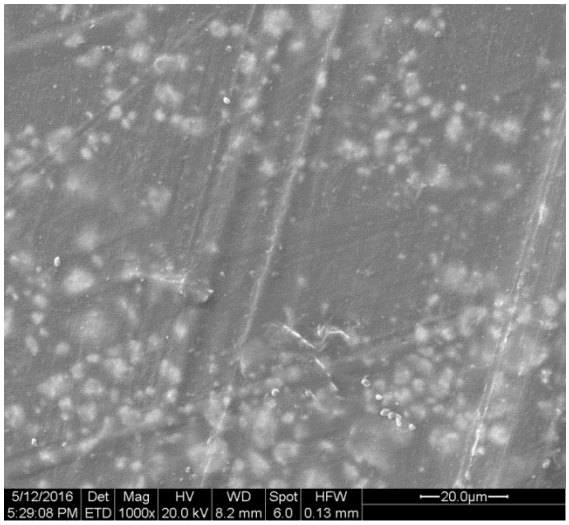

Figure 103. Coating surface from 5 wt% CeO_2/20 wt% 33DDS/75 wt% glycidyl POSS Method 1 disk at 1000X.

Light gray, cerium rich areas were common on the surface. Elemental analysis gave an average Ce concentration of 14.12 +/- 0.07 wt% at the surface. Again, this surface was originally the bottom of the disk during cure, allowing for the sedimentation of cerium (IV) oxide and was then inverted after removal from the mold. The striations seen in the figure are due to the texture of the polymer surface used for mold release.

5 wt% CeO_2/20 wt% 33DDS/75 wt% glycidyl POSS – Method 2. Method 2 adds the coating above the matrix after gelation, so there is minimal mixing

between layers. The 5 wt% CeO_2 disks produced by this method had convex surfaces compared to disks from Method 1 because the coating was at the top of the mold during cure. This meant the coating was not contacting a flat surface and could also be overfilled since the mold had no top (Figure 104).

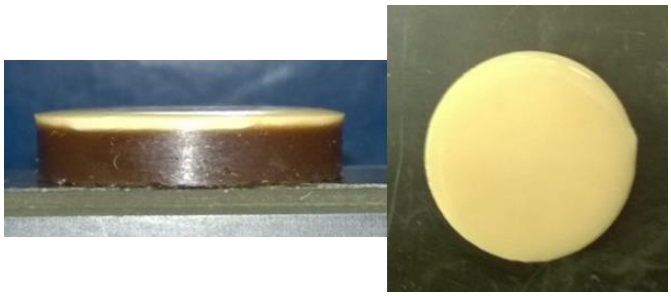

Figure 104. (L) Side and (R) top of 5 wt% CeO_2/20 wt% 33DDS/75 wt% glycidyl POSS Method 2 disk.

The lack of a mold surface at the top of the coating in Method 2 accounts for the lack of porosity compared to the Method 1 specimen of the same material as any gasses generated during cure are not trapped in the sample. Elemental analysis under SEM at 3000X showed the effects of changing the curing method with the majority of CeO_2 concentrated directly above the coating/matrix interface (Figure 105). In Method 1, the bottom of the coating during cure is the top of the disk, and this becomes the surface after the Method 1 disks are removed from the mold and inverted. However, in Method 2, the coating is cast over the matrix, so the bottom of the coating is always the bottom as there is no need for inversion of the disks. The settling of CeO_2 was also seen in these samples but at the bottom of the coating layer as detailed in Table 11.

Table 11

Ce wt% by depth via EDS in 5 wt% CeO_2/20 wt% 33DDS/75 wt% glycidyl POSS Method 2 disk.

Position	Ce Weight Percent (wt%)
Coating Top	1.54 +/- 0.11
Coating Middle	5.13 +/- 0.13
Interface Coating/Matrix	17.57 +/- 0.17
Matrix	0.00 +/- 0.00

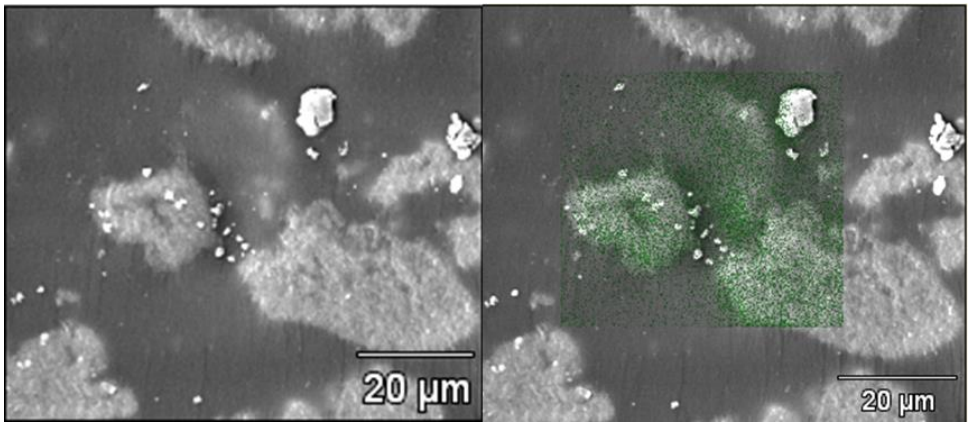

Figure 105. (L) Coating above interface and (R) Ce overlay (green) in 5 wt% CeO_2/20 wt% 33DDS/75 wt% glycidyl POSS Method 2 disk at 3000X.

As previously stated, in Method 2 the coating is cast over the matrix once gelation occurs. Therefore, if CeO_2 moves via a sedimentation mechanism, it will fall in the coating until it encounters the viscous, partially cured matrix layer. This illustrates the major impact of processing methods on the location of cerium (IV) oxide particulates. Method 1 creates a CeO_2 rich area over CeO_2, crosslinker, and POSS, whereas Method 2 sequesters the CeO_2 region under the general mixture as sketched in Figure 106.

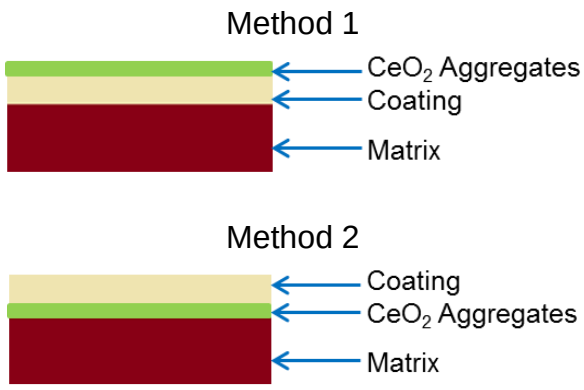

Figure 106. Location of layer of CeO_2 aggregates in Method 1 versus Method 2.

33 wt% CeO_2/17 wt% 33DDS/50 wt% glycidyl POSS – Method 1. Coatings with the highest feasible loading level of CeO_2 were made to provide multiple options for CeO_2 loading. This loading level was established by adding CeO_2 into glycidyl POSS until the oxide could no longer be suspended in the POSS. The ratio of 0.6:1 CeO_2:glycidyl POSS was the largest possible while still wetting all of the CeO_2 with glycidyl POSS. This resulted in coatings having 33 wt% CeO_2, 50 wt% glycidyl POSS, and 20 wt% 33DDS. However, the solution had a higher viscosity than the 5 wt% CeO_2 coating and was more difficult to cast into the mold at a consistent thickness even when heated to 80 °C for 15 to 20 minutes. This dense mixture resulted in the thickest coating layers of 0.109 +/- 0.032 in (Figure 107).

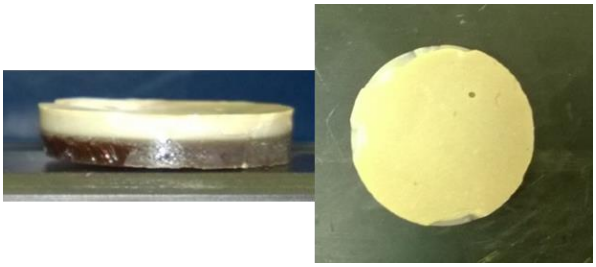

Figure 107. (L) Side and (R) top of 33 wt% CeO_2/17 wt% 33DDS/50 wt% glycidyl POSS Method 1 disk.

Porosity was seen at the top of the coating similar to the 5 wt% CeO_2 Method 1 disk. Chipping at coating edges was attributed to the decrease in ductility of the coating with the addition of more CeO_2. The depthwise distribution of CeO_2 in the 33 wt% CeO_2 Method 1 specimen recorded in Table 12 was different than the 5 wt% CeO_2 Method 1 specimen. Higher levels of Ce were seen in the coating both at the surface and right above the coating matrix interface rather than just at the top of the coating of the 5 wt% CeO_2 Method 1 specimen. This could be attributed to the saturation of the coating with CeO_2.

Table 12

Ce wt% by depth via EDS in 33 wt% CeO_2/20 wt% 33DDS/75 wt% glycidyl POSS specimen Method 1.

Position	Ce Weight Percent (wt%)
Coating Top	24.50 +/- 0.11
Coating Middle	17.39 +/- 0.12
Interface Coating/Matrix	22.35 +/- 0.09
Matrix	0.00 +/- 0.00

One commonality with other sample types was the lack of detectable CeO_2 in the matrix. This was also expected in 33 wt% CeO_2 Method 2 specimens.

33 wt% CeO_2/17 wt% 33DDS/50 wt% glycidyl POSS – Method 2.

Specimens with the CeO_2 saturated coating cast over the matrix had significant issues with thickness consistency. One example is presented in Figure 108.

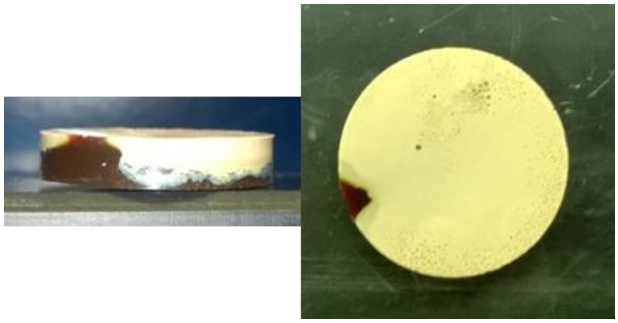

Figure 108. (L) Side and (R) top of 33 wt% CeO_2/17 wt% 33DDS/50 wt% glycidyl POSS Method 2 specimen.

Porosity was seen at the surface even with the Method 2 processing where the coating surface is exposed to air. This was not seen with the 5 wt% CeO_2 Method 2 disks. Therefore, the 33 wt% CeO_2 coating may have been more viscous 5 wt% CeO_2 coating, and therefore, trapped off-gassing from the underlying matrix.

Cerium-rich areas (highlighted in green) were seen at the top of the Method 2 coating layer in Figure 109. This was also the top of the coating during fabrication as Method 2 disks were not inverted after cure. This was an unexpected observation given that coatings fabricated using a lower loading level of CeO_2 and Method 2 produced Ce-rich areas directly above the interface (Figure 109).

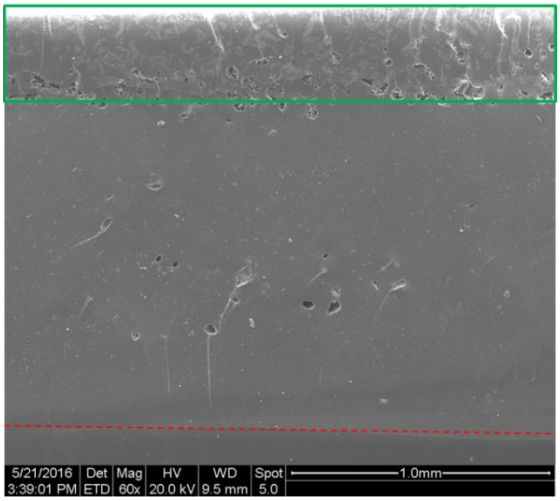

Figure 109. Coating layer of 33 wt% CeO_2/17 wt% 33DDS/50 wt% glycidyl POSS Method 2 over matrix (interface as dotted red line) with Ce-rich areas noted by the green rectangle at 60 X.

Elemental analysis of sample cross-sections by EDS is summarized in Table 13.

This does show less Ce deeper into the coating, compared to the 33 wt% CeO_2 Method 1 sample.

Table 13

Ce wt% by depth via EDS in 5 wt% CeO_2/20 wt% 33DDS/75 wt% glycidyl POSS specimen Method 2

Position	Ce Weight Percent (wt%)
Coating Top	11.11 +/- 0.11
Coating Middle	8.97 +/- 0.15
Interface Coating/Matrix	2.46 +/- 0.08
Matrix	0.03 +/- 0.03

Elemental analysis was also conducted on the top surfaces of both the Method 1 and Method 2 33 wt% CeO_2 coatings. The surface of Method 1 had a Ce concentration of 10.32 +/- 0.05 and the surface of Method 2 had 14.98 +/- 0.07 wt% Ce.

10 wt% 33DDS/90 wt% glycidyl POSS – Method 1 and 2. Coatings with only glycidyl POSS and 33DDS were also made. The minimum amount of 33DDS needed was found to be 10 wt% as combinations of glycidyl POSS and less than 10 wt% 33DDS remained tacky after cure. Due to the lack of cream colored CeO_2 additive, these layers were harder to distinguish visually from the matrix for measurement purposes, as shown in Figure 110.

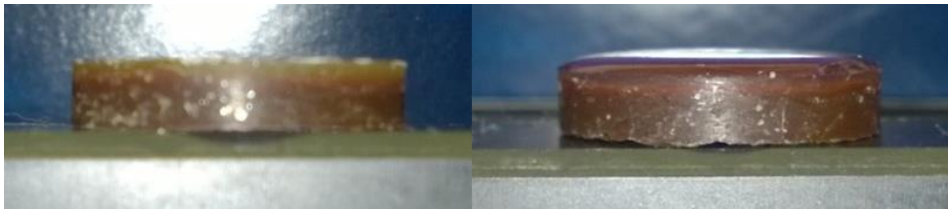

Figure 110. Disks of 10 wt% 33DDS/90 wt% glycidyl POSS using (L) Method 1 and (R) Method 2.

Both coatings were translucent up to the coating matrix interface. It was not possible to manually separate the coating and matrix layers with samples of either method.

Overall, the sedimentation behavior of CeO_2 in CeO_2/glycidyl POSS/33DDS layers indicated a lack of strong interactions between CeO_2 and glycidyl POSS. There was no capture of the CeO_2 by the glycidyl functional group to disperse CeO_2 throughout the matrix. However, preparation of the dual layer composites proved the ability to bond POSS-rich layers to an epoxy matrix through the amine crosslinker. In addition, the sedimentation mechanism of CeO_2 aggregation highlighted the importance of processing methods.

Plasma Treatment of Surface Coated Disks

Surface coated disks were produced for plasma exposure at Surfx Plasma in an effort to induce glassification of the POSS-rich coatings. Three types of samples were produced for exposure. These were distinguished by their coating composition and processing method:

1. 0 wt% 33DDS/90 wt% glycidyl POSS coating, Method 2
2. 5 wt% CeO_2/20 wt% 33DDS/75 wt% glycidyl POSS coating, Method 1
3. 5 wt% CeO_2/20 wt% 33DDS/75 wt1% glycidyl POSS coating, Method 2

Two disks of each of the three sample types were treated using an Atomflo 500 plasma system at Surfx Plasma in Redondo Beach, California. The plasma produced was from a 100:1 ratio of argon to oxygen gas at a power level of 120 W. One pass at 1 mm/s was made with the instrument over the coating surface of each disk at a 4 mm distance.

Water Contact Angle. Three water contact angle measurements were made on each coating surface before and after exposure. The initial contact angle values decreased with increasing amounts of CeO_2 at the surface (Table 14), indicating that this species created a more hydrophilic surface than just glycidyl POSS and crosslinker.

Table 14

Water contact angle measurements

90 wt% Glycidyl Method 2		**5 wt% CeO_2 Method 1**		**5 wt% CeO_2 Method 2**	
Before	After	Before	After	Before	After
100.70 +/- 0.02	9.10 +/- 0.52	83.60 +/- 3.75	58.70 +/- 3.39	90.30 +/- 3.32	9.10 +/- 3.84

After plasma treatment, the contact angles of the 90 wt% glycidyl POSS and 5 wt% CeO_2 Method 2 surfaces were significantly reduced. The decrease in contact angle from about 100º to about 9º indicates surface oxidation. However, the change in contact angle after plasma treatment was less evident for the 5 wt% CeO_2 Method 1 disks. Since Ce^{4+}, as found in CeO2, is the highest oxidation state of cerium, its presence at the coating surface (Figure 103) limits the species available for plasma oxidation, and therefore, minimizes measurable changes in surface free energy.

ATR FT-IR. As previously described, the mechanism of POSS glass formation is thought to be the ablation of carbon-rich pendant groups leading to the rearrangement of the cage into a SiO_x layer.[74] Spectra of unexposed and exposed surfaces were compared to look for growth in Si-O bonding at 1100-1000 cm^{-1} with corresponding decreases in the –CH2-CH2- (2950, 2850 cm^{-1}) and C-O (3600-3250 cm^{-1}) peaks of the glycidyl pendant group.[148]

Both the 90 wt% glycidyl POSS and 5 wt% CeO_2 Method 2 processed disks had nearly identical spectra before and after plasma exposure (Figures 111 and 112)

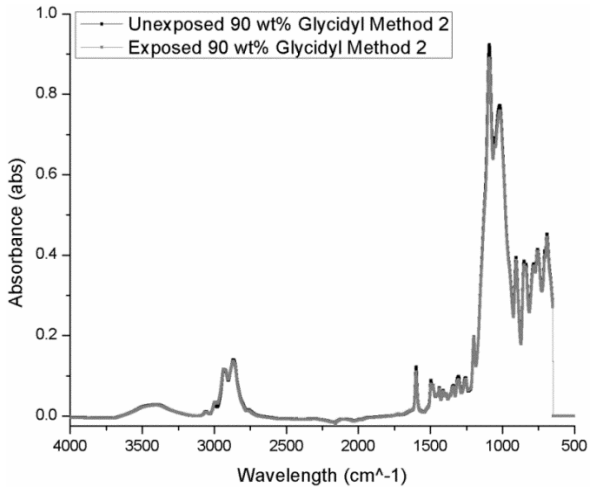

Figure 111. ATR FT-IR spectra of 90 wt% glycidyl POSS Method 2 coating before (black) and after (gray) plasma.

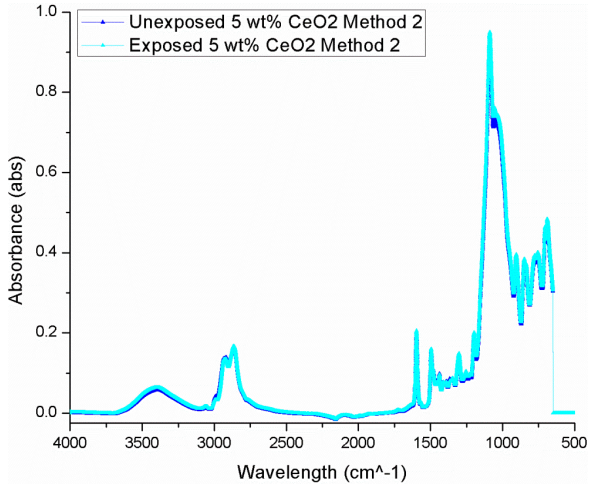

Figure 112. ATR FT-IR spectra of 5 wt% CeO_2 Method 2 coating before (dark blue) and after (light blue) plasma.

The Si-O peak from the POSS cage was highly pronounced in each spectra at approximately 1100 cm^{-1} regardless of whether plasma treatment had been conducted or not. Each spectrum also contained $–CH_2-$ bands at 2950 and 2850 cm^{-1} with a broad C-O stretch centered at 3400 cm^{-1}. Although surface oxidation was indicated by contact angle changes, it was not revealed by changes in the carbon or silicon based peaks.

Results differed with the 5 wt% CeO_2 Method 1 sample with CeO_2 aggregates at the coating surface. Plasma treatment almost eliminated the C-O and $–CH_2-$ bands but also significantly reduced the Si-O peak (Figure 113). It should be noted that both of these spectra were measured at relatively low attenuation, producing low absorbance across both spectra. This is a consequence of the roughened surfaces produced by CeO_2 surface particulates. In ATR FT-IR spectroscopy, good surface contact of the sample with the crystal produces stronger signal compared to weak sample contact.[99] Therefore, it is possible that all peaks on the exposed surface were simply decreased in comparison to the unexposed disk due to surface roughness. Elemental analysis from SEM/EDS could confirm this hypothesis that the chemical composition did not change and that the ATR FT-IR data was simply a reflection of surface roughness.

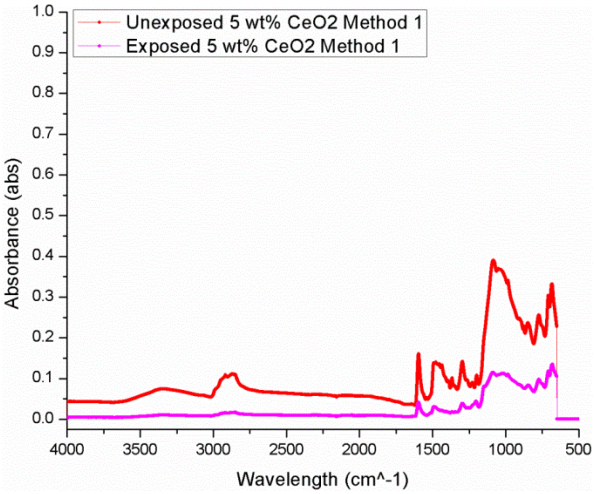

Figure 113. ATR FT-IR spectra of 5 wt% CeO_2 Method 1 coating layer before (red) and after (magenta) plasma.

SEM/EDS. Visually, plasma treated disks did not look altered except for a slight increase in surface sheen. Therefore, SEM was used to examine surface morphology on sputter coated disk sections. The 90 wt% glycidyl POSS coating before exposure was free from aggregates except for surface artifacts from spreading the coating over the matrix (Figure 114 L). However, after exposure, these artifacts were not apparent (Figure 114 R). In addition, the surface became dotted with ~0.5-1 μm debris and slight pitting.

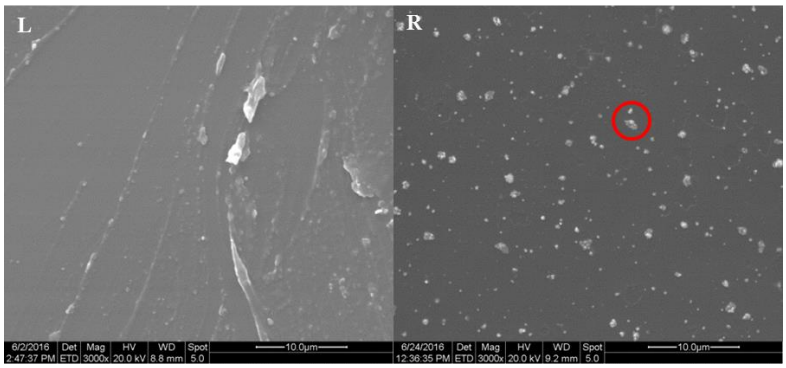

Figure 114. . Unexposed (L) and exposed (R) 90 wt% glycidyl POSS Method 1 coating layer surface at a magnification of 3000X. Surface erosion circled in red.

This erosion was expected from the plasma treatment. However, POSS glass appears as a smooth, aggregate free surface. It is possible that so this sample may not have been plasma treated for sufficient time to allow glassification.[12]

The 5 wt% CeO_2 Method 2 sample surface was similar to the 5 wt% CeO_2 Method 1 sample. The original, untreated surface was smooth but the exposed surface displayed both ~0.5-1 μm debris and a smaller, more uniform dotted pattern at high magnification, as displayed in Figure 115. Although focusing was sometimes difficult, these features were estimated to be <0.1 μm in diameter.

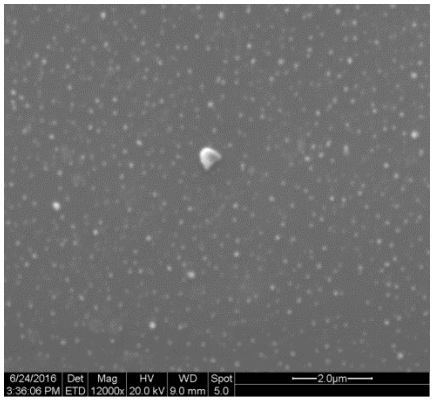

Figure 115. Exposed 5 wt% CeO_2 Method 2 coating surface at a magnification of 12000 X.

Analysis with EDAX did not reveal any elemental differences between these dots and the surrounding surface. This may be due to the size of the features being below the resolution of the instrument in this experiment.

The unexposed 5 wt% CeO_2 Method 1 surface confirmed the presence of cerium-rich aggregates that showed up as lighter areas of the sample. The textured lines seen in Figure 116 were a result of the Teflon used to line the bottom of the mold.

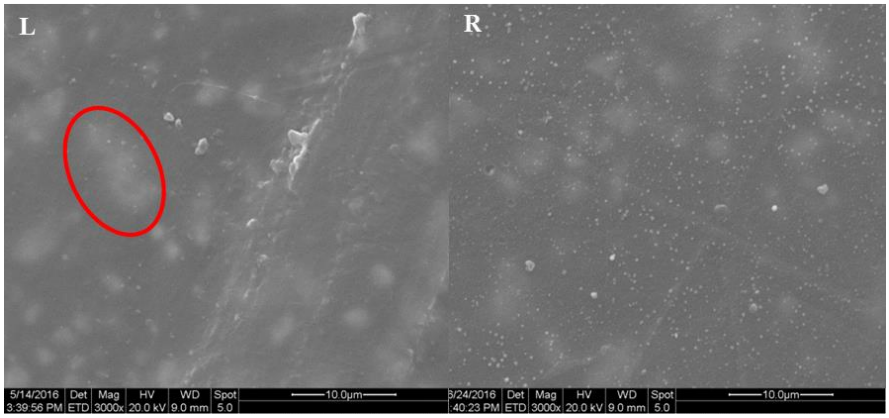

Figure 116. Unexposed 5 wt% CeO_2 Method 1 coating surface (L) with CeO_2 aggregation circled in red and exposed 5 wt% CeO_2 mold coating surface (R) at a magnification of 3000 X.

After exposure, these aggregates were unaltered but there was a similar pattern of ~0.1 μm diameter dots across the surface as with the 5 wt% CeO_2 Method 2 surface. However, larger, defined aggregates were not as common as with the previous two sample types. This supports the idea derived from contact angle results that the higher surface concentration of CeO_2 in the mold-side processed sample inhibited plasma related oxidation.

Elemental analysis from EDAX supports this conclusion (Table 15). Significant increases in oxygen weight percent and decreases in carbon weight percent were seen in the 90 wt% glycidyl POSS and 5 wt% CeO_2 Method 2 samples, indicating oxidation of the surface and some removal of carbon-rich POSS pendant groups. This removal, however, was not detected by ATR FT-IR spectra. This indicates a lack of substantial POSS glassification. With the 5 wt% CeO_2 Method 1 sample, there was a slight increase in oxygen wt% but no statistically significant differences in carbon wt% before and after treatment, again supporting the conclusion that cerium-rich aggregates block oxidation due to plasma exposure.

Table 15

EDAX Elemental results at 3000X

	90 wt% Glycidyl		**5 wt% CeO_2 Method 1**		**5 wt% CeO_2 Method 2**	
wt%	Before	After	Before	After	Before	After
Si	12.15 +/- 0.02	13.18 +/- 0.02	12.91 +/- 0.03	9.01 +/- 0.02	11.77 +/- 0.02	11.16 +/- 0.02
O	17.06 +/- 0.23	34.41 +/- 0.20	7.41 +/- 0.31	13.01 +/- 0.25	18.67 +/- 0.23	27.28 +/- 0.17
C	61.34 +/- 1.39	44.89 +/- 1.18	49.13 +/- 2.64	49.48 +/- 1.96	60.69 +/- 1.46	53.79 +/- 1.49

In summary, the objective of the plasma treatment experiment was to induce glassification of POSS-rich coating layer. However, ATR FT-IR spectra

measured before and after exposure did not record significant changes except in the 5 wt% CeO_2 Method 1 surface, which was attributed to surface roughness. This casts doubt on any potential POSS glassification. Scanning electron microscopy showed changes in surface morphology across all three sample types although these features were less pronounced in the 5 wt% CeO_2 Method 1 surface. Elemental analysis by EDS confirmed the increase in oxygen content at coating surfaces on all three sample types. This change was less pronounced on the 5 wt% CeO_2 Method 2 surface and there was no change in carbon concentration at this surface compared to the carbon weight percent decrease in the other two coatings. While POSS glassification did not definitively occur in any coating, it was valuable to learn that the presence of CeO_2 at a treated surface impedes the effects of plasma oxidation.

Cerium-POSS Reactions

Previous results indicate that cerium (IV) oxide sediments to the bottom of POSS-rich coatings when all components are blended together. In addition, coatings with as little as 5 wt% CeO_2 are not translucent. An alternative strategy to better disperse CeO_2 in POSS-rich coatings is to react it with a trisilanol POSS. These POSS moieties have one corner of the POSS cage opened and replaced by three silanol groups, as shown in Figure 117.

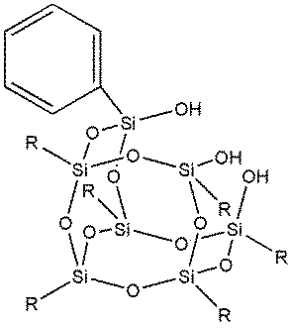

Figure 117. Structure of trisilanol phenyl POSS where R = phenyl.[107]

If the open cage POSS is more miscible in a given matrix, it will also disperse the attached oxide. This method was employed by Wheeler et al. to reduce the aggregate size of TiO_2 in polypropylene.[99] The TiO_2 was reacted with trisilanol isobutyl POSS at a 10:1 ratio by mixing the two reagents in hexanes at room temperature for 1 hour.[99] The proposed mechanism was hydrogen bonding between the reagents that led to a condensation reaction that formed a covalent bond between a silanol and the titanium center of TiO_2, as shown in Scheme 7.

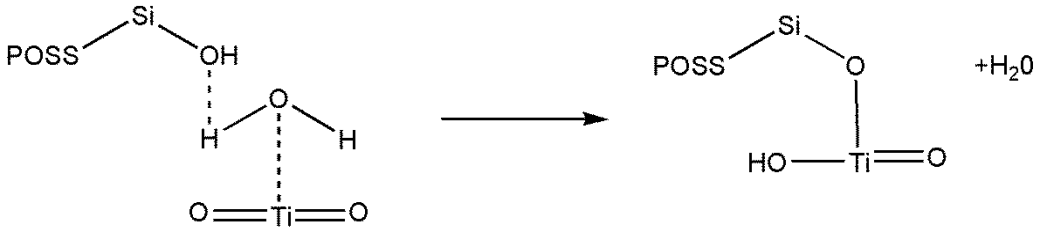

Scheme 7. Proposed reaction of TiO_2 with a trisilanol POSS.[72,99]

This method did decrease the average TiO_2 aggregate diameter from 70.6 +/- 31.9 nm to 33.2 +/- 11.6 nm.[99] However, thermogravimetric analysis (TGA) determined that there was only 3 wt% trisilanol isobutyl POSS in the product, a significant decrease from the original 10:1 CeO_2: POSS ratio of reagents.[99]

CeO_2-POSS Reactions. Following the method of Wheeler et al., CeO_2 and trisilanol phenyl (TSP) POSS were mixed in hexanes for 1 hour.[99,149] Trisilanol

phenyl POSS was chosen because of concerns that trisilanol isobutyl POSS with its aliphatic pendant would be less miscible in the aromatic epoxy matrix. The reagents were combined in a weight ratio of 5:1 CeO_2:TSP POSS in an attempt to have a higher ratio of POSS in the product compared to the 95 wt% oxide product that resulted from the 10:1 TiO_2:POSS mixture used by Wheeler et al.[99] A more balanced ratio of POSS and CeO_2 was targeted for the final product to capture the atomic oxygen protection of POSS in addition to the UV absorbance of CeO_2. Trisilanol phenyl POSS was used because it had aromatic pendant groups, which were thought to be more miscible in an aromatic epoxy matrix compared to commercially available alternatives with aliphatic POSS pendants. After mixing, solvent was evaporated using a rotary evaporator. Any residual solids were washed several times with hexanes and then the solvent was evaporated again. The remaining solid was a dry, slightly cream colored powder. This color was similar to the CeO_2 reagent, indicating that CeO_2 was probably present in the recovered solid. Thermogravimetric analysis was conducted on CeO_2, TSP POSS, and the recovered powder. Samples were heated from 40 to 800 °C at 10 °C/min and the weight loss was measured as a function of temperature. These curves are shown in Figure 118 where CeO_2 is in maroon, TSP POSS is in blue, and the CeO_2-POSS mixture is shown in orange.[149]

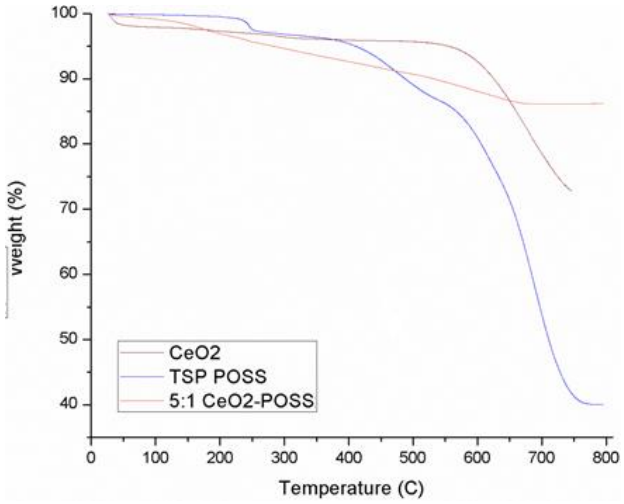

Figure 118. TGA curves of CeO_2, TSP POSS, and 5:1 CeO_2: POSS mixture.[149]

From this data, it was determined that the mixture was majority CeO_2 as the mixture curve did not have the same magnitude of mass loss beginning at 400 and 550 °C as dis the TSP POSS. This trend did not seem to alter with the ratios of 4:1, 3:1, 2:1, and 1:1 CeO_2: TSP POSS.[149] At this point, ATR FT-IR was not available to determine chemical composition due to instrumentation issues. The original procedure of mixing 5:1 CeO_2: TSP POSS was repeated in ethanol, acetone, tetrahydrofuran (THF), hexanes and other solvents. However, all mixtures remained overwhelmingly CeO_2 according to TGA.

One possibility was that the possible condensation reaction could need acid catalysis.[150] Both reagents were dissolved in 0.1 M HCl and stirred at 70 °C for 6 hours.[150] The solid recovered was vacuumed filtered from solution. However, the TGA curve of this recovered solid was very close to the curve for trisilanol phenyl POSS. One possibility from the acid catalyst and the previous method was that miscibility differences between the two reagents in a given

solvent could block the desired reaction of trisilanol phenyl POSS and cerium (IV) oxide.

$Ce(NO_3)_3$-POSS Reaction. From previous attempts to react CeO_2 with trisilanol phenyl POSS, it was concluded that the major issues were solubility and reactivity. Cerium-containing compounds have been integrated into anti-corrosion silane coatings.[151-153] However, these studies have used $Ce(NO_3)_3 \cdot 6H_2O$ or other Ce^{3+} species, rather than the Ce^{4+} found in CeO_2.[151-153] Cerium (III) nitrate hexahydrate is miscible in a wider range of solvents than CeO_2 and is the less stable of the two cerium oxidation states, making it more reactive.[151-154] Therefore, in consultation with collaborators at Hybrid Plastics, the decision was made to switch from CeO_2 to $Ce(NO_3)_3 \cdot 6H_2O$ in an effort to enhance solubility and increase reactivity with TSP POSS.

A 1:1 weight ratio of $Ce(NO_3)_3 \cdot 6H_2O$ and TSP POSS were stirred in an excess of acetone for 30 minutes at room temperature. Originally, a small amount of diglyme was added to act as a chelating agent at a ratio of 1:1:0.05 $Ce(NO_3)_3 \cdot 6H_2O$: TSP POSS: diglyme. However, diglyme or the lack thereof did not appear to influence the spectroscopic or thermal properties of the recovered solid so the use of diglyme was discontinued to avoid extra washing steps at the end of the reaction. After stirring, the mixture was poured into metal pans and the solvent evaporated overnight at ambient temperature and pressure. The resultant solid was a light cream colored powder caked onto the bottom of the metal pans. This powder was scraped off, heated overnight, at 75 °C and atmospheric

pressure, to remove any remaining acetone, and then the powder was weighed. This material was termed “CePOSS”.

The weight of the recovered CePOSS mixture was 49.6 +/- 2.5 % of the combined masses of the original $Ce(NO_3)_3 \cdot 6H_2O$ and TSP POSS. This was significantly lower than expected since it was assumed that a condensation reaction would occur between the two reagents and water would be lost. Assuming that reaction, a 1:1 ratio of Ce and TSP POSS in the product, the loss of all water associated with $Ce(NO_3)_3 \cdot 6H_2O$, and no other substantial losses during processing, the mass of the CePOSS product would be 92.08 % of the combined masses of the two original reagents. This is shown in the calculations below.

Assumed product molecular weight:

$$931.34\frac{g}{mol}\ TSP\ POSS + 434.22\frac{g}{mol}\ g\ Ce(NO3)3 \cdot 6H20 = 1365.56\ g/mol$$

Loss of 6 H_2O:

$$\left(\frac{1257.44\frac{g}{mol}}{1365.56\frac{g}{mol}}\right) * 100 = 92.08\ \%$$ remaining mass

Actual recovered mass = 49.6 % of original reagent mass

The discrepancy between calculated mass and the actual recovered mass was attributed to evaporation of material during the evaporation of the acetone. More spectroscopy and other property measurements were done with the new solid.

Thermal Characterization of CePOSS. Thermogravimetric analysis was conducted on cerium (III) nitrate hexahydrate, TSP POSS, and the powder that resulted from mixing these two compounds termed CePOSS. The results are shown in Figure 119.

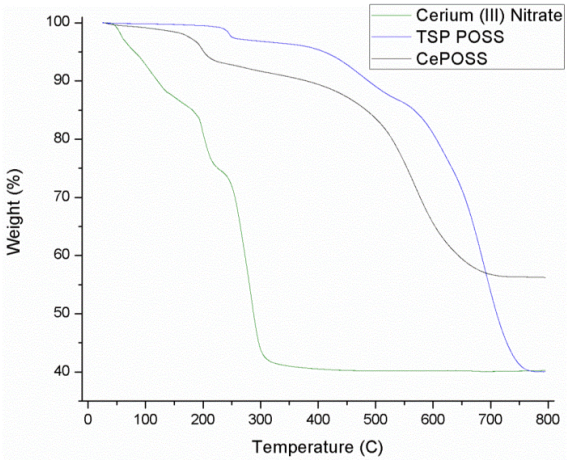

Figure 119. TGA curves for cerium (III) nitrate hexahydrate (green), TSP POSS (blue), and CePOSS (black).

The CePOSS mixture loses a small molecule byproduct, possibly water or unevaporated acetone, at approximately 180-200 °C. Above those temperatures, the degradation of CePOSS resembled that of cerium (III) nitrate hexahydrate but did not match it exactly.

Differential scanning calorimetry was also conducted on CePOSS (Figure 120). The sample was heated 10 °C/min to 250 °C to complete any reactions and eliminate thermal stresses. It was then cooled 10 °C/min to -50 °C and heated again at 10 °C/min to 250 °C

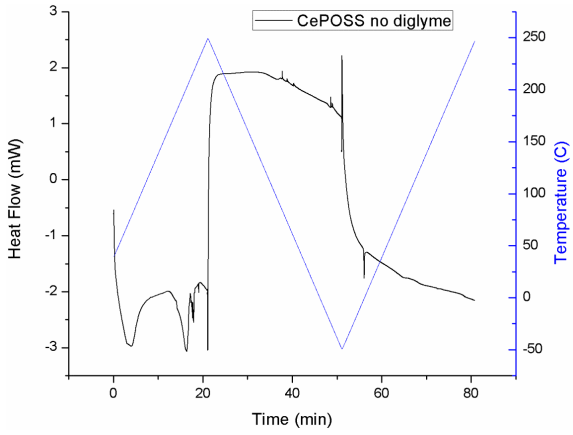

Figure 120. DSC curve of CePOSS, exo up.

On the first heat from 0 to approximately 20 min, there were two broad endothermic events. These events were not repeated during the second heat from approximately 50 to 80 min. Thus the endothermic events in the first heat were attributed to loss of water or residual solvent.

ATR FT-IR of CePOSS. Attenuated total reflectance Fourier transmission infrared (ATR-FTIR) spectroscopy identified functional groups shared between the reagents and CePOSS in Figure 121.

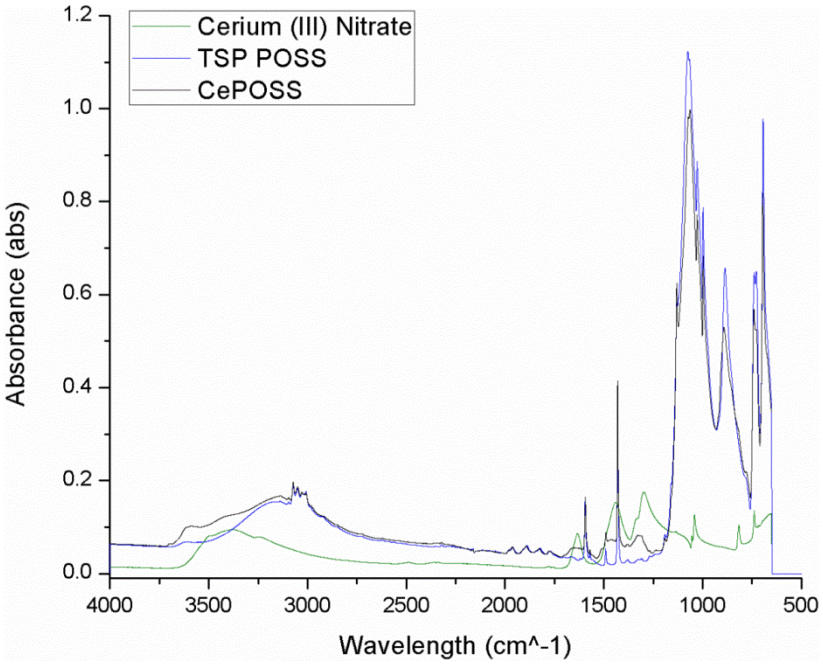

Figure 121. ATR FT-IR spectra of for cerium (III) nitrate hexahydrate (green), TSP POSS (blue), and CePOSS (black).

The defining peak from the TSP POSS was the strong Si-O peak from 1100-1000 cm^{-1}.[148] This showed up as well in the CePOSS, validating the TGA curve that predicted the presence of TSP POSS in CePOSS. The peaks between 3200-3000 cm^{-1} are indicative of phenyl groups, and also both show up in TSP POSS and CePOSS spectra.[148] Cerium (III) nitrate hexahydrate is also present in

CePOSS because of the nitrate group peaks at approximately 1650, 1450, and 1300 cm^{-1} present in both reagent and CePOSS spectra.[148] Therefore, ATR FT-IR establishes that CePOSS contains both POSS and cerium (III) nitrate hexahydrate functionalities. However, this data does not establish whether these reagents are covalently bonded and, if so, through what type of bond. Ce-O bonds present from 800-500 cm^{-1} in FT-IR, and therefore, were not detectable underneath the POSS peaks.[155]

CePOSS Solubility in Solvents. CeO_2, $Ce(NO_3)_3 \cdot 6H_2O$, trisilanol phenyl POSS, and CePOSS were mixed at 10 mg in 1000 mg of either acetone, cyclohexane, dichloromethane, deionized (DI) water, ethyl acetate, isopropanol, methyl isobutyl ketone, THF, and toluene. Teas diagrams were plotted for each solute with points labeled in red for immiscible mixtures, yellow for partially miscible, and green for miscible. Figures 122, 123, 124, and 125 show Teas diagrams for CeO_2, $Ce(NO_3)_3 \cdot 6H_2O$, trisilanol phenyl POSS, and CePOSS, respectively.

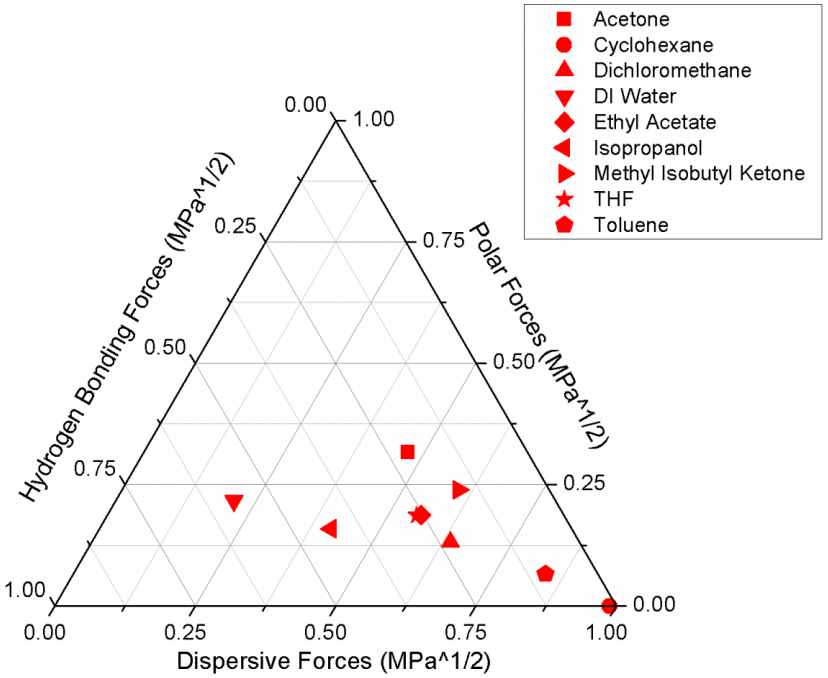

Figure 122. Teas diagram of CeO_2.

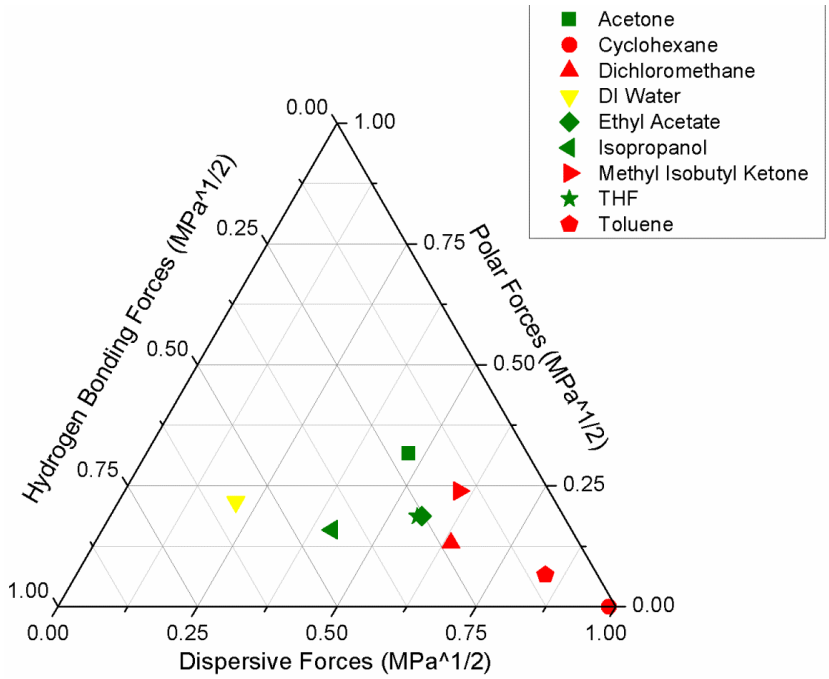

Figure 123. Teas diagram of $Ce(NO_3)_3 \cdot 6H_2O$.

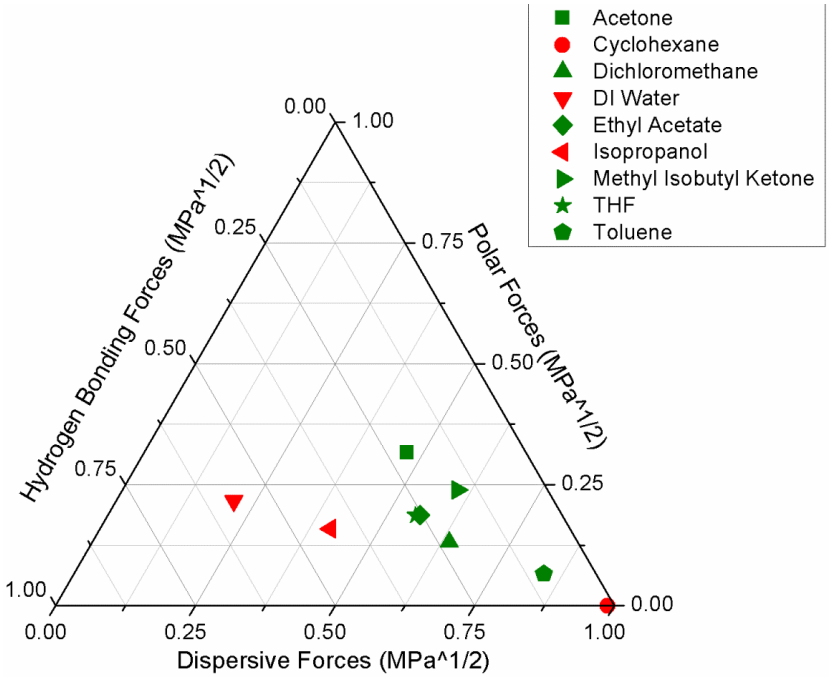

Figure 124. Teas diagram of trisilanol phenyl POSS.

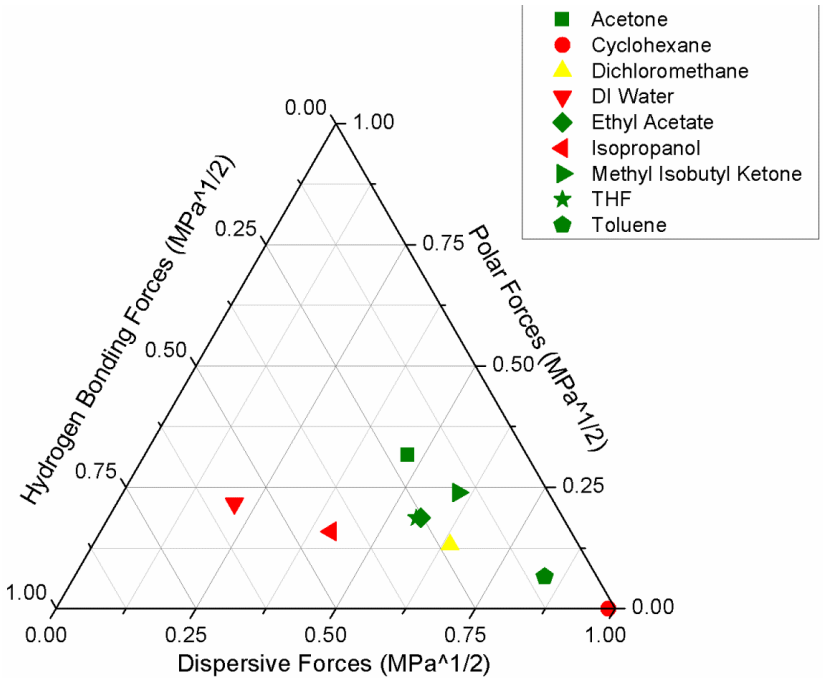

Figure 125. Teas diagram of CePOSS.

Cerium (IV) oxide precipitated in all solvents whereas the cerium (III) nitrate hexahydrate was miscible in the more polar organic solvents, acetone, ethyl acetate, isopropanol, and THF. The trisilanol phenyl POSS was miscible in acetone, dichloromethane, ethyl acetate, methyl isobutyl ketone, THF, and toluene, creating a region of solubility near the lower right corner of the Teas diagram. The CePOSS mixture was not soluble in deionized water compared to $Ce(NO_3)_3 \cdot 6H_2O$ and was only partially soluble in dichloromethane as opposed to trisilanol phenyl POSS, which was miscible in dichloromethane. Otherwise, the CePOSS mixture was soluble in the same five solvents as TSP POSS: acetone, ethyl acetate, methyl isobutyl ketone, THF, and toluene. The $Ce(NO_3)_3 \cdot 6H_2O$ was not miscible in methyl isobutyl ketone or toluene. Therefore, the trisilanol phenyl POSS may be acting as a dispersant for the cerium (III) nitrate hexahydrate.

Nuclear Magnetic Resonance of CePOSS. H, ^{13}C, and ^{29}Si NMR was performed on both trisilanol phenyl POSS and CePOSS in an attempt to determine the structure of CePOSS. The samples were 40 mg of TSP POSS in 1 mL of deuterated acetone and 80 mg of CePOSS in 1 mL of deuterated acetone. The increase in concentration of CePOSS was due to CePOSS being a theoretically 1:1 ratio of TSP POSS and cerium (III) nitrate hexahydrate, so both samples would have an equal amount of TSP POSS. The standard used was excess tetramethylsilane (TMS). Figures 126 and 127 show the ^{29}Si NMR for TSP POSS and CePOSS, respectively. The O_2Si-phenyl peaks for TSP POSS are at -77.29 and -78.18 ppm and were -76.78 and -78.18 ppm for CePOSS.[11] The Si-OH ^{29}Si peak was at -69.67 ppm for both samples. The peak at 0 ppm is

the TMS standard and the broad peak centered at -112.36 ppm is the silicate glass of the NMR sample tube.[156]

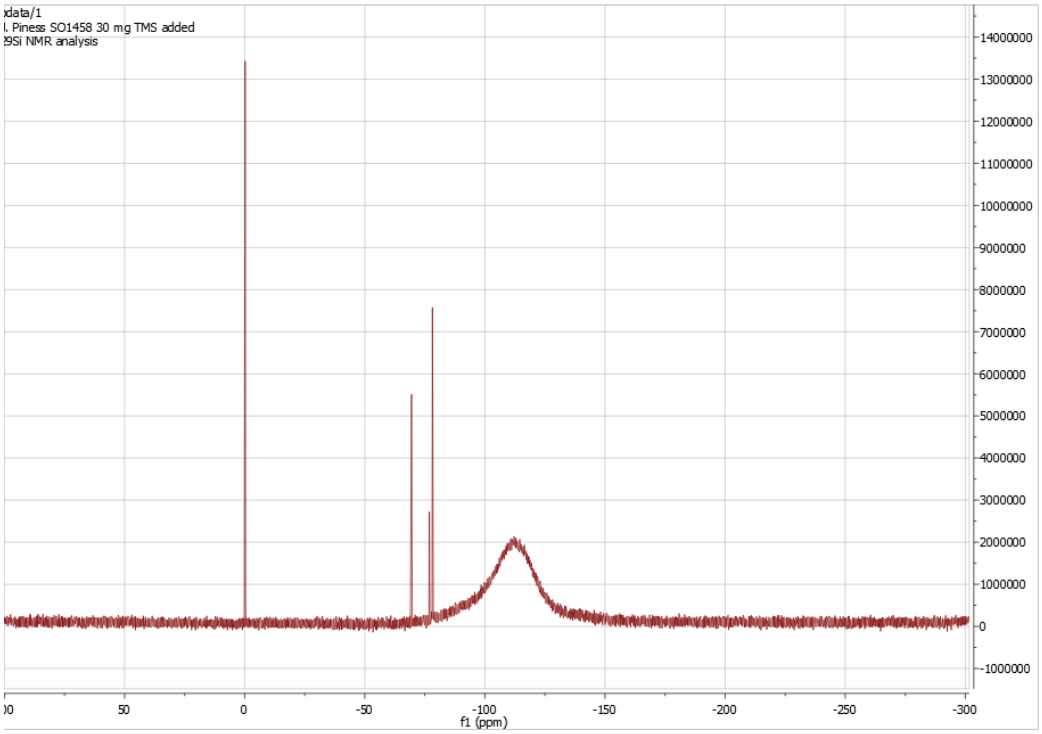

Figure 126. ^{29}Si NMR of TSP POSS.

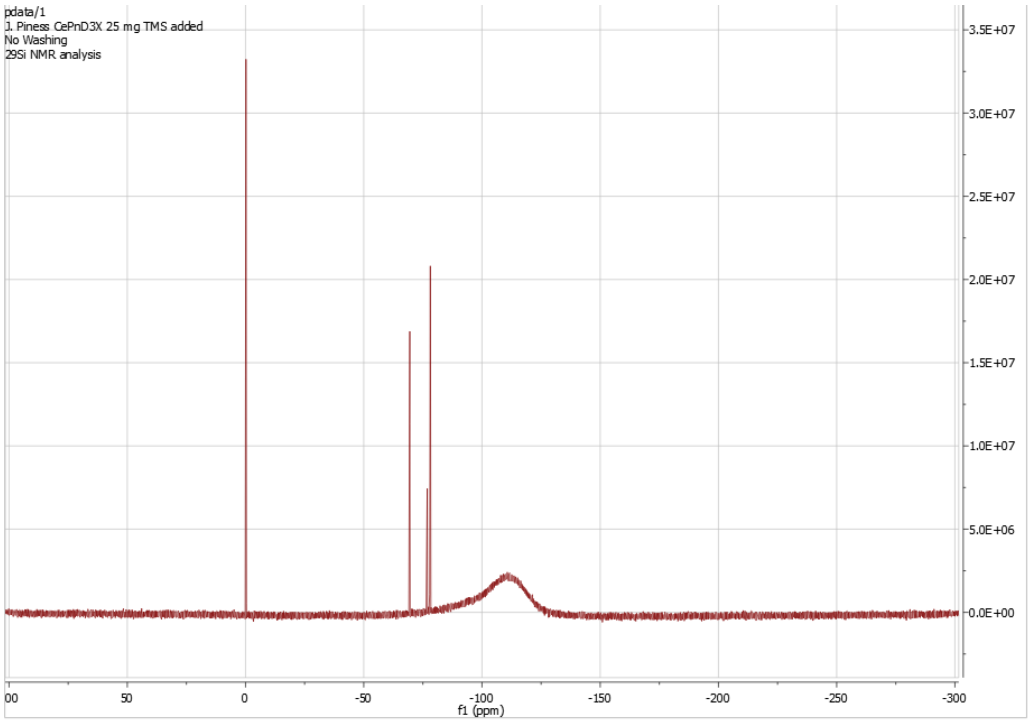

Figure 127. ^{29}Si spectra of CePOSS.

However, some changes in peak splitting between the two materials were observed when peaks were magnified (Figure 128 and 129).

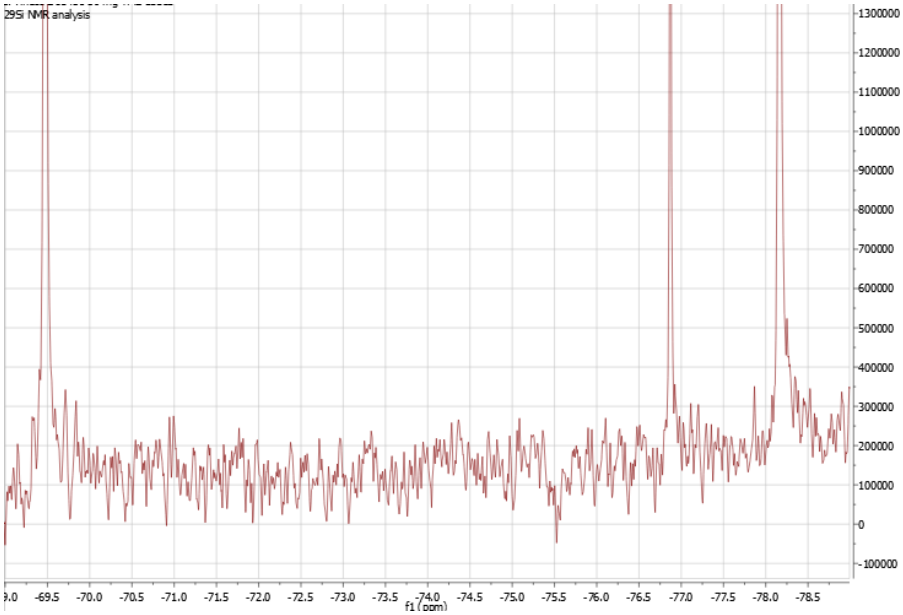

Figure 128. Selected area of TSP POSS ^{29}Si NMR spectrum.

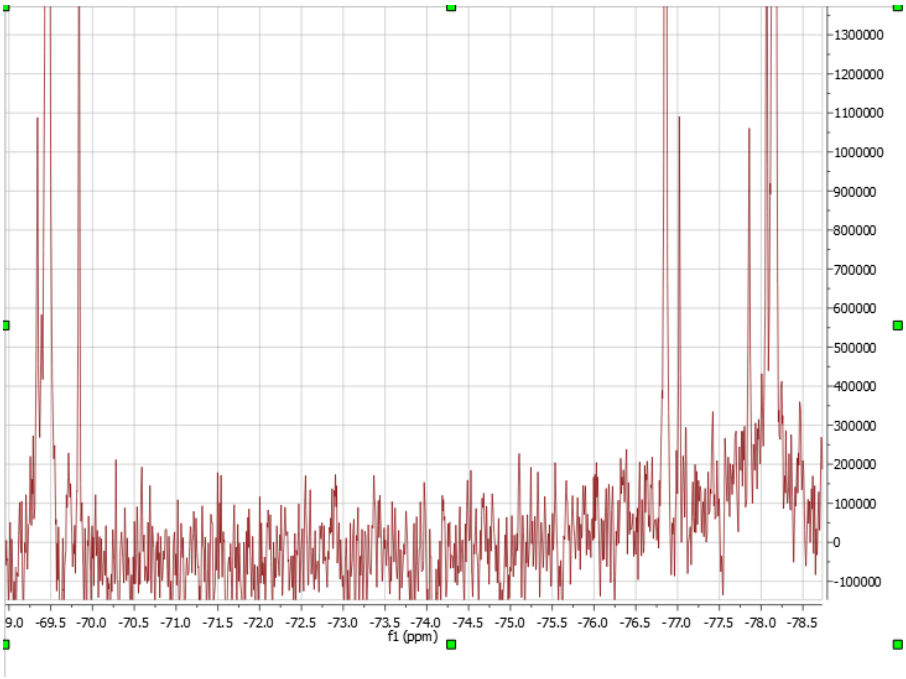

Figure 129. Selected area of CePOSS ^{29}Si NMR spectrum.

Splitting could indicate some alterations to the cage but it cannot be determine whether any alterations would be due to reaction between trisilanol phenyl POSS and cerium (III) nitrate hexahydrate or with other issues with the POSS cage due to the production of CePOSS.

In addition, some changes were seen in the ^{13}C phenyl peaks from the phenyl rings on the trisilanol phenyl POSS although the overall spectra did not show significant shifts (Figure 130, 131). Figure 132 shows the peaks from 137-126 ppm for trisilanol phenyl POSS with the same region from the CePOSS sample below in Figure 133.

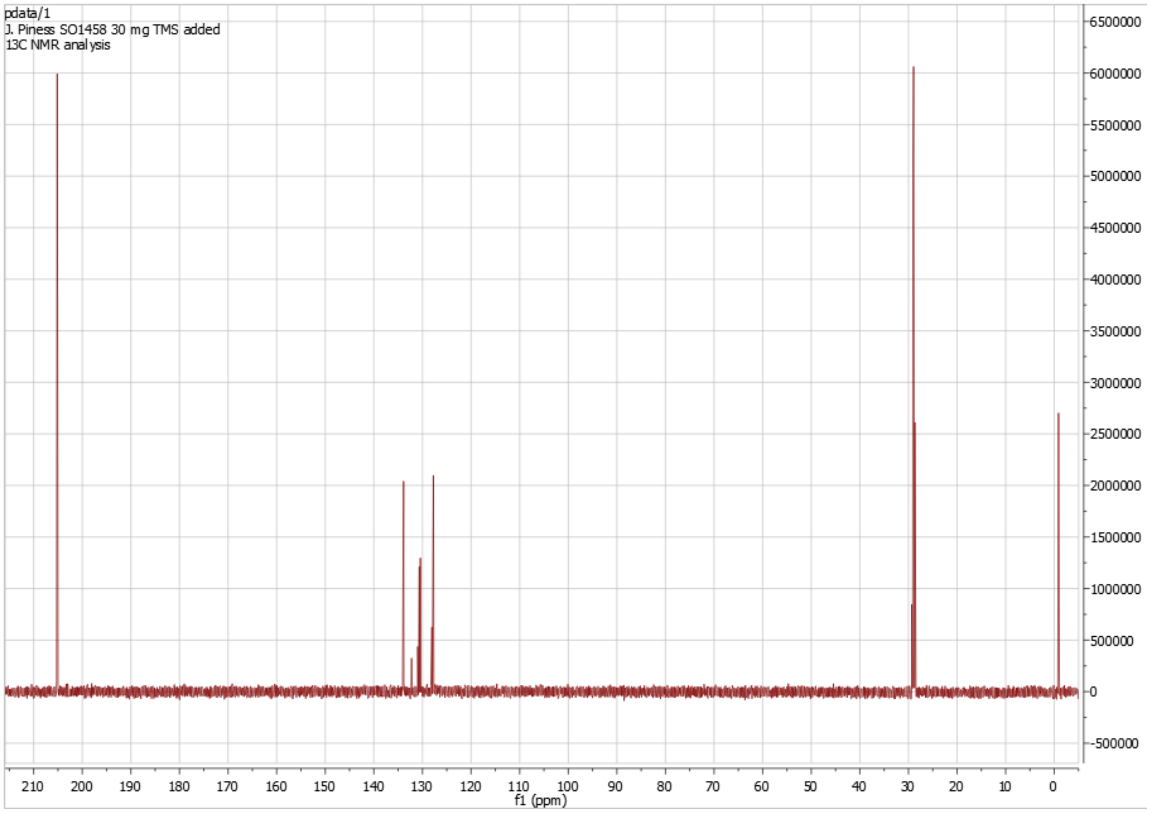

Figure 130. ^{13}C spectrum of trisilanol phenyl POSS.

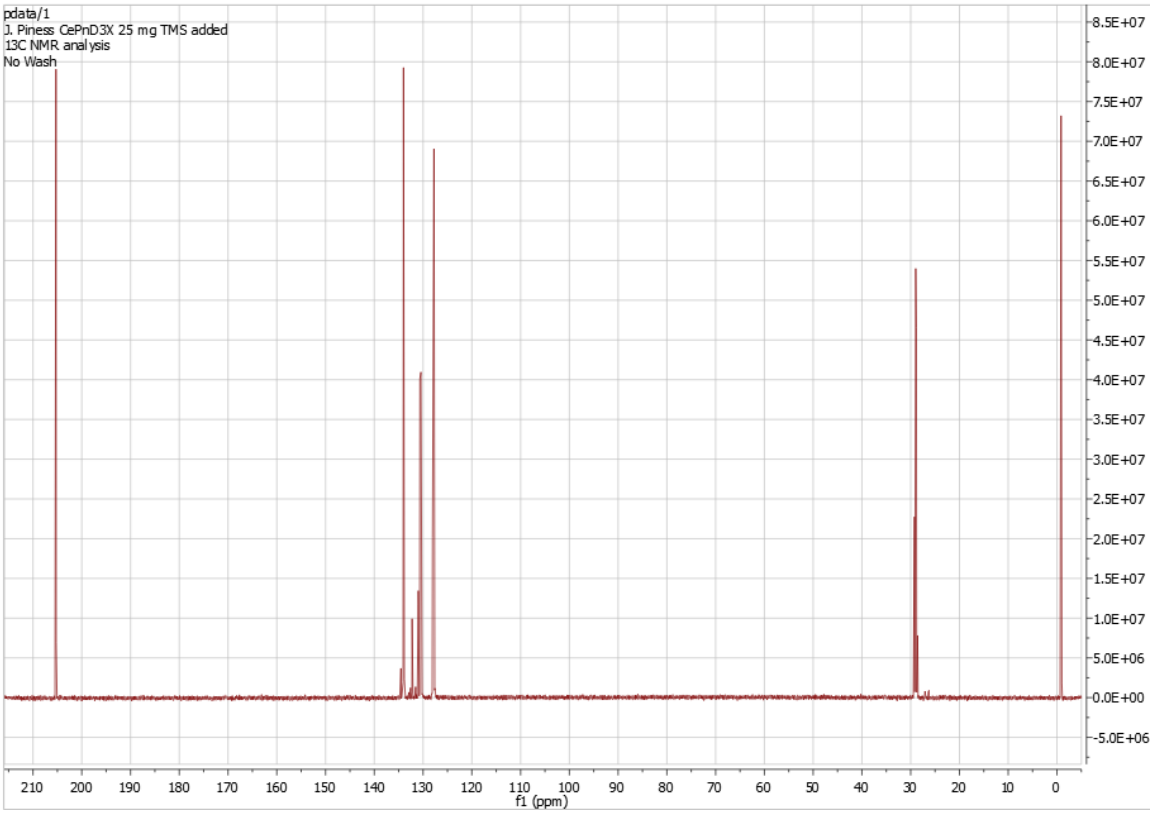

Figure 131. ^{13}C spectrum of CePOSS.

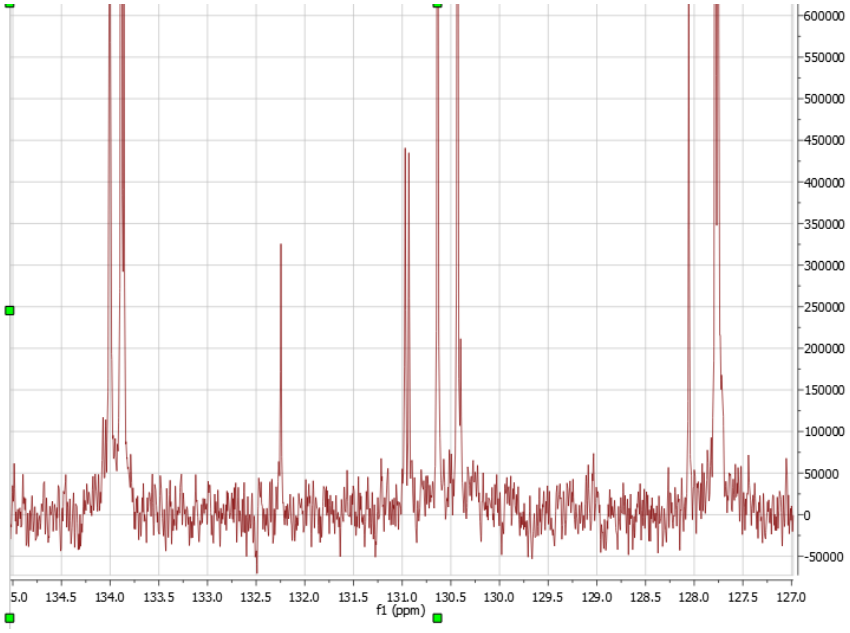

Figure 132. ^{13}C phenyl peaks from 135-127 ppm for trisilanol phenyl POSS.

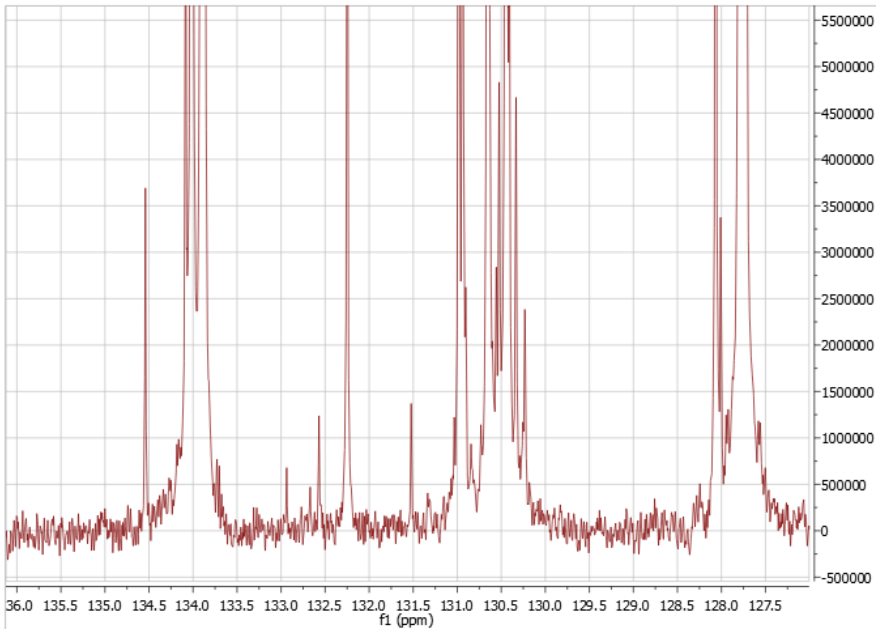

Figure 133. ^{13}C phenyl peaks from 136-127 ppm for CePOSS.

The CePOSS spectra showed extra smaller peaks and the larger, original peaks were split more than in the trisilanol phenyl POSS spectra. However, it was not possible to determine whether the nitrate functionalities from the cerium (III) nitrate hexahydrate specifically reacted with the phenyl rings.

Some differences were seen in the ^{1}H spectra as seen Figure 134 and 135. The TMS peaks were truncated in these spectra to focus on the POSS ^{1}H peaks.

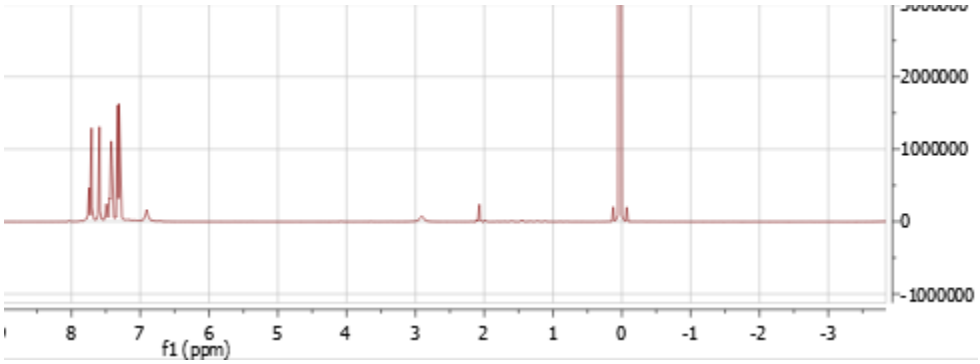

Figure 134. Selected area of TSP POSS ^{1}H NMR spectrum.

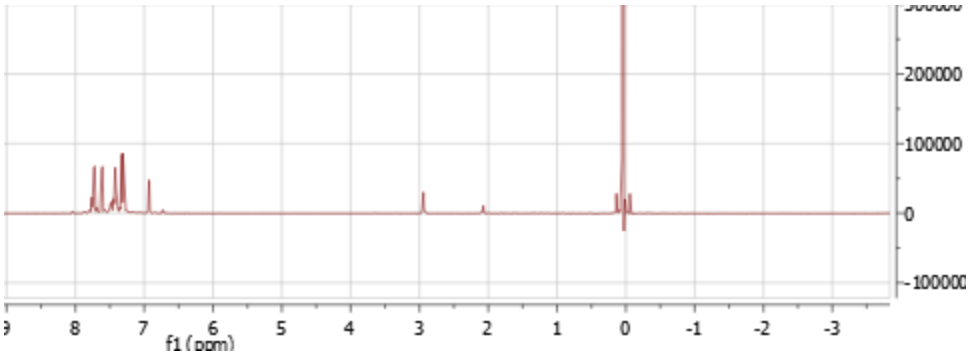

Figure 135. Selected area of CePOSS ^{1}H NMR spectrum.

The main phenyl peaks from approximately 7.25-7.75 ppm did not shift from TSP POSS to CePOSS.[120] The peak at 3.1 ppm was attributed to the H_2O in the cerium (III) nitrate hexahydrate and the smaller peak at 2.05 ppm was from the deuterated acetone solvent.[157] The main change was a seemingly new ^{1}H peak at 7 ppm in the CePOSS spectrum. However, upon magnification (Figure 136), this peak did appear in the trisilanol POSS spectrum and was possibly split in the CePOSS spectrum (Figure 137).

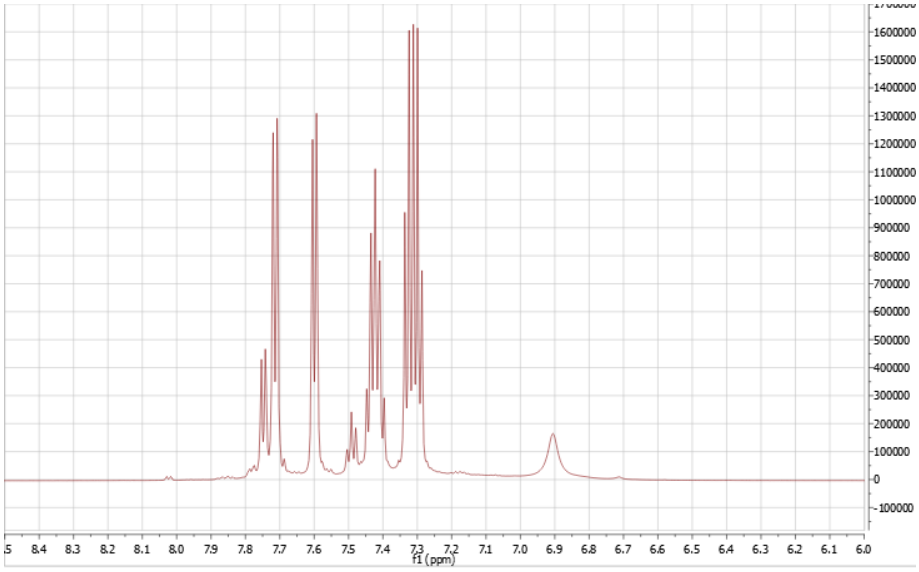

Figure 136. Area of TSP POSS ^{1}H NMR spectrum focused on aromatic and silanol protons.

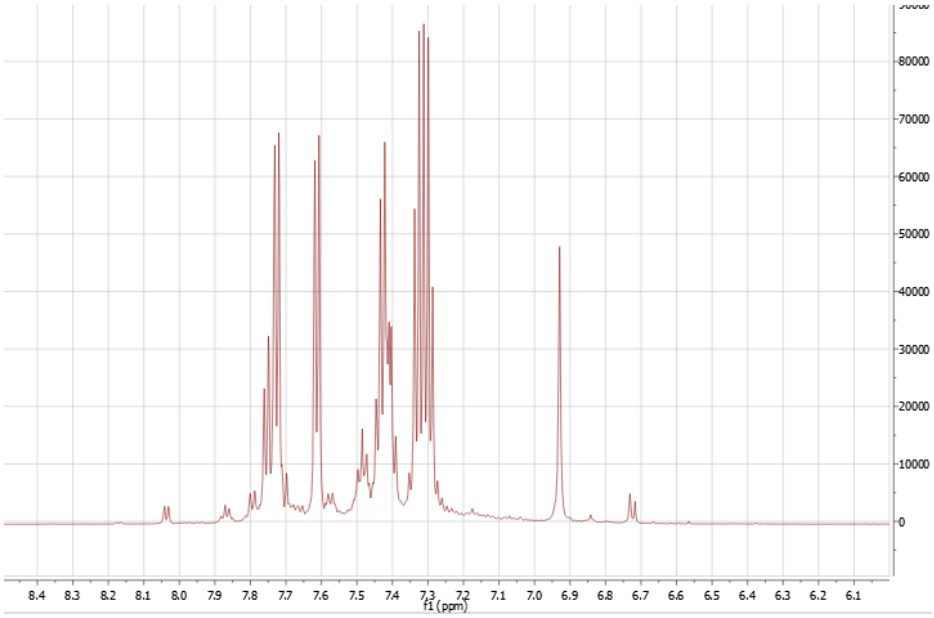

Figure 137. Area of CePOSS ^{1}H NMR spectrum focused on aromatic and silanol protons.

This shift and possible split could be attributed to hydrogen bonding between the silanol and nitrates or water that were part of cerium (III) hexahydrate.

Elemental Composition and Molecular Weight of CePOSS. In addition to NMR, molecular weight, and elemental composition were measured in order to determine if reaction had occurred between TSP POSS and $Ce(NO_3)_3 \cdot 6H_2O$. Initially, attempts were made to determine the crystal structure of CePOSS by slowly evaporating saturated solutions and collecting the crystallites. However, the solids recovered in all cases were a combination of amorphous cerium (III) nitrate hexahydrate and crystalline TSP POSS. This was determined through SEM/EDS as shown in Figure 138.

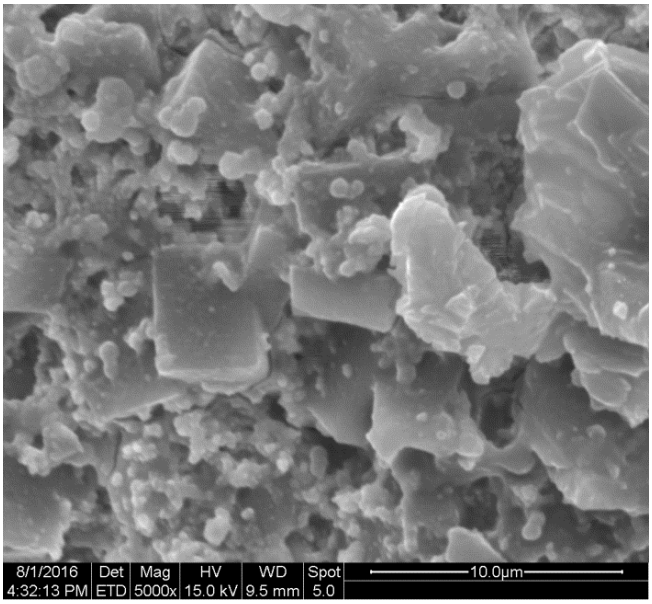

Figure 138. CePOSS material at 5000X.

At 5000X, square, Si-rich crystallites were observed as embedded in amorphous Ce-rich material. After solvent washing, only Si-rich material remained. This continued regardless of solvent, therefore, x-ray crystallography could not be used to find a crystal structure of CePOSS.

Elemental analysis was successfully completed on two distinct batches of CePOSS. If CePOSS is a complex of a 1:1 ratio of $Ce(NO_3)_3 \cdot 6H_2O$ and TSP POSS, the molecular weight would be 1365.56 g/mol with a formula of $C_{42}H_{50}N_3O_{27}Si_7Ce$. Using this formula, theoretical atomic contributions to total molecular weight can be compared to results from elemental analysis, as shown in Table 16. Elemental analysis detected the atom percent of C, H,N, Si, and Ce in CePOSS, and oxygen was assumed to make up the rest of the compound.

Table 16

Theoretical and experimental atom % results from elemental analysis

Atom	Theoretical Atom %	Experimental Atom %
C	36.93	49.43 +/- 1.59
H	3.69	3.55 +/- 0.12
N	3.08	0.70 +/- 0.34
O*	31.63	24.53 +/- 5.55
Si	14.40	19.28 +/- 5.91
Ce	10.26	2.51 +/- 1.00

*Calculated from sum of other atom % subtracted from 100%

From this data, it can be concluded that there is not a 1:1 $Ce(NO_3)_3 \cdot 6H_2O$ to TSP POSS in CePOSS. Given the proportions of Si and Ce from the experimental results, the ratio is1:5.4 $Ce(NO_3)_3 \cdot 6H_2O$ to TSP POSS. However, the high amount of carbon was unexpected and could indicate contamination during the production of CePOSS. In addition, a sample was analyzed that was made from a 5:1 blend of $Ce(NO_3)_3 \cdot 6H_2O$ to TSP POSS in an effort to boost cerium content. Unexpectedly, the Si:Ce ratio was 28.48 wt% to 2.16 wt%. This result raised the possibility that there is a limit on the amount of cerium that the CePOSS material can contain or that the elemental analysis method may not be sufficient to characterize the material.

Matrix-assisted laser desorption/ionization (MALDI) mass spectrometry was used as an characterization method to determine molecular weight.[120] Cerium (III) nitrate hexahydrate, trisilanol phenyl POSS, and CePOSS was dissolved in acetone and combined with a matrix of sinapinic acid based on the mass spectroscopy work of Wallace et al with POSS.[122] The molecular weights of TSP POSS and $Ce(NO_3)_3 \cdot 6H_2O$ are 931.34 g/mol and 434.22 g/mol, respectively.[107,158] Given the high ratio of TSP POSS to $Ce(NO_3)_3 \cdot 6H_2O$ from elemental analysis, it was expected that the molecular weight would be

significantly above the 1365.56 g/mol molecular weight estimated from the combination 1 molecule of TSP POSS and 1 molecule of $Ce(NO_3)_3 \cdot 6H_2O$ without small molecule loss. Spectra are shown in Figures 139-141.

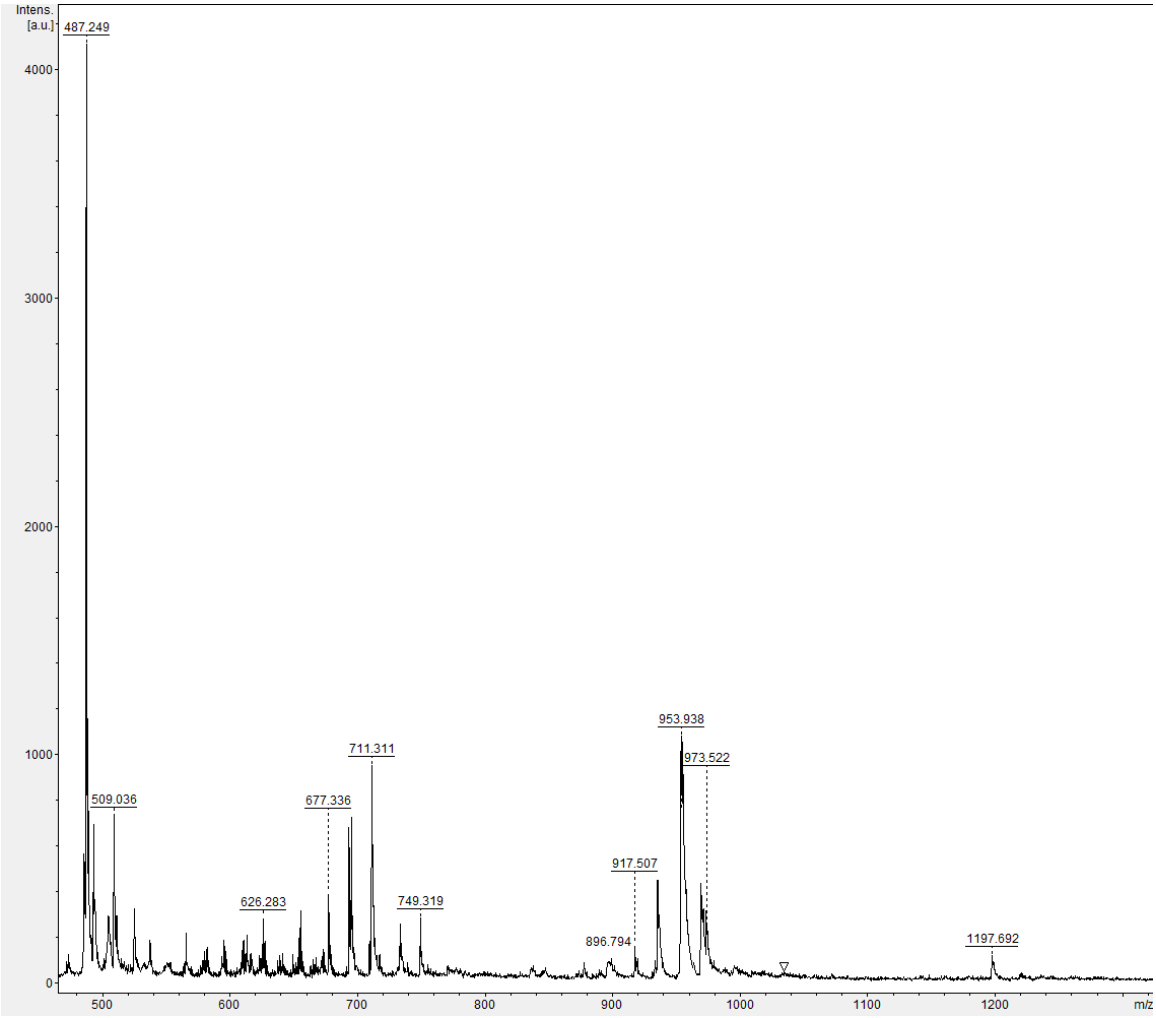

Figure 139. Mass spectroscopy spectrum of trisilanol phenyl POSS.

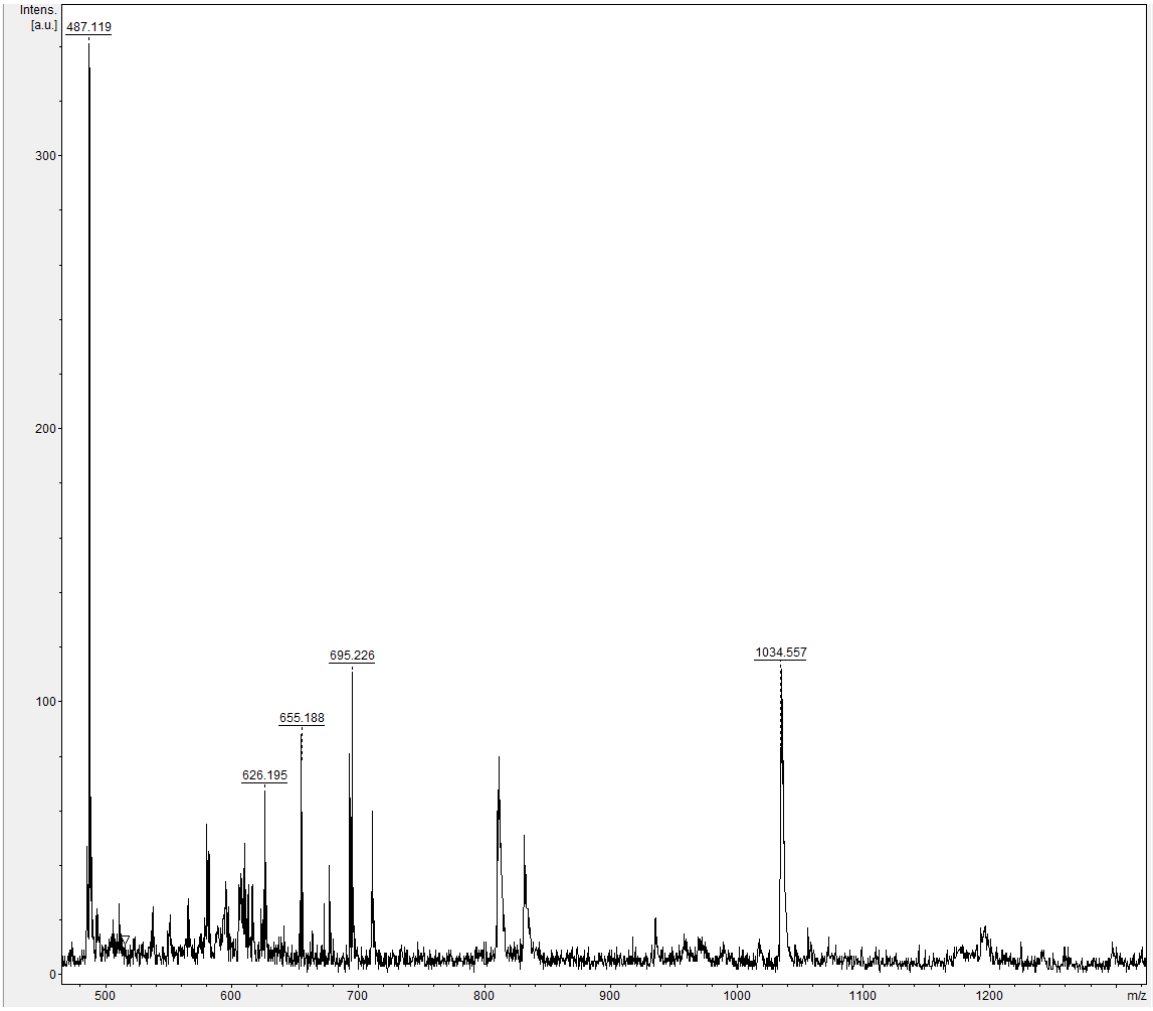

Figure 140. Mass spectroscopy spectrum of cerium (III) nitrate.

Neither the trisilanol phenyl POSS spectrum nor the cerium (III) nitrate spectrum contained peaks corresponding to the known molecular weights of these compounds.

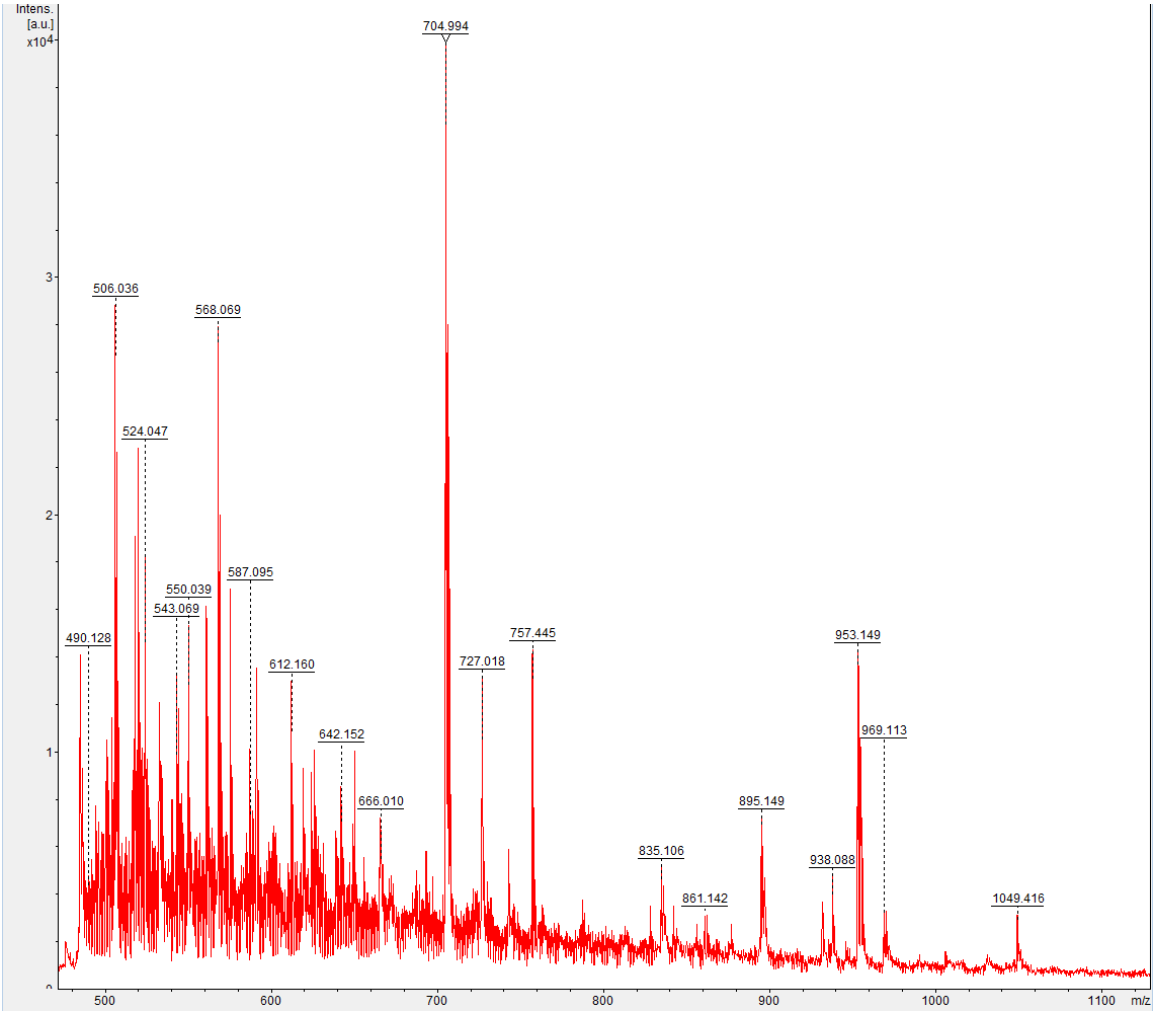

Figure 141. Mass spectroscopy spectrum of CePOSS.

In addition, the highest value peak in the CePOSS spectrum was 1049.416 amu. This is only 118.076 g/mol more than the molecular weight of TSP POSS. The molecular weight of one cerium atom is 140.1 g/mol, more than the difference between the CePOSS maximum peak and the molecular weight of TSP POSS. Therefore, it can be concluded that the CePOSS material is a mixture rather than a compound containing a covalent bond between cerium (III) nitrate and trisilanol phenyl POSS.

Complexation of CePOSS. From the previous NMR data especially, it appears that CePOSS is primarily a mixture of cerium (III) nitrate hexahydrate and trisilanol phenyl POSS. There are indications that hydrogen bonding is present between the silanol functional group and the water or the nitrate associated with the cerium (III) hexahydrate. Salazar-Sandoval et al. reported complexation between Ce^{3+} and carbonyl and hydroxyl groups.[159] Based upon this publication, dehydrated cerium (III) nitrate was combined with TSP POSS. If a material formed with the same characteristics as Ce POSS, this would be evidence of complexation through hydrogen bonding between the silanol and the nitrate groups. However, the experiments were not repeatable and convincing evidence of complex formation was not demonstrated by this approach.

ATR FT-IR was used in an attempt to detect hydrogen bonding by seeking shifts in peaks associated with water and nitrate in the spectrum of $Ce(NO_3)_3 \cdot 6H_2O$. Such an approach was used by Lochhead et al. to characterize the primary intermolecular interactions between montmorillonite clays and polyelectrolytes.[160] The specific peaks selected were:[148]

- O-H stretching: ~3650-2750 cm^{-1}
- H-O-H bend: ~1650 cm^{-1}
- N-O (in NO3) symmetric stretch: ~1430 cm^{-1}
- N-O (in NO3) asymmetric stretch: ~1300 cm^{-1}

Measured shifts are displayed in Table 17.

Table 17

Peak shifts from Ce(NO3)3·6H2O to CePOSS.

	O-H stretching		**H-O-H bend**	
	cm^{-1}	abs	cm^{-1}	abs
$Ce(NO_3)_3{\cdot}6H_2O$	3374.879	0.536	1632.944	0.370
CePOSS	3224.159	0.223	1637.886	0.096
CePOSS minus $Ce(NO_3)_3{\cdot}6H_2O$	**-150.720**		**+4.942**	
	N-O (in NO_3) symmetric stretch		**N-O (in NO_3) asymmetric stretch**	
	cm^{-1}	abs	cm^{-1}	abs
$Ce(NO_3)_3{\cdot}6H_2O$	1432.807	0.721	1289.499	0.837
CePOSS	1455.045	0.137	1326.561	0.165
CePOSS minus $Ce(NO_3)_3{\cdot}6H_2O$	**-22.238**		**-37.062**	

The major shift is downfield in the O-H stretch, indicating a high probability of hydrogen bonding between silanols on trilsilanol phenyl POSS and the hydrate functionality on $Ce(NO_3)_3{\cdot}6H_2O$.[160,161] Hydrogen bonding draws electrons farther from their original atom, changing the resonance of surrounding bonds and shifting those bonds to lower wavenumbers in FT-IR. The N-O peaks also had downfield shifts above the 2 cm^{-1} resolution of the instrument. These results demonstrate that hydrogen bonding occurred between the water of hydration and the silanol groups and also between the nitrate and the silanol groups.

UV-vis Spectroscopy of CePOSS. Cerium was added to POSS with the intent to improve the UV absorption of POSS, especially in the UVb (320-280 nm) and UVc (280-100 nm) ranges.[19] The UV absorption of CeO_2, TSP POSS, and CePOSS in THF at 0.25 mg/mL was measured from 230-500 nm. The comparative results are shown in Figure 142.

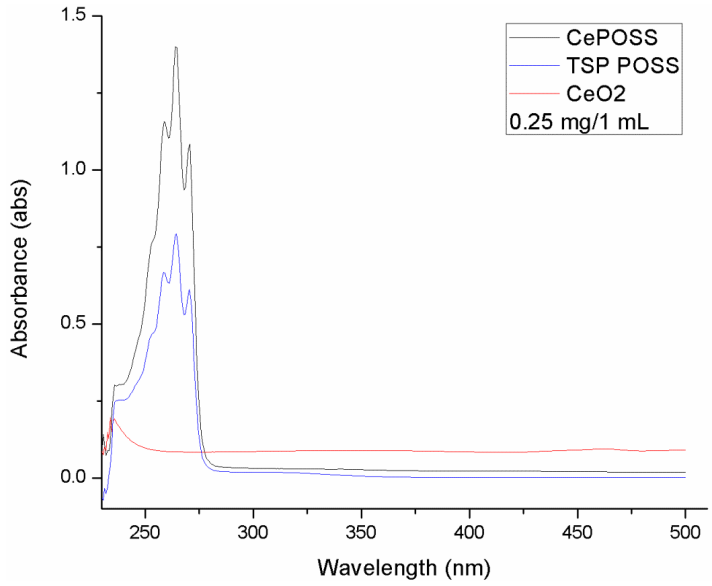

Figure 142. UV-vis spectra of CePOSS (black), TSP POSS (blue), and CeO_2 (red) at 0.25 mg/mL in THF.

When considering spectra at equal concentrations, CePOSS increased UV absorption between approximately 235-275 nm compared to TSP POSS and did so significantly compared to CeO_2. The next step was to then assess the miscibility of CePOSS as filler in POSS-rich coatings.

CePOSS Solubility in Polymers. In order to test the miscibility of CePOSS with epoxy resins, the Ce POSS filler was mixed into two commercially available POSS-rich coatings, IM9330 and EP3510. IM9330 is a proprietary polyimide-POSS copolymer that is solvent cast in propylene glycol monomethyl ether acetate (PGMEA).[114] EP3510 is a POSS-epoxy coating composed of 68.6 wt% glycidyl POSS, 29.4 wt% diglycidyl ether of bisphenol F, and 2 wt% Lindax 1 imidazole curative.[114] These coatings were chosen in consultation with collaborators at Hybrid Plastics because each coating has a high level of POSS, which should allow for glassification. In addition, both of these coatings can be

cast over already cured disks of TGDDM-glycidyl POSS-Lindax 1, creating a viable route to dual layer disks with POSS-rich coating layers.

Mixing CePOSS in each coating produced visible aggregates. In order to seek better dispersion, the CePOSS was mixed with various other POSS moieties as shown in Figure 143.

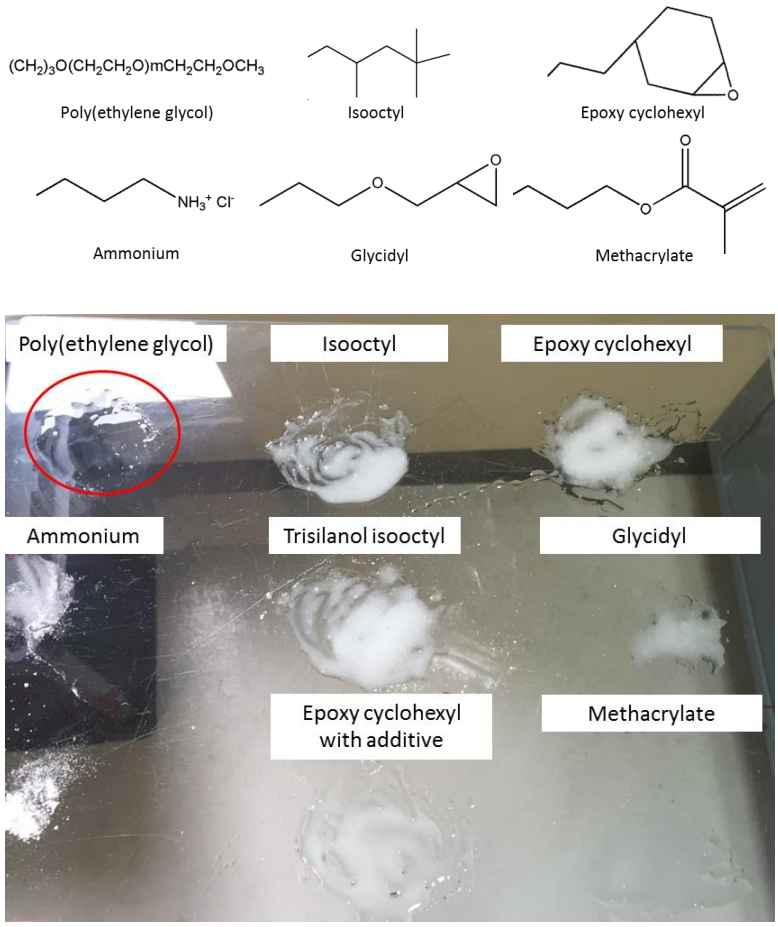

Figure 143. Mixtures of CePOSS with various POSS moieties.

The only transparent mixture was CePOSS with octapoly(ethylene glycol)POSS, or “PEG POSS”. According to the Teas diagram of PEG POSS in Figure 144, PEG POSS is miscible in acetone, ethyl acetate, THF, and toluene, which are also compatible solvents for CePOSS.

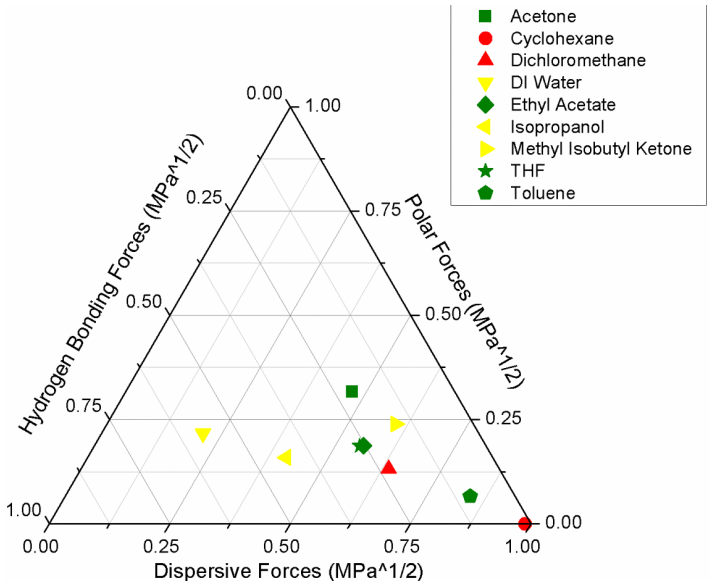

Figure 144. Teas diagram of PEG POSS.

The miscibility of these two components may be due to the long, polar chains on the PEG POSS moiety that could interact favorably with the water in CePOSS.

When the CePOSS-PEG POSS mixture was placed in EP3510, the POSS-epoxy coating, it produced a transparent coating at 5 wt% CePOSS-PEG POSS. However, this mixture was not precisely measured. To better chart the properties of CePOSS-PEG POSS in POSS-rich coatings, 1:1 and 2:1 weight ratios of CePOSS:PEG POSS were blended with a specialized dremel known as a tissue tearor. These blends were then incorporated into IM9330 and EP3510 at the following concentrations per blend:

1:1 CePOSS:PEG POSS

- 0.5 wt% CePOSS – 0.5 wt% PEG POSS
- 1.0 wt% CePOSS – 1.0 wt% PEG POSS
- 2.0 wt% CePOSS – 2.0 wt% PEG POSS
- 3.0 wt% CePOSS – 3.0 wt% PEG POSS

2:1 CePOSS:PEG POSS

- 0.67 wt% CePOSS – 0.33 wt% PEG POSS
- 1.33 wt% CePOSS – 0.67 wt% PEG POSS
- 2.67 wt% CePOSS – 1.33 wt% PEG POSS
- 4.0 wt% CePOSS – 2.0 wt% PEG POSS

The IM9330 matrix was initially clear (Figure 145a). Solvent casting produced level films. However, addition of any level of CePOSS-PEG POSS produced cloudy regions and aggregates, as shown in Figure 145b.

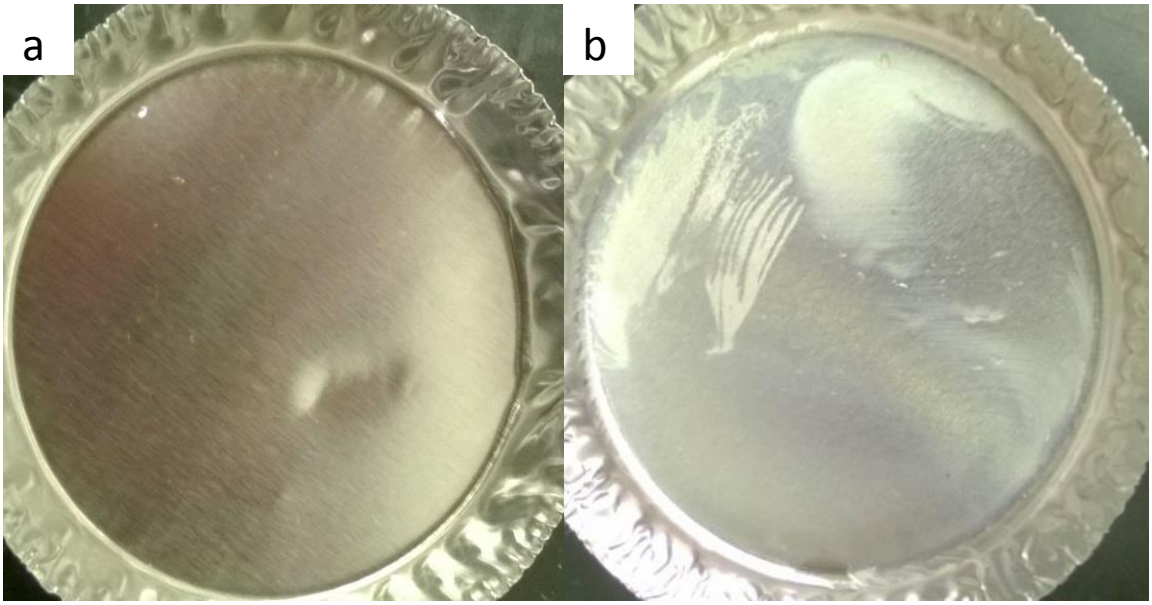

Figure 145. Coatings of a) neat IM9330 and b) 2 wt% CePOSS – 2 wt% PEG POSS in IM9330.

As a result, this coating was discarded in favor of the POSS-epoxy matrix, EP3510. Neat EP3510 was a reddish-orange color depending on thickness, as shown in Figure 146a.

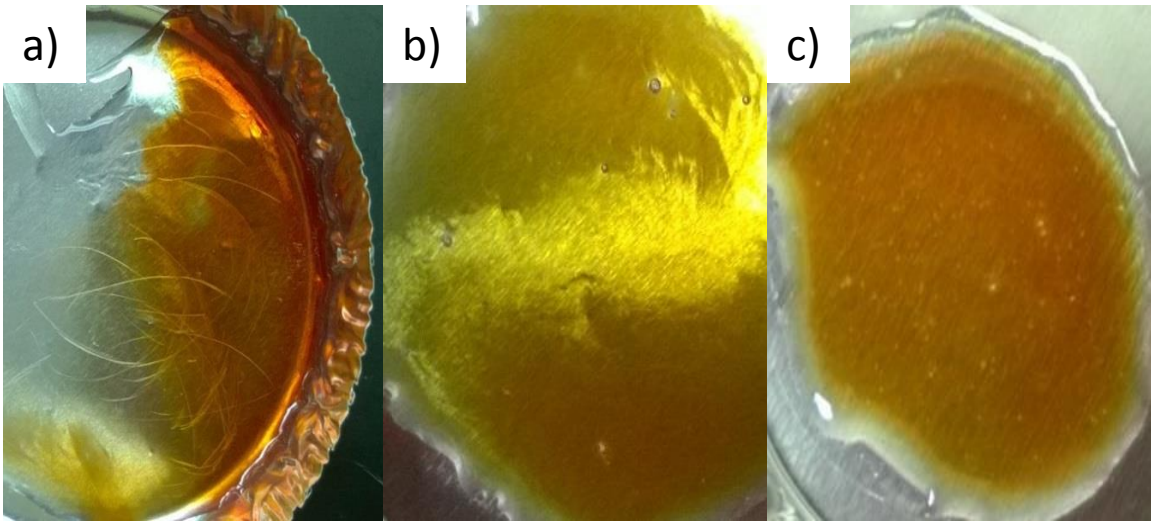

Figure 146. Coatings of a) neat EP3510, b) 2 wt% CePOSS – 2 wt% PEG POSS, and c) 4 wt% CePOSS – 2 wt% PEG POSS in EP3510.

Inclusion of CePOSS-PEG POSS lightened the coating (Figure 146b), but no aggregates appeared until 4 wt% CePOSS – 2 wt% PEG POSS (Figure 146c).

EP3510 was more viscous than the solvent rich IM9330 and this caused difficulty in attempts to level the sample surfaces. To address this issue, a drawdown bar was used to cast coatings of 1 mil on glass slides before the thermal cure with varying levels of CePOSS-PEG POSS, always at a 2:1 ratio. Some dust did settle on samples during this process, but overall the finished coatings were transparent. The coatings are displayed in Figure 147. Of note, the smudge in the 2.5 wt% CePOSS – 1.25 wt% PEG POSS coating was sample that cured on the bottom of the slide, not an impurity or aggregation region


Neat EP3510

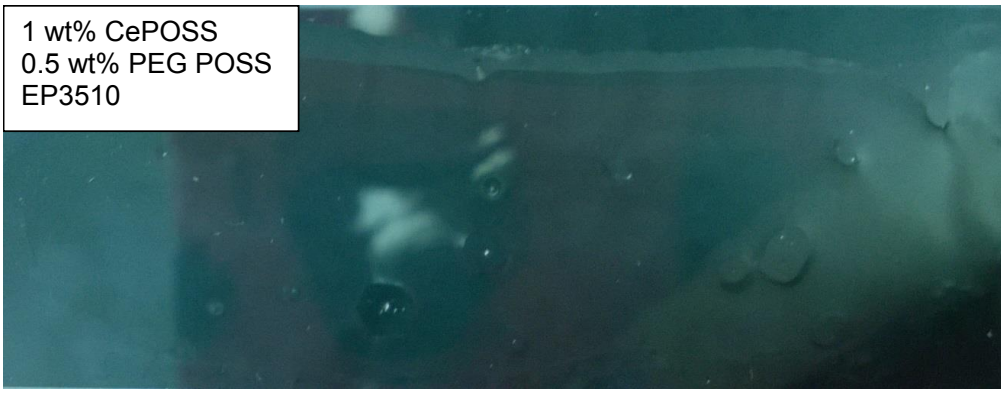
1 wt% CePOSS
0.5 wt% PEG POSS
EP3510

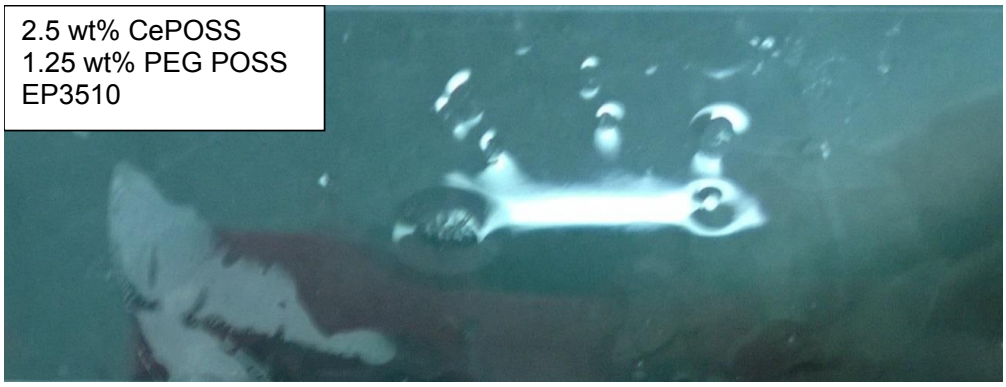
2.5 wt% CePOSS
1.25 wt% PEG POSS
EP3510

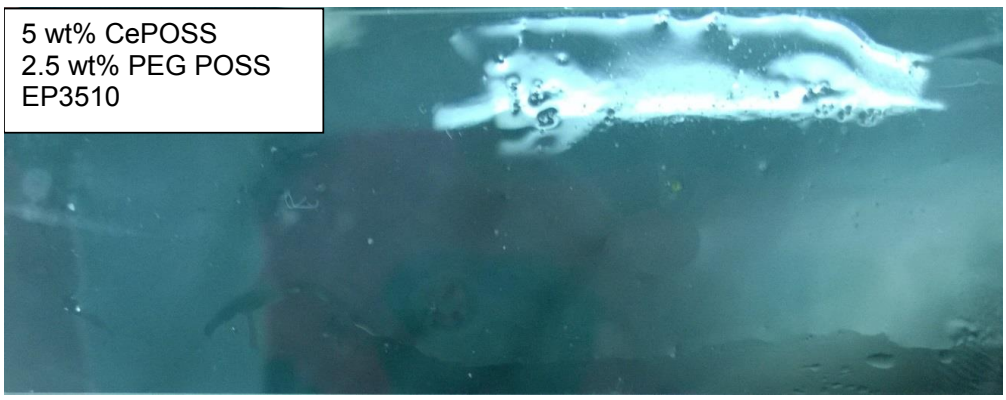
5 wt% CePOSS
2.5 wt% PEG POSS
EP3510

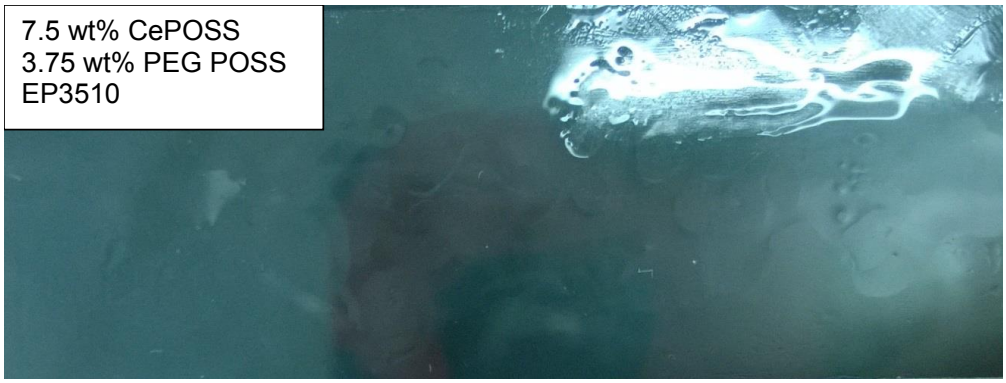
7.5 wt% CePOSS
3.75 wt% PEG POSS
EP3510

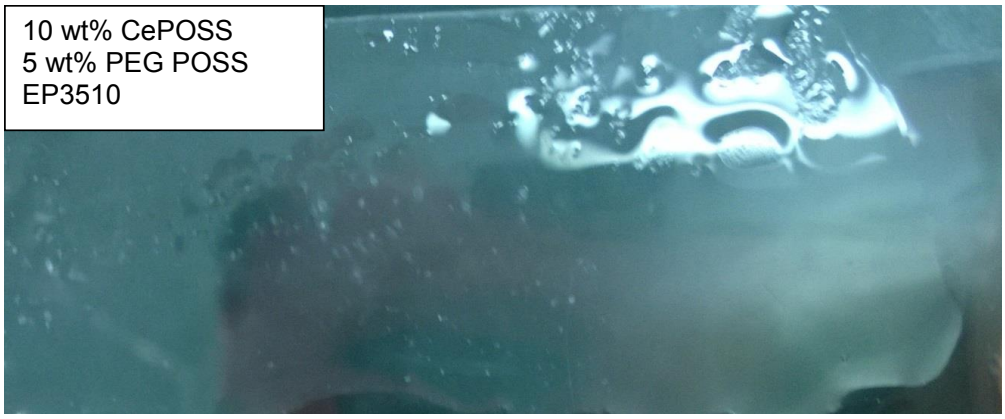
10 wt% CePOSS
5 wt% PEG POSS
EP3510

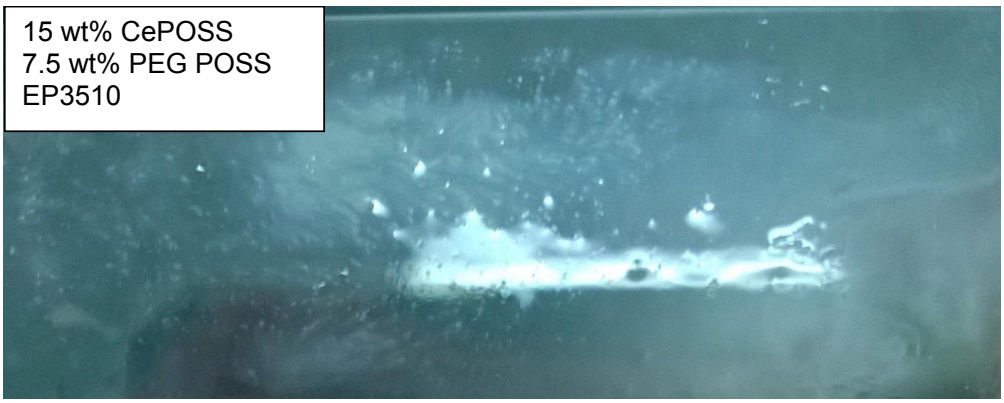
15 wt% CePOSS
7.5 wt% PEG POSS
EP3510

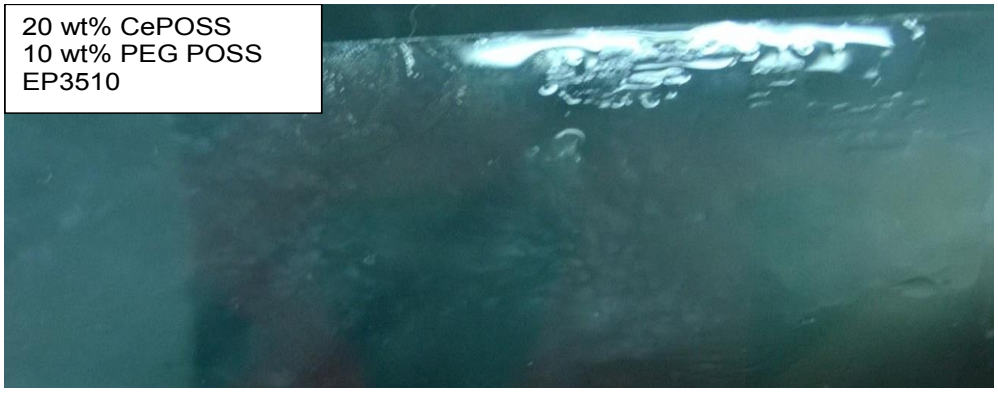
20 wt% CePOSS
10 wt% PEG POSS
EP3510

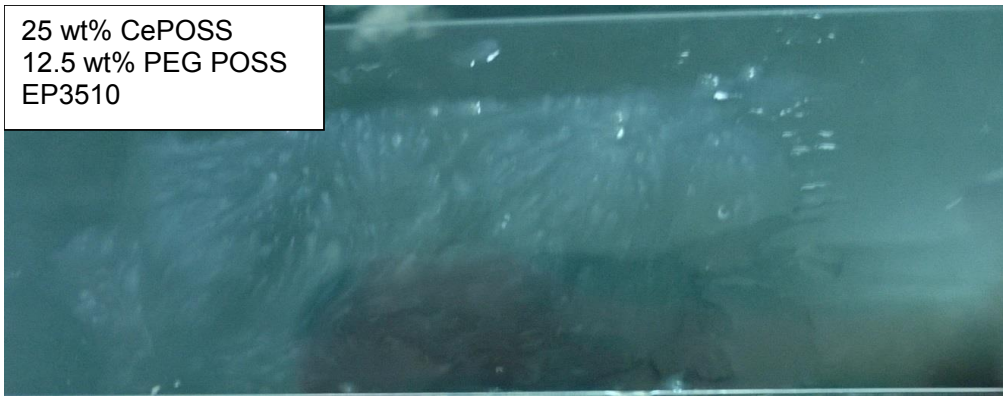

Figure 147. CePOSS-PEG POSS at various loading levels in EP3510.

The EP3510 coatings were transparent up to a loading of 5 wt% CePOSS – 2.5 wt% PEG POSS. At this loading level, white flecks with diameters less than 1 μm were occasionally seen at or above a loading of 10 wt% CePOSS –5 wt% PEG POSS. These aggregates were eliminated by increasing mixing time of the 2:1 CePOSS:PEG POSS mixture with the tissue tearor. Another issue was that all coatings above 1 wt% CePOSS – 0.5 wt% PEG POSS were slightly tacky after the cure protocol was complete. This was issue was solved by increasing the amount of Lindax 1® curative to 5 wt% of the overall formulation, which completed cure and did not visibly change optical properties.

At loadings of 7.5 wt% CePOSS – 3.75 wt% PEG POSS EP3510 coating, white aggregates and cloudy areas became common. Cloudiness especially increased significantly at 15 wt% CePOSS – 7.5 PEG POSS. This may indicate that the solubility limit of the system has been reached. This induced a loss of optical quality as shown in the above photos. Therefore, the decision was made to use the fillers only up to 5 wt% CePOSS – 2.5 wt% PEG POSS for further testing to avoid loss of optical properties.

Conclusions

Cerium (IV) oxide is used for UV protection of polymers. However, it is difficult to disperse.[9,10] Incorporating cerium oxide in glycidyl POSS enhanced dispersion and resulted in opaque, cream-colored layers. These layers could be cohesively bonded to a POSS/epoxy matrix during cure. The location of cerium-rich aggregates depth-wise in the POSS-cerium oxide layer could be influenced by orientation during cure. After plasma exposure, it was concluded that cerium-rich aggregates at the surface impeded oxidation of the surface but that the oxygen plasma source used was not powerful enough to cause detectable POSS glassification.

Morgan et al. reacted titanium dioxide with an open cage silanol POSS to better disperse titanium dioxide in polypropylene.[99] In the present study, a similar approach was attempted with cerium (IV) oxide and trisilanol phenyl POSS to improve the dispersion of cerium in a POSS-rich matrix. However, the cerium (IV) oxide was not uniformly dispersed by this method. Cerium (III) nitrate hexahydrate formed a dispersible mixture with POSS. Mass spectroscopy and nuclear magnetic resonance spectroscopy suggested that there was probably no reaction to form covalent bonds between the Cerium and POSS moieties. However, attenuated total reflectance Fourier transform infrared spectroscopy suggested hydrogen bonding between the POSS silanols and water, and silanols and nitrates of the cerium (III) nitrate hexahydrate. The resulting material, which we named Ce POSS, showed noticeably more absorbance than cerium (III)

nitrate hexahydrate or trisilanol phenyl POSS at UV wavelengths between 235 and -275 nm.

CePOSS initially produced micron-sized aggregates in POSS-polyimide and POSS-epoxy coatings. When CePOSS was combined with a POSS with eight poly(ethylene glycol) pendants at a 2:1 PEG POSS:CePOSS ratio, this produced transparent coatings in the POSS-epoxy matrix, EP3510, up to a loading of 5 wt% CePOSS-2.5 wt% PEG POSS. Above this loading level, the coating became cloudy with white aggregates indicating the solute had reached its solubility limit.

No combination of CePOSS-PEG POSS produced transparent POSS-polyimide coatings. Therefore, films of various levels of CePOSS-PEG POSS in EP3510 were chosen along with neat EP3510 and neat EPON 862 (the base epoxy of EP3510) for exposure to UV/ozone and UV transmittance analysis. Glassification of POSS is an important mechanism for protection of organic materials in low Earth orbit and this study attempted to assess the advantages of including cerium on this process.

CHAPTER V – UV TRANSMITTANCE AND UV/OZONE EXPOSURE OF POSS COATINGS

Introduction

The combination of cerium (III) nitrate hexahydrate and trisilanol phenyl POSS produced enhanced UV absorbance from 235-275 nm compared to cerium (IV) oxide or neat trisilanol phenyl POSS. Unlike Cerium oxide, the combination was also able to be incorporated into a POSS-epoxy coating, EP3510, to produce a transparent material. This was accomplished by pre-blending at a 2:1 ratio with PEG POSS at up to 5 wt% CePOSS and 2.5 wt% PEG POSS. Samples of the neat epoxy EPON 862, neat EP3510, and EP3510 with 1 wt% CePOSS-0.5 wt% PEG POSS, 2.5 wt% CePOSS-1.25 wt% PEG POSS, or 5 wt% CePOSS-2.5 wt% PEG POSS were examined by UV-vis spectroscopy to determine whether CePOSS would also increase UV absorbance when in a coating.

One of the primary reasons for using POSS in low Earth orbit is its transformation to a passivating SiO_2 layer under atomic oxygen.[12] Therefore, it was of interest to see how the presence of cerium affected this process. A conventional 18 W laboratory plasma oven was not powerful enough to glassify POSS. Instead, the method of Özçam et al. was adapted wherein samples were exposed to a combination of UV radiation and ozone. The effects of this treatment were evaluated by x-ray photoelectron spectroscopy, scanning electron microscopy, and contact angle measurement. UV-vis spectroscopy was

conducted on samples before and then after exposure to UV radiation and ozone.

Results and Discussion

The implicit reason for combining cerium (III) nitrate hexahydrate with trisilanol phenyl POSS to form the CePOSS material was to enhance the UV absorbance of POSS. Moreover, POSS is transformed to a layer of silica under atomic oxygen exposure. This silica layer can protect underlying organic material from erosion.[67] It was unknown how this transformation would be affected by the inclusion of cerium.

UV Transmittance Measurements

As shown in the previous chapter, CePOSS had higher UV absorbance than trisilanol phenyl POSS in the range of electromagnetic radiation wavelengths 235 to 275 nm. In order to enhance miscibility in the epoxy-amine matrix, CePOSS was mixed with PEG POSS at a 2:1 ratio and then included in EP3510, a thermally cured POSS-epoxy coating, at 1/0.5, 2.5/1.25, and 5/2.5 wt% concentrations of CePOSS/PEG POSS. UV-vis spectroscopy was conducted on the CePOSS/PEG POSS materials in addition to neat EP3510 and neat EPON 862, which is the base epoxy used for EP3510. The base epoxy sample served as the non-POSS, non-CePOSS control. Films of each material were cast on UV transparent quartz using the same amount of material and a 0.5 mil (0.0127 mm) drawdown bar to attempt to achieve equivalent thicknesses between films.

After cure, films ranged in thickness from 1.23-1.58 mm. For the five materials, films closest in thickness were compared for transmittance between 200-500 nm, as shown in Figure 148.

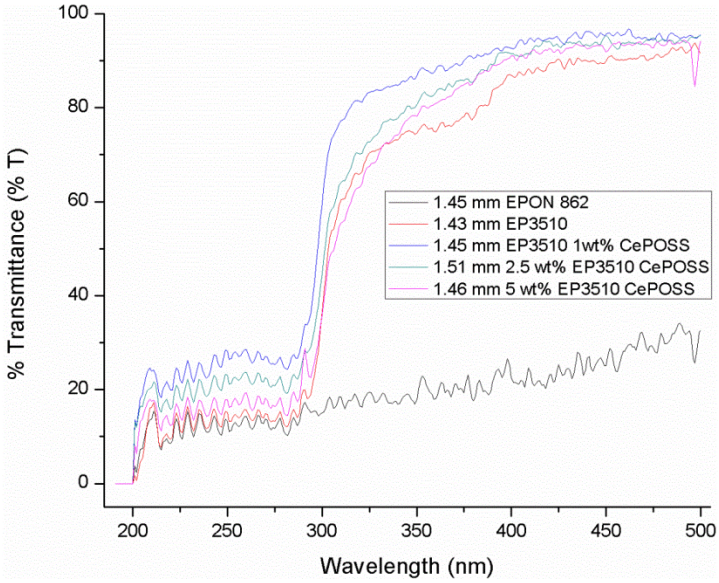

Figure 148. UV transmittance of EPON 862, EP3510, and EP3510 with CePOSS from 200-500 nm.

The epoxy-only EPON 862 transmitted only between 10 and 30 percent of the electromagnetic radiation over the entire wavelength range that was investigated. The POSS-epoxy EP3510 and EP3510 coatings with CePOSS transmitted between 10 and 30 % of the radiation in the wavelength range200 to 300 nm. However, in the wavelength range 300 to 500 nm, the POSS-epoxy EP3510 samples with and without CePOSS, transmitted 80 to 95 percent of the radiation. The electromagnetic radiation signature of these latter materials is significant because they are essentially opaque in the ultraviolet region and transparent in the visible region. The roughness displayed in the spectra was due to fluctuations in beam intensity when passing through films.

Although Figure 148 gives a general idea of the transmittance properties of the five materials considered, the films used had similar but not matching thicknesses. Therefore, the percent transmittance was recorded at 250, 300, 350, and 400 nm for each sample and divided by the thickness of the sample in millimeters. There were 3 to 5 samples for each type of material, so an average and standard deviation of percent transmittance per unit thickness could be determined for each of the 4 selected wavelengths. The results of these calculations are shown in Figures 149-152.

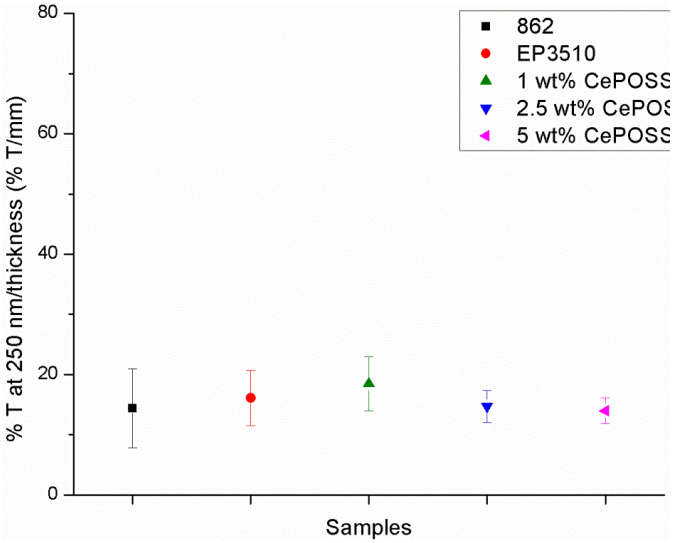

Figure 149. Percent transmittance at 250 nm/film thickness.

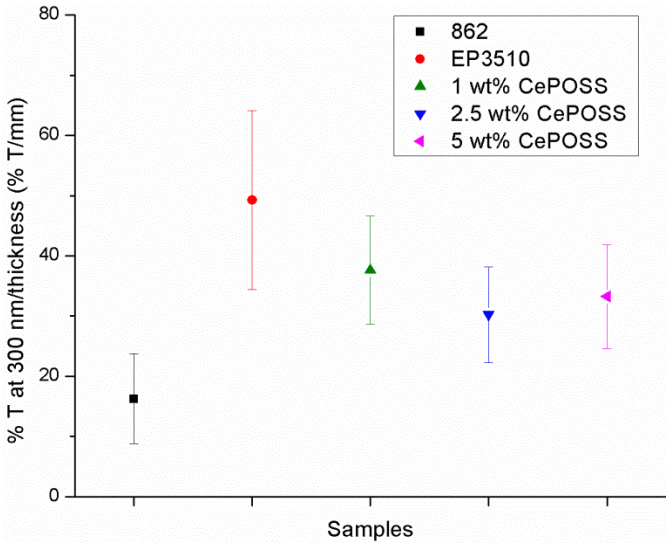

Figure 150. Percent transmittance at 300 nm/film thickness.

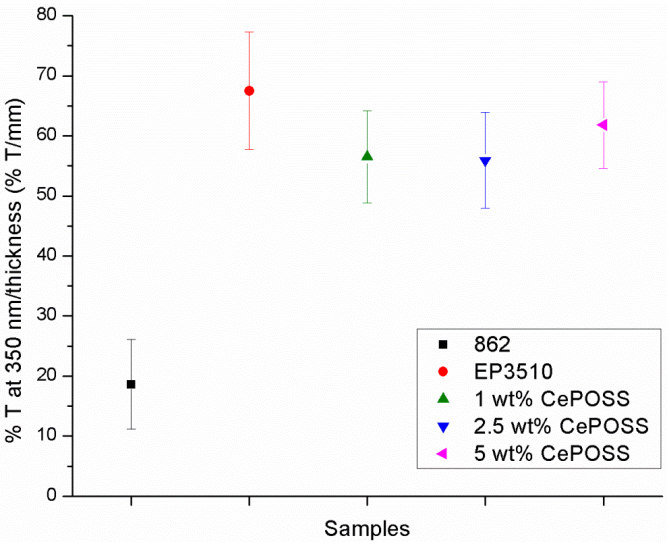

Figure 151. Percent transmittance at 350 nm/film thickness.

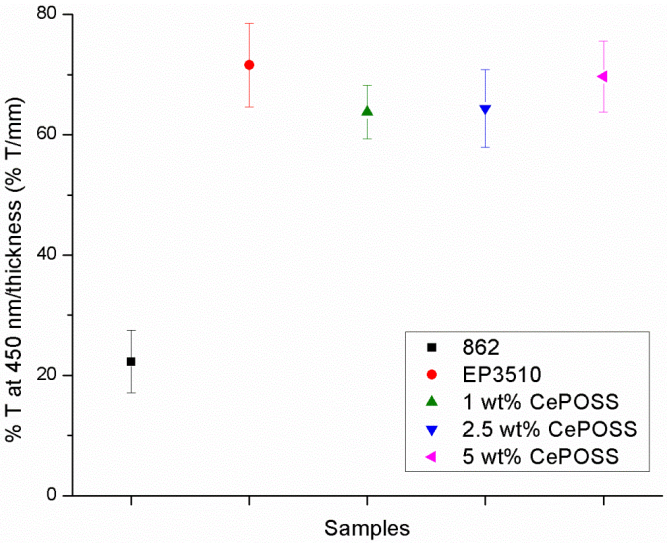

Figure 152. Percent transmittance at 450 nm/film thickness.

Accounting for thickness, there was no statistically significant difference between EPON 862 and POSS/ CePOSS -inclusive materials at 250 nm. Above 300 nm, all POSS/ CePOSS -inclusive samples allowed significantly more electromagnetic radiation transmission compared to the neat epoxy, EPON 862. In addition, there was no statistically significant difference in transmission at any of the selected wavelengths between neat EP3510 and EP3510 with CePOSS. Previous UV-vis data presented in Chapter 4 indicated that CePOSS was more absorbent from approximately 235-275 nm compared to neat trisilanol phenyl POSS. From this result, it was assumed that the inclusion of CePOSS would decrease the UV transmission of a POSS-rich material. Decreased UV transmission in the presence of CePOSS was not observed in this study. This fact that the effect of CePOSS on UV transmittance was not observed could be attributed to the low Ce loading level of 5 wt percent, or possibly that the effect of the Ce was hidden by the opacity of the epoxy base in the UV range.

An additional conclusion from the UV-vis spectroscopy was the strong increase in transmission above 300 nm for the POSS-epoxy coatings (EP3510, and EP3510 with CePOSS) compared to the neat epoxy EPON 862. UV transmittance of epoxies can be affected by the amount and nanoscale distribution of additives.[162] Changes in the distribution and loading level of additives such as POSS also affects the morphology of epoxies.[163] Therefore, it may be that well dispersed POSS modified the nanostructural morphology of the EPON 862 to increase transmittance above 300 nm.

Glassification Attempts in Laboratory Plasma Oven

The use of POSS in low Earth orbit is based on its ability to glassify and protect underlying organic material against atomic oxygen and other hazards.[27,87] Some POSS-polymer systems have been glassified with oxygen plasma.[94] Therefore, this method was attempted to determine the effect of CePOSS on glassification. The first exposures completed were with neat EP3510 in a plasma oven producing oxygen plasma at 18W power.[131] Bundles of three slides coated with EP3510 at 1 mil and one drop of EP3510 cured onto a SEM post were exposed for durations of 1, 2.5, 5, 10, 15, 30, and 45 min. After exposure, SEM/EDS was performed on each sample to examine morphology and compositional changes. Any significant decrease in carbon could indicate glassification and suggest a candidate for more expensive XPS testing.[69] Figure 153 charts changes in silicon, oxygen, and carbon atom percent according to exposure time.

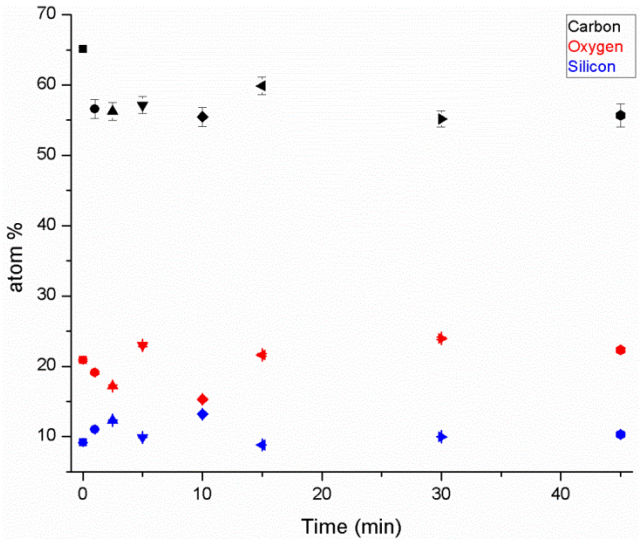

Figure 153. Changes in carbon (black), oxygen (red), and silicon (blue) atom percent in neat EP3510 after exposure to 18 W oxygen plasma.

SEM/EDS results show that carbon content decreased after only 1 min of exposure to the plasma, but remained constant with additional exposure. Oxygen and silicon content fluctuated until 15 min of exposure and leveled out afterward. The overall increase in oxygen atom percent was approximately 2 to 3 atom percent. This was less than reported for POSS glassification as verified by XPS in other studies.[69] In addition; no morphological changes were seen after any duration of exposure.

Water contact angle was also measured on three unexposed neat EP3510 coatings and three neat EP3510 samples that had been exposed for 45 min. The contact angle dropped from 52.71 +/- 1.03° without exposure to 27.50 +/- 1.99° with 45 min of exposure. This was indicative of a more hydrophilic surface. However, the lack of significant carbon atom percent decrease in SEM/EDS led to the conclusion that the plasma cleaned and oxidized the surface but was not powerful enough to glassify POSS.

Xeel UV/Ozone Exposures

Atomic oxygen does glassify POSS and other silicon-rich substances, but techniques used to expose samples to atomic oxygen are time and cost intensive.[12,31,73.74] In work done in 2014, Özçam et al. glassified poly(dimethyl siloxane) and poly(vinyl methyl siloxane) using a combination of UV radiation and ozone.[132] Samples were placed in an ozone chamber 5 mm away from a 8.2 mW/cm^2 fused quartz UV lamp.[132] The ozone concentration was not specified. Surface glassification was confirmed by decreased water contact angle, decreased elastic modulus of films, and bond shifts in XPS, with substantial changes occurring after 30 min of exposure.[132] Efimenko et al. estimated that the poly(dimethyl siloxane) glassified up to 5 nm deep into the sample from x-ray diffraction analysis.[128,132] In contrast, the poly(vinyl methyl siloxane) glassified completely through the entire ~700 nm thickness of the films due to the ability of the vinyl side chains to participate in reactions and transmit radicals through the bulk of the polymer.[132] Given the success of this UV/ozone method to glassify polysiloxanes, it was decided to attempt the same combination of degradants to glassify POSS-rich coatings.

Coatings with POSS and CePOSS were exposed to UV radiation and ozone at Xeel Corporation.[133] The main characterization method used to verify glassification was x-ray photoelectron spectroscopy (XPS). Unlike SEM/EDS, XPS can verify the type of bonding present at the surface in addition to elemental composition. This is done by bombarding the surface with x-rays and then correlating the binding energies of the ejected electrons to values of electrons

excited in specific nuclei.[72] This technique does only penetrate 1-2 nm into the surface, as opposed to SEM/EDS but XPS has been a standard technique to verify glassification.[12,65,73,74]

XPS on UV/ozone Exposed Samples. Surface analysis was conducted on the same samples before and after exposure with XPS. The neat EPON 862 was not expected to glassify but the surface still oxidized. This was shown in Figure 154, which shows the unexposed (black) and exposed (red) XPS spectra through the full energy range measured.

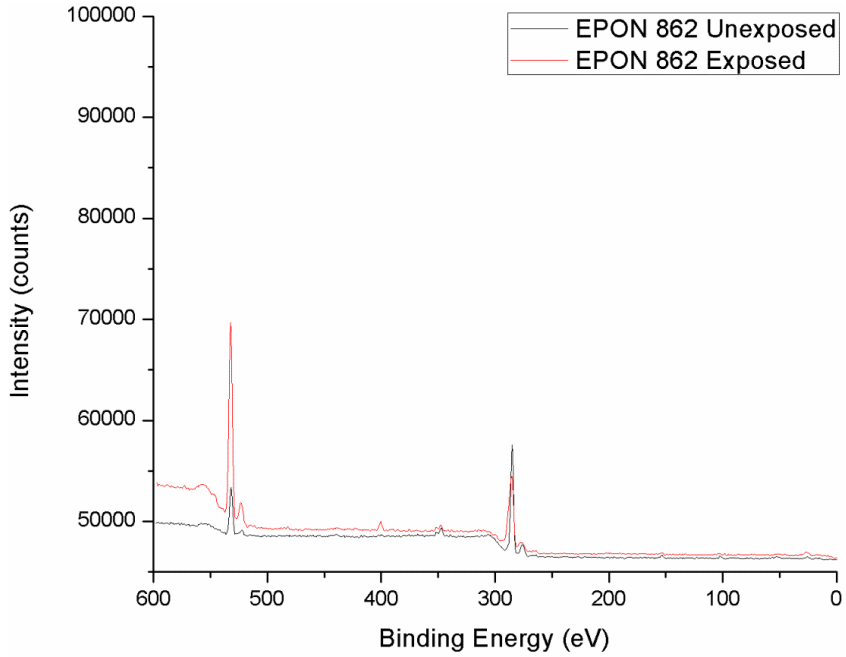

Figure 154. Unexposed (black) and exposed (red) EPON 862 XPS spectra from 0-600 eV.

The O 1s peak at approximately 532 eV increased significantly in intensity after exposure, confirming oxidation as a result of the UV/ozone exposure.[164]

In contrast, the Si 2p peak at 102.3 eV decreased in intensity. The EPON 862 material did not contain POSS but may have picked up silicon-based

contaminates at some point before analysis. The Si 2p peaks from silicon-based contaminants in unexposed and exposed EPON 862 spectra are shown in Figure 155 and 156, respectively.

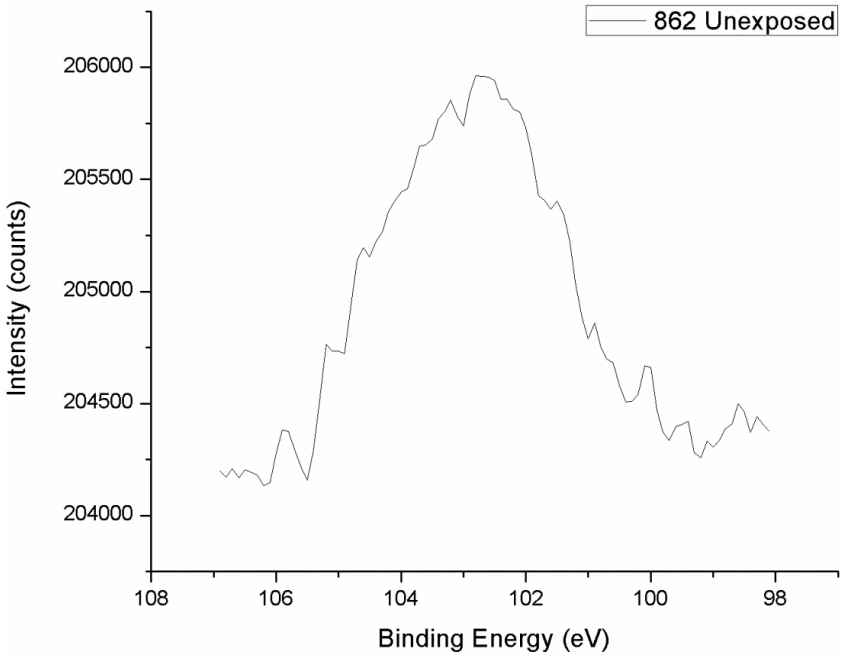

Figure 155. XPS Si 2p spectra from 98-107 eV for unexposed EPON 862.

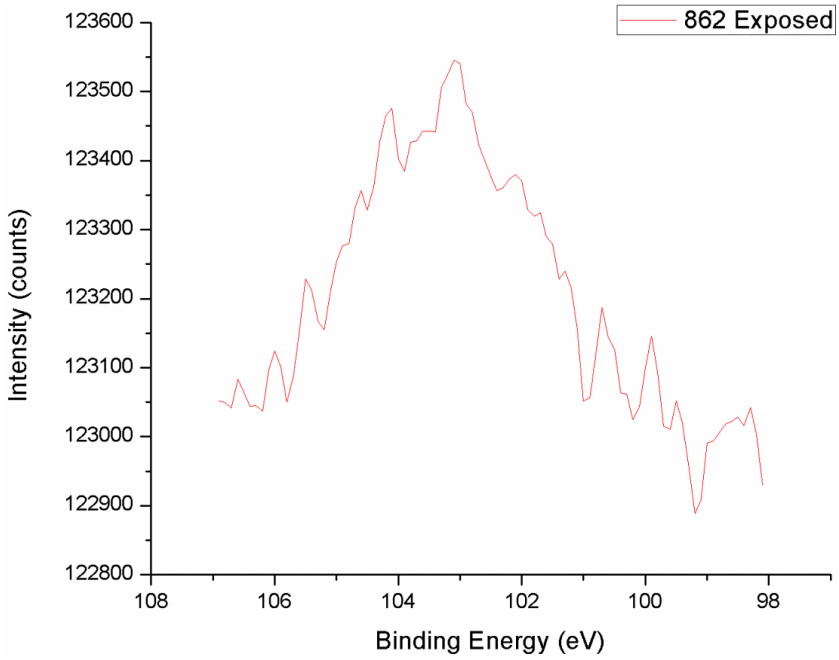

Figure 156. XPS Si 2p spectra from 98-107 eV for exposed EPON 862.

The Si 2p peak only shifted from 102.3 eV to 102.6 eV after exposure. The oxidation of the surface made the composition less uniform, as seen by increasing roughness after exposure. This confirms the damage done to epoxies that do not include POSS. In addition, the intensity of the Si 2p decreased drastically. This also happened with the C 1s peak, as shown in Figure 157.

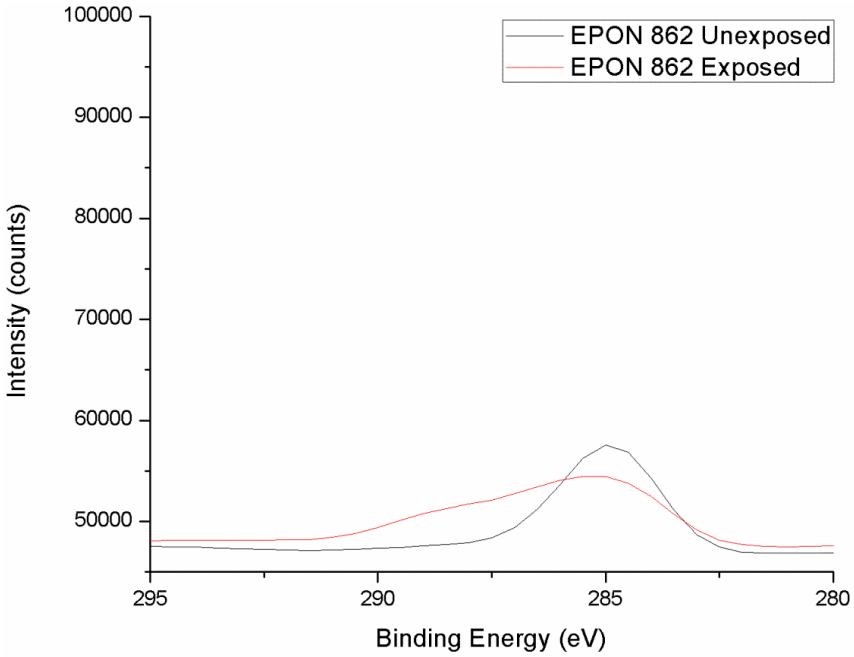

Figure 157. XPS C 1s spectra from 280-295 eV for unexposed (black) and exposed (red) EPON 862.

The intensity drop for both the Si 2p and C 1s peaks reflects a surface dominated by oxygen after UV/ozone exposure. In addition, the broadening of the C 1s peak reflected an increase in C-O bonds.

Neat EP3510 did glassify as predicted with a shift in the Si 2p peak and an increase in the magnitude of the O 1s peak (Figure 158).

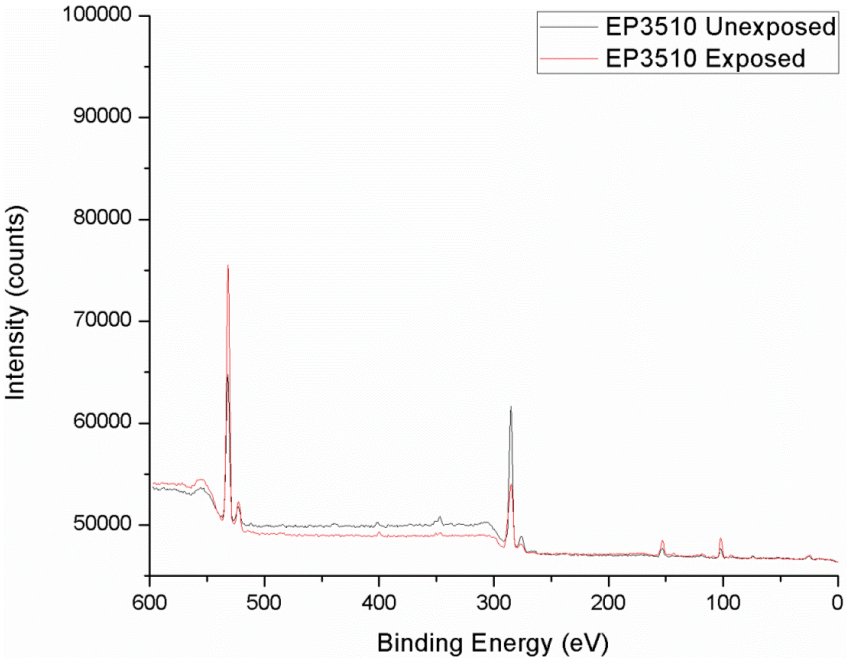

Figure 158. Unexposed (black) and exposed (red) neat EP3510 XPS spectra from 0-600 eV.

The change in the Si 2p peak bonding is shown in Figure 159.

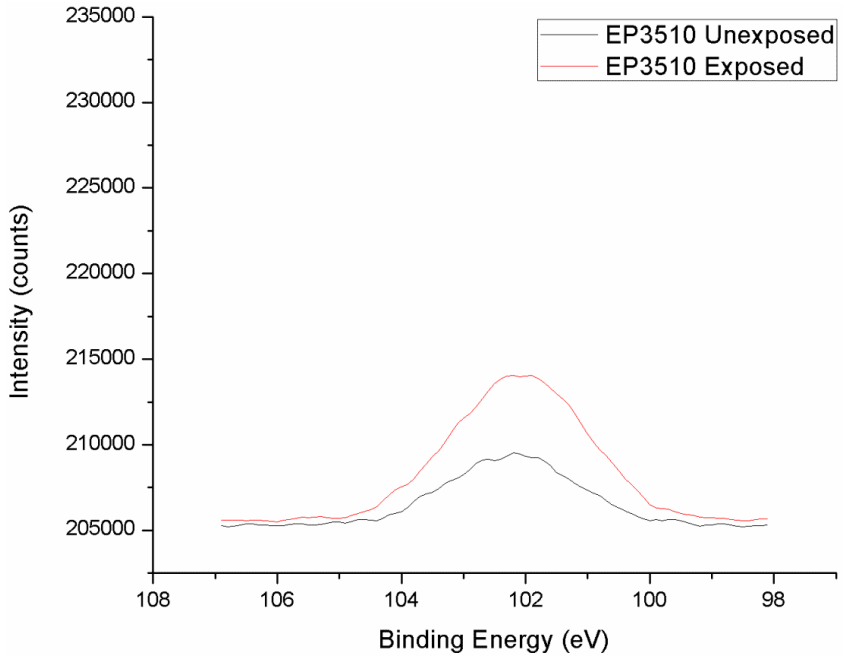

Figure 159. XPS Si 2p spectra from 98-107 eV for unexposed (black) and exposed (red) neat EP3510.

The binding energy of the unexposed EP3510 Si 2p peak had a maximum of at 102 eV corresponding to the Si_3N_4 species with a shoulder at 100.4 eV for SiC bonding. When exposed, this binding energy shifted to 103.2 eV, centered between SiO_2nH_2O at 103.5 eV and SiO_2 at 103 eV. This is typical of the bonding shift seen with glassification of POSS.[75] In addition, the exposed peak was more uniform in shape indicating a more chemically uniform surface after exposure.

Carbon content decreased after exposure, as expected (Figure 160).

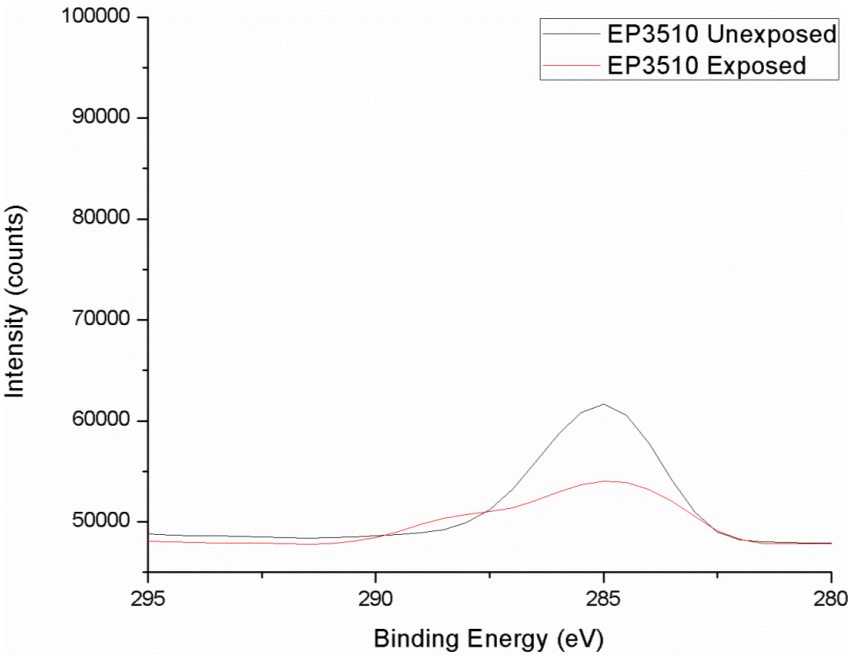

Figure 160. XPS C 1s spectra from 280-295 eV for unexposed (black) and exposed (red) neat EP3510.

The decrease in intensity corresponds to the removal of the organic pendant groups from POSS during the transformation of POSS to silica. As with the EPON 862 surface, the EP3510 C 1s peak also shifted to higher bonding energies, indicating more carbon-oxygen bonding.

The main objective of this testing was to determine whether the presence of CePOSS would impede POSS glassification. Figure 161 shows the full XPS spectra of unexposed and exposed for 1 wt% CePOSS – 0.5 wt% PEG POSS in EP3510.

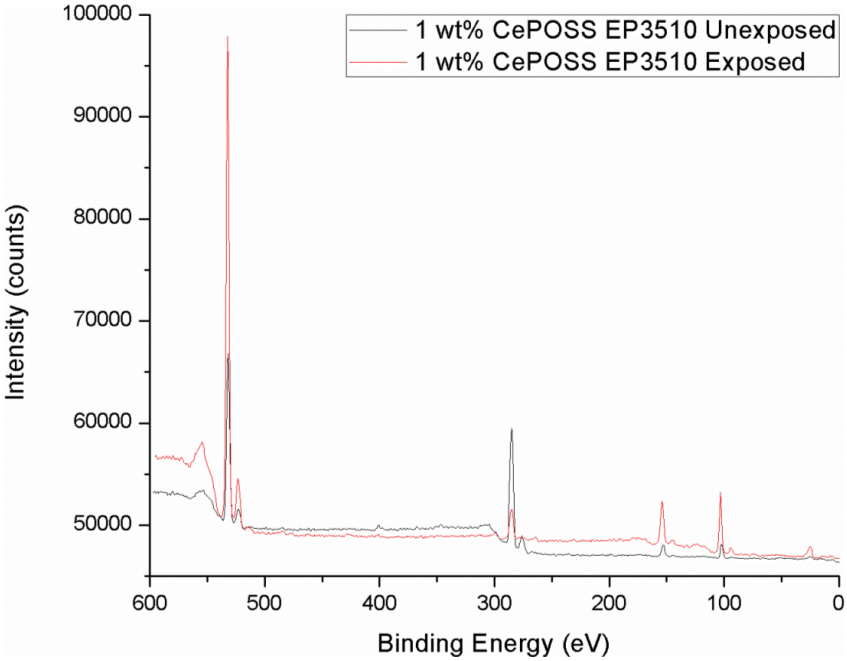

Figure 161. Unexposed (black) and exposed (red) EP3510 with 1 wt% CePOSS-0.5 wt% PEG POSS XPS spectra from 0-600 eV.

The defining features of the full spectra are the strong increases in oxygen (~532 eV) and silicon peaks (~103 eV) as well as the decrease in carbon (~285 eV). The Si 2p peak shift can be better observed in Figure 162.

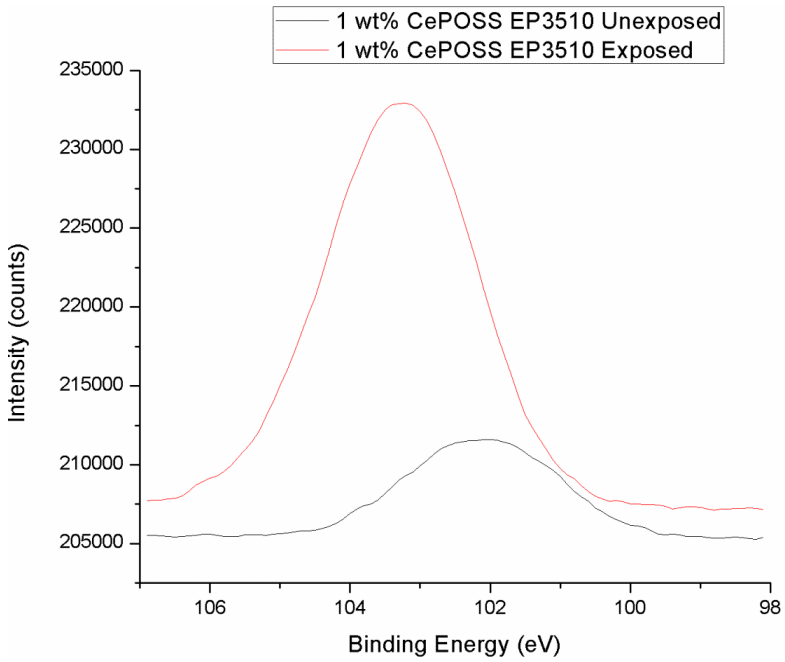

Figure 162. XPS Si 2p spectra from 89-107 eV for unexposed (black) and exposed (red) EP3510 1 wt% CePOSS – 0.5 wt% PEG POSS.

The shift in the EP3510 1 wt% CePOSS – 0.5 wt% PEG POSS sample was more pronounced than the EP3510. The Si 2p peak maximum shifted from to 102.1 to 103.4 eV. The exposed peak also reflected a more uniformly bonded surface in terms of the smooth and narrower peak.

The carbon 1s peak decreased in intensity as displayed in Figure 163.

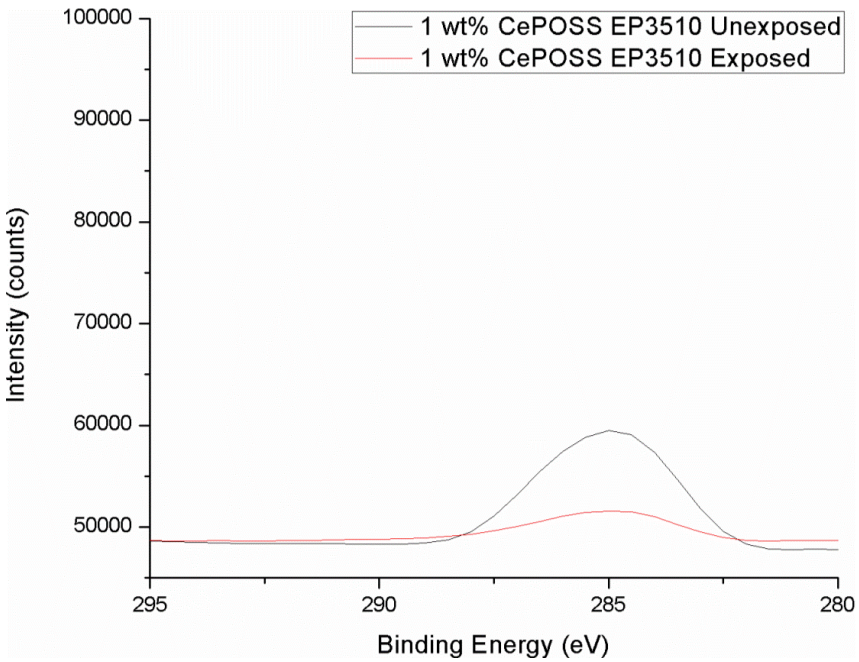

Figure 163. XPS C 1s spectra from 280-295 eV for unexposed (black) and exposed (red) EP3510 1 wt% CePOSS – 0.5 wt% PEG POSS.

Again, this is characteristic of glassification of POSS, which reduces surface carbon content.

The EP3510 2.5 wt% CePOSS – 1.25 wt% PEG POSS sample followed the same trends as the 1 wt% CePOSS sample with increases in oxygen and silica peak intensities while carbon decreased (Figure 164).

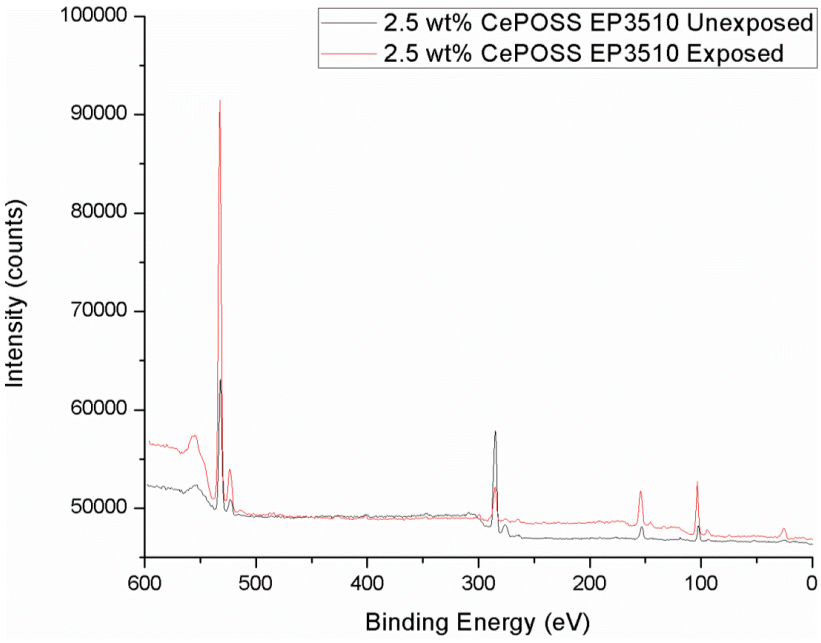

Figure 164. Unexposed (black) and exposed (red) EP3510 with 2.5 wt% CePOSS-1 wt% PEG POSS XPS spectra from 0-600 eV.

The EP3510 2.5 wt% CePOSS – 1.25 wt% PEG POSS Si 2p shift also exceeded that of the neat EP3510 as shown in Figure 165.

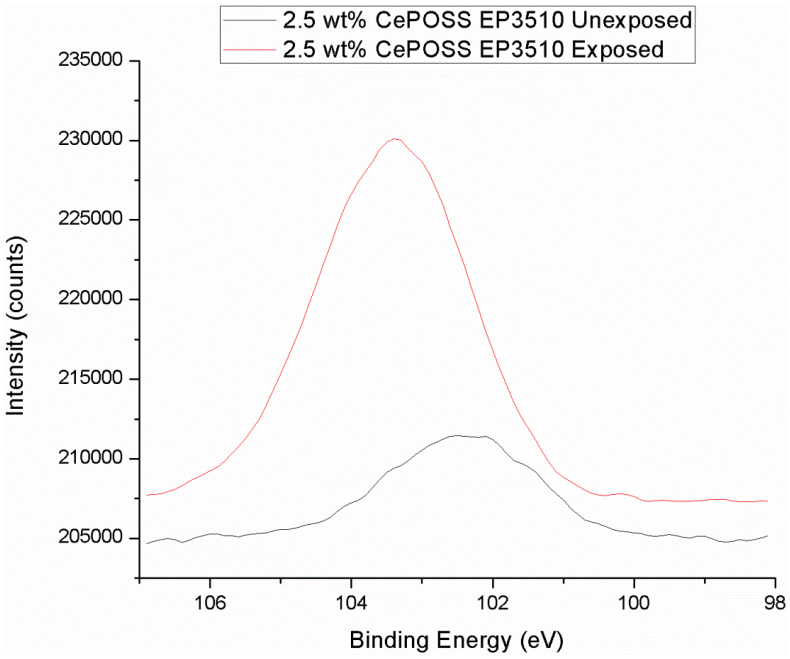

Figure 165. XPS Si 2p spectra from 98-107 eV for unexposed (black) and exposed (red) EP3510 2.5 wt% CePOSS – 1.25 wt% PEG POSS.

The original unexposed EP3510 2.5 wt% CePOSS – 1.25 wt% PEG POSS Si 2p peak was centered on 102.4 eV. This shifted to 103.4 eV, similar to the EP3510 1 wt% CePOSS – 0.5 wt% PEG POSS sample and the Si 2p was again centered between the SiO_2nH_2O and SiO_2 species.

Another similarity to the 1 wt% CePOSS film, shown in the EP3510 2.5 wt% CePOSS – 1.25 wt% PEG POSS sample was the decrease in the C 1s peak intensity as displayed in Figure 166.

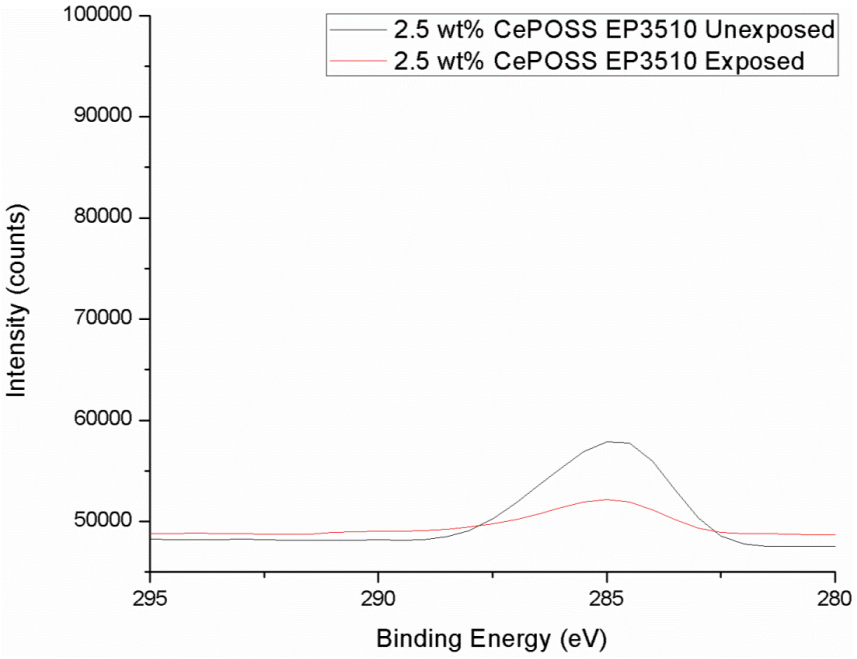

Figure 166. XPS C 1s spectra from 280-295 eV for unexposed (black) and exposed (red) EP3510 2.5 wt% CePOSS – 1 wt% PEG POSS.

The exposed peak was also broadened, indicating that carbon was bonded to more elements in more configurations than before exposure.

The highest loading level used was 5 wt% CePOSS – 2.5 wt% PEG POSS. Above this, aggregates and discolorations appeared in the EP3510. If the EP3510 5 wt% CePOSS – 2.5 wt% PEG POSS samples glassified then it would

be concluded that CePOSS does not affect glassification when used at levels that do not impact the optical quality of the base EP3510 coating. Figure 167 shows the XPS spectra before and after exposure.

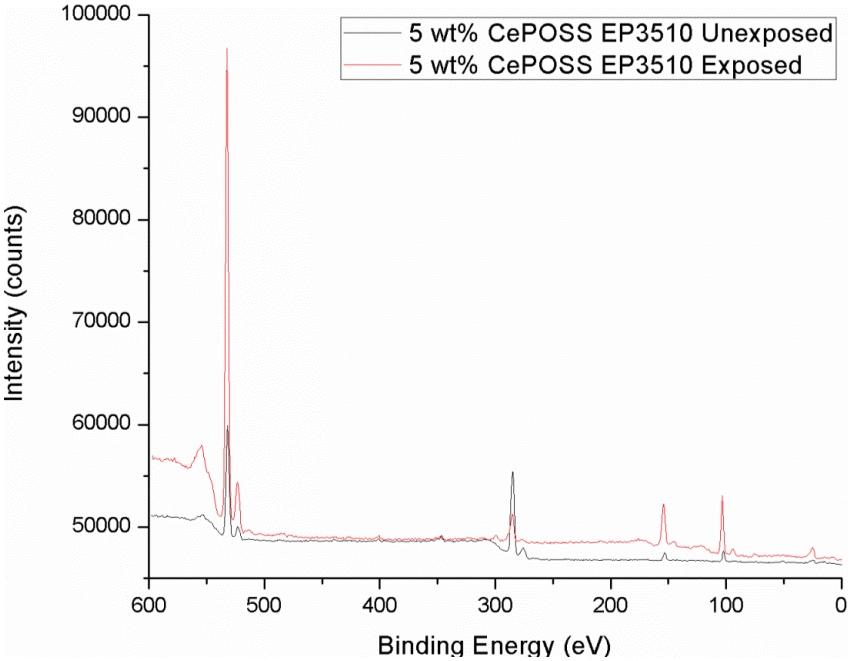

Figure 167. Unexposed (black) and exposed (red) EP3510 with 5 wt% CePOSS-2.5 wt% PEG POSS XPS spectra from 0-600 eV.

The EP3510 with 5 wt% CePOSS-2.5 wt% PEG POSS material underwent surface oxidation during UV/ozone exposure as evidenced by increases in oxygen and silicon peak intensity with a decrease in the carbon peak intensity.

The Si 2p peak shifted 1 eV after exposure as shown in Figure 168.

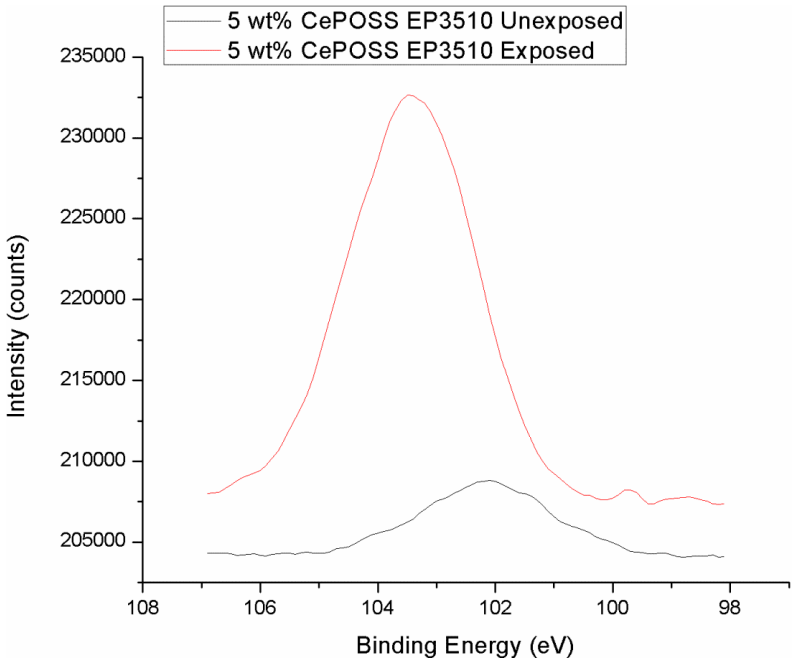

Figure 168. XPS Si 2p spectra from 98-107 eV for unexposed (black) and exposed (red) EP3510 5 wt% CePOSS – 2.5 wt% PEG POSS.

As with the previous samples, the Si 2p peak shifted downfield in this specific case from 102.2 eV to 103.2 eV, indicating POSS glassification. Silicon bonding shifted from Si_3N_4 to SiO_2 and SiO_2nH_2O. In addition, the Si 2p bonding was more uniform after treatment as indicated by the width and smoothness of the peak.

The intensity of the carbon 1s peak also decreased for the EP3510 5 wt% CePOSS-2.5 wt% PEG POSS material after exposure (Figure 169).

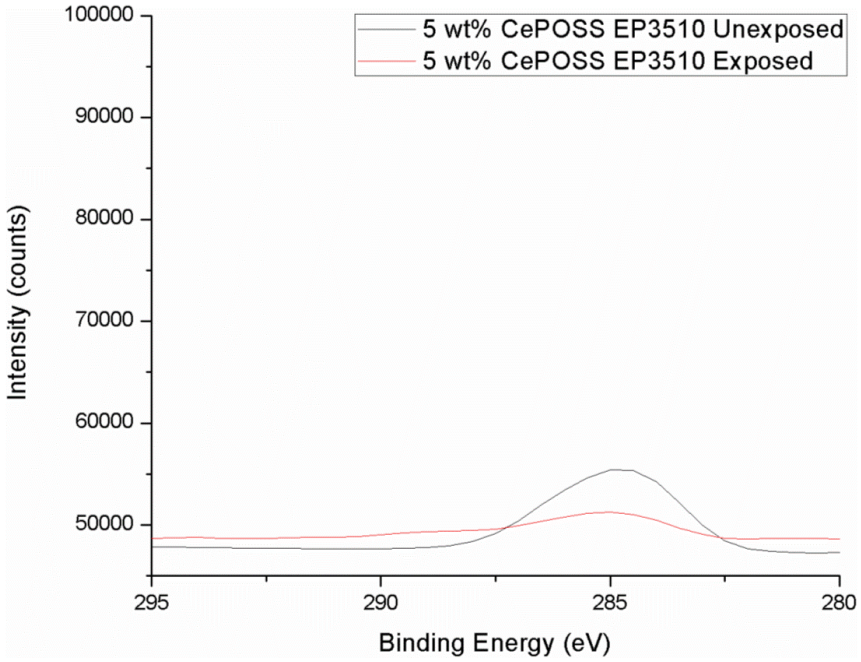

Figure 169. XPS C 1s spectra from 280-295 eV for unexposed (black) and exposed (red) EP3510 5 wt% CePOSS – 2.5 wt% PEG POSS.

In addition to the decrease in intensity, the C 1s peak after exposure was broader, indicating more C-O bonding. This helps to confirm surface oxidation.

The surface compositions before and after exposure for each material are shown in Table 18.

Table 18

XPS surface composition of materials before and after exposure to UV/ozone

	Carbon wt%		Silicon wt%		Oxygen wt%	
Material	**Pre exposure**	**Post exposure**	**Pre exposure**	**Post exposure**	**Pre exposure**	**Post exposure**
EPON 862	85.6	61.7	1.2	0.7	11.9	34.1
EP3510	72.0	21.4	5.0	23.1	21.2	54.9
EP3510 1 wt% CePOSS - 0.5 PEG POSS	67.8	16.6	7.4	25.0	23.0	58.4
EP3510 2.5 wt% CePOSS - 1.25 PEG POSS	66.5	21.6	9.9	21.4	21.9	57.0
EP3510 5 wt% CePOSS - 2.5 PEG POSS	69.4	17.3	6.3	23.5	22.7	59.3

EPON 862 was synthesized from epoxy and imidazole curative only. However, XPS picked up 1.2 wt% Si in this material before exposure and 0.7 wt% after exposure. This could be from silicon contaminants such as dust. After exposure, oxygen content in EPON 862 increased from 11.9 to 34.1 wt%. Carbon content decreased from 85.6 to 61.7 wt%, and this could be attributed to the added oxygen. This decrease was not as large as for the EP3510-based coatings. This could be due to the exposure only oxidizing the surface of the EPON 862 and not continuing to remove large amounts of carbon.

The four POSS-rich samples showed a carbon content decrease on average of 49.7 +/- 3.3 wt%. All four materials had a carbon weight percent decrease over 50 wt% except for the EP3510 2.5 wt% CePOSS-1.25 wt% PEG POSS, which had its carbon content decreased by 44.9 wt%. Silicon content increased for neat EP3510 and the three EP3510 films with CePOSS at an average of 16.1 +/- 3.1 wt%. Again, all films showed an increase of at least 17 wt% Si except for the except for the EP3510 2.5 wt% CePOSS-1.25 wt% PEG POSS. The EP3510 2.5 wt% CePOSS-1.25 wt% PEG POSS showed an increase in silicon of 11.5 wt%. The increase in oxygen across the four EP3510-based coatings was 35.2 +/- 1.2 wt%. The increase for neat EP3510 was 33.7 wt% whereas all coatings with CePOSS were above 35 wt%. While the EP3510 2.5 wt% CePOSS-1.25 wt% PEG POSS oxidized as well as the other CePOSS-containing samples, it would be of interest to run more exposures and XPS with this material to determine if the results in terms of silicon and carbon content are typical.

Overall, it appears that the presence of the CePOSS additive did not impede POSS glassification, which would indicate that the protective capability of POSS against atomic oxygen would likely remain intact Bond energy shifts of the Si 2p peak are recorded in Table 19.

Table 19

Si 2p XPS bond shifts

	Si 2p	
Material	**Pre exposure (eV)**	**Post exposure (eV)**
EPON 862	102.3	102.6
EP3510	102.1	103.2
EP3510 1 wt% CePOSS - 0.5 PEG POSS	102.1	103.4
EP3510 2.5 wt% CePOSS - 1.25 PEG POSS	102.4	103.4
EP3510 5 wt% CePOSS - 2.5 PEG POSS	102.2	102.7

The neat EP3510 Si 2p peak shifted +1.1 eV towards oxidized Si, whereas the shifts with 1, 2.5, and 5 wt% CePOSS were +1.3, +1.0, and +0.5 eV, respectively. More testing would be of interest to see whether a low concentration of CePOSS (≤ 1.0 wt%) consistently produces a greater Si 2p shift. Cerium generally acts as an anti-oxidant and these results indicate that the presence of Cerium at 5 percent loading, does not offer protection against oxidation for the epoxy-amine materials tested in this study.[9]

SEM/EDS on UV/ozone Exposed Samples. Analysis by XPS revealed that the UV/ozone exposure oxidized the EPON 862 surface and glassified the EP3510 and CePOSS-PEG POSS-EP3510 surfaces. Samples were cured onto SEM posts and then exposed to the UV/ozone treatment as made. The EP3510 sample can be shown in Figure 170. Samples were approximately 3-4 mm thick. The darker colors in Figure 170 show where the Lindax 1® curative has concentrated in the thicker center of the sample, compared to the thinner,

transparent edges. This phenomenon was confirmed by ATR FT-IR spectroscopy.

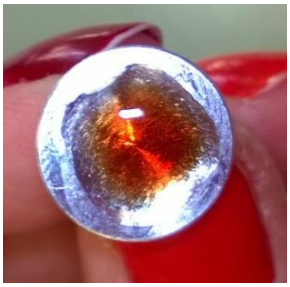

Figure 170. EP3510 cured onto SEM post for exposure.

One set of five samples was examined before exposure and another set withheld and examined after exposure. All samples were sputter coated with silver 2 to 3 times and examined on a Zeiss Sigma VP FEG-SEM. The accelerating voltage was held as low as possible (10-20 kV) to try to avoid damage of the sample by the electron beam, but some surface burning did occur and could not be prevented regardless of beam voltage. Some lower magnification, non-EDS work was done on an FEI Quanta 200 SEM.

EPON 862 oxidized during exposure to UV/ozone but did not lose substantial amounts of carbon, according to XPS. Since this material did not use POSS in its formulation, it was expected that the EPON 862 surface would show significant degradation. The unexposed EPON 862 surface is shown in Figure 171 and the exposed surface is shown in Figure 172.

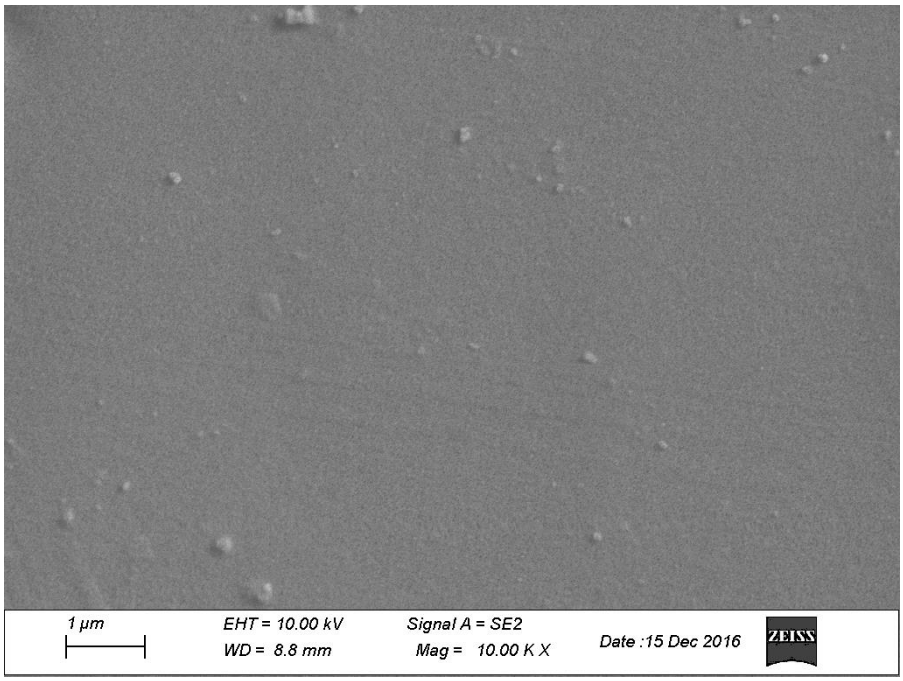

Figure 171. Unexposed surface of EPON 862 at 10000X.

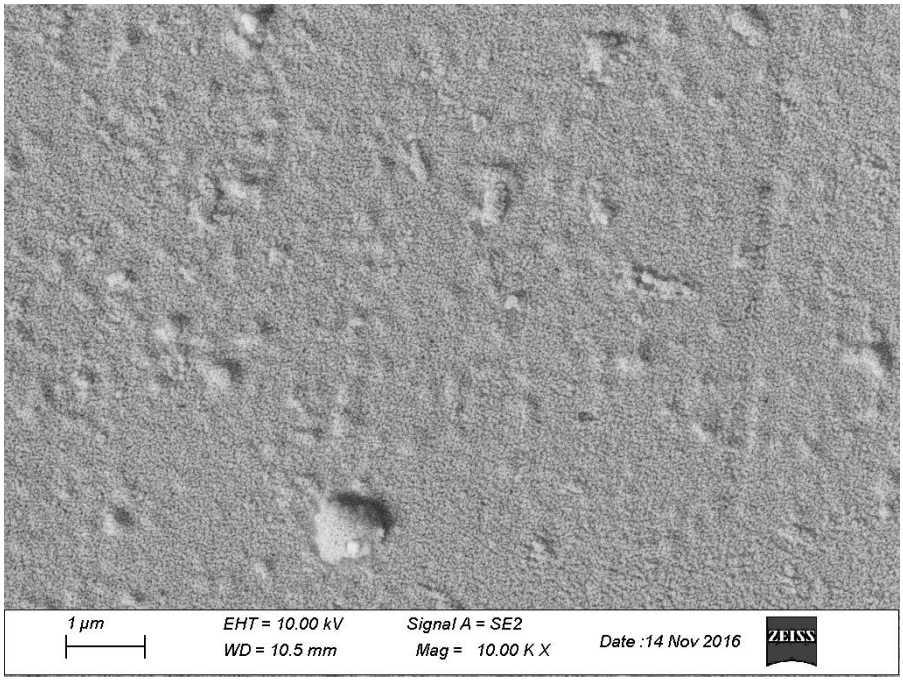

Figure 172. Exposed surface of EPON 862 at 10000X.

Initially, the EPON 862 surface was smooth with minor surface particulates attributed to dirt or other contaminants. After exposure, the surface became more pitted and appeared bumpy. Scanning electron microscopy cannot measure depth, but this pattern may indicate erosion during testing.

EP3510 was the neat POSS-epoxy material without any additional CePOSS-PEG POSS. The unexposed EP3510 sample is shown in Figure 173 with the exposed surface below in Figure 174. Darker spots, especially in the middle of the unexposed micrograph, are caused by burning due to the SEM electron beam.

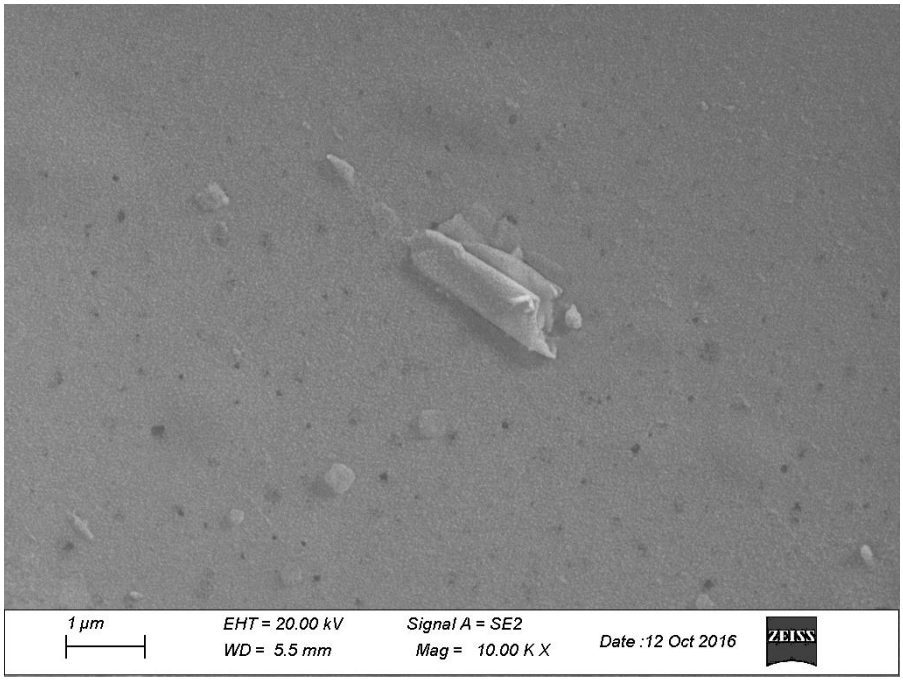

Figure 173. Unexposed surface of EP3510 at 10000X.

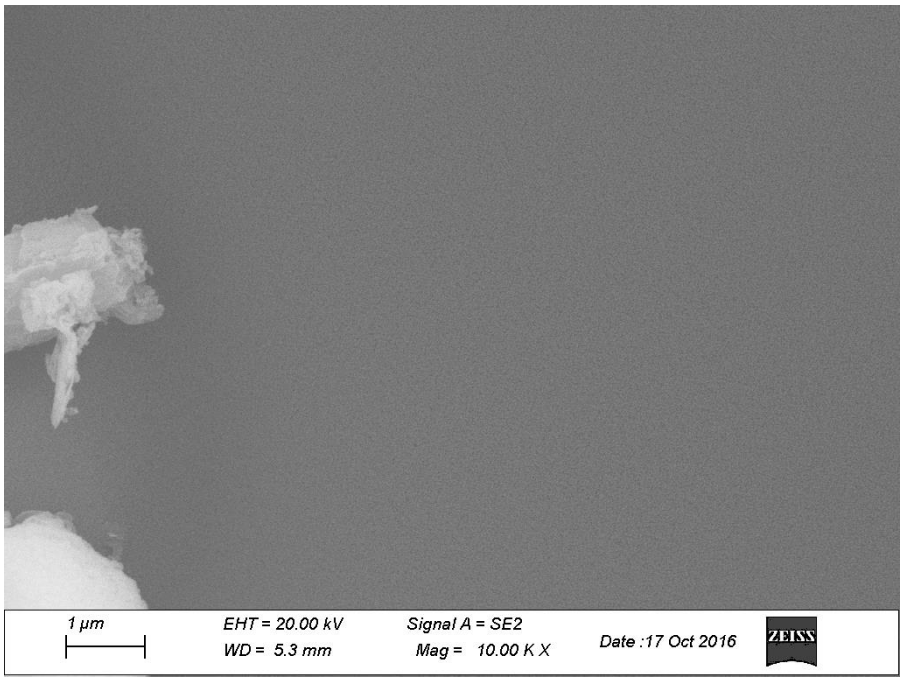

Figure 174. Exposed surface of EP3510 at 10000X.

The EP3510 surface displayed similar debris to the EPON 862 before exposure, but the UV/ozone treatment smoothed the surface to the extent that there were no discernable sub-micron features remaining. Some debris did remain, but there were generally fewer particulates. However, cracking was seen at lower magnifications (Figure 175).

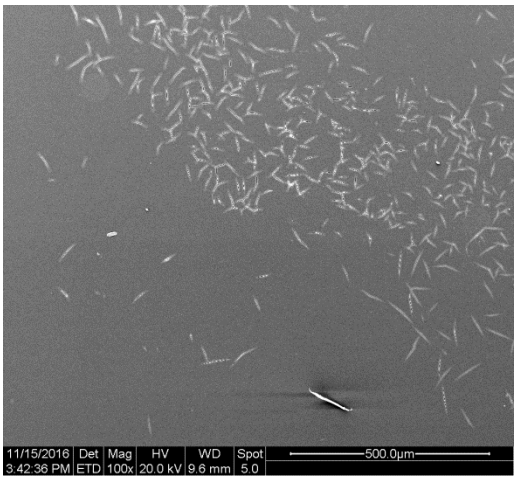

Figure 175. Exposed surface of EP3510 at 100X.

Surface cracking has been reported after glassification of silicones when exposed to atomic oxygen so this was not entirely unexpected.[42] However, it is a concern for the proposed application when considering thermal cycling in LEO.

Analysis by XPS showed POSS glassification even with the presence of CePOSS. Some morphological changes were observed in CePOSS-inclusive samples, however. The unexposed surface of 1 wt% CePOSS – 0.5 wt% PEG POSS EP3510 is shown in Figure 176. Darker spots, especially on the right side of the micrograph, are burning due to the SEM electron beam.

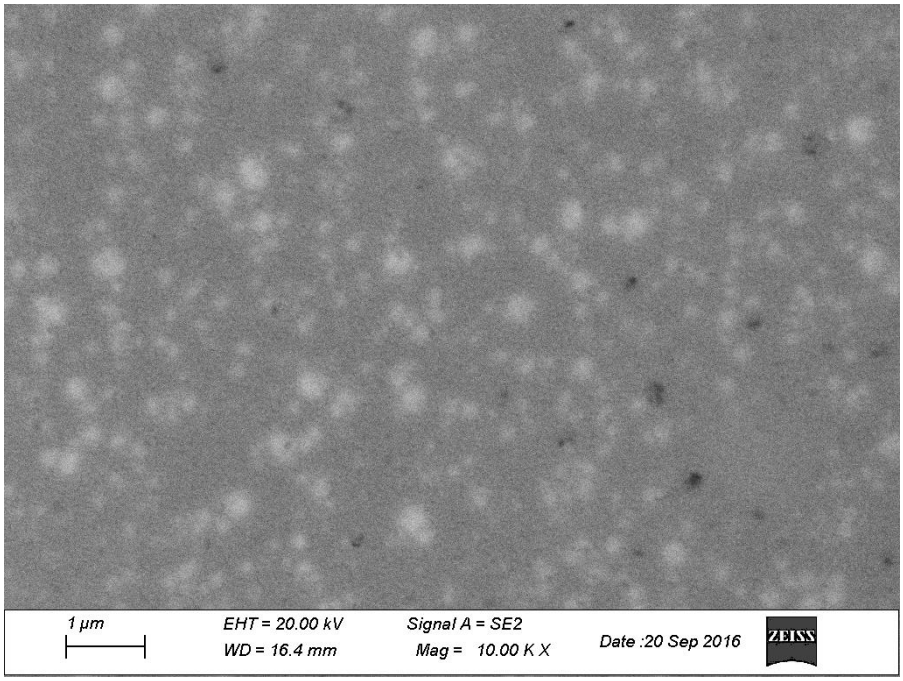

Figure 176. Unexposed 1 wt% CePOSS – 0.5 wt% PEG POSS in EP3510 at 10000X.

The lighter regions were assumed to be cerium-rich, as similar lighter colored regions were observed in the CeO_2-glycidyl POSS-33DDS coating layers shown in the dual layer disk cross sections in Chapter 4. However, the EDS could not

specifically resolve these regions due to their small size. The surface of this material was more uniform after exposure as shown in Figure 177.

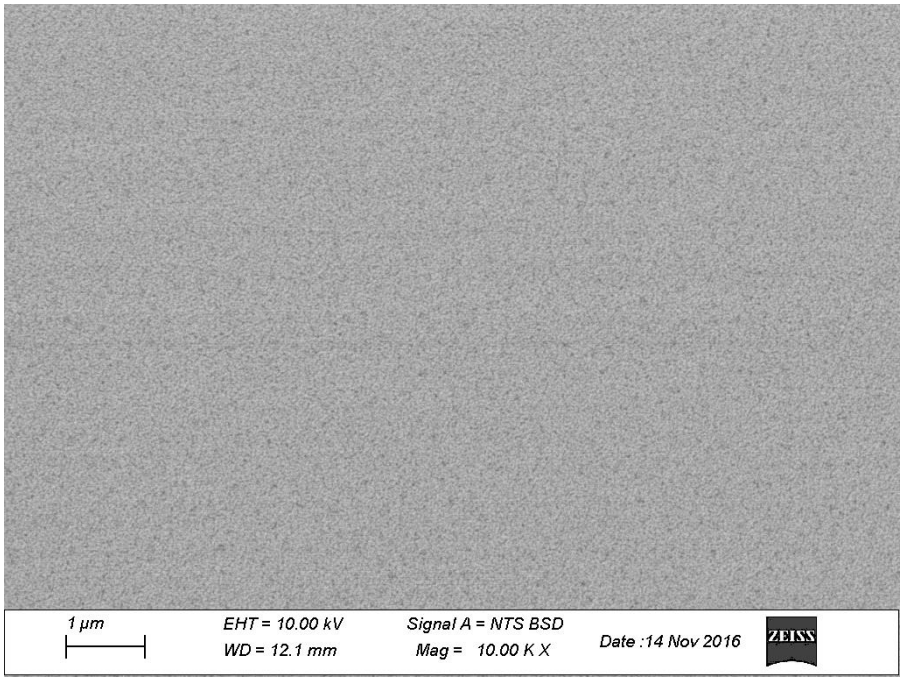

Figure 177. Exposed 1 wt% CePOSS – 0.5 wt% PEG POSS in EP3510 at 10000X.

This appeared to be a highly textured, yet uniform surface. Similar erosion patterns of small, conical structures, have been observed in Kapton H® exposed to atomic oxygen terrestrially and Teflon® exposed to low Earth orbit (LEO) on the Long Duration Exposure Facility (LDEF) as shown in Figure 178.[3]

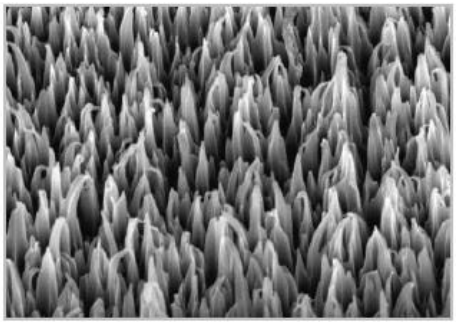

Figure 178. Surface erosion in Kapton H® exposed to 2.3×10^{20} atoms/cm^2.[3]

Cerium-rich areas were not seen distinctly in unexposed 2.5 wt% CePOSS – 1.25 wt% PEG POSS in EP3510 (Figure 179). EDS was used to verify the presence of that element. Occasional burn marks were also observed on this sample.

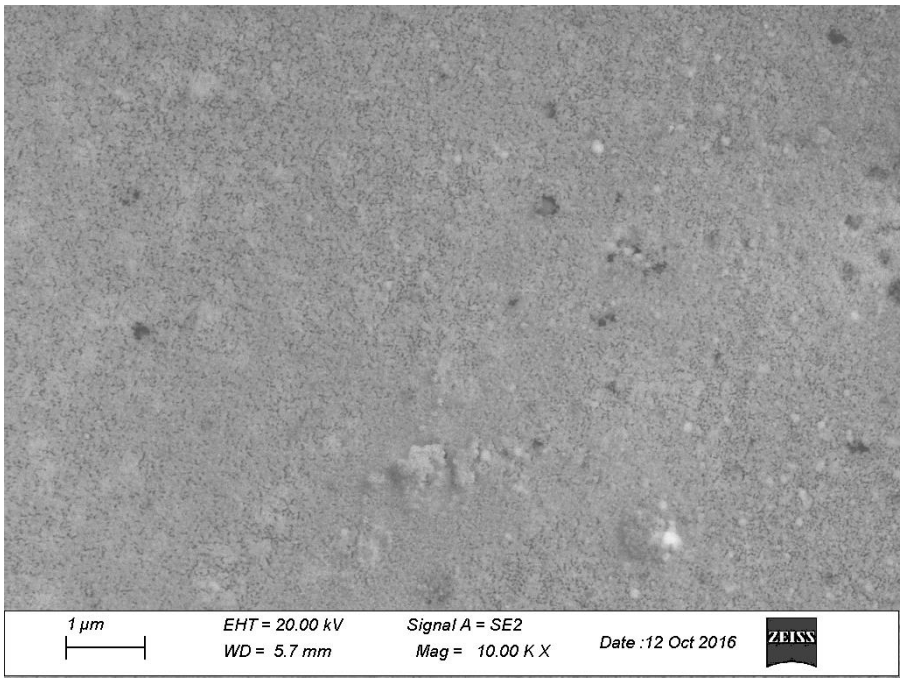

Figure 179. Unexposed 2.5 wt% CePOSS – 1.25 wt% PEG POSS in EP3510 at 10000X.

The exposed surface of the 2.5 wt% CePOSS – 1.25 wt% PEG POSS in EP3510 was also textured (Figure 180).

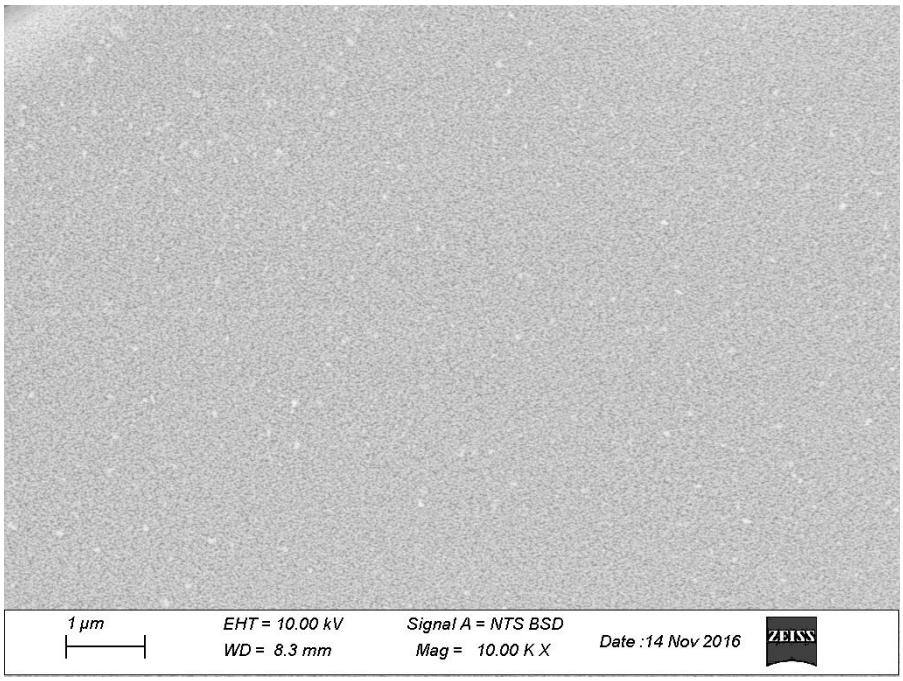

Figure 180. Exposed 2.5 wt% CePOSS – 1.25 wt% PEG POSS in EP3510 at 10000X.

Unlike the 1 wt% CePOSS – 0.5 PEG POSS sample, cracking was seen at the surface, as shown in Figure 181.

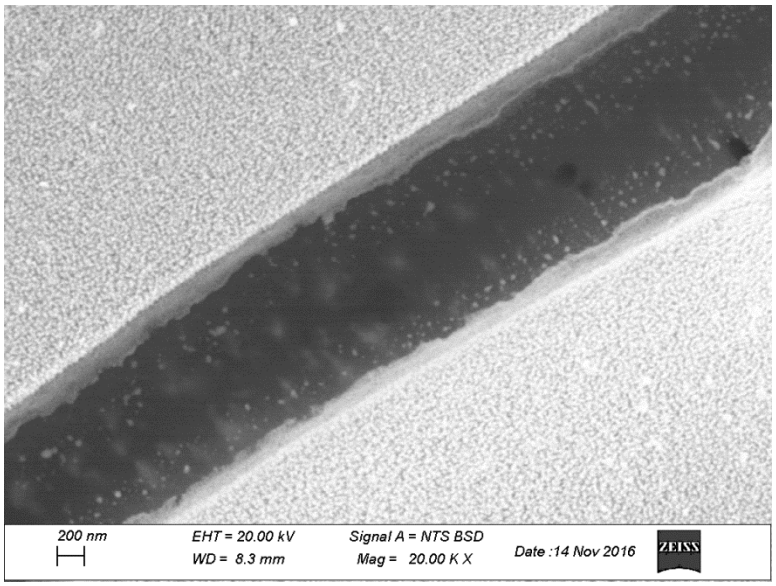

Figure 181. Crack in exposed 2.5 wt% CePOSS – 1.25 wt% PEG POSS in EP3510 at 20000X.

These cracks were more interconnected and could be seen at higher magnification than the ones present in the exposed 2.5 wt% CePOSS – 1.25 wt% PEG POSS EP3510 sample (Figure 182).

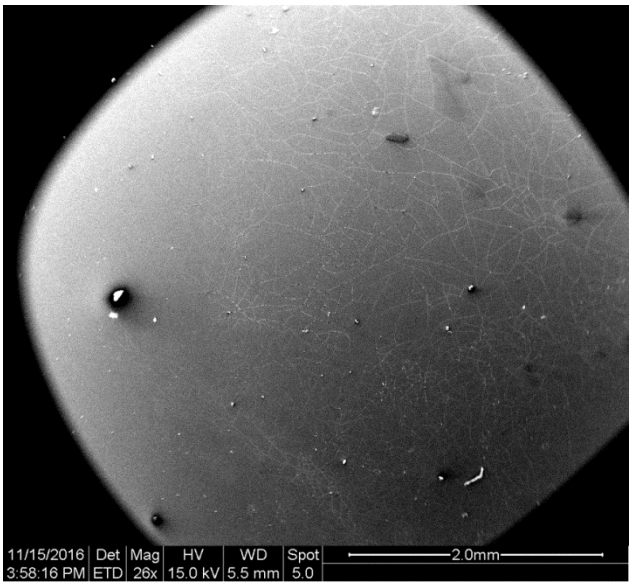

Figure 182. Crack network on surface of 2.5 wt% CePOSS – 1.25 wt% PEG POSS at 26X.

Initially, it was thought that the presence of CePOSS induced cracking. However, cracking was also seen in the neat EP3510 after exposure. In addition, cracking was not seen in the 1 wt% CePOSS-0.5 wt% PEG POSS or 5 wt% CePOSS – 2.5 wt% PEG POSS samples.

Before exposure, the 5 wt% CePOSS material showed some pitting and texture at the surface as shown in Figure 183. Darker spots, especially on the right side of the micrograph, are burning due to the SEM electron beam.

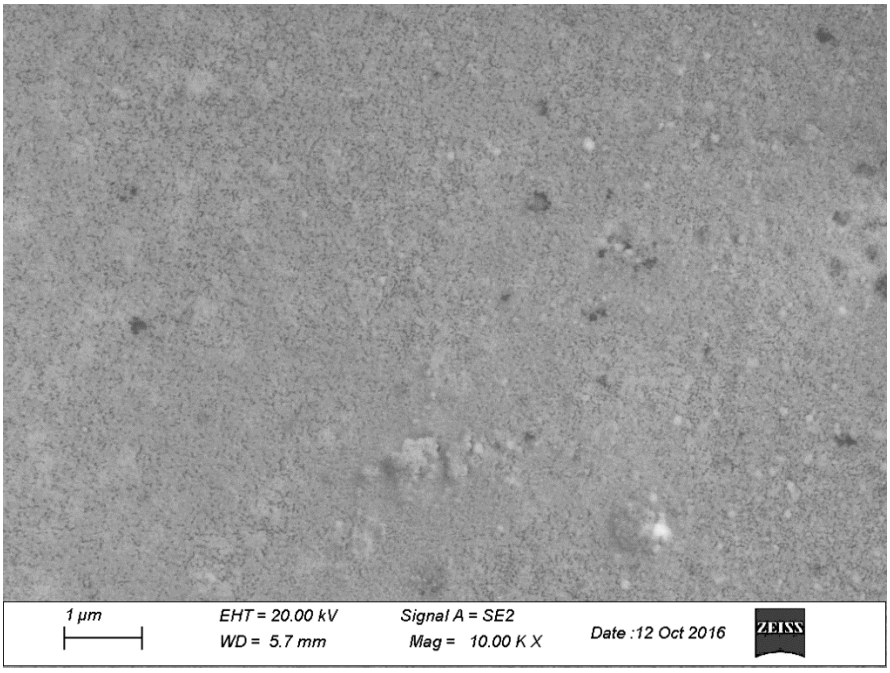

Figure 183. Unexposed 5 wt% CePOSS – 2.5 wt% PEG POSS at 10000X.

After exposure, the surface was more uniform, similar to the other CePOSS-inclusive samples (Figure 184).

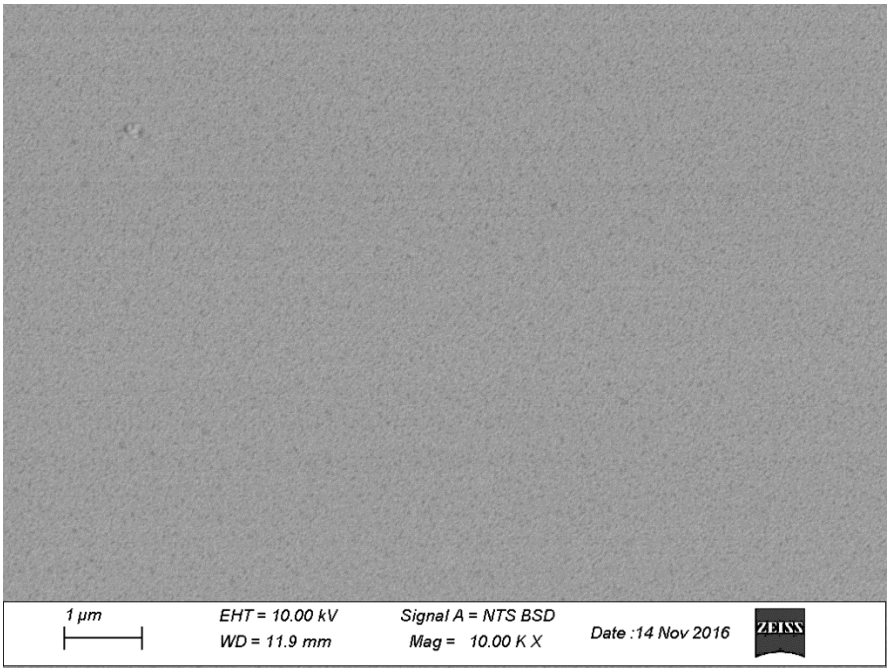

Figure 184. Exposed 5 wt% CePOSS – 2.5 wt% PEG POSS in EP3510 at 10000X.

A higher magnification view of this morphology is shown in Figure 185.

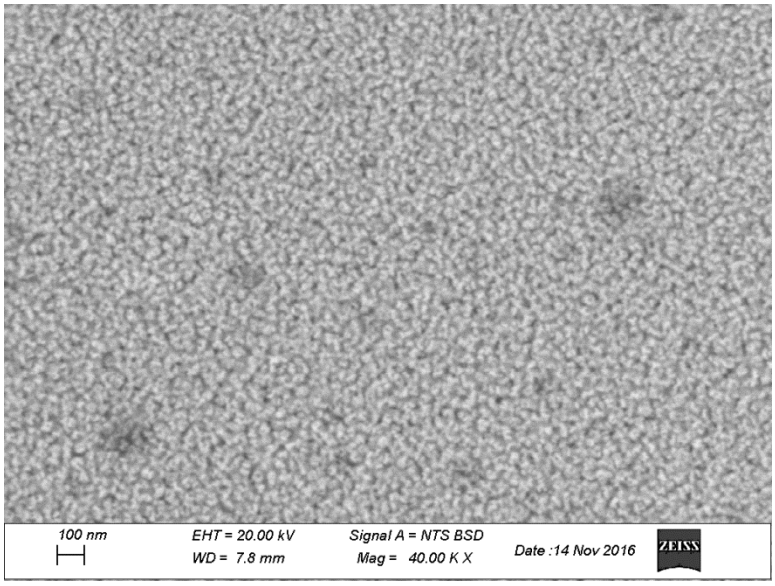

Figure 185. Exposed 5 wt% CePOSS – 2.5 wt% PEG POSS in EP3510 at 40000X.

The morphology appeared to be an interconnected, uniform network of nodular structures. Again, this is somewhat similar to the effects of atomic oxygen damage seen in polymers.[3] The darker spots in Figure 185 are burn marks from the SEM electron beam. This occurred even at a fairly low accelerating voltage of 10 kV compared to the 20 kV normally used for SEM with EDS.

No surface cracking was observed in the 5 wt% CePOSS – 2.5 wt% PEG POSS EP3510 sample. The only samples that cracked were neat EP3510 and 2.5 wt% CePOSS – 1.25 wt% PEG POSS EP3510. There appeared to be no trend in terms of increasing cracking with increasing CePOSS. However, only one sample of each material was exposed, so the sample size per material may not have been large enough to fully explore the morphological effects of UV and ozone treatment.

The majority of POSS glassification papers considered in the introduction did not attempt to measure the thickness of the final SiO_2 layer. Eon et al. estimated the thickness of this layer at 1.4-3.2 nm based on XPS peaks.[94] Therefore, in the present study, the exposed neat EP3510 sample was cross-sectioned for examination by SEM to look at the interior of the sample from the surface to the base of the disk. This surface was then microtomed, mounted, and sputtered coated. A view of this surface is shown in Figure 186 with the top of the disk at the top of the micrograph.

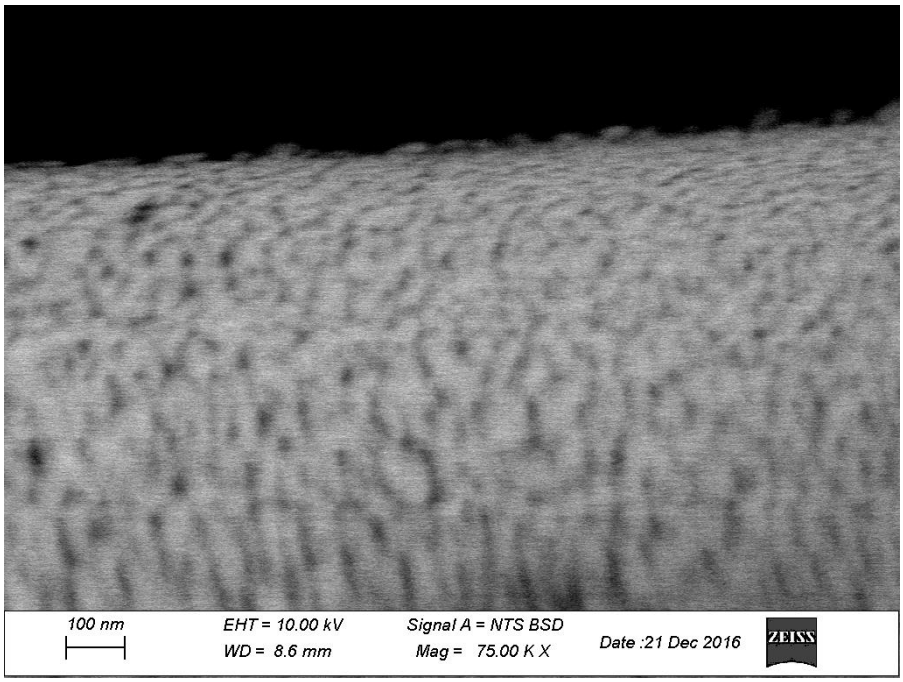

Figure 186. Top of cross-section of exposed EP3510 at a magnification of 75000X.

The sample was examined at a magnification of 75,000X and above, but no discernible layer was seen. In addition, sample vibration was amplified at these high magnifications so EDS analysis was unable to be performed. Therefore, no layer measurement could be completed. In the future, it could be useful to use

focused ion beam to etch layers off of the surface with EDS measurements between etching to determine the extent of the lack of carbon, and therefore, the extent of the SiO_2 layer.[165]

Contact Angle on UV/ozone Exposed Samples. Contact angle was also measured on unexposed and exposed films using water and diiodomethane.[128] Using two liquids allowed the surface energy to be calculated for each film by a method that takes into can separate the dispersion and polar components of the surface free energy.[129] Results are shown in Tables 20 and 21.

Table 20

Contact angle results for unexposed and exposed films

	Water Contact Angle (°)		Diiodomethane Contact Angle (°)	
Material	**Pre exposure**	**Post exposure**	**Pre exposure**	**Post exposure**
EPON 862	66.8 +/- 0.5	46.3 +/- 0.6	33.2 +/- 4.2	39.3 +/- 0.5
EP3510	55.4 +/- 0.7	33.1 +/- 0.9	35.9 +/- 0.8	47.0 +/- 0.3
EP3510 1 wt% CePOSS - 0.5 PEG POSS	64.1 +/- 2.1	35.3 +/- 1.3	38.5 +/- 0.8	41.2 +/- 1.0
EP3510 2.5 wt% CePOSS - 1.25 PEG POSS	50.4 +/- 1.2	36.3 +/- 1.3	33.6 +/- 1.0	41.6 +/- 1.0
EP3510 5 wt% CePOSS - 2.5 PEG POSS	50.9 +/- 2.0	37.7 +/- 1.0	31.9 +/- 0.8	41.0 +/- 1.3

Table 21

Surface free energy results for unexposed and exposed films

	Polar Surface Free Energy (mJ/m^2)		Dispersive Surface Free Energy (mJ/m^2)		Total Surface Free Energy (mJ/m^2)	
Material	**Pre exposure**	**Post exposure**	**Pre exposure**	**Post exposure**	**Pre exposure**	**Post exposure**
EPON 862	8.17 +/- 0.50	20.12 +/- 0.22	42.21 +/- 1.91	39.96 +/- 0.14	50.38 +/- 1.41	60.08 +/- 0.22
EP3510	14.24 +/- 0.42	29.67 +/- 0.27	41.61 +/- 0.18	35.93 +/- 0.10	55.84 +/- 0.24	65.60 +/- 0.27
EP3510 1 wt% CePOSS - 0.5 PEG POSS	10.07 +/- 1.25	26.78 +/- 0.42	40.34 +/- 0.04	39.01 +/- 0.29	50.40 +/- 1.30	65.79 +/- 0.42
EP3510 2.5 wt% CePOSS - 1.25 PEG POSS	16.58 +/- 0.95	26.34 +/- 0.48	42.68 +/- 0.47	38.83 +/- 0.31	59.26 +/- 0.47	65.17 +/- 0.46
EP3510 5 wt% CePOSS - 2.5 PEG POSS	16.01 +/- 1.21	25.12 +/- 0.46	43.44 +/- 0.14	39.70 +/- 0.66s	59.45 +/- 1.36	64.82 +/- 0.44

All material surfaces showed an increase in polar surface energy and a decrease in dispersive surface energy after UV/ozone exposure. This reflects the oxidation seen in all five materials in the XPS data presented earlier. The inclusion of POSS resulted in more hydrophilic surfaces/higher polar surface energies but this effect did not seem to be as significant with the inclusion of CePOSS.

UV-vis Spectroscopy on UV/ozone Exposed Samples. Previous data showed that POSS increased UV transmission in epoxies above 300 nm. Therefore, it was of interest to see if this was altered by surface glassification. All work was done on 2 mm thick disks. Figure 187 shows the UV transmittance of EPON 862 before and after exposure from 190-700 nm. Noise is due to wavelengths at which there was insufficient data.

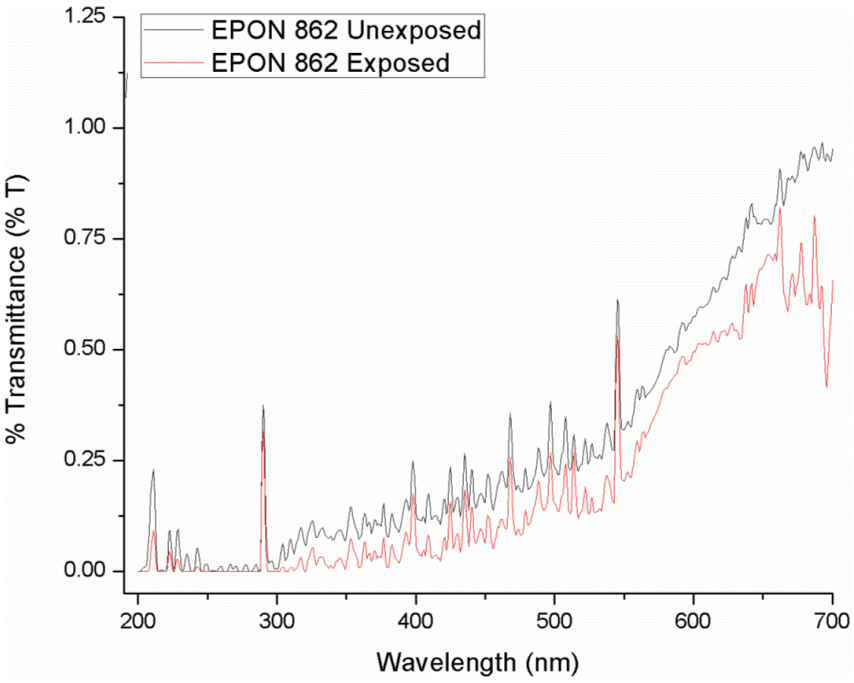

Figure 187. UV transmittance from 190-700 nm of unexposed (black) and exposed (red) EPON 862.

The exposure decreased transmittance throughout the entire wavelength range but did not change the overall shape of the transmittance spectrum. The unexposed and exposed spectra for neat EP3510 are displayed in Figure 188.

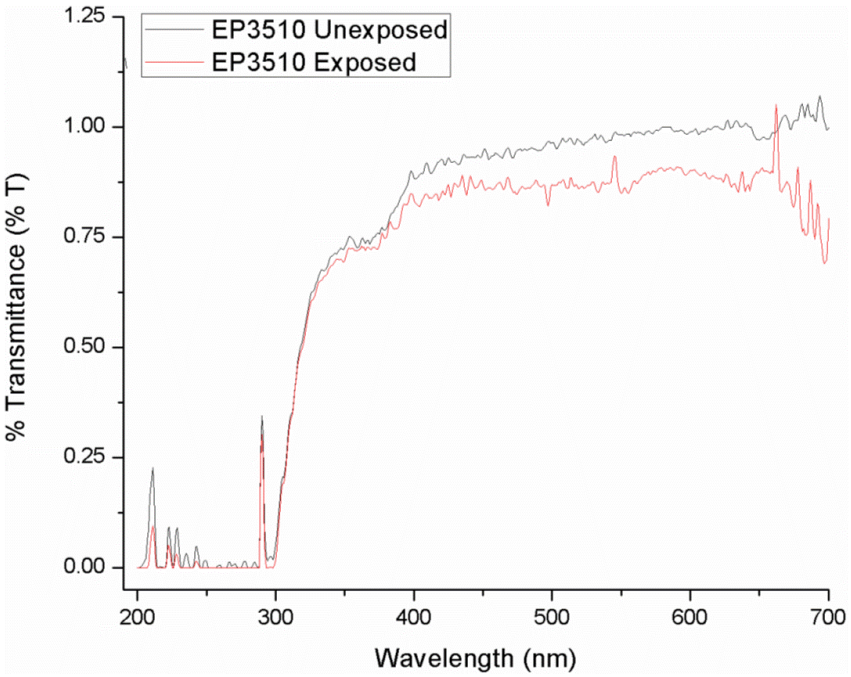

Figure 188. UV transmittance from 190-700 nm of unexposed (black) and exposed (red) EP3510.

Until approximately 375 nm, the spectra were extremely similar. A decrease in transmittance was seen in the exposed sample above that wavelength, probably due to the oxidized silica surface.

Data for the EP3510 1 wt% CePOSS-0.5 wt% PEG POSS, 2.5 wt% CePOSS-1.25 wt% PEG POSS, and 5 wt% CePOSS-2.5 wt% PEG POSS films are shown in Figures 189-191.

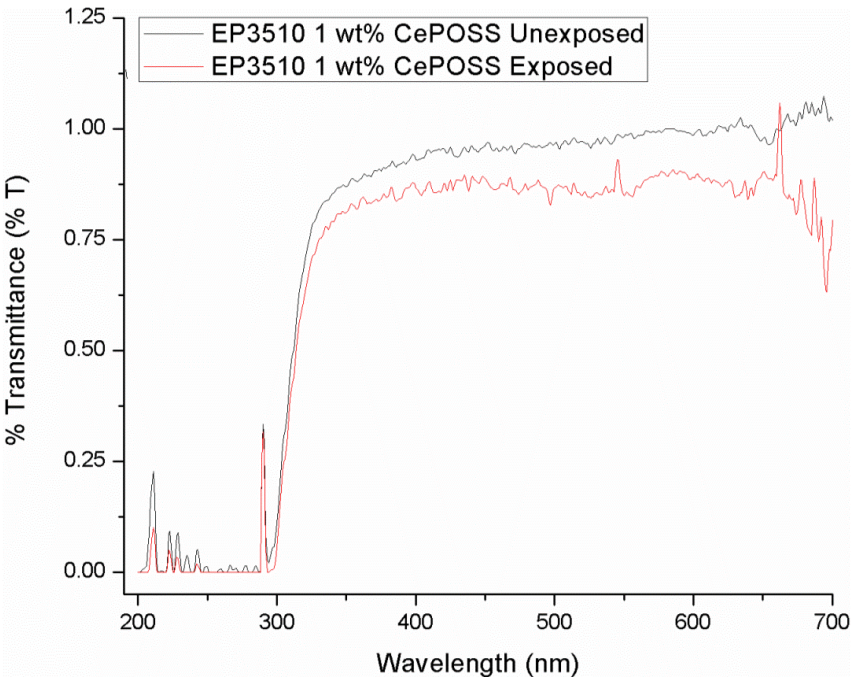

Figure 189. UV transmittance from 190-700 nm of unexposed (black) and exposed (red) EP3510 1 wt% CePOSS-0.5 wt% PEG POSS.

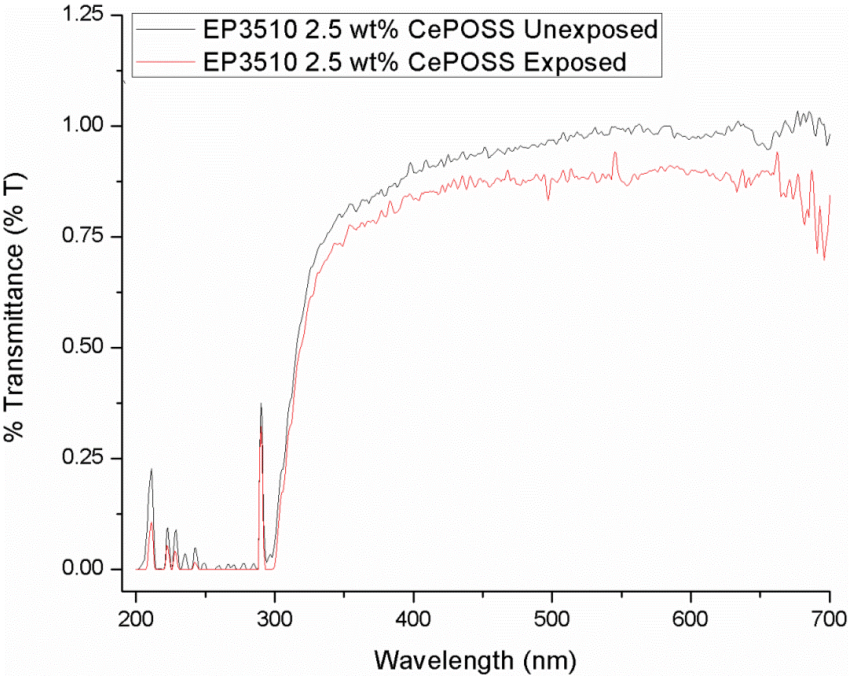

Figure 190. UV transmittance from 190-700 nm of unexposed (black) and exposed (red) EP3510 2.5 wt% CePOSS-1.25 wt% PEG POSS.

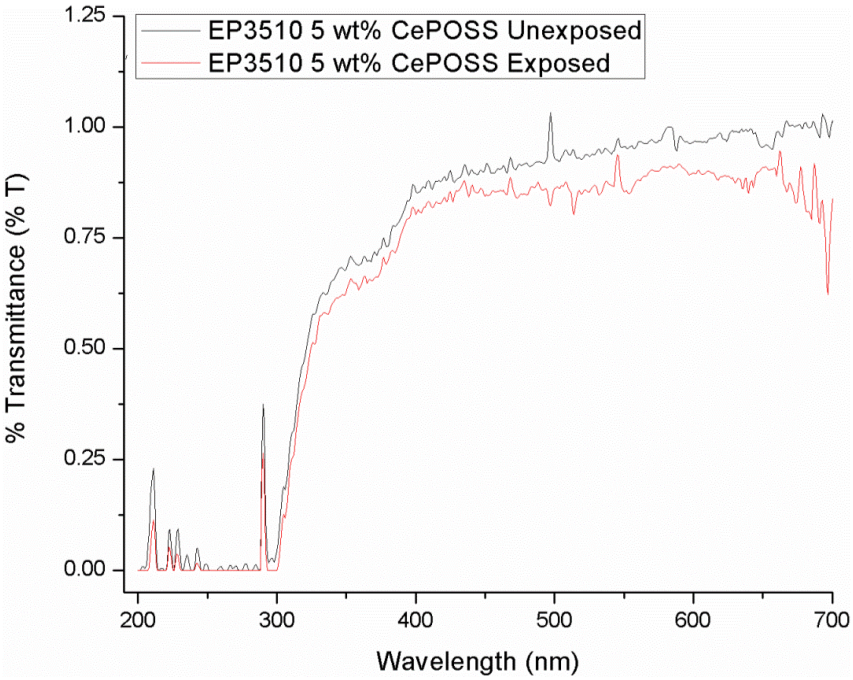

Figure 191. UV transmittance from 190-700 nm of unexposed (black) and exposed (red) EP3510 5 wt% CePOSS-2.5 wt% PEG POSS.

The CePOSS-rich samples had similar pre and post exposure spectra in the UV region below wavelengths of approximately 300 nm. Above this wavelength, transmittance increased but the transmittance was lowered by sample exposure to UV/ozone.

Conclusions

The presence of CePOSS did not appear to significantly decrease the UV transmittance of POSS when normalized by thickness. However, the transmittance of the aromatic epoxy EPON 862 was significantly increased, above wavelengths of 300 nm and in the visible light region, by the presence of POSS with or without CePOSS.

Samples of EPON 862, EP3510, EP3510 1 wt% CePOSS-0.5 wt% PEG POSS, EP3510 2.5 wt% CePOSS-1.25 wt% PEG POSS, and EP3510 5 wt%

CePOSS-2.5 wt% PEG POSS were exposed to a combination of UV radiation and ozone similar to a method used by Özçam et al. to glassify poly(dimethyl siloxane) and poly(vinyl methyl siloxane).[132] X-ray photoelectron spectroscopy confirmed shifts in the POSS-containing films from Si_3N_4 to SiO_2 and $SiO_2 \cdot nH_2O$. This shift did not seem to be affected by the presence of CePOSS and the largest magnitude shift was with 1 wt% CePOSS. In addition, all 5 materials confirmed the oxidation of the surface through increases in oxygen surface. The POSS-rich films also showed a decrease in carbon as was expected. Scanning electron microscopy of surface morphology revealed erosion on the epoxy EPON 862 sample after exposure compared to a fine nodular structure with POSS-rich surfaces. This morphology has been seen in other polymers exposed to atomic oxygen.[3] Cracking was seen in the neat EP3510 and 2.5 wt% CePOSS – 1.25 wt% PEG POSS EP3510 samples after exposure. There appeared to be no trend in terms of increasing cracking with increasing CePOSS. An attempt was made to image the SiO_2 layer at the top of neat EP3510 but failed due to unavoidable sample vibration in the instrument. Finally, contact angle measurements also confirmed surface oxidation and POSS glassification due to an increase in surface hydrophilicity and surface energies.

Given the increased transmittance at wavelengths higher than 300nm, caused by the addition of POSS to EPON 862, it was of interest to see whether this phenomenon continued after glassification. All five materials had very similar shapes to their pre- and post-exposure spectra from 190-700 nm. Transmittance decreased slightly above 375 nm for EP3510 and above 300 nm for CePOSS-

rich samples. CePOSS at 5 weight percent loading had little or no observable effect on oxidation of the surface.

CHAPTER VI – CONCLUSIONS

Low Earth orbit presents a variety of challenges for organic materials including atomic oxygen and UV radiation.[3] Composites are used in space applications but degradation of polymer matrices can decrease mechanical and thermal properties.[36,44,54] One additive that decreases erosion and mass loss in polymers exposed to atomic oxygen is polyhedral oligomeric silsesquioxane (POSS).[12] It achieves this through a process termed glassification where the POSS is converted to an inert layer of silica glass after atomic oxygen exposure, and this protects the underlying polymer.[75] POSS also has the ability to absorb UVb and UVc radiation.[81] The class of POSS materials comprise a $SiO_{1.5}$ cage with generally eight organic pendant groups bonded to the cage corners.[11] The compatibility of the pendant group used in the surrounding polymer governs the dispersion of the POSS moiety.[102]

In previous studies, POSS was dispersed throughout polymers, meaning that some erosion must occur before enough POSS is exposed to glassify.[12,27,67,69,73,74,75,85,86,87,88,91.92] The original objective of this work was to create nanocomposites with POSS-rich surfaces in an attempt to offer atomic oxygen protection with less mass loss. The epoxy-amine system diglycidyl ether of bisphenyl-A (DGEBA) monomer and 4,4’-diaminodiphenyl sulfone crosslinker was used as the thermoset matrix. This epoxy-amine system has been well-characterized in composite materials and it is a commonly used epoxy-amine for researchers.[48,52] Initially, DGEBA-44DDS was mixed with octamethyl and octaphenyl POSS at loading levels up to 5 wt% and cured for 3 hours at 180 °C.

The octamethyl POSS was thought to be the least miscible in the matrix and this was verified by construction of Teas diagrams. The octaphenyl POSS was more miscible due to its phenyl pendant group. However, initial experiments that tried to incorporate octaphenyl POSS resulted in large, millimeter-sized aggregates spread throughout sample bars. In-situ dielectric spectroscopy was used to analyze cure and found a window with low ion viscosity from approximately 100-175 °C while the oven was heating 1 °C/min to 180 °C before crosslinking started to accelerate. Therefore, the cure cycle was altered to a 1-hour hold at 110 °C, followed by a ramp of 1 °C/min to 180 °C and then the original hold of 3 hours at 180 °C. This pause was to allow POSS time to sediment into a layer at the bottom of the mold. In addition, a third POSS moiety was added with glycidyl pendants. This was the most miscible of the three POSS moieties used and it reacted homogeneously throughout the polymer matrix.

The deposition of a sedimented POSS layer was observed at the bottom surface of samples at the highest loading level, 5 wt%, of octamethyl POSS, which was the most immiscible moiety. The POSS-rich bottom surfaces of samples with 2.5 wt% octamethyl, octaphenyl, or glycidyl POSS were exposed to an atomic oxygen fluence of $1x10^{21}$ atoms/cm^2 at NASA Glenn Research Center. POSS-inclusive samples did not decrease overall exposure-induced mass loss compared to exposed neat DGEBA-44DDS. In addition, no evidence was seen for glassification of POSS. Instead, highly eroded surfaces were revealed by scanning electron microscopy. It was concluded that the surface density of the POSS was insufficient to result in glassification.

The second objective of this work was to evaluate the use of POSS to disperse cerium compounds. Cerium (IV) oxide is used as an effective absorber across the UV spectrum but is difficult to disperse in polymers.[9,10] Initially, it was postulated that the epoxy rings at the end of glycidyl POSS pendants could form a complex around cerium (IV) oxide through intermolecular forces. It was envisaged that such a mixture could be cast over an epoxy matrix and bonded together through crosslinking by 5-10 wt% of amine crosslinker in the mixture. Although the strategy of creating a dual layer composite of POSS-cerium (IV) oxide over epoxy matrix was successful, the cerium (IV) oxide always aggregated. Depending on the orientation of the coating during processing, this aggregation was either at the top or bottom of the coating. Oxygen plasma exposure carried out at Surfx Plasma did oxidize the surface of these coatings but did not prompt glassification. In addition, it was noted that cerium (IV) oxide aggregates at the surface of the coating did not enhance the performance of POSS in protecting the surface from oxidation.

Morgan et al. reacted open cage trisilanol POSS with titanium dioxide to reduce the size of TiO_2 aggregates in polypropylene.[99] In this study, the more miscible POSS helped to disperse the attached oxide. Therefore, this procedure was attempted with cerium (IV) oxide. After several unsuccessful attempts, cerium (III) nitrate hexahydrate was used instead of cerium oxide.[151-154] Blending of trisilanol phenyl POSS and cerium (III) nitrate in acetone followed by drying resulted in a powder that contained both POSS and nitrate groups. This material was termed CePOSS and was miscible in a different range of solvents compared

to cerium (III) nitrate hexahydrate and trisilanol phenyl POSS. The reason for the enhanced miscibility was investigated. Proton, carbon and silicon NMR spectroscopy revealed no major structural changes compared to trisilanol phenyl POSS although there was some additional peak splitting that may have indicated side reactions or contaminants. ATR FT-IR shifts indicated that CePOSS was a material held together primarily through hydrogen bonding between the POSS silanols and water and nitrates associated with cerium (III) nitrate hexahydrate. CePOSS showed greater UV absorbance at wavelength from approximately 235 to 275 nm compared to cerium (IV) oxide, cerium (III) nitrate, or trisilanol phenyl POSS.

CePOSS was incorporated into two POSS-rich coatings, one epoxy based with a thermal cure and one polyimide based and solvent cured. It was possible to incorporate CePOSS at loading levels up to 5 wt% in the POSS-epoxy coating, EP3510, when premixed at a 2:1 ratio with PEG POSS. The resultant material was transparent in the visible region but opaque in the UV region at wavelengths below 300nm.

Coatings of EP3510, EP3510 with CePOSS-PEG POSS, and EPON 862 (the POSS-free epoxy used in EP3510) were examined by UV-vis spectroscopy. It was hypothesized that the incorporation of CePOSS would decrease the UV transmission of the POSS-epoxy EP3510 coating. However, there was no statistically significant difference between EP3510 absorbance with and without CePOSS from 200-500 likely at loading levels up to 5 weight percent CePOSS.

Above 300 nm, EP3510 significantly increased transmission compared to EPON 862 regardless of the presence of CePOSS.

EPON 862, neat EP3510 and EP3510 with CePOSS-PEG POSS were exposed to a combination of UVc radiation and ozone in an attempt to glassify the POSS-rich coatings and understand the effect of cerium on glassification. All POSS-inclusive materials glassified as seen through Si 2p bond shifts in XPS measurements. The EPON 862 showed a substantial increase in surface oxygen content and this was also observed in the EP3510-based materials. Scanning electron microscopy revealed a nodular, sub-millimeter morphology in the EP3510 samples, which has also been seen in polymers exposed to atomic oxygen.[3] The neat EP3510 and 2.5 wt% CePOSS-1.25 wt% PEG POSS EP3510 sample cracked at the surface but there was no apparent reason why these materials cracked as opposed to other glassified samples. Decreases in contact angle and surface energy as measured with water and diiodomethane also confirmed surface oxidation.

UV-vis spectroscopy was done on disks before and after UV/ozone exposure and subsequent surface oxidation and glassification. No major changes were seen in the shape of transmission spectra from 190-700 nm before and after exposure. However, glassified POSS-based materials showed a decrease in transmission above 375 nm for neat EP3510 and above 300 nm for EP3510 CePOSS-PEG POSS films.

Overall, the initial objective of this work to layer was achieved: to concentrate POSS at a polymer surface by a sedimentation mechanism in the

DGEBA-44DDS system. Moreover, it was shown that POSS could be combined with a cerium-containing molecule. However, unexpectedly the inclusion of Cerium offered no more protection than POSS against oxidation or UV-induced damage. This CePOSS material when mixed with PEG POSS could form a POSS-epoxy coating, EP3510. This material was transparent in the visible region, with loadings up to up to 5 wt% CePOSS/2.5 wt% PEG POSS. This loading was not sufficient to decrease the UV transmittance compared to neat EP3510 but all POSS-inclusive coatings did show a window of transmittance above 300 nm compared to the base epoxy. In addition, the presence of cerium did not prevent oxidation or UV damage over the presence of PEG POSS alone.

CHAPTER VII – FUTURE WORK

The CePOSS material drives many of the suggestions for future work. In Chapter 4, it was concluded that CePOSS is a complex dominated by hydrogen bonding between cerium (III) nitrate hexahydrate and trisilanol phenyl POSS. However, some additional split peaks were seen in the carbon and silicon NMR. The exact reason for the increase in compatibility apparently caused by hydrogen bonding between the POSS and the Cerium compound is an area that should be studied. Understanding the reason for this enhanced solubility could have far-reaching impact that goes beyond mere Cerium and POSS combinations.

A major finding was that the inclusion of POSS in epoxy greatly increases UV transmittance above 300 nm compared to the neat epoxy. The exact cause of this phenomenon should be explored with the possibility of developing more materials that are opaque in the ultraviolet spectrum and transparent in the visible spectrum.

Neat EP3510 and EP3510 with 2.5 wt% CePOSS-1.25 wt % PEG POSS SEM samples cracked after exposure to UV radiation and ozone. Since cracking did not seem to correspond to any increase or decrease in the CePOSS additive, it would be of interest to repeat the testing with more samples to see whether surface cracking is random or whether it occurs specifically in those two materials.

Finally, it would be of interest to investigate surfaces after POSS glassification to see how homogenous the glass is across the surface and how thick it is. The homogeneity could be achieved through multiple XPS Si 2p bond

energy measurements across a surface. The depth measurement could be achieved through a technique such as focused ion beam where the surface can slowly be cut away and then examined with SEM/EDAX to determine at what depth carbon content was not affected by surface changes.

REFERENCES

1. Engineering Materials – Engineering Toolbox http://www.engineeringtoolbox.com/engineering-materials-properties-d_1225.html (accessed December 29, 2016).

2. “Space Environmental Effects on Spacecraft: LEO Materials Selection Guide” United States. NASA. *NASA Contractor Report 4661 Part 1*. NASA-4661-1. Washington, DC, 1995.

3. “Spacecraft Polymers Atomic Oxygen Durability Handbook” United States. NASA. *NASA Technical Handbook*. NASA-HDBK-6024. Washington, DC, 2014.

4. Timm, D.C.; Ayorinde, A.J.; Foral, R.F. *Br. Polym. J.* **1985,** *17*, 227-232.

5. Malshe, V.C.; Waghoo, G. *Prog. Org. Coat.* **2004,** *51,* 267-272.

6. Jaworske, D.A. *Thin Solid Films*. **1998,** *332,* 30-33.

7. “Effect of Radiation on Cerium-Doped Solar-Cell Cover Glass” United States. NASA. *NASA Technical Note D-6024*. NASA TN D-6024. Washington, DC, 1970.

8. “Low Earth Orbit Atomic Oxygen Interactions With Materials” United States. NASA. *NASA Technical Memorandum 2004-213223*. NASA-TM-2004-213223. Washington, DC, 2004.

9. Reyes-Acosta, M.A.; Torres-Huerta, A.M.; Dominguez-Crespo, M.A.; Flores-Vela, A.I.; Dorantes-Rosales, H.J.; Andraca-Adame, J.A. *Polymers* **2015,** *7,* 1638-1659.

10. Smeenk, N.J.; Mooney, C.; Feenstra, J.; Mulder, P.; Rohr, T.; Semprimoschnig, C.O.A.; Vlieg, E.; Schermer, J.J. *Polym. Degrad. Stab.* **2013,** *98,* 2503-2511.

11. Cordes, D.B.; Lickiss, P.D.; Rataboul, F. *Chem. Rev.* **2010,** *110,* 2081-2173.
12. Gilman, J.W.; Schlitzer, D.S.; Lichtenhan, J.D. J. Appl. Polym. Sci. 1996, 60, 591-596.

13. Long Term Exposure Facility (LDEF). http://www.nasa.gov/centers/marshall/history/ldef01.html (accessed October 4, 2016).

14. NASA, Catalog of Earth Satellite Orbits http://earthobservatory.nasa.gov/Features/OrbitsCatalog/ (accessed July 4, 2016).

15. Harris, J.T., Stimler, F.J. Expandable Structures for Space. In *Structures Technology: Historical Perspective and Evolution;* Noor, A.K., Ed.; AIAA: Reston, VA, 1998, pp 429-436

16. Ungar, E.W. Applications of Materials to Solid-Rocket Nozzles. In *Structures Technology: Historical Perspective and Evolution;* Noor, A.K., Ed.; AIAA: Reston, VA, 1998, pp 511-520.

17. National Space Society http://www.nss.org/articles/falconheavy.html#appendix (accessed September 9, 2016).

18. National Research Council. *Technology for Small Spacecraft;* The National Academies Press, 1994; pp 42-49.

19. Webb, A.R. *Radiat. Prot. Dosim.* **1997,** *72,* 207-216.

20. Atkins, P.; and de Paula, J. *Physical Chemistry for the Life Sciences*, W.H. Freedman and Company: New York, 2006.

21. Honle UV America Inc, Fundamental Principles of UV Reactive Manufacturing Processes http://www.honleuv.com/news/2014/5/28/fundamental-principles-of-uv-reactive-manufacturing-processe.html (accessed July 16, 2016).

22. Warneck, P. *Chemistry of the Natural Atmosphere;* Academic Press, 2000; pp 99-119.

23. Lerouge, S.; Fozza, A.C.; Wertheimer, M.R.; Marchand, R.; Yahia, L.H. *Plasmas Polym.* **2000,** *5,* 31-46.

24. Dever, J.A.; McCracken, C.A. *High Perform. Polym.* **2004,** *16,* 289-301.

25. Ghosh, L.; Fadhilah, M.F.; Kinoshita, H.; Ohmae, N. *Polymer* **2006,** *47,* 6836-6842.

26. Dever, J.A.; Banks, B.A.; Yan, L. *J. Spacecr. Rockets.* **2006,** *43,* 386-392.

27. Minton, T.K.; Wright, M.E.; Tomczak, S.J.; Marquez, S.A.; Shen, L.; Brunsvold, A.L.; Cooper, R.; Zhang, J.; Vij, V.; Guenthner, A.J.; Petteys, B.J. *Appl. Mater. Interfaces* **2012,** *4,* 492-502.

28. Bratolyubova-Tsulukidze, L.S.; Grachev, E.A.; Grigoryan, O.R.; Kunitsyn, V.E.; Kuzhevskij, B.M; Lysakov, D.S.; Nechaev, O.Y.; Usanova, M.E. *Adv. Space Res.* **2004,** *34,* 1815-1818.

29. Musto, P.; Abbate, M.; Pannico, M.; Scarinzi, G.; Ragosta, G. *Polymer* **2012,** *53,* 5016-5036.

30. Hartmann-Thompson, C. *Applications of Polyhedral Oligomeric Silsesquioxanes*, 1st ed.; Springer Netherlands, 2011.

31. "Comparison of Atomic Oxygen Erosion Yields of Materials at Various Energy and Impact Angles" United States. NASA. *NASA Technical Memorandum 2006-214363*. NASA-TM-2006-214363. Washington, DC, 2006.

32. "MISSE 2 PEACE Polymers Experiment Atomic Oxygen Erosion Yield Analysis" United States. NASA. *NASA Technical Memorandum 2010-216903*. NASA-TM-2010-216903. Washington, DC, 2010.

33. Grossman, E.; Gouzman, I. *Nucl. Instr. And Meth. In Phys. Res.* **2003,** *208,* 48-57.

34. ARES: Orbital Debris Program Office http://www.orbitaldebris.jsc.nasa.gov/ (accessed July 16, 2016).

35. Shin, K-B.; Kim, C-G.; Hong, C-S.; Lee, H-H. *Composites Part B*. **2000,** *31,* 223-235.

36. Park, S.Y.; Choi, H.S.; Choi, W.J.; Kwon, H. *Composites Part B.* **2012,** *43,* 726-738.

37. Han, J-H.; Kim, C-G. *Compos. Struct.* **2006,** *72,* 218-226.

38. *Loctite EA 956 Aero Part A;* MSDS No. 936906; Henkel, Aug 6, 2014.

39. *Loctite EA 956 Aero Part B;* MSDS No. 936907; Henkel, Sep 26, 2014.

40. Dever, J.; Banks, B; De Groh, K.; Miller, S. Degradation of Spacecraft Materials. In *Handbook of Environmental Degradation of Materials*; Kutz, M.,2nd Ed.; Elsevier: 2012; pp 717-770.

41. Dever, J.A.; de Groh, K.K.; Banks, B.A.; Townsend, J.A. *High Perform. Polym.* **1999,** *11,* 123-140.

42. "Space Environment Effects on Silicone Seal Materials" United States. NASA. *NASA Technical Memorandum 2010-216332*. NASA-TM-2010-216332. Washington, DC, 2010.

43. Viers, B.D.; Gonzales, R.I.; Phillips, S.H. *POSS Polymers for Space: Entrepreneurial Research:* Technical Report for Air Force Research Laboratory: Edwards Air Force Base, CA, 2009.

44. Tennyson, R. *Composites in Space – Challenges and Opportunities* In Proceedings of Tenth International Conference on Composite Materials, Whistler, Canada, August 14-18, 1995.

45. Chemistry and Technology of Cyanate Ester Resins; Hamerton, I. Eds.; Springer, 1994.

46. Polyimides. In *Encyclopedia of Polymer Science and Engineering;* Mark, H.F.; Bikales, N.M.; Overberger, C.G.; Menges, G.; Kroschwitz, J. Eds.; John Wiley & Sons Inc., 1988; Vol. 12, pg. 364-383

47. Tetrafluoroethylene Polymers In *Encyclopedia of Polymer Science and Engineering;* Mark, H.F.; Bikales, N.M.; Overberger, C.G.; Menges, G.; Kroschwitz, J. Eds.; John Wiley & Sons Inc., 1988; Vol. 16, pg. 577-648

48. Epoxy Resins In *Encyclopedia of Polymer Science and Engineering;* Mark, H.F.; Bikales, N.M.; Overberger, C.G.; Menges, G.; Kroschwitz, J. Eds.; John Wiley & Sons Inc., 1988; Vol. 16, pg. 322-382

49. Silicates In *Encyclopedia of Polymer Science and Engineering;* Mark, H.F.; Bikales, N.M.; Overberger, C.G.; Menges, G.; Kroschwitz, J. Eds.; John Wiley & Sons Inc., 1988; Vol. 4, pg. 204-308

50. Scroog, C.E. *Prog. Polym. Sci.* **1991,** *16,* 561-694.

51. Stevens, M. *Polymer Chemistry: An Introduction*, 3rd ed.; Oxford University Press: New York, 1999.

52. Composite Fabrication In *Encyclopedia of Polymer Science and Engineering;* Mark, H.F.; Bikales, N.M.; Overberger, C.G.; Menges, G.; Kroschwitz, J. Eds.; John Wiley & Sons Inc., 1988; Vol. 4, pg. 1-36.

53. Boyle, M.A.; Martin, C.J.; Neuner, J.D. Epoxy Resins. In *ASM Handbook Volume 21: Composites;* Miracle, D.B.; Donaldson, S.L., Ed.; ASM International: Ohio, 2001: p 78.

54. Ungar, E.W. Applications of Materials to Solid-Rocket Nozzles. In *Structures Technology: Historical Perspective and Evolution;* Noor, A.K., Ed.; AIAA: Reston, VA, 1998, pp 511-520.

55. "Performance of Rocket Nozzle Materials with Several Solid Propellants" United States. NASA. *NASA Technical Note D-3428*. NASA-TN-D-3428. Washington, DC, 1966.

56. Hexion – EPON 825 Resin. http://www.hexion.com/Products/TechnicalDataSheet.aspx?id=3936 (accessed Nov 16, 2016).

57. *4-aminophenyl sulfone* MSDS No. A74807; Sigma Aldrich, February 4, 2013.

58. Royce International – Epoxy Curing Agents. http://www.royceintl.com/products/epoxy-curing-agents (accessed Nov 16, 2016).

59. Cho, K.; Lee, D.; Park, C.E.; Huh, W. *Polymer* **1996,** *37,* 813-817.

60. "Leveling Coatings for Reducing the Atomic Oxygen Defect Density in Protected Graphite Fiber Epoxy Composites" United States. NASA. *NASA Technical Memorandum 105732*. NASA-TM-1992-105732. Washington, DC, 1992.

61. *EPO-TEK 301 Part A*; MSDS; Epoxy Technology, Apr 25, 2016.

62. Cui, H.; Zayat, M.; Parejo, P.G.; Levy, D. *Adv Mater* **2008,** *20,* 65-68.

63. Simple Method of Measuring the Band Gap Energy Value of TiO_2 in the Powder Form using a UV/Vis/NIR Spectrometer https://www.perkinelmer.com/lab-solutions/resources/docs/APP_UVVISNIRMeasureBandGapEnergyValue.pdf (accessed Oct 5, 2016).

64. Saadat-Monfared, A.; Mohseni, M. *Colloids Surf., A* **2014,** *441,* 752-757.

65. R. L. Crabb, Evaluation of Cerium Stabilized Microsheet Cover Slips for Higher Solar Cell Outputs. IEEE 9th Photovoltaic Specialist Conference, Silver Springs, USA, 1972, p. 329.

66. Tasis, D.; Tagmatarchis, N.; Bianco, A.; Prato, M. *Chem. Rev.* **2006,** *106,* 1105-1136.

67. Atar, N.; Grossman, E.; Gouzman, I.; Bolker, A.; Murray, V.J.; Marshall, B.C.; Qian, M.; Minton, T.K.; Hanein, Y. *Appl. Mater. Interfaces* **2012,** *7,* 12047-12056.

68. Hybrid Plastics: Bulk Chemicals http://hybridplastics.com/products/bulk-chemicals/ (accessed Nov 15, 2016).

69. Gonzales, R.I.; Tomczak, S.J.; Minton, T.K.; Brunsvold, A.L.; Hoflund, G.B. Proceedings of the 9th International Symposium on Materials in a Space Environment, Noordwijk, The Netherlands, June 16-20, 2003.

70. Toub, M.; Finney, D.L. Temperature Resistant Elastomers – E. Silicone Elastomers; In *Basic Elastomer Technology*; Rubber Division American Chemical Society: Baltimore, MD, 2001; pp. 499-514.

71. "Atomic Oxygen Protection of Materials in Low Earth Orbit" United States. NASA. *NASA Technical Memorandum 2002-211360*. NASA-TM-2002-211360. Washington, DC, 2002.

72. Campbell, D.; Pethrick, R.A.; White, J.R. *Polymer Characterization: Physical Techniques*, 2nd ed.; Stanley Thornes Ltd: Cheltenham, UK, 2000.

73. Gonzales, R.I.; Phillips, S.H.; Hoflund, G.B. *J. Spacecr. Rockets* **2000,** *37,* 463-467.

74. Phillips, S.; Gonzales, R.; Chaffee, K.; Haddad, T.; Hoflund, G.; Hsiao, B.; Fu, B. *POSS Polymers for Space: Entrepreneurial Research:* Technical Report for Air Force Research Laboratory: Edwards Air Force Base, CA, 2009.

75. Hoflund, G.B; Gonzalez, R.I.; Phillips, S.H. *J. Adhesion. Sci. Technology* **2001,** *15,* 1199-1211.

76. Li, G.; Wang, L.; Ni, H.; Pittman, C.U. *J. Inorg. Organomet. Polym.* **2001,** *11,* 123-154.

77. Lee, A.; Lichtenhan, J.D. *Macromolecues*, **1998,** *31,* 4970-4974.

78. Phillips, S.H.; Haddad, T.S.; Tomczak, S.J. *Curr. Opin. Solid State Mater. Sci.* **2008,** *8,* 21-29.

79. Misra, R.; Fu, B.X.; Plagge, A.; Morgan, S.E. *J. Polym. Sci. Part B: Polym. Phys.* **2009,** *47,* 1088-1102.

80. Jones, P.J.; Cook, R.D.; McWright, C.N.; Nalty, R.J.; Choudhary, V.; Morgan, S.E. *J. Appl. Polym. Sci.* **2011,** *121,* 2945-2956.

81. Dintcheva, N.T.; Morici, E.; Arrigo, R.; La Mantia, F.P.; Malatesta, V.; Schwab, J.J. *Polym. Degrad. Stab.* **2012,** *97,* 2313-2322.

82. Engardio, T.J.; Hu, G.Y.; Kang, D.K.; Rorye, E.S. Scratch-Resistant Coatings with Improved Adhesion to Inorganic Thin Film Coatings. US20100249265 A1, September 30, 2010.

83. Novak, E. *Understanding the Capabilities of Your Surface Measurement System*; Bruker NSB Stylus and Optical Unit R&D Status Update: Tucson, AZ, June 2012.

84. De Oliveira, R.R.L.; Albuquerque, D.A.C.; Cruz, T.G.S.; Yamaji, F.M.; Leite, F.L. Measurement of the Nanoscale Roughness by Atomic Force Microscopy: Basic Principles and Applications; In *Atomic Force Microscopy – Imaging, Measuring and Manipulating Surfaces at the Atomic Scale*; InTech; 2012; pp. 147-174.

85. Brunsvold, A.L.; Minton, T.K.; Gouzman, I.; Grossman, E.; Gonzales, R. *High Perform. Polym.* **2004,** *16,* 303-318.

86. Tomczak, S.J.; Marchant, D.; Svejda, S.; Minton, T.K.; Brunsvold, A.L.; Gouzman, I.; Grossman, E.; Schatz, G.C.; Troya, D.; Sun, L.; Gonzales R.I. In *Materials for Space Applications,* Proceedings of the Materials Research Society Symposium Proceedings Volume 851, January, 2004.

87. Tomczak, S.; Marchant, D.; Mabry, J.; Vij, V.; Minton, T.; Brunsvold, A.; Wright, M.; Petteys, B.; Guenthner A. Proceedings of Pacifichem 2005, Honolulu, HI, December 15-20, 2005.

88. Wright, M.E.; Petteys, B.J; Guenther, A.J.; Fallis, S.; Yandek, G.R.; Tomczak, S.J.; Minton, T.K.; Brunsvold, A. *Macromolecules* **2006,** *39,* 4710-4718.

89. Kuo, S-W.; Chang, F-C. *Prog. Polym. Sci.* **2011,** *36,* 1649-1696.

90. Pittman, C.U.; Li, G-H.; Ni, H. *Macromol. Symp.* **2003,** *196,* 301-325.

91. Verker, R.; Grossman, E.; Gouzman, I.; Eliaz, N. *High Perform. Polym.* **2008,** *20,* 475-491.

92. Lei, X-F.; Qiao, M-T.; Tian, L-D.; Yao, P.; Ma, Y.; Zhang, H-P.; Zhang, Q-Y. *Corros. Sci.* **2015,** *90,* 223-238.

93. Satellite Life Extension: Reaching for the Holy Grail http://www.satellitetoday.com/publications/2013/03/01/satellite-life-extension-reaching-for-the-holy-grail/ (accessed December 16, 2016).

94. Eon. D.; Raballand, V.; Carty, G.; Cardinaud, C.; Vourdas, N.; Argitis, P.; Gogolides E. *J. Vac. Sci. Technol. B.* **2006,** *24,* 2678-2688.

95. Mirabella, F.M. *Spectroscopy* **1990,** *5,* 28-30.

96. What is Ellipsometry? https://www.jawoollam.com/resources/ellipsometry-tutorial/what-is-ellipsometry (accessed Oct 24, 2016).

97. Augustine, B.H.; Hughes, W.C.; Zimmermann, K.J.; Figueiredo, A.J.; Guo, X.; Chusuei, C.C.; Maidment, J.S. *Langmuir* **2007,** *23,* 4346-4350.

98. Wenzel, R.N.; *Ind. Eng. Chem.* **1936,** *28,* 988-994.

99. Wheeler, P.A.; Misra, R.; Cook, R.D.; Morgan, S.E. *J. Appl. Polym. Sci.* **2008,** *108,* 2503-1508.

100. Gomathi, A.; Gopalakrishnan, K.; Rao, C.N.R. *Mater. Res. Bull*. **2010,** *45,* 1894-1898.

101. XPS vs EDS – Depth of Chemistry Information http://www.nanolabtechnologies.com/K-Alpha-Thermo (accessed Oct 26, 2016).

102. Misra, R.; Alidedeouglu, A.H.; Jarrett, W.L.; Morgan, S.E. *Polymer* **2009,** *50,* 2906-2918.

103. Milliman, H.W.; Boris, D.; Schiraldi, D.A. *Macromolecules*. **2012,** *45,* 1931-1936.

104. Hansen, C.M. *Hansen Solubility Parameters: A User's Handbook*, 1st ed.; CRC Press: Boca Raton, FL, 2000.

105. Barton, A.M. CRC Handbook of Solubility Parameters and Other Cohesion Parameters; CRC Press: Boca Raton, 1983; pp 153-161.

106. Rosu, D.; Cascaval, C.N.; Mustata, F.; Ciobanu, C. *Thermochim. Acta* **2002,** *383,* 119-127.

107. Hybrid Plastics – R&D Chemicals http://hybridplastics.com/products/rd-chemicals/ (accessed Nov 30, 2016)

108. *Cerium (IV) Oxide* MSDS No. 342955; Sigma Aldrich, February 4, 2013.

109. Bang, J.H.; Suslick, K.S. *Adv. Mater.* **2010,** *22,* 1039-1059.

110. *RAR-912* MSDS; Royce International: East Rutherford, NJ, August 19, 2011.

111. *Lindax 1* MSDS; Lindau Chemicals: Columbia, SC, May 18, 2005.

112. Tissue-Tearor – Thomas Scientific http://www.thomassci.com/Equipment/Homogenizers/_/TISSUE-TEAROR (accessed Nov 30, 2016)

113. Hexion.com – EPON 862 Resin http://www.hexion.com/Products/TechnicalDataSheet.aspx?id=3950 (accessed December 10, 2016).

114. Lichtenhan, J.D. Hybrid Plastics, Hattiesburg, MS. Personal communication, 2016.

115. Dielectric Spectroscopy of Reactive Polymers. http://www.novocontrol.de/pdf_s/APND2.PDF (accessed Nov 5, 2016).

116. Dielectric Spectroscopy on the Dynamics of Amorphous Polymeric Systems. http://www.novocontrol.de/pdf_s/APND1.PDF (accessed Nov 5, 2016).

117. Piness, J; Hassan, M.K.; & Wiggins, J.S. “Network Conversion Studies of POSS-Epoxy-Amine Nanocomposites” *SAMPE Tech 2014*. Seattle, WA, June 2014.

118. Larson, R.G. *The Structure and Rheology of Complex Fluids*; Oxford University Press: New York, 1999.

119. Piness, J.; Wiggins, J.S. “UV Protective Oxide Coatings for Cyanate Esters” *SAMPE Tech 2016*. Long Beach, CA, May 2016.

120. Silverstein, R.M.; Webster, F.X.; Kiemle, D.J. *Spectrometric Identification of Organic Compounds*; John Wiley & Sons, Inc.: Hoboken, NJ, 2005.

121. 8.2 The Nuclear Overhauser Effect https://www.chem.wisc.edu/areas/reich/nmr/08-tech-02-noe.htm (accessed December 24, 2016).

122. Wallace, W.E.; Guttman, C.M.; Antonucci, J.M. *J. Am. Soc. Mass. Spectrom.* **1998,** *10,* 224-230.

123. Scope of Services – Microanalysis Lab – School of Chemical Sciences – University of Illinois http://scs.illinois.edu/microanalysis/ (accessed December 16, 2016).

124. Piness, J.; Miller, S.K.; Knauer, K.M.; Morgan, S.E.; Wiggins, J.S. “Atomic Oxygen Exposure Testing of Novel Layered POSS Thermoset Nanocomposites” *International Astronautical Congress.* Jerusalem, Israel, October 2015.

125. ASTM D638-14 Standard Test Method for Tensile Properties of Plastics; ASTM Standard: West Conshohocken, PA, 2014.

126. ASTM D638-15 Standard Test Methods for Flexural Properties of Unreinforced and Reinforced Plastics and Electrical Insulating Materials; ASTM Standard: West Conshohocken, PA, 2015.

127. Holmes-Farley, S.R.; Bain, C.D.; Whitesides, G.M. *Langmuir.* **1988,** *4,* 921-937.

128. Efimenko, K.; Wallace, W.E.; Genzer, J. *J. Colloid Interface Sci.* **2002,** *245,* 306-315.

129. Owens, D.K.; Wendt, R.C. *J. Appl. Polym. Sci.* **1969,** *13,* 1741-1747

130. Wells, B.K. Xeel Corporation, Notasulga, Al. Personal Communication, 2016.

131. Basic Plasma Cleaner – Harrick Plasma http://harrickplasma.com/products/basic-plasma-cleaner (accessed January 6, 2017).

132. Özçam, A.E.; Efimenko, K.; Genzer, J. *Polymer*, **2014,** *55,* 3107-3119.

133. Su, X.; Jing, X. *J. Appl. Polym. Sci.* **2007,** *106,* 737-742.

134. Cho, K.; Lee, D.; Park, C.E.; Huh, W. *Polymer* **1996,** *37,* 813-817.

135. POSS User's Guide Version 2.06; Hybrid Plastics, Hattiesburg, MS.

136. Bergshoef, M.M.; Vancso, G.J. *Adv. Mater.* **1999,** *11,* 1362-1365.

137. *Dielectric Spectroscopy of Polymeric Materials: Fundamentals and Applications.*; Runt J.P.; Fitzgerald J.J., Eds.; American Chemical Society, Washington, DC, 1997.

138. Kim, H.S.; Lee, D.G. *Compos. Sci. Technol.* **2007,** *67,* 29–44.

139. Ungarish, M.; Joseph, R.; Vittoser, J.; Kenig, S. *Composites* **1990,** *21,* 481–486.

140. *Handbook of Epoxy Resins;* Lee, H.L.; Neville, K., Eds.; McGraw-Hill,New York, 1967.

141. Bidstrup, S.A.; Simpson, J.O. *J. Polym. Sci., Polym. Phys.* **1995,** *33,* 43-54.

142. Kolesar, E.S. Dielectric Measurements for Monitoring the Cure of Epoxies and Composite Materials. In *Comprehensive Composite Materials*; Carlsson, L.; Crane, R.L.; Uchino, K., Eds. New York, 2000; Vol 5.

143. Ultrasonication. http://www.rsc.org/publishing/journals/prospect/ontology.asp?id=CMO:0001708 (accessed Nov 4, 2016).

144. Jenekhe, S.A.; Roberts, M.F. *Macromolecules* **1993,** *26,* 4981-4983.

145. Callister, W.D. *Materials Science and Engineering: An Introduction*, 7th ed.; John Wiley & Sons Inc: New York, 2007.

146. Piness, J.; Knauer, M.K.; Wiggins, J.S. "Atomistic and Macro-scale Mechanical Property Testing of POSS Nanocomposites for Space Applications" *SAMPE Tech 2015*. Baltimore, MD May 2015.

147. New York Times, U.S. Military Space Plane Begins a Fourth (Mostly) Secret Mission. http://www.nytimes.com/2015/05/20/science/space/secret-vessel-to-test-durability-of-materials-in-space-nasa-says.html (accessed May 19, 2015).

148. Coates, J. Interpretation of Infrared Spectra, A Practical Approach. In *Encyclopedia of Analytical Chemistry*; Meyers, R.A., Eds. John Wiley and Sons, Inc.: 2006; pp 1-23.

149. Piness, J.; Knauer, K.M.; Morgan, S.E.; Wiggins, J.S. Novel POSS-Cerium Oxide Thermoset Nanocomposites for UV Degradation Mitigation*, Proceedings of the AIAA SPACE 2015 Conference and Exposition*, Pasadena, CA, Aug 31 – Sep 2, 2015.

150. Godnjavec, J.; Znoj, B.; Veronovski, N.; Venturini, P. *Prog. Org. Coat.* **2012,** *74,* 654-659.

151. Hammer, P.; Schiavetto, M.G.; dos Santos, F.C.; Benedetti, A.V.; Pulcinelli, S.H.; Santilli, C.V. *J. Non-Cryst. Solids.* **2010,** *356,* 2606-2612

152. Shi, H.; Lui, F.; Han, E. *Mater. Chem. Phys.* **2010,** *124,* 291-297.

153. Gonzalez, E.; Pavez, J.; Azocar, I.; Zagal, J.H.; Zhou, X.; Melo, F.; Thompson, G.E.; Paez, M.A. *Electrochim. Acta.* **2011,** *56,* 7586-7595.

154. Montemor, M.F.; Pinto, P.; Ferreira, M.G.S. *Electrochim. Acta* **2009,** *54,* 5179-5189.

155. Wilson, S.P.; Andrews, L. *J. Phys. Chem. A.* **1999,** *103,* 3171-3183.

156. NMR Spectroscopy Tubes – Sigma Aldrich http://www.sigmaaldrich.com/analytical-chromatography/spectroscopy/learning-center/nmr-spectroscopy/nmr-tubes.html (accessed December 9, 2016).

157. NMR Solvent Data Chart – Cambridge Isotope Laboratories Inc. http://www2.chem.umd.edu/nmr/reference/isotope_solvent.pdf (accessed December 9, 2016).

158. *Cerium (III)Nitrate Hexahydrate* MSDS No. 238538; Sigma Aldrich, January 23, 2017.

159. Salazar-Sandoval, E.J.; Aguirre, M.; Paulis, M.; Leiza, J.R.; Johansson, M.; Ahniyaz, A. *RSC Adv.* **2014,** *4,* 61863-61868.

160. Lochhead, R.Y.; Boykin, C.M. An Investigative Study of Polymer Absorption to Smectite Clay: Polyelectrolytes and Sodium Montmorillonite. In Polymer Nanocomposites Synthesis, Characterization, and Modeling; ACS Symposium Series 804; American Chemical Society: Washington D.C., 2002; pp 85-98.

161. Zagar, E.; Grdadolnik, J. *J. Mol. Struct.* **2003,** *658,* 143-152.

162. Gutierrez, J.; Tercjak, A.; Mondragon, I. *J. Phys Chem. C* **2010,** *114,* 22424-22430.

163. Ni Y.; Zheng, S. *Macromolecules* **2007,** *40,* 7009-7018.

164. NIST X-ray Photoelectron Spectroscopy Database https://srdata.nist.gov/xps/ (accessed January 18, 2017).

165. An Introduction to Electron Microscopy – Focused Ion Beams Systems and DualBeam™ Systems https://www.fei.com/introduction-to-electron-microscopy/fib/ (accessed January 21, 2017).